Surf Wave Hydrodynamics in the Coastal Environment

Salmon, James

DOI
10.4233/uuid:b038f8a2-d2db-46fc-8419-3141f21faa1c

Publication date
2016

Document Version
Final published version

Citation (APA)
Salmon, J. (2016). *Surf Wave Hydrodynamics in the Coastal Environment*. [Dissertation (TU Delft), Delft University of Technology]. https://doi.org/10.4233/uuid:b038f8a2-d2db-46fc-8419-3141f21faa1c

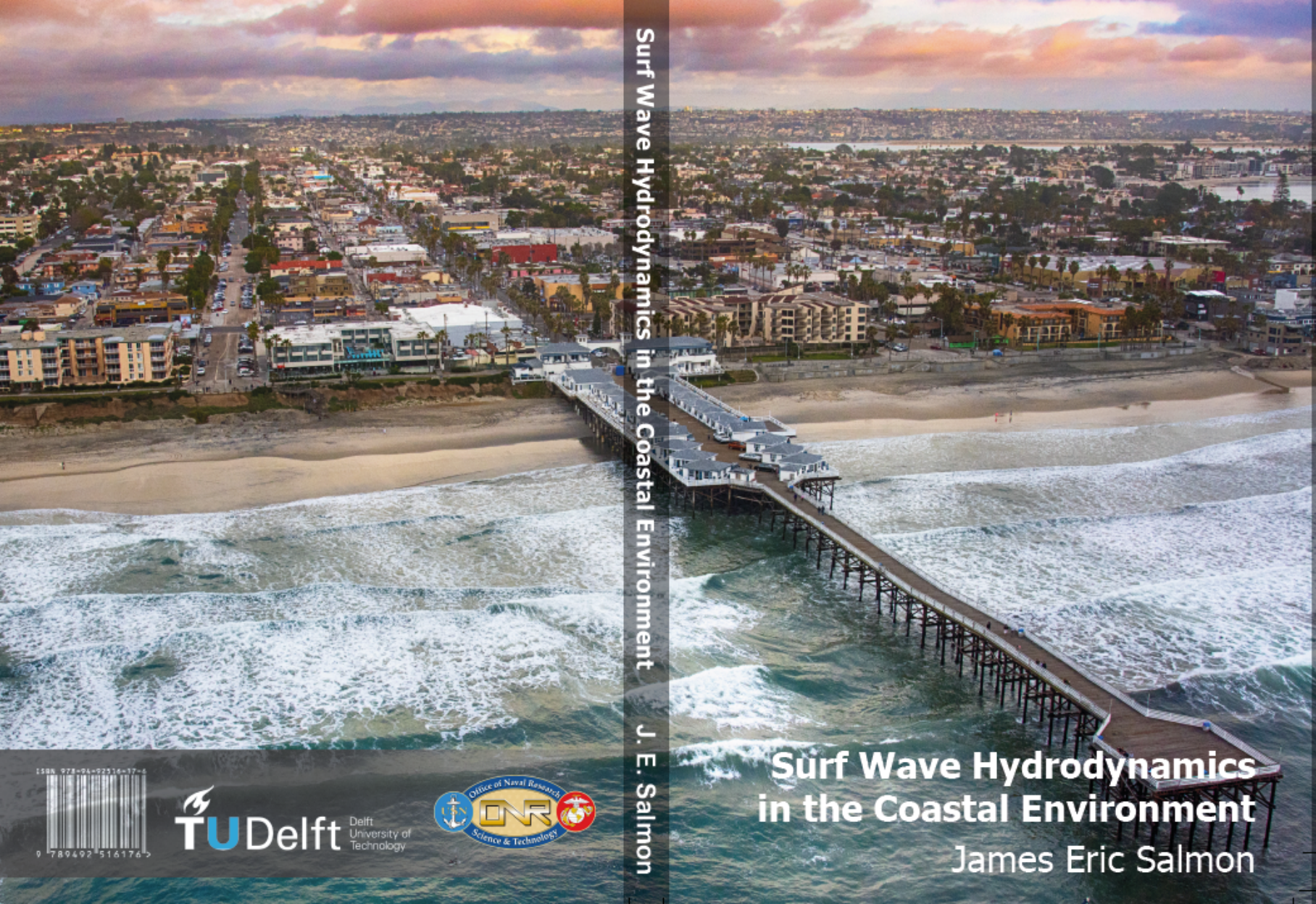

Surf Wave Hydrodynamics in the Coastal Environment

J. E. Salmon

ISBN 978-94-92516-17-6

TU Delft Delft University of Technology

Office of Naval Research ONR Science & Technology

Surf Wave Hydrodynamics in the Coastal Environment

James Eric Salmon

Invitation

to my public defense on

Surf Wave Hydrodynamics in the Coastal Environment

Tuesday, 15th November 2016 at 10:00

Senaatzaal of the Auditorium of Delft University of Technology

Aula Congress Centre
Building 20
Mekelweg 5
2628 CC Delft
The Netherlands

At 09:30 an introductory presentation on the doctoral work will be given.

A reception will follow the defence.

James Eric Salmon
salmonjames@gmail.com

Stellingen

behorende bij het proefschrift

SURF WAVE HYDRODYNAMICS IN THE COASTAL ENVIRONMENT

door

James SALMON

1. Een gecombineerde weging voor diepte geïnduceerde golfbreking die gebaseerd is op zowel het lokale bodemprofiel als de lokale golfparameters komt beter overeen met de literatuur en golfobservaties dan voorgaande wegingen.

   Dit proefschrift, Hoofdstuk 3 en 4.

2. De huidige implementatie van unidirectionele triad-brontermen in 2D stochastische golfmodellen is inconsistent.

   Dit proefschrift, Hoofdstuk 5.

3. Om vooruitgang te boeken in spectrale golfmodellering dient het parameterisatie paradigma wat betreft de brontermen te verschuiven van 1D idealisaties naar idealisaties die de golfspreiding in beschouwing nemen.

   Dit proefschrift, Hoofdstuk 3, 4 en 5.

4. Kustingenieurs moeten problemen vanuit een multidisciplinair oogpunt benaderen en de onzekerheden in hun oplossingen omarmen.

   Zie e.g. KAMPHUIS, J.W. (2006). Coastal engineering — quo vadis? *Coastal Engineering*, **53** (2-3), pp. 133–140.

5. De ontwikkelingen in data management technieken zoals Big Data zullen een belangrijke rol spelen in de vooruitgang van de Civiele Techniek.

   Zie e.g. BOYD, D. and CRAWFORD, K. (2012). Critical questions for big data: Provocations for a cultural, technological, and scholarly phenomenon. *Information, Communication & Society*, **15** (5), pp. 662–679.

6. Strikte loyaliteit aan de wetenschappelijke methode is nadelig voor de vooruitgang van de wetenschap.

   Zie e.g. CASTILLO, M. (2013). The scientific method: a need for something better? *American Journal of Neuroradiology*, **34** (9), pp. 1669–1671.

7. Wetenschappelijke methoden zijn geschikt voor het maken van waardeoordelen.

   Zie e.g. KURTZ, P. (2004). Can the sciences help us to make wise ethical judgments? *Skeptical Inquirer*, **28** (5), pp. 18–24.

8. Voorzichtigheid is geboden wanneer men oneliners gebruikt om complexe ideeën te beschrijven.

   Zie e.g. LUCAS, J.R. (1965). Against equality. *Philosophy*, **40** (154), pp. 296–307.

9. Het is ons eigen bestaan wat leed veroorzaakt.

10. Onverschilligheid is de grootste uitdaging van de mensheid.

Deze stellingen worden opponeerbaar en verdedigbaar geacht en zijn als zodanig goedgekeurd door de promotor prof. dr. J. D. Pietrzak.

Propositions

accompanying the dissertation

SURF WAVE HYDRODYNAMICS IN THE COASTAL ENVIRONMENT

by

James Eric SALMON

1. A joint scaling for depth-induced wave breaking based on both local bathymetry and local wave parameters provides better consistency with the literature and wave observations than previous scalings.

   This thesis, Chapters 3 and 4.

2. The current implementation of unidirectional triad source terms in 2D stochastic wave models is inconsistent.

   This thesis, Chapter 5.

3. To advance spectral wave modelling, the parameterization paradigm for source terms must shift from 1D idealizations to include effects of wave directionality.

   This thesis, Chapters 3, 4 and 5.

4. Coastal Engineers must approach problems from a multidisciplinary perspective and embrace uncertainty in their solutions.

   See e.g. KAMPHUIS, J.W. (2006). Coastal engineering — quo vadis? *Coastal Engineering*, **53** (2-3), pp. 133–140.

5. Advances in data management techniques such as Big Data will play a significant role in the advancement of Civil Engineering.

   See e.g. BOYD, D. and CRAWFORD, K. (2012). Critical questions for big data: Provocations for a cultural, technological, and scholarly phenomenon. *Information, Communication & Society*, **15** (5), pp. 662–679.

6. Strict adherence to the Scientific Method is detrimental to the advancement of the sciences.

   See e.g. CASTILLO, M. (2013). The scientific method: a need for something better? *American Journal of Neuroradiology*, **34** (9), pp. 1669–1671.

7. Scientific methods are suitable for making value judgments.

   See e.g. KURTZ, P. (2004). Can the sciences help us to make wise ethical judgments? *Skeptical Inquirer*, **28** (5), pp. 18–24.

8. Caution must be used when using labels which represent complex ideas.

   See e.g. LUCAS, J.R. (1965). Against equality. *Philosophy*, **40** (154), pp. 296–307.

9. It is our own existence which causes suffering.

10. Apathy is humanity's greatest challenge.

These propositions are regarded as opposable and defendable, and have been approved as such by the supervisor prof. dr. J. D. Pietrzak.

SURF WAVE HYDRODYNAMICS IN THE COASTAL ENVIRONMENT

SURF WAVE HYDRODYNAMICS IN THE COASTAL ENVIRONMENT

Proefschrift

ter verkrijging van de graad van doctor
aan de Technische Universiteit Delft,
op gezag van de Rector Magnificus prof. ir. K. C. A. M. Luyben,
voorzitter van het College voor Promoties,
in het openbaar te verdedigen op dinsdag 15 november 2016 om 10:00 uur

door

James Eric SALMON

Master of Engineering and Associateship of the City and Guilds of London Institute,
Imperial College London, Verenigd Koningkrijk
geboren te Londen, Verenigd Koningkrijk

Dit proefschrift is goedgekeurd door de promotor:

Prof. dr. J. D. Pietrzak

copromotor:

Dr. ir. L. H. Holthuijsen

Samenstelling promotiecommissie:

Rector Magnificus,	voorzitter
Prof. dr. J. D. Pietrzak,	Technische Universiteit Delft, promotor
Dr. ir. L. H. Holthuijsen,	Technische Universiteit Delft, copromotor
Onafhankelijk leden:	
Prof. dr. ir. A. W. Heemink,	Technische Universiteit Delft
Prof. J. Monbaliu,	Katholieke Universiteit Leuven, België
Prof. dr. ir. A. J. H. M. Reniers,	Technische Universiteit Delft
Dr. L. Cavaleri,	Istituto di Scienze Marine, Italië
Dr. ir. H. L. Tolman,	NOAA, Verenigde Staten
Prof. dr. ir. G. S. Stelling,	Technische Universiteit Delft, reservelid

Keywords: wave dynamics; numerical modelling; coastal systems; wave breaking; nonlinear interactions; stochastic models

Printed by: Gildeprint Drukkerijen, Enschede, The Netherlands

Author e-mail: salmonjames@gmail.com

Typeset with MiKTEX 2.9 using LyX 2.1.4. Original TU Delft document class available at: http://huisstijl.tudelft.nl/.

ISBN 978-94-92516-17-6

An electronic version of this dissertation is available at: http://repository.tudelft.nl/.

Dedicated to Douglas Roy Salmon
nil illegitimi carborundum

1930-2011

ACKNOWLEDGMENTS

LOOKING back over the last 5^+ years of my PhD, it is clear that it has been one of the most fun, rewarding and sometimes challenging experiences I've had to date; both in- and outside of the office. Without a doubt, it has been the people around me which have made my PhD period such a memorable experience and I would like to dedicate these pages to them.

First, I would like to thank Leo Holthuijsen for getting me into the amazing world of stochastic wave modelling and for being an inspiring supervisor: from his interesting Short Waves and Wind Waves courses to our daily discussions on spectral wave modelling and holidaying in the UK! Equally, I am grateful to the rest of the SWAN team: Gerbrant van Vledder for sharing his expertise and enthusiasm on many different aspects of wave hydrodynamics and Marcel Zijlema for navigating me through the SWAN source code and his expertise in numerics. I am also indebted to the SWAN team for securing the ONR funding, without which this research could not have been undertaken.

I am also grateful to Guus Stelling who acted as my Promotor during the first half of my PhD and to Julie Pietrzak who kindly took over and has supported me over the second half of my PhD; particularly with getting my papers and thesis together and securing additional funding allowing me to complete my research. In this regard, I am grateful to Wim Uijttewaal and Ad Reniers who approved the extra funding from the Environmental Fluid Mechanics section to extend my PhD. Thanks also goes to Environmental Fluid Mechanics support staff, particularly Otti Kievits for simplifying the university administration and providing advice on a multitude of issues, and also to Andre Brouwer who minimized my computer woes at the beginning of my PhD.

It cannot be overstated the scientific and moral support of my fellow PhD and Postdoc colleagues in the Environmental Fluid Mechanics Section (or otherwise!) have provided; from our casual to heated discussions to the Thursday afternoon section drinks. First, thanks to my predecessors: Pieter Smit, Matthijs Bénit and Paul van der Ham who helped me with my first few steps with wave modelling. In particular, thanks to Pieter for being a great conference travelling companion, PhD role model and co-author! From the 2^{nd} floor, thanks goes to Dirk Rijnsdorp and Xuexue Chen for also being great conference companions and for being part of the thesis-writing team and sharing their successes and sorrows! Thanks Dirk for our discussions on phase-resolving wave modelling to his expertise on a variety of Dutch topics and to Xuexue for our discussions on hydraulic structures to Chinese culture and food! Particular gratitude goes to Dirk Rijnsdorp and Sabine Rijnsburger who worked tirelessly to translate the Samenvatting and Stellingen, and also to Gerbrant van Vledder for translation suggestions and Daniel Boonman for checking these translations. Additional thanks goes to Carine van der Boog for assistance with the cover design.

I am also grateful to the PhDs who I have had the pleasure of sharing an office with: Tu Pham, Víctor Chavarrías, Sabine Rijnsburger, Sotiria Georgiou, Steffie Ypma and Floris

de Wit, and also to the MSc students and guest researchers, of which there are too many to name here! Thanks for the many and varied discussions and not commenting too harshly on the 'organisation' of my desk space! Without your helpful suggestions, this thesis could never have been realised in LaTeX. Also thanks to Ocean Cui, Olga Kleptsova, Gu Stecca, Nils Brüggemann, Marion Tissier and Adam Candy for adding to the great working culture on the 2nd floor by being there for our daily lunchtime discussions and for their help with various educational tasks over the years! Finally, thanks to the other half of the Environmental Fluid Mechanics Section PhDs and Postdocs working in the laboratory or elsewhere: Andres, Binh, Bram, Clara, Cynthia, Frank, Gonzalo, Jakob, Lodewijk, María, Marco, Miguel, Nici, Shahid, Steven, Willem, Yorick and anyone else I've missed (!) for the drinks, food, cakes and comradery over the years .

Last, but certainly not least, a mention must go to my friends and family. Thanks to my family back in the UK for their unconditional support whilst I have been abroad. Thanks for you patience and understanding over what has sometimes been a hard period of adjustment. I also thank all my friends here in the Netherlands that have helped make my stay here as fun and comfortable as a second home over the years. Thanks go to all my previous house mates: the guys at Geertsemastraat 6A (2009-2010) and Roland Holstlaan 652 (2010); Anne Krimp (and the cats!); Shahin Azad; Jan Wessels; Tunmise Odediran and the guys at Woudseweg 6A (2016). Thank you for putting up with me and everything! Very finally, a mention must go to the guys at the Board of European Students of Technology Delft who have been a constant presence over the years in both my social life and personal development outside academia - all the BEST!

James Eric Salmon
Chelmsford, March 2016

SAMENVATTING

SURF WAVE HYDRODYNAMICS IN THE COASTAL ENVIRONMENT

STOCHASTISCHE golfmodellen spelen een centrale rol in ons hedendaags modelleervermogen. Ze worden veelvuldig gebruikt om schattingen te maken van de golfstatistiek, om randvoorwaardes te genereren en om golfeffecten in gekoppelde model systemen te beschrijven. Zulke modellen zijn oorspronkelijk ontwikkeld om de golftransformatie in diep water te kunnen voorspellen, waar de aannames van de Gaussische statistiek over het algemeen geldig zijn. In de afgelopen decennia zijn deze modellen echter ook toegepast in ondiepere kustgebieden waar de geldigheid van de stochastische representatie van de dominante golfprocessen twijfelachtig is, dit komt met name door de toename van de niet-lineariten in het golfveld en de in dit gebied dominante diepte-geïnduceerde golfprocessen.

De twee meest dominante golfprocessen in de brandingszone, diepte-geïnduceerd golfbreken en niet-lineaire drie golf (triad) interacties, zijn echter de minst begrepen en gerepresenteerde processen in stochastische golfmodellen. Dit komt zowel door hun complexiteit, als door de schaarste aan analytische oplossingen voor realistische golfvelden. Daarmee vertegenwoordigen deze twee processen het grootste obstakel om een nauwkeurige voorspelling te geven van de golfdynamica in een kustgebied. Zulke voorspellingen zijn daarentegen essentieel om praktische kustbeheer en kustontwerp vraagstukken te kunnen beantwoorden. Zulke ontwikkelingen zijn noodzakelijk om ons begrip van deze golf geïnduceerde processen te vergroten, om de kosten van het kustbeheer te reduceren en om hedendaagse kwesties zoals onzekerheden in de zeespiegelstijging te beschouwen.

Door de complexiteit van diepte-geïnduceerd golfbreken bestaat er nog geen complete beschrijving van dit proces voor zowel stochastische als deterministische modellen. Ook al is er uitgebreid onderzoek gedaan om dit proces te parametriseren in stochastische modellen, dergelijke parametrisaties zijn inconsistent met theorie, observaties en (deterministische) model voorspellingen. Hedendaagse model standaarden presteren met name slecht over (bijna) horizontale bodems, waar het energieverlies van lokaal opgewekte golven wordt overschat en het energieverlies van deining wordt onderschat. Evenzeer geven stochastische golfmodellen een matige beschrijving van de triadinteracties door het sluitingsprobleem en de oplopende rekenkosten van meer nauwkeurige beschrijvingen. In het bijzonder geeft de meest toegepaste parametrisatie in de golfliteratuur een verkeerde voorspelling van de evolutie van de spectrale vorm, en van de convergentie naar het evenwicht in de hoogfrequente staart diep in de brandingszone. Het correct oplossen van deze kwesties is essentieel om de vele kustactiviteiten te kunnen beheren; van het ontwerp van kustverdedigingswerken tot de haalbaarheidsstudies van golfenergieomzetters, van havenactiviteiten tot scheepsnavigatie, van ecologie tot visserij, en van toerisme tot kustveiligheid.

In deze studie onderzoeken we het diepte-geïnduceerd golfbreken door middel van een uitgebreide literatuurstudie en een vergelijking van de model prestaties. We maken gebruik van een uitgebreide set aan golfmetingen welke een breed scala aan golfcondities en bodemliggingen omvat. De analyse toont aan dat geen van de beschikbare brontermen in staat is om op een adequate manier het diepte-geïnduceerd golfbreken te beschrijven. Dit komt overeen met de golfliteratuur, aangezien bestaande parametrisaties dan wel de golfdissipatie van lokaal gegenereerde golven overschat, ofwel de dissipatie van niet-lokaal gegenereerde golven over relatief vlakke bodems onderschat. Vanwege deze kwestie stellen we een nieuwe gecombineerde weging voor, welke is gebaseerd op zowel de lokale golfcondities als de bodemligging. Door gebruik te maken van zowel het genormaliseerde karakteristieke golfgetal als de lokale bodemhelling kan men de twee benaderingen welke gangbaar zijn in de golfliteratuur verenigen. Deze nieuwe formulering verbeterd de prestaties van het model wat betreft de dissipatie van zowel de lokale als de niet-lokale genereerde golven over relatief vlakke bodems.

Verder is de geldigheid van de aanname dat de golfdissipatie kan worden beschreven met een eendimensionale watersprong onderzocht. Vervolgens is er een heuristische richtingsmodificatie geïntroduceerd voor de diepte-geïnduceerde golfbreking dissipatie modellen. Deze benadering partitioneert het tweedimensionale golfspectrum in een aantal richtingspartities welke uni-directioneel worden verondersteld. Deze partitionering verminderd de golfdissipatie en vergroot de significante golfhoogte, wat in overeenstemming is met veldmetingen. Deze aanpassing is niet alleen toepasbaar voor de in deze studie voorgestelde gecombineerde weging golfbreking parametrisatie, maar ook voor de gerenommeerde parametrisaties.

De effecten van de voorgestelde weging en richtingsmodificatie worden vervolgens bekeken in een operationele context door ze te vergelijken met de hedendaagse brontermen, veldmetingen en een hypothetische storm welke representatief is voor de Nederlandse ontwerpcondities. We verwachten dat deze ontwerpcondities representatief zijn voor de globale ontwerpcondities. In een omgeving waar de intensiteit van stormen toe kunnen nemen, bijvoorbeeld door de opwarming van de aarde, wordt de invloed van golfbreking bij de kust van grotere relevantie in het geval van zulke extreme condities. De verwachting is dat de invloed van golfbreking modellen in gekoppelde model systemen nieuwe belangrijke inlichtingen oplevert wat betreft ons begrip van de golfgedreven processen in kustgebieden.

Vervolgens bestuderen we de beschrijving van de triad-interacties in stochastische golfmodellen. In het bijzonder komen we terug op de collineaire aanname welke wordt gebruikt om 1D triad-brontermen te transformeren voor gebruik in 2D stochastische golfmodellen. Deze aannames zijn noodzakelijk uit het oogpunt van reken efficiëntie. De gangbare collineaire aanname blijkt inconsistent in de unidirectionele limiet, waar de door stochastische modellen berekende energie overdachten onbegrensd worden. Dit resulteert in een dimensionele kalibratie coëfficiënt welke ten minste een orde van grootte kleiner is dan de gene uit de golfliteratuur. Om die reden is, in het geval van richting gespreide golfcondities, de 1D triad-bronterm (gebaseerd op de gangbare collineaire aanname) niet in staat om de golftransformatie correct te beschrijven. Om dit probleem op te lossen presenteren we een nieuwe collineaire aanname welke rekening houdt met de golfenergie binnen een eindige directionele bandbreedte. Deze colline-

aire benadering convergeert op een correcte wijze in de unidirectionele limiet en komt overeen met de voorspellingen van een tweede orde nauwkeurig deterministisch golfmodel. Betere overeenstemming is met name gevonden in de voorspellingen van de spectrale vorm en gerelateerde integrale parameters zoals de golfperiode in het geval van geïdealiseerde golfcondities. In een aantal condities zijn de verbeteringen significanter dan de verschillen tussen de onderliggende triad-modellen.

Dit werk laat zien dat, hoewel de onderliggende theorien van de stochastiche golfmodellen twijfelachtig zijn in het kustgebied, dat het accuraat modelleren van de golfstatistiek in zulke gebieden mogelijk is. Met de voortgang gepresenteerd in dit werk, de nieuwe brontermen komen beter overeen met de hedendaagse golfliteratuur en bieden significante stappen voorwaarts ten opzichte van de bestaande brontermen. We anticiperen dat de gepresenteerde ontwikkelingen de basis vormen voor toekomstig onderzoek naar brontermen en dat ze gebruikt kunnen worden om de dominante golffysica in kustgebieden te beschrijven in operationele golfmodellen.

ABSTRACT

SURF WAVE HYDRODYNAMICS IN THE COASTAL ENVIRONMENT

STOCHASTIC wave models play a central role in our present-day wave modelling capabilities. They are frequently used to compute wave statistics, to generate boundary conditions and to include wave effects in coupled model systems. Historically, such models were developed to predict the wave field evolution in deep water where the conditions of Gaussianity generally hold. However, in recent decades, such models have been applied to the shallower coastal environment where the stochastic representation of the dominant wave physics becomes questionable. This is primarily due to the increased influence of wave nonlinearity and the additional depth-induced wave processes that are dominant in this region.

Unfortunately, the two most dominant wave processes in the surf zone: depth-induced wave breaking and nonlinear triad wave-wave interactions are also the least well represented and understood. This is due to both their complexity and the scarcity of analytical solutions for realistic wave fields. As such, they represent a significant obstacle in the accurate modelling of the wave dynamics in the coastal region. Providing accurate representations of these wave processes is essential to answering the questions demanded from stochastic wave models from coastal engineers for coastal management and design. Such advancements are necessary to improve our understanding of wave-induced processes, to reduce costs in managing the coastal environment and to tackle contemporary issues such as uncertainties with respect to increased sea level rise.

Due to the complexity of depth-induced wave breaking, a complete representation of this wave process does not exist for both stochastic and deterministic modelling frameworks. Although there is extensive literature on the subject of parameterizing depth-induced wave breaking in a stochastic sense, these parameterizations are inconsistent with theory, observations and (deterministic) model predictions. In particular, present-day modelling defaults perform poorly over (near-)horizontal bathymetries with over-enhanced wave dissipation of locally-generated waves and insufficient dissipation of swell waves. Equally, nonlinear triad wave-wave interactions are poorly represented in stochastic wave models due to the problem of closure and the impractical computational expense of more accurate representations. In particular, the most commonly applied parameterization in the wave literature incorrectly predicts the evolution of the spectral shape, and the convergence to an equilibrium high-frequency tail deep in the surf zone. Correctly resolving these issues is essential for the management of many of the activities occurring at the coast; from the design of coastal defenses to feasibility studies for wave energy converters, from port operation and availability to vessel navigation, from understanding the ecology at the coast to the fisheries, and from managing leisure and tourism to safety at the coast.

In this work, we investigate the process of depth-induced wave breaking through a comprehensive analysis of the literature and a comparison of modelling performance.

Here, we use an extensive set of wave observations representing a large range of wave conditions and bathymetric profiles. The analysis demonstrates that no currently available depth-induced breaking source term is capable of sufficiently representing the process of depth-induced wave breaking. This is shown to be in agreement with the wave literature with parameterizations either over-predicting wave dissipation for locally generated waves or under-predicting wave dissipation for non-locally generated waves over (near-)horizontal bathymetries. To address this issue, a new joint scaling using both local wave and bathymetric conditions is proposed. Using both the normalized characteristic wave number and local bottom slope unifies two approaches prevalent in the wave literature. This is shown to improve the model performance for the dissipation of both locally and non-locally generated waves over (near-)horizontal bathymetries.

Furthermore, the validity of the assumption that wave dissipation can be modelled as analogous to a 1D dissipative bore is explored. Subsequently, a heuristic directional modification is introduced for depth-induced wave breaking dissipation models. This directionally partitions the 2D spectrum into several directional partitions that are assumed to be unidirectional. Model results demonstrate that the effect of the directional partitioning is to reduce the dissipation of wave energy and to enhance the significant wave height; in agreement with field measurements. Not only is this modification shown to be applicable to the joint wave breaking parameterization proposed in this study, but also for well-established parameterizations.

The effects of both the proposed scaling and directional modification are then reviewed from an operational context and are compared to state-of-the-art source terms, field observations and a hypothetical storm representative of Dutch design conditions. Such design conditions are expected to be representative of design conditions found globally. In an environment where storm intensities may be increasing, for example due to global warming, the results of wave breaking models near the coast under such extreme conditions become of greater relevance. The influence of wave breaking models in coupled model systems is anticipated to provide important new insights in understanding the various wave-driven processes along our coasts.

Next, the representation of the nonlinear triad wave-wave interactions in stochastic wave models is reviewed. In particular, the collinear approximation used to transform 1D triad source terms for implementation in 2D stochastic wave models is revisited. These approximations are necessitated by considerations of computational efficiency. The conventional collinear approximation is shown to be inconsistent at the unidirectional limit and to be a primary source of modelling error. Instead of converging to the values predicted by the 1D triad source terms at the unidirectional limit, the energy transfers as computed by stochastic wave models are shown to become unbounded. This results in a dimensional calibration coefficient which is at least an order of magnitude smaller than that found in the wave literature. Consequently, for directional wave conditions, 1D triad source terms implemented with the conventional collinear approximation insufficiently capture the wave evolution. To address this problem, a new collinear approximation is presented which accounts for the wave energy contained within a finite directional bandwidth. This collinear approximation is shown to converge correctly at the unidirectional limit and to agree well with predictions from a second-order accurate deterministic wave model. In particular, better agreement is shown in the

modelling prediction of the spectral shape and related integral parameters, e.g. wave period, under idealized wave conditions. Under certain conditions, these error reductions are shown to be more significant than differences between the underlying triad models.

The contribution of this work demonstrates that while the underlying theory underpinning stochastic wave modelling in the coastal environment still remains questionable, the accurate determination of wave statistics in the coastal zone is tenable. With the advancements presented in this study, the new source terms correspond better with the current wave literature and are shown to provide significant steps forward over existing default source terms. The developments presented here are anticipated to form the foundation for future source term research, and to be used for the representation of the dominant wave physics in the coastal environment in operational wave models.

Contents

1

INTRODUCTION

THE oceans have always been a source of fascination, mystery and awe. On the one hand, they represent a rich source of biodiversity, of valuable natural resource and a place of both economic and recreational value. On the other, the oceans are a source of fear and terror; an unpredictable force of nature to which man has fought against since time immemorial. It is therefore of little surprise that few people remain apathetic to the oceans. With a significant proportion of the world population living in the coastal region[1], the ocean has played, and continues to play, a central role in their livelihoods.

Arguably, the most spectacular and frequently recognised feature of the oceans are its surface waves. These waves are generated over the deep ocean basins under the influence of wind over the oceanic surface. Due to gravity, these waves then propagate as swell towards our coastlines where they shoal, steepen and inevitably dissipate. It is this evolution of the waves - from generation to dissipation - which is of much interest for our economic (e.g. port operations and fisheries), engineering (e.g. coastal defence and wave energy harvesting), environmental (e.g. influence on ecology and morphology), recreational (e.g. surfing conditions and swimmer safety) and, of course, scientific interest. However, despite our long history in studying ocean wave dynamics (see Phillips, 1977), it was military interests during the D-Day landings of World War II which catalyzed our present-day modelling developments and capabilities to both describe and predict ocean waves (see Komen et al., 1994).

Since then, with the advent of the era of modern computers, a plethora of wave models have been developed and been made available. All of these models are based on the Navier-Stokes equations with varying degrees of approximation introduced to facilitate computational efficiency. With the least level of approximation are the Large Eddy Simulation (LES) and Reynolds-Averaged Navier-Stokes class of models which are capable of representing all spatial and temporal scales of wave motion up to turbulence. Although such models have been applied to the study of waves (e.g. Lin and Liu, 1998; Lubin and Glockner, 2015), for operational engineering applications they are unsuitable due their

[1] Estimated to be over 40% of the world population (e.g. Martínez et al., 2007).

1

considerable requirements for computational resources; even by today's standards! Instead, a number of computationally more efficient model classes have been developed for predicting oceanic surface waves; each with their own advantages and limitations (see Fig. 1.1). Battjes (1994) identifies two main categories of wave models suitable for nearshore modelling: phase-resolving (deterministic) and phase-averaging (stochastic).

The classical phase-resolving approach for modelling waves are the depth-averaged Boussinesq equations whereby a velocity potential is introduced by assuming irrotationality and the vertical coordinate is eliminated by replacing vertical derivatives with their horizontal counterparts. The vertical structure is then given by the horizontal derivatives. By including only the lowest-order dispersion term and neglecting the nonlinear terms, the lowest-order Boussinesq equations of Peregrine (1967) are derived. Since then, much progress has been made to extend the range of applicability of Boussinesq-type equations such as the inclusion of higher order terms, inclusion of wave breaking and the improvement of the frequency-dispersion characteristics (see e.g. Madsen and Schaffer, 1999; Kirby, 2003; Brocchini, 2013).

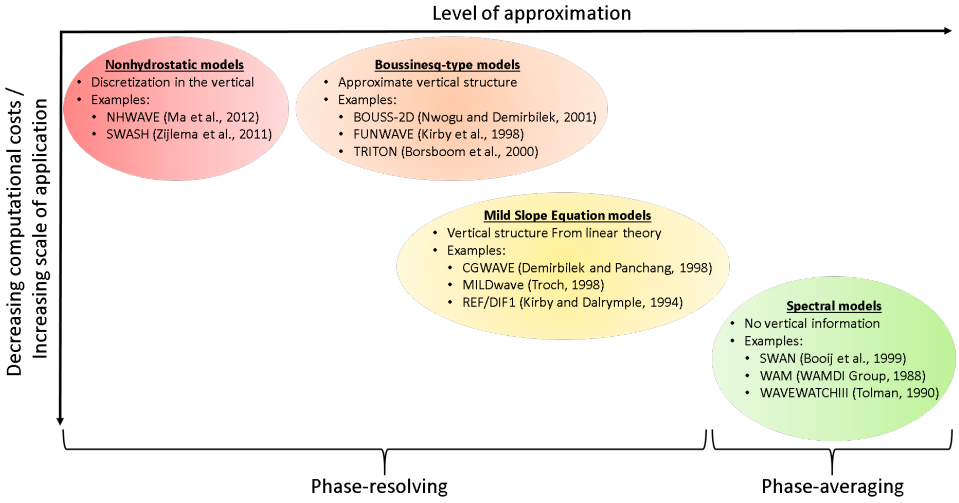

Figure 1.1: Commonly applied operational Eulerian wave models classes categorized into phase-resolving and phase-averaging.

An alternative approach to eliminate the dependency on the vertical is to assume a vertical structure based on linear wave theory which results in the mild-slope equations. Although the classical model (Berkoff, 1972) was limited to linear waves and gently sloping bathymetries, progress has been made to extend its range of applicability including: nonlinear conditions, steeper slopes and wave breaking (see e.g. Dingemans, 1997).

A recent advancement in nearshore wave modelling has come from from the non-hydrostatic approach (Stelling and Zijlema, 2003). Unlike the previous two wave models, the vertical structure is not imposed but is discretized and is therefore computed. Such models are promising as they have been demonstrated to have comparable computational efficiency to Boussinesq-type models (Zijlema et al., 2011) and have been shown

to be able to capture much of the physical phenomena relevant in the surf zone (e.g. Smit et al., 2014; Rijnsdorp et al., 2015).

Arguably, for the prediction of nearshore waves, where wave properties may vary rapidly due to nonlinear processes such as wave breaking and nonlinear wave interactions, the phase-resolving or deterministic approach to wave modelling such as Boussinesq-type models (e.g. Peregrine, 1967; Madsen and Sørensen, 1992; Nwogu, 1993; Lynett, 2006; Klopman et al., 2010), non-hydrostatic wave models (e.g. Zhou and Stansby, 1998; Zijlema et al., 2011) or others (e.g. Dalrymple and Rogers, 2006) should be employed. These deterministic models are advantageous as they predict the actual surface elevation $\eta(\mathbf{x}, t)$ as a function of space $\mathbf{x} = (x, y)$ and time t. Therefore, such models often include many of the physical processes which influence the wave dynamics, including wave refraction, diffraction and nonlinear wave-wave interactions. However, these models are also limited, by both their relatively high computational expense (due to requiring a high spatial resolution; typically a small fraction of the wavelength) and their inability to include wave generation due to wind. Therefore, over extended areas (say $>O(10)$ wavelengths) such models become impractical for operational purposes.

An alternative to the phase-resolving approach is phase-averaging where the sea surface is described by a wave spectrum. The surface elevation is then represented through the superposition of many sinusoidal waves, each of which represents a single independent freely propagating linear wave. Stochastic wave models then compute the transport of conserved quantities such as wave energy or action and represent the wave dynamics such as the generation of wave by wind, dissipation of waves and nonlinear interactions through the use of (parametric) source terms. Although this comes at the cost of the loss of phase information, and therefore phase-related processes such as diffraction cannot be inherently accounted for (e.g. Holthuijsen et al., 2003), such models are significantly more computationally efficient than their phase-resolving counterparts. Therefore, they are applicable on regional to global scales with (spatial) computational grids of the order of many wavelengths and time scales of many wave periods.

Originally, such models were developed for offshore applications (e.g. WAM (e.g. WAMDI Group, 1988; Komen et al., 1994; Monbaliu et al., 2000); WAVEWATCH III (e.g. Tolman, 1990b, 2009; Tolman and Chalikov, 1996)) where the general requirement of Gaussianity is applicable. However, in recent decades, as with phase-resolving wave modelling, impressive progress has be made to extend the limits of applicability of the phase-averaged framework, i.e., towards the nearshore. Nowadays, such models provide an essential tool for many operational purposes e.g. wave hindcasting and forecasting; design of coastal defences; vessel and port operations. In particular, in regions where sufficient wave data is unavailable, stochastic models provide an invaluable source of synthetic data. Furthermore, stochastic wave models are increasingly coupled to other numerical models (e.g. Warner et al., 2008; Dietrich et al., 2012) to include the effects of waves to predict currents, sediment transport and set-up.

However, despite this, two of the dominant wave processes encountered in shallow water are still not well represented. Although much success has been demonstrated in the coupling of a unidirectional bore-based dissipation model (e.g. Battjes and Janssen, 1978) with a constant scaling parameter, e.g., $\gamma = 0.73$ under a variety of wave conditions (see e.g. Ris et al., 1999), recent studies have shown that dissipation computed in

this way is *overestimated* for conditions of local wave growth over relatively horizontal bathymetries (e.g. de Waal, 2001; Bottema and Beyer, 2002). Conversely, for the dissipation of swell over similar bathymetries, laboratory observations and field measurements, numerical model results and theory suggests that dissipation computed with $\gamma = 0.73$ is *underestimated* (e.g. Nelson, 1997; Massel, 1998; Katsardi, 2007). This issue is further complicated by the plethora of different dissipation models available and even greater number of scaling parameterizations based on a variety of different parameters such as bottom slope (e.g. Madsen, 1976; Sallenger Jr. and Holman, 1985; Rattanapitikon and Shibayama, 2000), normalized wave number (e.g. Ting, 2001; Ruessink et al., 2003) or wave steepness (e.g. Battjes and Stive, 1985; Vink, 2001).

In addition, the effect of nonlinear triad wave-wave interactions are crudely implemented in operational stochastic models, if at all, in view of their computational expense. Although some success has been demonstrated in the prediction of bulk parameters sensitive to the computed spectral shape (e.g mean wave periods; Ris et al., 1999; van der Westhuysen, 2007), typically the spectral shape is poorly reproduced (e.g. Booij et al., 2009). In particular, the Lumped Triad Approximation (LTA) model of Eldeberky (1996) cannot reproduce the equilibrium high-frequency tail observed deep in the surf zone (e.g. Smith, 2004; Kaihatu et al., 2007, 2008). This in part comes from the restriction to only self-self interactions made in the LTA model which only permits the generation of superharmonics. However, even with less restrictive triad models which includes all interactions (e.g. Becq-Girard et al., 1999), it can be shown that the model performance is dependent on the collinear approximation applied to transform the 1D triad source terms into a 2D[2] source term suitable for 2D stochastic wave models.

1.1. OBJECTIVE AND OUTLINE

The primary objective of the present work is to improve our modelling capabilities to represent and predict two of the dominant wave processes encountered in shallow water: depth-induced wave breaking and nonlinear triad wave-wave interactions (Holthuijsen et al., 2008). In particular, the performance of stochastic wave models to reproduce the total energy; represented by the significant wave height H_{m0} and to reproduce the basic shape of the spectrum; represented by the mean wave period T_{m02} is considered. The accurate reproduction of either parameter does not guarantee the accurate representation of the sea state (e.g. Dabbi et al., 2015), but these two parameters are arguably the minimum, and most important, parameters needed for coastal engineering applications. Through comparison with wave observations and with alternative models, the present study aims to develop, calibrate and validate new source terms and modelling frameworks for application in operational stochastic models.

Following this introduction, Chapter 2 provides an overview of stochastic wave modelling and current state-of-the-art source terms for depth-induced wave breaking and triad nonlinear wave-wave interactions which the later chapters build upon. In particular, the concept of the variance density spectrum is introduced along with the energy (or action) balance with source terms relevant to deep and shallow water. Furthermore,

[2] In the context of spectral wave models, 2D refers to frequency-direction (σ, θ; or equivalent) space as opposed to geographical space.

the classical dissipation model of Battjes and Janssen (1978) for depth-induced wave breaking is provided in detail as are the key steps for the derivation of the Lumped Triad Approximation model of Eldeberky and Battjes (1996).

The following chapters (Chapters 3 and 4) are devoted to the further development and verification of parametric models for representing depth-induced wave breaking. Chapter 3 provides a comprehensive overview of the depth-induced wave breaking literature and provides an extensive analysis over numerous data sets characteristic of a wide range of wave conditions. Based on this analysis, a new joint scaling dependent on both bottom topography and wave field characteristics is presented. Furthermore, a heuristic modification is introduced for dissipation models to account for directional wave conditions. In Chapter 4, the new parameterization is compared to the present default which uses a constant scaling and to the scaling based on nonlinearity of van der Westhuysen (2009, 2010) over a range of field cases with different wave and bottom characteristics. In particular, focus was made on the geographical differences and to their performance under design conditions for a hypothetical 1 in 4000 year storm.

Chapter 5 is dedicated to the parameterization of the nonlinear triad wave-wave interactions. Particular focus is made on the development of a new collinear approximation to extend unidirectional triad parameterizations for the prediction of unidirectional and directional wave conditions using a 2D wave model. To demonstrate the suitability of the collinear approximation, model results for the mean wave period and the spectral shape are compared to a deterministic model capable of representing the wave dynamics to second-order accuracy. Furthermore, the effect of using less restrictive triad source terms is demonstrated.

Finally, a summary of the conclusions from this thesis, including the operational aspects given in Appendix B is provided in Chapter 6. In addition, an outlook for the future of stochastic wave modelling in the coastal environment is presented.

2

STOCHASTIC WAVE MODELLING

ONE of the triumphs towards our modern day operational wave prediction capabilities of the ocean wave dynamics has been our progress towards describing wave statistics as a wave spectrum (e.g. Pierson Jr. et al., 1955; Komen et al., 1994) and to predict its spectral evolution due to various physical processes resulting from external forcing and the conditions imposed by the local environment through an energy or action balance equation (e.g. Hasselmann et al., 1973; Phillips, 1977; WAMDI Group, 1988; Komen et al., 1994; WISE Group, 2007). Unlike the deterministic approach to wave modelling which predicts the instantaneous 2D free-surface elevation $\eta(\mathbf{x}, t)$ for each location $\mathbf{x} = (x, y)$ and time instance t, the stochastic approach represents the waves in terms of its spectral components, for example, radial frequency, σ and direction, θ. As such it describes averaged characteristics of the sea state.

2.1. THE WAVE SPECTRUM

Here, we briefly describe the wave spectrum. Excellent overviews may be found in LeBlond and Mysak (1981), Dalrymple and Dean (1991), Komen et al. (1994), Massel (1996), Emery and Thomson (2001), Holthuijsen (2007) and many others. If we assume that the 1D sea surface elevation can be assumed to be a zero-mean periodic (weakly) stationary and homogeneous process[1] then over a given time duration, T, we may represent the process as a superposition of an infinite number of independent discrete sinusoidal waves, e.g.:

$$\eta(\mathbf{x}, t) = \frac{a_0}{2} + \sum_{p=1}^{\infty} a_p cos\left(\sigma_p t - \mathbf{k}_p \mathbf{x} + \alpha_p\right) \tag{2.1}$$

where $a_0 = 0$ is the mean value, a_p is the wave amplitude, $\sigma_p = 2\pi p/T$ is the harmonic frequency, $\mathbf{k}_p$ is the wave number vector and α_p is the wave phase. As the discrete waves are independent of each other, α_p is uniformly (or randomly) distributed over the range $[0, 2\pi]$. Alternatively, Eq. (2.1) may be expressed in complex form at each location $\mathbf{x}$:

[1] Stationary referring to the invariance in time and homogeneous referring to invariance in geographical space.

$$\eta(t;\mathbf{x}) = \sum_{p=-\infty}^{\infty} A_p exp\left[i\sigma_p t\right] \tag{2.2}$$

where A_p is a complex Fourier amplitude. From the Wiener-Khinchin theorem, it is then possible to describe $\eta(t;\mathbf{x})$ as a spectral decomposition given by the energy (or power) spectrum by taking the Fourier transform of the autocorrelation[2] of η. The discrete contribution to the two-sided spectrum for each harmonic is then given as:

$$E_p^{'} = \int_{-\infty}^{\infty} R_{\eta\eta}(\tau)\, exp\left[-i\sigma_p\tau\right] d\tau \tag{2.3}$$

and:

$$R_{\eta\eta}(\tau) = E\left[\eta(t;\mathbf{x})\,\eta(t+\tau;\mathbf{x})\right] \tag{2.4}$$

with $E[\ldots]$ denoting the expected value[3] and τ representing a time lag.

In practice, it is difficult to compute $E[\ldots]$ (or even the ensemble average $\langle\ldots\rangle$) and instead the ergodic hypothesis is applied (see Kinsman, 1965) so that $\langle\ldots\rangle$ may be replaced by the time (or spatial) average at the limit $T\to\infty$. In reality, T is finite but is assumed to be sufficiently long to be representative of the wave conditions. As the time series is discrete, i.e., is sampled at N points so that $T = N\Delta t$, $R_{\eta\eta}(\tau)$ may then be estimated as:

$$R_{\eta\eta}(\tau) \approx \frac{1}{T}\sum_{n=1}^{N} \eta(n\Delta t;\mathbf{x})\,\eta(n\Delta t+\tau;\mathbf{x})\,\Delta t = \frac{1}{N}\sum_{n=1}^{N} \eta(n\Delta t;\mathbf{x})\,\eta(n\Delta t+\tau;\mathbf{x}) \tag{2.5}$$

In addition, for a discrete time series, we can re-write Eq. (2.2) as:

$$\eta(m\Delta t;\mathbf{x}) = \sum_{p=-N/2}^{N/2} A_p exp\left[i\sigma_p m\Delta t\right] \tag{2.6}$$

with its Fourier transform:

$$A_p = \frac{1}{N}\sum_{m=1}^{N} \eta(m\Delta t;\mathbf{x})\, exp\left[-i\sigma_p m\Delta t\right] \tag{2.7}$$

Substituting Eq. (2.6) and (2.7) into Eq. (2.5) and simplifying yields:

$$R_{\eta\eta}(\tau) = \sum_{p=-N/2}^{N/2} A_p A_p^{*} exp\left[i\sigma_p\tau\right] \tag{2.8}$$

where $*$ represent the complex conjugate. From Eq. (2.3), then:

[2] Occasionally this is used interchangeably with the autocovariance. However, whereas the autocorrelation is applied to the actual data series, the autocovariance is applied to a data series with the sample mean $\mu = a_0$ removed, i.e., $R_{vv}(\tau) = E\left[\left(v(t)-\mu_v\right)\left(v(t+\tau)-\mu_v\right)\right]$. Therefore, for a zero-mean process, these two definitions are equivalent. Further confusion also arises from the use of the term autocorrelation for the autocovariance normalized by the variance (Emery and Thomson, 2001).

[3] Occasionally this is used interchangeably with the ensemble average $\langle\ldots\rangle$ which is the average over N realizations rather than $N\to\infty$ implied by $E[\ldots]$, i.e., $E[v(t)] = \lim_{N\to\infty} N^{-1}\sum_{q=1}^{N} v_q(t)$.

$$E_p' = A_p A_p^* = |A_p|^2 \tag{2.9}$$

In practice, the use of a singular time series leads to only one realization of an amplitude per frequency and results in large errors (e.g. Holthuijsen, 2007). Therefore different techniques may be employed to give more realizations so that:

$$E_p' = \left\langle A_p A_p^* \right\rangle \tag{2.10}$$

where $\langle \ldots \rangle$ represents a (quasi-)ensembled average. Finally, expressing Eq. (2.10) as a one-sided continuous variance spectrum by distributing the discrete contribution over the frequency bandwidth $\Delta\sigma$ yields for $p > 0$:

$$E(\sigma_p) = 2\frac{|A_p|^2}{\Delta\sigma} \tag{2.11}$$

where:

$$\langle \eta^2(t) \rangle = \int_0^\infty E(\sigma)\, d\sigma \tag{2.12}$$

By using various measurement techniques, it is possible to incorporate directional information such the mean direction, θ_0 and the directional width, σ_θ. However, additional assumptions are often required to derive the *two-dimensional* wave spectra (see e.g. COST Action 714 Working Group, 2005), i.e., $E(\sigma,\theta)$. Often a directional distribution $D(\theta;\sigma)$ for each frequency is applied as a function of θ_0 and σ_θ so that:

$$E(\sigma,\theta) = E(\sigma)\, D(\theta;\sigma) \tag{2.13}$$

where $\int_0^{2\pi} D(\theta;\sigma)\, d\theta = 1$. Common unimodal models for $D(\theta;\sigma)$ include the $cos^2\theta$ model and the $cos^{2s}\theta$ model (e.g. Longuet-Higgins et al., 1963; Mitsuyasu et al., 1975).

2.2. THE ENERGY/ACTION BALANCE EQUATION

Although the numerical techniques employed by stochastic wave models vary, they all compute the evolution of the wave spectrum by solving the Eulerian balance for either the energy or action density as given in Eq. (2.14). The most widely used stochastic wave models include WAM (e.g. WAMDI Group, 1988; Komen et al., 1994; Monbaliu et al., 2000), WAVEWATCH III (e.g. Tolman, 1990b, 2009; Tolman and Chalikov, 1996), TOMAWAC (Benoit et al., 1996), SWAN (e.g. Booij et al., 1999; Ris et al., 1999; Zijlema, 2010), CREST (Ardhuin et al., 2001), MIKE21SW (Sørensen et al., 2004) and WWM (Roland et al., 2006; Roland, 2009). Typically, the action balance is computed as this quantity is conserved in the presence of currents (Bretherton and Garett, 1968). The action balance[4] is written in the form (e.g. Hasselmann et al., 1973; Phillips, 1977; Komen et al., 1994):

$$\left\{ \frac{\partial}{\partial t} + \nabla_{\mathbf{x}} \cdot c_{g,\mathbf{x}} + \frac{\partial c_\sigma}{\partial \sigma} + \frac{\partial c_\theta}{\partial \theta} \right\} N(\sigma,\theta;\mathbf{x},t) = S_{total}(\sigma,\theta;\mathbf{x},t) \tag{2.14}$$

[4] The action or energy balance equation is also referred to as the Radiative Transport Equation (RTE).

where $N = E/\sigma$ is the action density, $\nabla_{\mathbf{x}} = [\partial_x, \partial_y]$, c_g are the propagation velocities and S_{total} represents the source terms. The LHS of Eq. (2.14) represent the conservative wave kinematics. The first term represents the time dependent term which may be ignored if the wave conditions are stationary. The next term represent the wave propagation in geographical space and the last two terms represent the propagation of wave energy in σ-space (the Doppler effect) and θ-space (refraction).

Whereas the LHS has remained largely unchanged since the introduction of third-generation stochastic wave models (e.g. WAMDI Group, 1988; Komen et al., 1994)[5], the RHS has been the subject of much research (see WISE Group, 2007). The RHS represents the wave dynamics and may expressed as the linear sum of various source terms:

$$S_{total} = S_{wind} + S_{dissipation} + S_{nl} \tag{2.15}$$

The first term on the RHS of Eq. (2.15) represents the generation of waves by wind (e.g. Miles, 1957; Phillips, 1957; Cavaleri and Rizzoli, 1981; Snyder et al., 1981; Komen et al., 1994; WISE Group, 2007) and, in deep water, the remaining two terms represent the the dissipation of waves due to white capping (e.g. Hasselmann, 1974; Komen et al., 1994; WISE Group, 2007) and quadruplet wave-wave interactions (e.g. Phillips, 1960; Hasselmann, 1962), respectively.

Figure 2.1 illustrates the balance between these three source terms: S_{wind} provides the source of energy which causes waves to grow which is balanced by dissipation through white capping, S_{wcap}. The effect of the cubic nonlinearities (quadruplet interactions, S_{nl4}) is to (conservatively) redistribute the wave energy near the peak to lower and higher frequencies. In general, the spectral evolution provided by Eqs. (2.14) and (2.15) provides reasonable predictions in deep water as the constraints of being (weakly) stationary and homogeneous on the wave field are typically valid as variations on the wave field typically act over relatively long temporal and spatial scales and therefore the conditions remain predominantly Gaussian.

2.3. SHALLOW WATER SOURCE TERMS

In shallow water, the prediction of spectral evolution becomes significantly more complex as additional processes must be accounted for and typically variations in the bathymetry and currents become important. Additional dissipative effects such as the effect of the bed and vegetation and depth-induced wave breaking become important and cubic nonlinearities shift to quadratic nonlinearities (e.g. Elgar and Guza, 1985; Herbers and Burton, 1997; Janssen, 2006; Holthuijsen, 2007). Such processes can often occur over relatively short length (time) scales, i.e., only a few wavelengths and therefore the original assumptions of spatial and temporal invariance become questionable. Nevertheless, various studies (e.g. Ris et al., 1999; van der Westhuysen, 2007) have shown the merit of the stochastic approach in the coastal region with the supplementation of additional source terms (see Fig. 2.2).

[5] A notable exception is found in Smit and Janssen (2013) who derive a generalized form of (2.14) to include coherent wave effects.

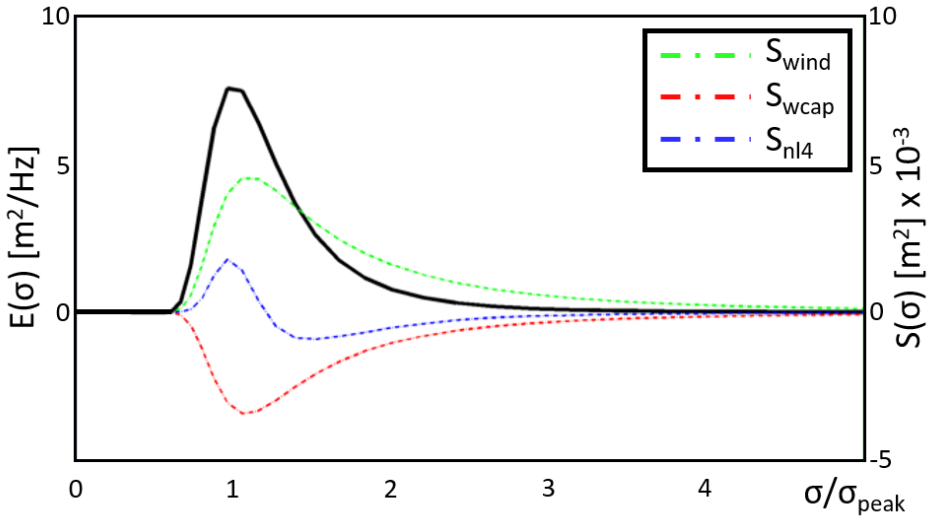

Figure 2.1: Deep water source terms $S(\sigma)$ computed using SWAN for a JONSWAP spectrum (H_{m0} = 3.5 m; T_{peak} = 7 s) at water depth d = 10 m (following Holthuijsen, 2007). S_{wind} is computed with the source term of Snyder et al. (1981) as re-scaled by Komen et al. (1984); S_{wcap} is computed using the pulse model of Hasselmann (1974) as re-scaled by WAMDI Group (1988); and S_{nl4} is computed using the near-exact WRT method (van Vledder, 2006) with WAM depth scaling.

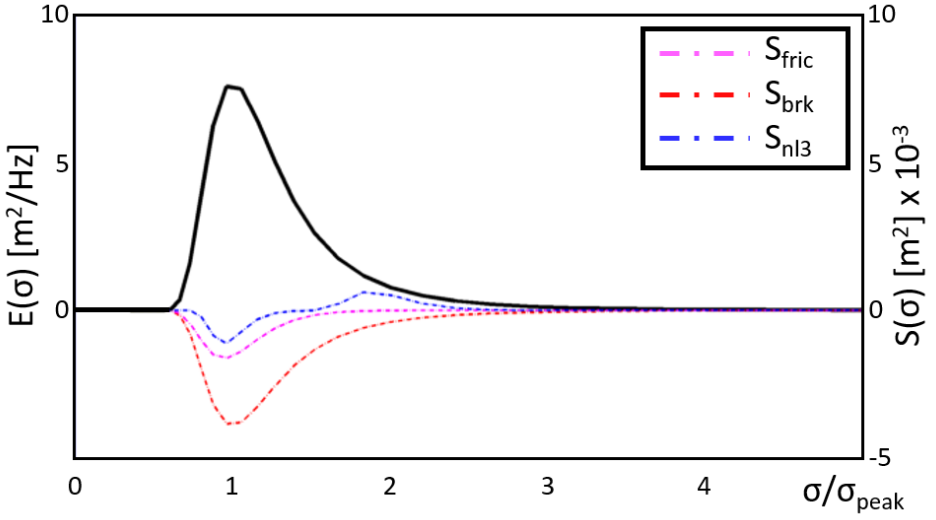

Figure 2.2: Shallow water source terms $S(\sigma)$ computed using SWAN for a JONSWAP spectrum (H_{m0} = 3.5 m; T_{peak} = 7 s) at water depth d = 10 m (following Holthuijsen, 2007). S_{fric} is computed with the JONSWAP source term of Hasselmann et al. (1973); S_{brk} is computed using the bore dissipation model of Battjes and Janssen (1978); and S_{nl3} is computed using the LTA model of Eldeberky and Battjes (1996).

Typically Eq. (2.15) is augmented with $S_{dissipation}$ to include dissipation of wave energy due to bottom friction S_{fric} (e.g. Collins, 1972; Hasselmann et al., 1973; Madsen et al., 1988; Zijlema et al., 2012), depth-induced wave breaking S_{brk} (e.g. Battjes and Janssen, 1978; Thornton and Guza, 1983; Baldock et al., 1998), and other effects such as vegetation (e.g. Suzuki et al., 2012). The nonlinear terms, S_{nl} is also often extended to include (1D) cross-spectral transfer of wave energy due to triad wave-wave interactions S_{nl3} (e.g. Eldeberky and Battjes, 1996; Becq-Girard et al., 1999).

The complexity of the interplay between depth-induced wave breaking and nonlinear triad interactions is schematized in the wave profile evolution shown in Figure 2.3A. Initially, at the wavemaker a monochromatic wave train is generated which has a sinusoidal wave profile. This is represented as a unimodal wave spectrum as shown in Panel B at Location 1 with a near-symmetrical measured surface elevation. As the waves progress into shallow water (between Locations 2 to 6), the waves begin to shoal and due to nonlinear interactions the wave profile becomes distorted.

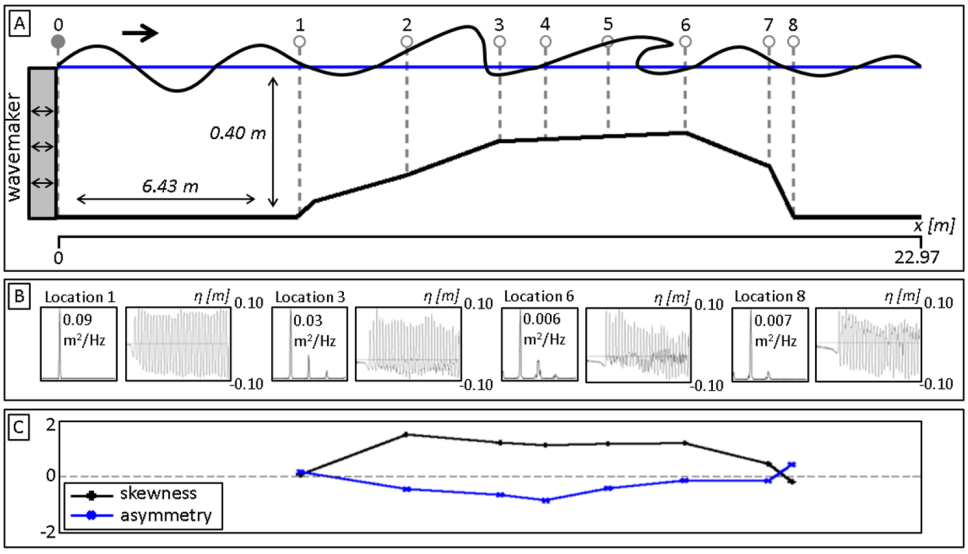

Figure 2.3: Record 31 (monochromatic waves with $H_{m0} \approx 0.2$ m and $T_p = 1.7778$ s at the wavemaker) of the Sochi (2004)[6] laboratory flume experiment. Panel A presents the configuration of the flume and the schematized evolution of the wave profile. Panel B shows the computed spectra with the peak variance density level and observed time series at Locations 1, 3, 6 and 8. Panel C shows the computed skewness and asymmetry computed from the measured time series.

Initially, the wave profile is distorted along the horizontal axis with sharper crests and flatter troughs (Stokes-type waves) and this effect is measured by the wave skewness (see Panel C; solid black line). This corresponds to the generation of bound harmonics which are locked in phase with the primary wave. Conceptually, this may be seen as the superposition of the harmonics and is demonstrated in the distinct spectral signatures seen at

[6]Data provided by A. Romanov, K. Zvezdun, S. Kuznetsov, V. Shakhin and Y. Saprykina. This research was supported under the Russian Foundation for Basic Reasearch project 03-05-64561.

integer multiples of the peak frequency in Panel B. Note that in this case, the wave components are no longer independent and the wave phases are *not* uniformly distributed. From a spectral perspective this is represented by the transfer of wave energy to different wave frequencies. At Location 3, energy transfers to the higher frequencies, i.e., generation of superharmonics are clearly shown and by Location 6, energy transfers to the lower harmonics, i.e., subharmonics are also seen.

At this point, the waves may begin to break as the wave height increases and the waves becomes depth-limited. If dissipation does not occur, the bound harmonics may continue to grow and the wave profile further evolves with distortion occurring along the vertical axis with sharp forward slopes and gentler rear slopes, i.e., a saw-tooth profile. This is referred to as wave asymmetry (see Panel C; solid blue line). At this point, the wave profile becomes unstable as the crest propagates faster than the trough and the waves breaks.

In the example given in Figure 2.3, wave breaking starts between Locations 1 and 3 and continues breaking as a bore up to Location 5. As shown in Panel C, this corresponds to positively skewed and negatively asymmetric wave profiles. By Location 7, due to the effects of both nonlinear interactions and wave breaking, the wave profile returns to a near-sinusoidal profile with less wave skewness and symmetry. Between Locations 6 and 8, the water depth increases and the effect of the triad interactions is to transfer wave energy back to the primary peak in a process known as recurrence. This is demonstrated by the reduction of the superharmonics and increase of the energy level at the peak at Location 8 compared with Location 6.

Therefore, there is a balance between the effect of the triad interactions which transfer wave energy away from the spectral peak and distort the wave profile, and depth-induced wave breaking which dissipate wave energy across the wave spectrum. The effect of the energy transfers are captured in spectral wave models by the S_{nl3} term, whereas the dissipation due to depth-limited wave breaking is captured by the S_{brk} term. As the focus of the present work is on the both of these processes, for completeness an overview of the most commonly implemented parameterizations from the literature is outlined here.

2.3.1. DEPTH-INDUCED WAVE BREAKING

The classical method for representing shallow water wave attenuation due to depth-induced wave breaking involves the coupling of an idealized dissipation model for a single wave with a probability density function to represent the wave conditions (e.g. Battjes and Janssen, 1978; Thornton and Guza, 1983; Baldock et al., 1998). This method was first introduced by Battjes and Janssen (1978) who used an analogy of a 1D bore to represent the dissipation of a single breaking wave and a truncated Rayleigh distribution to represent the *unbroken* wave conditions.

In this parameterization, the dissipation of a single breaking wave is given as (per unit time, per unit area; Lamb, 1932; Stoker, 1957 and Le Méhauté, 1962):

$$\varepsilon_0 = -\frac{1}{4d}\alpha \bar{f} \rho g H_{brk}^3 \tag{2.16}$$

where α is a tunable coefficient of $O(1)$, d is the local water depth, $\bar{f}$ is a characteristic

wave frequency measure (typically f_{m01}; see Section 2.4.2), g is the gravitational acceleration, ρ is the density of water and H_{brk} is a characteristic height for the breaking waves. The bulk dissipation for an ensemble of breaking waves is then obtained by introducing the probability density function, $p(H_{brk})$:

$$\langle \varepsilon_{brk} \rangle = -\frac{1}{4d} \alpha_{brk} \bar{f} \rho g \int_0^\infty H_{brk}^3 p(H_{brk}) \, dH_{brk} \tag{2.17}$$

Battjes and Janssen (1978) assume a Rayleigh distribution for the *unbroken* waves and truncate this distribution at a characteristic maximum wave height H_{max} so that the *broken* waves are represented by a delta function at the limit $H = H_{max}$:

$$p(H) = \begin{cases} 2CHexp\left[-CH^2\right] & 0 \le H < H_{max} \\ 1 & H \ge H_{max} \end{cases} \tag{2.18}$$

where C is an arbitrary scaling parameter. This implies that all breaking or broken wave heights have a wave height H_{max} and this value is larger than that of the broken waves. Although this may be a crude approximation, the exact form for $p(H_{brk})$ is not required for estimating integral quantities and these simplifications have been shown to yield reasonable and robust results (e.g. Battjes and Janssen, 2008) for the prediction of integral quantities. Integrating $p(H)$ yields the cumulative distribution function:

$$F(H) = Pr\left\{\underline{H} \le H\right\} = \begin{cases} 1 - exp\left[-CH^2\right] & 0 \le H < H_{max} \\ 1 & H \ge H_{max} \end{cases} \tag{2.19}$$

where the underscore denotes a random variable. From the above definitions, the probability of a wave having broken or breaking, Q_b is:

$$Q_b = Pr\left\{\underline{H} = H_{max}\right\} = exp\left[-CH_{max}^2\right] \tag{2.20}$$

where the rms wave height is:

$$H_{rms}^2 = \int_0^\infty H^2 dF(H) = C^{-1}(1 - Q_b) \tag{2.21}$$

By applying an 'order of magnitude' relationship $H_{brk}/d \approx 1$ and noting that we only consider a single breaking wave height with probability Q_b, Eq. (2.17) reduces to:

$$\langle \varepsilon_{BJ} \rangle = -\frac{1}{4} \alpha_{BJ} \bar{f} \rho g Q_b H_{max}^2 \tag{2.22}$$

and by eliminating C in Eq. (2.20) and (2.21):

$$\frac{(1 - Q_b)}{lnQ_b} = -\left(\frac{H_{rms}}{H_{max}}\right)^2 \tag{2.23}$$

The resulting expressions have two free parameters: α_{BJ} and H_{max}. Battjes and Janssen (1978) showed that by setting these parameters to $\alpha_{BJ} = 1$ and $H_{max} = \gamma_{BJ} d$ with $\gamma_{BJ} = 0.80$ they were able to reproduce their observations.

Invariably, alternatives to the Battjes and Janssen (1978) approach in stochastic wave modelling follow two main routes; either through modification of the probability distribution or in the scaling of the resulting bulk dissipation model through γ. In the former case, the two most prominent alternatives are based on the models of Thornton and Guza (1983) and Baldock et al. (1998)[7]. From observed wave data, Thornton and Guza (1983) propose a weighting function for the Rayleigh probability distribution to place greater emphasis on the waves with larger wave height. The resulting bulk dissipation is expressed as:

$$\langle \varepsilon_{TG} \rangle = -\frac{3\sqrt{\pi}}{16d} \alpha_{TG} \bar{f} \rho g H_{rms}^3 H_{r,TG}^2 \left[1 - \left(1 + H_{r,TG}^2 \right)^{-5/2} \right] \tag{2.24}$$

where $H_{r,TG} = H_{rms} / \left(\gamma_{TG} d \right)$ and $\gamma_{TG} = 0.42$.

Baldock et al. (1998) present an explicit form for Q_b and demonstrate improved modelling performance over steep beach profiles. Their expressions, neglecting their original 'order of magnitude' assumption (which is not applicable for $H_b = \gamma_B d$ (Janssen, 2006)) are:

$$Q_b = exp\left[-\left(H_b / H_{rms} \right)^2 \right] \tag{2.25}$$

and:

$$\langle \varepsilon_B \rangle = -\frac{3\sqrt{\pi}}{16d} \alpha_B \bar{f} \rho g H_{rms}^3 \left[1 + \frac{4}{3\sqrt{\pi}} \left(H_{r,B}^{-3} + \frac{3}{2} H_{r,B}^{-1} \right) exp\left[-H_{r,B}^{-2} \right] - erf\left(H_{r,B}^{-1} \right) \right] \tag{2.26}$$

where $H_{r,B} = H_{rms} / H_b$ and H_b is a characteristic breaking wave height.

In many stochastic wave models, γ is taken to be a constant which is somewhat justified by the work of Miche (1944) who provides limits for the maximum wave height for *regular* waves over constant water depths at the shallow and deep water wave limits. At the shallow limit, the maximum wave height is show to be proportional to the local water depth with $H_{max} = 0.88d$. Although the justification of such a scaling is still questionable as operational wave models deal with *irregular* waves propagating over variable topography, numerous studies (e.g. Ris et al., 1999) have demonstrated the applicability of a constant in a variety of wave environments, albeit with different values, e.g., $H_{max} = 0.73d$. Typically, the deep water limit $H_{max} = 0.88k^{-1}$, which represents a limiting wave steepness, is treated separately in the white capping source term. A notable exception is the dissipation model of Filipot and Ardhuin (2012) who retain a Miche-type breaking criterion and present a model applicable to both deep and shallow water.

An alternative to the coupled approach is the approach proposed by Dally et al. (1985) and further developed by Rattanapitikon and Shibayama (1998a,b) and Rattanapitikon et al. (2003a) for irregular waves. This model is essentially a relaxation model where dissipation is proportional to the local energy flux and the defined stable energy flux. In the form proposed by Rattanapitikon et al. (2003b), the bulk dissipation is:

$$\langle \varepsilon_R \rangle = -\frac{1}{8d} c_g \rho g \left[H_{rms}^2 - H_{rms,stable}^2 \right] \tag{2.27}$$

[7] Later corrected by Janssen (2006); Janssen and Battjes (2007); Alsina and Baldock (2007).

where the stable wave height can be defined in a form suitable for operational wave models $H^2_{rms,stable} = \gamma_R d$ where $\gamma_R = 0.266$ (Rattanapitikon, 2007).

In order to express the bulk dissipation in the form of a source term, it is further assumed that the shape of the wave spectrum is unaffected by wave breaking (see Beji and Battjes, 1993) and therefore the bulk dissipation is distributed proportionally to the energy density spectrum:

$$S_{brk}(\sigma,\theta) = \langle \varepsilon_{brk} \rangle \frac{E(\sigma,\theta)}{\rho g E} \tag{2.28}$$

Although a proportional weighting as given in Eq. (2.28) is used in the present study, recent studies (e.g Mase and Kirby, 1992; Chen et al., 1997; Kaihatu and Kirby, 1995; Smit et al., 2014) suggest that the depth-induced wave breaking dissipation is in fact distributed by the frequency-squared, i.e., weighted more heavily to the higher frequencies.

2.3.2. NONLINEAR TRIAD WAVE-WAVE INTERACTIONS

Two of the most commonly applied triad source terms are based on extended Boussinesq-type equations of Madsen and Sørensen (1993). Following their work, the surface elevation $\eta(x,t)$ can be represented by:

$$\eta(x,t) = \sum_{p=-\infty}^{\infty} \widetilde{A}_p(x)\, exp\left[i\left(\sigma_p t - \psi_p(x)\right)\right] \tag{2.29}$$

where ψ_p is the linear contribution to the phase and the evolution equation for the complex amplitude $\widetilde{A}_p$ for a unidirectional wave field over a mildly sloping bottom given by:

$$\frac{d\widetilde{A}_p}{dx} = -W_p^{linear}\widetilde{A}_p - i\sum_{m=-\infty}^{\infty} W_{m,p-m}\widetilde{A}_m\widetilde{A}_{p-m} exp\left[i\Delta\psi_{m,p-m}\right] \tag{2.30}$$

where $\Delta\psi_{m,p-m} = \psi_p - \psi_m - \psi_{p-m}$ is the phase mismatch and W represents the real nonlinear shoaling coefficient given by Madsen and Sørensen (1993) as:

$$W_{m,p-m} = \frac{R_{m,p-m}}{S_p} = \frac{\left(k_m + k_{p-m}\right)^2\left[\frac{1}{2} + c_m c_{p-m}\left(gd\right)^{-1}\right]}{-2\left(k_p d\right)^2\left[2\beta + \left(k_p d\right)^{-2} - \left(\beta + \frac{1}{3}\right)c_p^2\left(gd\right)^{-1}\right]} \tag{2.31}$$

where k is the wave satisfying the dispersion relationship, $c_p = \sigma_p / k_p$ is the phase velocity and $\beta = 1/15$. The first term on the RHS of Eq. (2.30) is the linear shoaling term and the second term represents the nonlinear interactions between a triad of wave components: p, m and $p-m$. Eldeberky (1996) shows that Eq. (2.30) can be written as an evolution equation for A_p by substituting $\widetilde{A}_p = A_p exp[-i\psi_p]$[8]:

$$\frac{dA_p}{dx} = -i\left(k_p A_p + \sum_{m=-\infty}^{\infty} W_{m,p-m}A_m A_{p-m}\right) \tag{2.32}$$

[8] In complex notation $A_p = |A_p| exp\left[-i\phi_p\right]$ where ϕ_p represents the phase due to the linear propagation ψ_p and nonlinear interactions θ_p.

where the linear shoaling term is excluded for convenience. As the contribution to the wave spectrum is proportional to $\left\langle A_p A_p^* \right\rangle$ (Eq. 2.10), the evolution of the wave spectrum may be expressed as:

$$\frac{dE_p^{'}}{dx} = \frac{d}{dx}\left\langle A_p A_p^* \right\rangle \tag{2.33}$$

Applying the product rule to the RHS of Eq. 2.33 and from Eq. 2.32 yields:

$$\frac{dE_p^{'}}{dx} = i \sum_{m=-\infty}^{\infty} W_{m,p-m}\left[\left\langle A_p A_m^* A_{p-m}^* \right\rangle - \left\langle A_p^* A_m A_{p-m} \right\rangle\right] \tag{2.34}$$

The triple product pair of complex amplitudes are in fact complex conjugates of each other and by introducing the next-order bispectrum $B_{m,p-m} = \left\langle A_m A_{p-m} A_p^* \right\rangle$:

$$\frac{dE_p^{'}}{dx} = 2 \sum_{m=-\infty}^{\infty} W_{m,p-m} Im\{B_{m,p-m}\} \tag{2.35}$$

where $Im\{\ldots\}$ represents the imaginary part of the argument. The 1D (frequency) source term for the nonlinear triad interactions may then expressed by factoring in the corresponding group velocity $c_{g,p}$ and splitting the sum interaction ($\sigma_m, \sigma_p - \sigma_m$) and difference interaction ($\sigma_m, \sigma_p + \sigma_m$) contributions, respectively:

$$S_{nl3,p} = 2c_{g,p}\left[\sum_{m=1}^{p-1} W_{m,p-m} Im\{B_{m,p-m}\} - 2\sum_{m=1}^{\infty} W_{m,p} Im\{B_{m,p}\}\right] \tag{2.36}$$

Therefore, at the lowest-order, the evolution of the wave spectrum is dependent on the third-order cumulant; the bispectrum. This presents the fundamental problem of Eq. (2.36) as it depends upon knowledge of $B_{m,p-m}$ which in turn depends upon increasingly higher-order cumulants, i.e., the trispectrum, and so on resulting in an open set of evolution equations. Following Eq. (2.33), the next order evolution equation is:

$$\frac{dB_{m,p-m}}{dx} = \frac{d}{dx}\left\langle A_m A_{p-m} A_p^* \right\rangle \tag{2.37}$$

Expanding Eq. (2.37) and substituting Eq. (2.32) yields:

$$\begin{aligned}\frac{dB_{m,p-m}}{dx} = i\Bigg[\Delta k_{m,p-m} B_{m,p-m} + \sum_{q=-\infty}^{\infty}\Big(&W_{q,p-q} T_{m,p-m,-p} - W_{q,m-q} T_{p-m,-p,m} \\ &- W_{q,p-m-q} T_{m,-p,p-m}\Big)\Bigg]\end{aligned} \tag{2.38}$$

where $\Delta k_{m,p-m} = k_p - k_m - k_{p-m}$ is the wave number mismatch and $T_{m,p-m,-p} = \left\langle A_m A_{p-m} A_q^* A_{p-q}^* \right\rangle$ is the trispectrum. This results in the classical problem of closure similar to that found in turbulence (see e.g Orszag, 1974; Janssen, 2006). As such, the bispectrum is parameterized using some form of closure approximation.

The simplest and most computationally efficient triad approximation model is the Lumped Triad Approximation (LTA) proposed by Eldeberky (1996). To close the set of equations, a quasi-normal approximation (e.g. Herbers and Burton, 1997) is applied which assumes that the fourth-order contributions can be written in terms of the second order contributions:

$$\frac{dB_{m,p-m}}{dx} = i\left(\Delta k_{m,p-m} B_{m,p-m} + 2\widetilde{Q}'_{m,p-m}\right) \tag{2.39}$$

where $\widetilde{Q}'_{m,p-m} = W_{m,p-m} \times \left[E'_m E'_{p-m} - E'_p\left(E'_m + E'_{p-m}\right)\right]$ represents the fourth-order statistics in terms of second-order statistics. Note that for the expression for $\widetilde{Q}$, Eldeberky (1996) assumes that all three weighting coefficients in Eq. (2.38) are equivalent, i.e., $W_{m,p-m} = W_{p,-m} = W_{p,m-p}$. To reduce the computational costs associated with the coupled spectral and bispectral evolution equation, Eq. (2.39) is spatially integrated and only the steady contribution is retained. The imaginary part of the bispectrum is then estimated in terms of its magnitude and phase, $Im\{B_{m,p-m}\} = |B_{m,p-m}|\, sin(\varphi_{m,p-m})$ (Kim and Powers, 1979) where $|B_{m,p-m}| = 2\widetilde{Q}'_{m,p-m}/\Delta k_{m,p-m}$. Therefore from Eq. (2.36):

$$S_{nl3,p} = 4c_{g,p}\, sin|\varphi_{Ur}| \left[\sum_{m=1}^{p-1} \frac{W_{m,p-m}\widetilde{Q}'_{m,p-m}}{\Delta k_{m,p-m}} - 2\sum_{m=1}^{\infty} \frac{W_{m,p}\widetilde{Q}'_{m,p}}{\Delta k_{m,p}}\right] \tag{2.40}$$

where $\varphi_{Ur} = \pi\left[tanh(0.2/Ur) - 1\right]/2$ (Doering and Bowen, 1995; Eldeberky, 1996) and Ur is the spectral Ursell number based on the local moments of the wave spectra (see Section 2.4):

$$Ur = \frac{gH_{m0}}{8\sqrt{2}}\left(\frac{T_{m01}}{\pi d}\right)^2 \tag{2.41}$$

Note that as φ_{Ur} only depends on local parameters, it is identical for both the sum and difference contributions. The influence of φ in Eq. (2.40) is to control the magnitude of the energy transfers between interacting wave components and can be interpreted as a transition from skewed second-order Stokes waves in deep water (where $Im\{B_{m,p-m}\} = 0$) to an asymmetric saw tooth-like profile as $\varphi \to -\pi/2$ and energy is transferred to the higher frequencies in the surf zone.

In terms of a continuous spectrum, from Eq. (2.11), Eq. (2.40) can be re-written as:

$$S_{nl3}(\sigma_p) = 2\pi c_{g,p}\, sin|\varphi_{Ur}| \left[\int_0^{\sigma_p} \frac{W_{m,p-m}\widetilde{Q}_{m,p-m}}{\Delta k_{m,p-m}} d\sigma_m - 2\int_0^{\infty} \frac{W_{m,p}\widetilde{Q}_{m,p}}{\Delta k_{m,p}} d\sigma_m\right] \tag{2.42}$$

where $\widetilde{Q}$ is $\widetilde{Q}'$ in terms of $E(\sigma)$. To significantly reduce the computational costs associated with Eq. (2.42), the LTA model approximates the integrals with the product of a representative value of the integrands, taken to be that of the self-self interactions, and an effective frequency interaction bandwidth $\delta\sigma$. By applying this approximation and arguing that $\delta\sigma$ and Δk scale with σ_p and k_p, the LTA source term is:

$$S_{LTA}(\sigma_p) = 2\pi\alpha_{LTA} c_{g,p} c_p\, sin|\varphi_{Ur}| \left[W_{p/2,p/2}\widetilde{Q}_{p/2,p/2} - 2W_{p,p}\widetilde{Q}_{p,p}\right] \tag{2.43}$$

where α_{LTA} is a calibration parameter and the subscripts $p/2$ and $2p$ relate to $\sigma_p/2$ and $2\sigma_p$, respectively.

As the effect of the sum contribution is to transfer half of the difference contribution of the frequency component $\sigma_p/2$ towards the frequency component σ_p, the S_{LTA} may be expressed solely in term of the sum contributions which further reduces the computational effort:

$$S_{LTA}(\sigma_p) = S^{+}_{LTA}(\sigma_p) - 2S^{+}_{LTA}(2\sigma_p) \tag{2.44}$$

Although the LTA model is computationally efficient, it has a number of shortcomings. The consideration of only the self-self interactions renders the LTA model capable of only generating superharmonics. In other words, given an initial unimodal spectrum with a peak at σ_{peak}, harmonics can only be generated at $\sigma = 2^n\sigma_{peak}$ for $n \in \mathbb{Z}$. This is in contrast to observations and numerical simulations (e.g. Smith, 2004; Kaihatu et al., 2007, 2008) who demonstrate that deep in the surf zone the tail of the spectrum becomes featureless. This has lead to ameliorative measures being taken by limiting the upper frequency to which interactions are computed (Ris et al., 1999). Furthermore, only energy transfers towards higher frequencies are permitted which precludes the process of recurrence whereby energy maybe transferred back down towards lower frequencies e.g. at the lee side of a shoal. Becq-Girard et al. (1999) also demonstrate that the LTA model is prone to artificial shoaling. This arises from the (linear) energy conservative form of the LTA (Eq. 2.44) where it is assumed that all waves are free and propagate with the linear group velocity c_g^l. In reality, the nonlinear group velocity c_g^{nl} associated with the bound higher harmonic should be used which is larger than c_g^l which results in an overestimation of the total wave energy when energy is transferred to higher harmonics. Finally, the application of the quasi-normal approximation is questionable as it may cause initial tendencies to unrealistically persist. Janssen (2006) demonstrates that in regions of strong nonlinearity, this leads to the over-prediction of the nonlinear coupling.

An alternative triad model is the Stochastic Parametric model based on Boussinesq equations (SPB) model derived by Becq-Girard et al. (1999). As with the LTA, the SPB is based on the Boussinesq-type equations of Madsen and Sørensen (1993) and it therefore has similar interaction coefficients W (Eq. 2.31). However, instead of fully neglecting the fourth-order contributions, they are assumed to be proportional to the bispectrum itself (e.g. Holloway and Hendershott, 1977; Holloway, 1980) by introducing an empirical parameter μ. In effect, this represents a length scale over which the bispectrum, in the absence of forcing, returns to zero. In contrast to Eq. (2.38), Eq. (2.37) can be written as:

$$\frac{dB_{m,p-m}}{dx} = i\left[\left(\Delta k_{m,p-m} + i\mu\right)B_{m,p-m} + \sum_{q=-\infty}^{\infty}\Big(W_{q,p-q}T_{m,p-m,-p} - W_{q,m-q}T_{p-m,-p,m} - W_{q,p-m-q}T_{m,-p,p-m}\Big)\right] \tag{2.45}$$

where $\mu = 0.95k_{peak,0} - 0.75$ and $k_{peak,0}$ is the offshore peak wave number from the peak frequency $f_{peak,0}$. By spatially integrating Eq. (2.45), again retaining only the steady contribution, the imaginary part of the bispectrum is given as:

$$Im\{B_{m,p-m}\} = 2Q'_{m,p-m}\left[E_p\left(W_{p,-m}E_m + W_{p,m-p}E_{p-m}\right) - W_{m,p-m}E_mE_{p-m}\right] \times \frac{\mu}{\left(\Delta k_{m,p-m}\right)^2+\mu^2} \tag{2.46}$$

where $Q'_{m,p-m} = \left[W_{m,p-m}E'_mE'_{p-m} - E'_p\left(W_{p,-m}E'_m + W_{p,m-p}E'_{p-m}\right)\right]$. Note that in comparison to Eq. (2.39), the weighting coefficients are not assumed to be equivalent. Substitution of Eq. (2.46) into Eq. (2.36) and re-writing in terms of a continuous spectrum gives the SPB source term:

$$S_{SPB}\left(\sigma_p\right) = 8\pi\alpha_{SPB}c_{g,p}\mu\left[\int_0^{\sigma_p}\frac{W_{m,p-m}Q_{m,p-m}}{\left(\Delta k_{m,p-m}\right)^2+\mu^2}d\sigma_m - 2\int_0^{\infty}\frac{W_{m,p}Q_{m,p}}{\left(\Delta k_{m,p}\right)^2+\mu^2}d\sigma_m\right] \tag{2.47}$$

where $\alpha_{SPB} = 1$ and Q is Q' in terms of $E(\sigma)$. Although significantly more computationally demanding than the LTA model, the SPB model is able to compute all the interactions between the frequencies and is therefore more suitable for predicting the high-frequency tail of the spectrum as well as the generation of subharmonics. However, it still shares common issues with the LTA regarding the reproduction of recurrence.

In most stochastic wave models, a collinear approximation is applied whereby it is assumed that the dominant contributions of the triad interactions occurs for collinear interactions. In this collinear approximation the triad source term for each directional bin is taken independently of other directional bins and the products of the 1D (directionally integrated) variance densities in Eqs. (2.43) and (2.47) are simply replaced with their 2D counterparts, i.e.,:

$$S_{LTA}\left(\sigma_p,\theta\right) = 2\pi\alpha_{LTA}c_{g,p}c_p sin\left(\varphi_{Ur}\right)\left[W^2_{p/2,p/2}\widetilde{Q}^{\theta}_{p/2,p/2} - 2W^2_{m,p}\widetilde{Q}^{\theta}_{p,p}\right] \tag{2.48}$$

and

$$S_{SPB}\left(\sigma_p,\theta\right) = 8\pi\alpha_{SPB}c_{g,p}\mu\left[\int_0^{\sigma_p}\frac{W_{m,p-m}Q^{\theta}_{m,p-m}}{\left(\Delta k_{m,p-m}\right)^2+\mu^2}d\sigma_m - 2\int_0^{\infty}\frac{W_{m,p}Q^{\theta}_{m,p}}{\left(\Delta k_{m,p}\right)^2+\mu^2}d\sigma_m\right] \tag{2.49}$$

where $E\left(\sigma_p\right) \rightarrow E\left(\sigma_p,\theta\right)$ and so forth for $Q^{\theta}_{m,p-m}$ and $\widetilde{Q}^{\theta}_{m,p-m}$.

A number of recent developments for the representation of triad interactions in stochastic wave models have been made in the past decade. They are however not routinely used in current operational wave models and are not pursued further in the present study. They are briefly outlined below for completeness.

Van der Westhuysen (2007) considered the combined model of SAM1D (a reduced version of the deterministic model of Janssen (2006)) and SWAN. As the SAM1D model solves for the coupled two-equation model, it provides a more complete representation of the triad interactions and can model both the resonant and near-resonant triad interactions exactly. This combined model was shown to provide improved modelling skill

in the prediction of the spectral shape in the absence of deep water source terms. However, its associated computational cost prohibits the combined model from operational applications.

The Distributed Collinear Triad Approximation (DCTA; Booij et al., 2009) was developed to heuristically capture the $k^{-4/3}$ equilibrium high-frequency tail expected at shallow water depths ($kd < 1$; e.g. Zakharov, 1999; Smith, 2004). Based on the general representation of the interaction between three wave components (e.g. Holloway, 1980, his Eq. 7), the resonance conditions can be relaxed to account for only the collinear interactions. The resulting equation can then be transformed from the wave number domain to the frequency domain. This results in two unknown coefficients which need to be defined. This is achieved by scaling the coefficients to be consistent with the LTA model and heuristically forcing the high-frequency tail to converge to the equilibrium $k^{-4/3}$ high-frequency tail. In its energy conservative form, the 1D source term may be expressed as:

$$\begin{aligned} S_{DCTA,E}(\sigma_p) \quad = \quad & \alpha_{DCTA,E} sin(\varphi_{Ur})\, d^{-2} \sigma_p^{-1} \int \frac{tanh(2\bar{k}d)}{2\bar{k}d} \bar{k}^{1-\kappa} E_m \\ & \times \left[\sigma_{p-m} c_{g,p-m} k_{p-m}^{\kappa} E_{p-m} - \sigma_p c_{g,p} k_p^{\kappa} E_p \right] d\sigma_m \end{aligned} \tag{2.50}$$

where $\alpha_{DCTA,E}$ is a calibration coefficient, $\bar{k} = (k_p + k_m + k_{p-m})/3$ is a characteristic wave number and $\kappa = 4/3$ is a shape coefficient to force the high-frequency tail.

Toledo and Agnon (2012) presents a modelling approach similar to the method employed by Eldeberky (1996) and Becq-Girard et al. (1999) but instead used the nonlinear shoaling coefficients of Agnon and Sheremet (2000) localized using the method of Stiassnie and Drimer (2006). This introduces nonlinear shoaling coefficients which are dependent on the spatial derivatives of the bathymetry. The resulting coefficients may then be written in the form:

$$W_{m,p-m} = \frac{1}{\Delta k_{m,p-m}} \times \frac{d}{dx} \left(\frac{\widetilde{W}_{m,p-m}}{\Delta_{m,p-m}} \right) \tag{2.51}$$

where $\widetilde{W}_{m,p-m}$ is given by Agnon and Sheremet (1997) and Eldeberky and Madsen (1999). Although this model was shown to compare well with the energy transfers as predicted by a deterministic nonlinear mild-slope equation model, in shallow water ($kd < 0.8$), the spectral energy transfers of energy away from the peak frequency appear to be overestimated. The reduced applicability of this model to shallow water depths was confirmed by Y. Toledo (pers. comm., 2013).

2.4. WAVE STATISTICS

If the conditions governing the surface elevations assumed throughout this chapter are realized, i.e., are (weakly) stationary and homogeneous; composed of the sum of a large number of independent waveforms; and ergodic, then from the application of the central limit theorem, waves in sufficiently deep water and/or sufficiently mild can be rep-

resented as a Gaussian random process (e.g. Ochi, 2005). It is then possible to fully describe the surface elevation, in an averaged statistical sense, from the wave spectrum. In the following, two of the most important parameters for engineering applications are briefly described: the significant wave height H_{m0} and the mean wave period T_{m01} or T_{m02}. A comprehensive discussion of these parameters and other parameters derived from the wave spectrum can be found in Dabbi et al. (2015).

2.4.1. SIGNIFICANT WAVE HEIGHT

If the wave field can be considered to be a narrow-band process, i.e., it is represented by a wave spectrum which is only non-zero for a small number of sequential frequencies, then it is possible to show that the wave height, assumed as $H \approx 2\eta$, follows a Rayleigh distribution. From this, various statistics related to the wave height can be computed. A commonly used wave parameter is the significant wave height which is defined as the mean wave height of the highest 1/3 waves in a given record. In practice however, rather than determining the significant wave height from a time series in this manner, for a narrow-band wave field, the significant wave height can be approximated from the wave spectra as:

$$H_{m0} = \sqrt{4m_0} \tag{2.52}$$

where m_0 is the zeroth-order moment of the wave spectrum, generally defined for the n-th order spectral moment as:

$$m_n = \iint \sigma^n E(\sigma,\theta)\, d\sigma d\theta \tag{2.53}$$

In reality, the constraint to a narrow-band process is too severe and for real observed time series, the sea surface elevation is typically more broad-banded. This can be interpreted as the presence of non-positive crests and non-negative troughs (see e.g. Locations 6 and 8 in Figure 2.3B) which arise from the superposition of frequency components with sufficient differences in frequency. As a result, significant wave heights as computed with Eq. (2.52) may overestimate the significant wave height as obtained directly from the time series by up to approximately 10% (see e.g. Ochi, 2005; Holthuijsen, 2007). Furthermore, nonlinear processes such as nonlinear interactions and wave breaking may act to increase this discrepancy (see Section 2.4.3).

2.4.2. MEAN WAVE PERIOD

If the surface elevation follows a Gaussian distribution, then the first few moments of the wave spectrum can be used to compute the mean wave frequency or period. The easiest to interpret wave period is that computed from the second-order moment which corresponds to the average of the zero crossing period (see e.g. Massel, 1996; Holthuijsen, 2007):

$$T_{m02} = f_{m02}^{-1} = 2\pi\sqrt{\frac{m_0}{m_2}} \tag{2.54}$$

In practice, the mean wave period as defined in Eq. (2.54) is sensitive to small errors which may arise from the analysis or measurement technique (Holthuijsen, 2007).

Furthermore, as shall be demonstrated in this study, operational wave models typically reproduce the high-frequency tail of the spectrum poorly which also results in a poor prediction of T_{m02}. Therefore, a more reliable measure of the characteristic wave period is often used:

$$T_{m01} = f_{m01}^{-1} = 2\pi \frac{m_0}{m_1} \tag{2.55}$$

The T_{m01} wave period is weighted towards the lower frequencies which are typically more accurately measured and better resolved by wave models than the higher frequencies.

2.4.3. RELEVANCE IN THE SURF ZONE

The previous definitions for the wave spectra, significant wave height and mean wave period are based on the premise that the surface elevation can be assumed to be a Gaussian random process. Whilst this assumption can been shown to be applicable to waves in sufficiently deep water and for sufficiently mild conditions in shallow water (Ochi, 2005), for the nonlinear conditions characteristic of the surf zone, the assumption of Gaussianity becomes invalid.

In this region, the propagation of waves in shallow water becomes weakly dispersive and a triad of wave components can approach resonance. Such quadratic nonlinear interactions can occur over relatively short temporal (or spatial; of order of wavelengths) scales and cause wave components to become phase-coupled. As a result the wave components can no longer be assumed to be independent of each other and therefore surface elevation as defined by their superposition can no longer be assumed to be a Gaussian random process. The effect of depth-induced breaking acts to further complicate the statistical description of the wave field as it may cause the distribution of the wave heights to deviate strongly from the Rayleigh distribution (e.g. Battjes and Groenendijk, 2000).

However, for the purposes of this study, the aforementioned definitions based on the spectral moments are still used. Although strictly speaking these wave statistics do not correspond to their physical interpretations, they still provide useful information characteristic of the wave spectrum. The significant wave height provides a measure of the amount of energy contained within the wave spectrum and the mean wave period provides a measure of the spectral shape. As a result, these parameters can be used as a basics for comparison between the observed and computed wave spectra, particularly for assessing the accuracy in capturing the wave dissipation and the cross-spectral transfer of energy. More complex parameters are available to quantify the agreement between wave spectra (e.g. Dabbi et al., 2015), however due to uncertainties in the equilibrium balance in the surf zone and therefore uncertainties in the computed spectral shape, these parameters are not pursuit further.

2.4.4. ADDITIONAL DEFINITIONS

Following the definition of the significant wave height and mean wave period, the following wave statistics based on the moments of the wave spectrum are used in this study.

- Total variance (= Total energy / ρg): $E = m_0 = \int E(\sigma)\, d\sigma$

- Root-mean-squared wave height: $H_{rms} = \sqrt{8m_0} = 2\sqrt{2m_0}$
- Minus first order moment wave period: $T_{m-10} = f_{m-10}^{-1} = 2\pi \frac{m_{-1}}{m_0}$
- Characteristic wave number: $\tilde{k} = k_{-1/2} = \left(\frac{\int k^{-1/2} E(\sigma) d\sigma}{m_0} \right)^{-2}$
- Local wave steepness: $s = \frac{H_{rms}\tilde{k}}{2\pi}$
- Directional standard deviation: $\sigma_\theta = 2\left[\int_{\theta_0-\pi}^{\theta_0+\pi} sin^2\left(\frac{\theta-\theta_0}{2} \right) D(\theta)\, d\theta \right]^{1/2}$

where θ_0 is the mean wave direction

- Normalized directional distribution: $D(\theta) = \int E(f,\theta)\, df / \int E(f)\, df$
- Spectrum-based Ursell number: $Ur = \frac{g}{8\sqrt{2}(\pi d)^2} H_{m0} T_{m01}^2$

3

SCALING DEPTH-INDUCED WAVE BREAKING IN TWO-DIMENSIONAL SPECTRAL WAVE MODELS

James SALMON, Leo HOLTHUIJSEN, Marcel ZIJLEMA, Gerbrant VAN VLEDDER, Julie PIETRZAK

Wave breaking in shallow water is still poorly understood and needs to be better parameterized in 2D spectral wave models. Significant wave heights over horizontal bathymetries are typically under-predicted in locally generated wave conditions and over-predicted in non-locally generated conditions. A joint scaling dependent on both local bottom slope and normalized wave number is presented and is shown to resolve these issues. Compared to the 12 wave breaking parameterizations considered in this study, this joint scaling demonstrates significant improvements, up to ~ 50% error reduction, over 1D horizontal bathymetries for both locally and non-locally generated waves. In order to account for the inherent differences between unidirectional (1D) and directionally spread (2D) wave conditions, an extension of the wave breaking dissipation models is presented. By including the effects of wave directionality, rms-errors for the significant wave height are reduced for the best performing parameterizations in conditions with strong directional spreading. With this extension, our joint scaling improves modeling skill for significant wave heights over a verification data set of 11 different 1D laboratory bathymetries, 3 shallow lakes and 4 coastal sites. The corresponding averaged normalized rms-error for significant wave height in the 2D cases varied between 8% and 27%. In comparison, using the default setting with a constant scaling, as used in most presently operating 2D spectral wave models, gave equivalent errors between 15% and 38%.

This chapter has been published as SALMON, J.E., HOLTHUIJSEN, L.H., ZIJLEMA, M., VAN VLEDDER, G.P. and PIETRZAK, J.D. (2015). Scaling depth-induced wave-breaking in two-dimensional spectral wave models. *Ocean Modelling*, **87**, pp. 30–47. Significant modifications are indicated in the footnotes.

3.1. INTRODUCTION

Predicting breaking waves in shallow water under complex 2D bathymetry and current conditions is important for understanding the natural development of oceanic islands and coastal regions, the design and management of man-made coastal structures, and risk assessment. Such waves usually dissipate in a relatively narrow 1D surf zone fringing the coast. However, occasionally a surf zone may occur suddenly and with catastrophic effect over a large 2D region when low-lying land, an island or a reef is inundated in a severe storm. Waves have been shown to be vitally important in understanding processes such as sediment re-suspension and transport in estuaries (e.g. Green and Coco, 2014) and the exchanges between the nearshore and inner shelf (Lentz et al., 2008). Furthermore, the increase in the need for interdisciplinary research to understand these complex processes has led to an increased use of coupling phase-averaging wave models to flow and circulation models (e.g. Dietrich et al., 2012).

Phase-averaged spectral wave models are widely used to describe the sea-state with waves described with a 2D energy spectrum, defined at each location and moment in time as the distribution of wave energy over frequency and direction of the constituent wave components (Phillips, 1977; WAMDI Group, 1988; Holthuijsen, 2007). Within the limitations of stationary Gaussian processes, a variety of statistical wave parameters can be estimated from the spectrum such as the significant wave height, defined as the mean wave height of the one-third highest waves (Longuet-Higgins, 1952). The most advanced of these models are the so-called third-generation wave models where the nonlinear quadruplet wave-wave interactions are explicitly represented, permitting a development of the wave spectrum that is unrestrained by a priori assumptions. This is in contrast to first- and second-generation wave models where quadruplet interactions are not represented or are represented by simple parameterizations Komen et al. (1994). This difference allows third-generation wave models to freely develop the spectrum in arbitrary 2D conditions of wind, currents and bathymetry as the spectral shape is not enforced a priori (Holthuijsen, 2007). We conform to this commonly accepted practice despite the fact that such models still typically use parametric expressions for the remaining wave processes e.g. white capping and wind input. Operational models of this type are WAM (WAMDI Group, 1988; Komen et al., 1994; Monbaliu et al., 2000), WAVEWATCH III (Tolman, 1990b, 2009; Tolman and Chalikov, 1996), TOMAWAC (Benoit et al., 1996), SWAN (Booij et al., 1999; Ris et al., 1999; Zijlema, 2010), MIKE21SW (Sørensen et al., 2004), CREST (Ardhuin et al., 2001) and WWM (Roland et al., 2006; Roland, 2009).

The default parameterization for depth-induced wave breaking dissipation, used in most of these models, is one based on an analogy of the dissipation in a 1D bore (Lamb, 1932; Stoker, 1957; Le Méhauté, 1962) introduced by Battjes and Janssen (1978). It combines the dissipation of a single breaking wave with a Rayleigh distribution for random wave heights. From this, three dissipation models were developed: Battjes and Janssen (1978), Thornton and Guza (1983) and Baldock et al. (1998). They are subsequently referred to as the BJ78, TG83 and B98 models. The essential difference is how they represent the statistics of the breaking waves (see Figure 3.1; top panel).

Battjes and Janssen (1978) truncate the distribution of the wave heights at an upper limit given by the maximum possible wave height for a given depth $H = H_{max}$ where they assume a delta function in the distribution (with a surface area equal to the probability

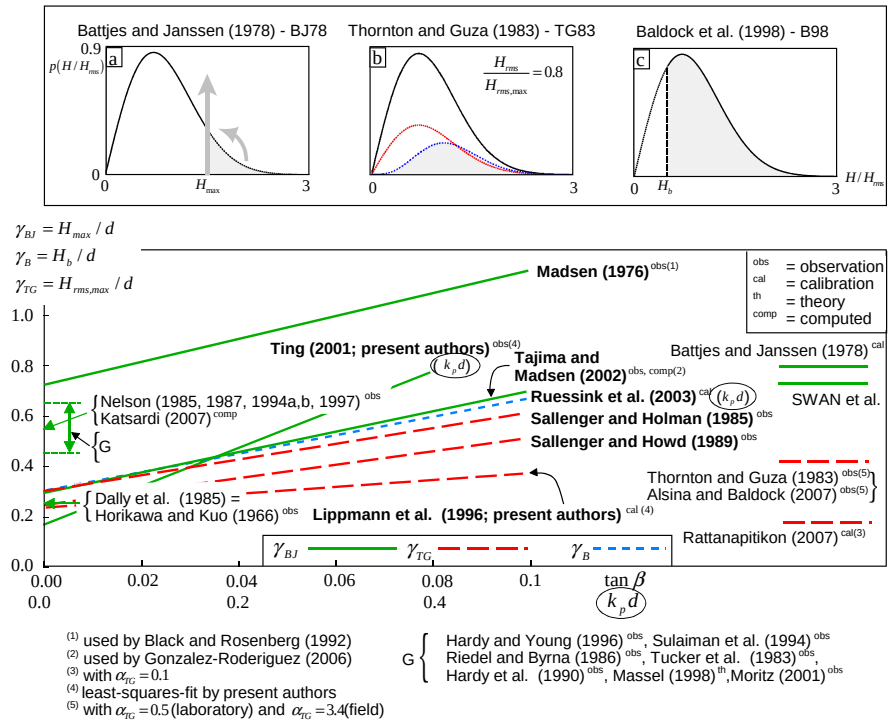

Figure 3.1: The parameterization of depth-induced wave breaking. The top panels illustrate the representation of the breaking waves with the Rayleigh probability density function (in black) for the A: Battjes and Janssen (1978, BJ), B: Thornton and Guza (1983, TG) and C: Baldock et al. (1998, B) dissipation models. The delta function used in BJ78 is represented by a vertical arrow in Panel A. Both expressions of Thornton and Guza (1983, their Eqs. (20) and (21)) are shown in Panel B as the red and blue lines respectively for $H_{rms}/\gamma_{TG}d = 0.8$. The lower panel presents the ratio of critical wave height over depth, which is used to scale the dissipation models, as a function of bottom slope $tan\beta$ or normalized wave number $k_p d$. The seven varying scalings considered in this study are labeled in bold type. All expressions are based on direct observations of individual waves except when indicated otherwise (see inset). All expressions have been derived for irregular waves (or have been used for irregular waves as indicated). The values of γ at $tan\beta = 0$ from reference group G cluster between 0.45 and 0.65. Constant values are indicated at the right-hand side of the diagram with horizontal lines. The commonly used value $\gamma_{BJ} = 0.73$ in third-generation models (indicated with SWAN et al.) has been added as reference.

of exceeding $H = H_{max}$ if the complete Rayleigh distribution would apply). As shown in Figure 3.1A, this delta function represents the assumption that all breaking waves have the same wave height H_{max}. A reduced breaking criterion of Miche (1944) is then used to scale the dissipation with a fixed ratio of the maximum possible wave height H_{max} and the local depth d, denoted as $\gamma_{BJ} = H_{max}/d$. Battjes and Janssen (1978) used $\gamma_{BJ} = 0.8$ in their computations, but most third-generation models use $\gamma_{BJ} = 0.73$, a value averaged from the more extensive data set of Battjes and Stive (1985, their Table 1). For convenience, we subsequently refer to this parameterization for dissipation and γ-scaling as the BJ model.

Thornton and Guza (1983, Figure 3.1B) suggest, on the basis of their field observations, using a Rayleigh distribution for the breaking waves shifted to higher wave heights instead. This is achieved through the use of a weighting function with a scaling coefficient $M_{TG} = \left(H_{rms}/\gamma_{TG}d\right)^n$ where $n = 2$ and $\gamma_{TG} = H_{rms,max}/d$ is the ratio of the maximum possible root-mean-square wave height to depth.

Baldock et al. (1998, Figure 3.1C) also suggest using a Rayleigh distribution but truncated at a lower limit of $H_b = \gamma_b d$ (the minimum breaker height) to represent the breaking wave height distribution. Their expression for dissipation is subsequently corrected by Janssen (2006), Janssen and Battjes (2007) and Alsina and Baldock (2007). An overview of variable parameterizations for γ_{BJ}, γ_{TG} and γ_B is given in Figure 3.1 (bottom panel) and a more extensive overview is presented in Appendix 3.A.

However, several studies have shown that when waves are locally generated over a (near-) horizontal bathymetry, the BJ model overestimates the dissipation (de Waal, 2001; Bottema and Beyer, 2002; Bottema et al., 2002; van der Westhuysen et al., 2007; Bottema and van Vledder, 2009; Groeneweg et al., 2008; van Vledder et al., 2008; Goda, 2009). Van der Westhuysen (2009, 2010) addresses this problem by scaling TG83 using bi-phase characteristics of the waves and shows that in a storm over the Wadden Sea, the under-prediction of the significant wave height is reduced. However, if waves are *not* locally generated but arrive from a distant source, we find that this formulation overestimates the significant wave height e.g. during storm observations in a $10 \times 10\,\mathrm{km}^2$ shallow coastal bay (Haringvliet; see Section 3.5.2).

In this paper, we present a new parameterization for depth-induced wave breaking for 2D spectral wave models which addresses this dichotomy by considering both the effects of local bottom slope and normalized wave number in a joint γ-scaling. Furthermore, we demonstrate the limitations of the assumption of a 1D bore in the parameterization when used for strongly 2D conditions and present an extension for these models to account for the enhanced wave directionality under such conditions.

This paper is structured as follows. First, in Section 3.2, we describe the wave model used in this study and in Section 3.3, we describe our methodology. In Section 3.4, we present our new scaling for γ which depends both on local bottom slope and normalized wave number. We also present an extension to include wave directionality. In Section 3.5, we demonstrate the shortcomings of currently available parameterizations used in all third-generation wave models through a comparison of computed significant wave heights with both laboratory and field observations. An analysis of the error characteristics highlights the need for a joint dependency on both local bottom slope and normalized wave number for γ which we investigate with our new parameterization in Section

3.6. Here, we show large improvements for significant wave heights for locally and non-locally generated waves over 1D horizontal bathymetries. Finally, in Section 3.7, we conclude with a discussion of our results with a particular focus on the 2D field cases and the extension to include wave directionality.

3.2. MODEL DESCRIPTION

The wave model used in this study is the third-generation wave model SWAN version 40.91 (Simulating WAves Nearshore; Booij et al., 1999). However, any of the third-generation wave models outlined in Section 3.1 are equally applicable. It solves the wave action density, defined as the ratio of energy over the relative frequency (Bretherton and Garett, 1968; Phillips, 1977, p. 26) with a spectral balance in Cartesian x, y coordinates:

$$\frac{\partial N(\sigma,\theta;x,y,t)}{\partial t}+\frac{\partial c_{g,x}N(\sigma,\theta;x,y,t)}{\partial x}+\frac{\partial c_{g,y}N(\sigma,\theta;x,y,t)}{\partial y}+\frac{\partial c_{\theta}N(\sigma,\theta;x,y,t)}{\partial \theta}+\frac{\partial c_{\sigma}N(\sigma,\theta;x,y,t)}{\partial \sigma}=\frac{S(\sigma,\theta;x,y,t)}{\sigma} \tag{3.1}$$

where $N(\sigma,\theta)=E(\sigma,\theta)/\sigma$ represents the action density with the energy density $E(\sigma,\theta)$ as a function of the relative radian frequency σ and spectral direction θ. The left-hand side terms of Eq. (3.1) represent, respectively, the rate of change of $N(\sigma,\theta)$ in time and the propagation of $N(\sigma,\theta)$ in geographical space, θ-space and σ-space with propagation velocities $c_{g,x}$, $c_{g,y}$, c_{θ}, c_{σ}. The right-hand side represents the source terms for action density including wave generation by wind, nonlinear wave–wave interactions (triad and quadruplet interactions) and dissipation terms for white capping, bottom friction and depth-induced breaking.

All computations with SWAN were carried out in stationary mode. For laboratory cases, we use only the source terms for triad wave–wave interactions (the Lumped Triad Approximation (LTA) of Eldeberky, 1996), bottom friction (Hasselmann et al., 1973) with bottom friction coefficient 0.038 m^2s^{-3} (Zijlema et al., 2012) and depth-induced breaking. Additionally, for field cases, we include the generation by wind of Snyder et al. (1981) as adapted by Komen et al. (1984) with wind drag coefficient calculated as described by Zijlema et al. (2012), quadruplet wave–wave interactions with the Discrete Interaction Approximation (DIA) of Hasselmann et al. (1985) scaled for shallow water as suggested by the WAMDI Group (1988) and white capping with the pulse model of Hasselmann (1974) as modified by the WAMDI Group (1988) and shifted to higher frequencies as suggested by Rogers et al. (2003). All these settings are the current default physics in SWAN from version 40.91A apart from the bottom friction and wind drag coefficient, and the depth-induced breaking source term which is the focus of this paper.

The only exception to the above was for our reef field case (Guam) where we used a spectral version of the bottom friction model of Thornton and Guza (1983) as bottom friction estimates were available for this friction model (Péquignet et al. 2011, see Appendix A). We distribute the corresponding bulk dissipation for bottom friction proportionally to the spectral density of the near-bottom velocity from linear theory (Graber and Madsen, 1988; Tolman, 1990a) given by:

$$S_{bf}(\sigma,\theta) = A\left(\frac{\sigma}{sinh(kd)}\right)^2 E(\sigma,\theta) \tag{3.2}$$

where A is such that the bulk dissipation is given by the Thornton and Guza (1983) model calculated with characteristic frequency f_{m01} (defined below).

All laboratory cases and, in view of their idealized character, all lake cases were computed in 1D. For the field cases, the computations were 2D using either regular grids (Haringvliet and Petten) or curvi-linear grids (Amelander Zeegat and Guam). For all laboratory cases, a logarithmic frequency distribution with frequency resolution $\Delta f = 0.05 f$ and directional resolution of $\Delta\theta = 0.5°$ was used. For all lake and field cases, $\Delta f = 0.1 f$ (a constraint of the DIA) and $\Delta\theta = 15°$. The default criteria for stopping SWAN computations was applied i.e., a change of less than 2% in the significant wave height and mean wave period over 98% of the spatial computational grid points between one iteration and the next; capped at 50 iterations. This cap was verified to be sufficient for the default stopping criteria.

All integral wave parameters such as the significant wave height and mean wave frequencies are estimated in the present study from the moments of the 1D variance density spectrum $m_n = \int \sigma^n E'(\sigma)\, d\sigma$ where $E'(\sigma) = \int E(\sigma,\theta)\, d\theta / (\rho g)$ with ρ, the density of water and g, the gravitational acceleration. The significant wave height is computed as $H_{m0} = 4\sqrt{m_0}$ and the mean frequency as $f_{m01} = (2\pi)^{-1} m_1 / m_0$.

3.3. METHODOLOGY

This section begins with our selection of parameterizations for wave breaking applicable for use in 2D spectral models over an extensive range of irregular (i.e., random) waves over 1D and 2D bathymetries. We subsequently present the observations used, including the selection of calibration and validation subsets, and our method of analysis.

3.3.1. DEPTH-INDUCED WAVE BREAKING MODELS

In this section, we select γ-scalings for depth-induced wave breaking suitable for irregular waves over 1D and 2D bathymetries. We include in our verification all three versions of the basic Battjes and Janssen (1978) dissipation model described in Section 3.1. However, we discount γ-scalings that are limited to 1D situations and are parameterized in terms of *incident* wave parameters as such scalings cannot be used in 2D wave models. Such parameters include offshore wave steepness (Battjes and Stive, 1985; Svendsen, 1987; Nairn, 1990; Rattanapitikon et al., 2003b; Holthuijsen and Booij, 2006; Camenen and Larson, 2007), offshore wave height (Apotsos et al., 2008) and deep water wavelength (Goda, 2004). For 2D situations, these parameters vary along the coast and lose much of their relevance for the surf zone when other processes apart from breaking, for instance refraction, affect the waves. In addition, van der Westhuysen (2010, his Fig. 9) demonstrates that offshore, or even local, wave steepness (Vink, 2001) is unable to represent γ_{BJ} satisfactory. Finally, we do not consider studies which obtain results for regular waves which do not seem to apply to irregular waves (Vincent, 1985; Kamphuis, 1991; Goda, 2010).

Based on the above arguments and the review of van der Westhuysen (2010), we se-

lect seven γ-scalings which vary with local parameters; namely local bottom slope or characteristic normalized wave number. These are presented in Fig. 3.1 (bottom panel). For Ruessink et al. (2003), we use both the original and corrected B98 model. We also include the recent versions of van der Westhuysen (2009) and Filipot and Ardhuin (2012) of the TG83 model as they offer alternatives to using a variable γ value. The BJ model, with a constant $\gamma_{BJ} = 0.73$, is included only as a reference.

The only conceptual alternative to the Battjes and Janssen (1978) approach, that we are aware of, is given by Dally et al. (1985) who presents a relaxation model for the dissipation of a breaking periodic wave. For irregular waves, Dally (1992) applied this approach on a wave-by-wave basis. Rattanapitikon and Shibayama (1998a,b) and Rattanapitikon et al. (2003a) propose estimating the wave energy as $E = \rho g H_{rms}^2/8$ and using a Miche-type criterion for estimating H_{stable} to define $E_{stable} = \rho g H_{stable}^2/8$. We subsequently refer to this model as the D85 dissipation model and use the constant breaking criterion for a stable root-mean-square wave height ($\gamma_D = H_{rms,st}/d = 0.266$) given by Rattanapitikon (2007).

In summary, 12 formulations are considered in the model comparison. These formulations are described in greater detail in Appendix 3.A.

3.3.2. DEPTH-INDUCED WAVE BREAKING OBSERVATIONS

LABORATORY OBSERVATIONS

To represent a large range of wave conditions, eight data sets with observations made in 1D wave flumes with waves propagating (with two exceptions) over a constant slope were used (see Fig. 3.2). Occasionally, we used the nominal incident spectrum, either unimodal or bimodal, but where available we used the observed incident spectrum. A $cos^m(\theta)$ directional distribution with $m = 800$ (i.e., directional spreading $\sigma_\theta = 2°$; Kuik et al., 1988) was used to characterize the long-crested waves.

To avoid redundancy and for reasons of economy, we select from each of the two large data sets of Wallingford (Coates et al., 1998; Hawkes et al., 1998; van der Meer et al., 2000) and Jensen (2002), each with 210 and 110 cases respectively, a representative sample. It comprised of (a) the cases closest to the central values of the experimental parameters (the significant wave height, mean wave period, spectral shape, etc.), (b) the cases at the extreme values of these parameters (representing the envelope) and (c) a random sample of 25 remaining cases. This resulted in 49 Wallingford cases and 45 Jensen (2002) cases. For the Wallingford data set, the observations are divided into two data sets; one containing observations on the slope and the other over the horizontal flat resulting in 98 cases. The remaining six laboratory data sets are included in their entirety.

IDEALIZED FIELD OBSERVATIONS

To include observations representing wave generation limited by depth-induced wave breaking, we include observations from three shallow lakes (see Fig. 3.3): Lake George in south–east Australia (Young and Babanin, 2006) and Lake IJssel and Lake Sloten in the Netherlands (Bottema and van Vledder, 2009). These authors presented their observations as dimensionless energy $\tilde{E} = g^2 m_0/U_{10}^4$ as a function of dimensionless depth $\tilde{d} = g d/U_{10}^2$, in which U_{10} is the average wind speed at 10 m elevation implying an idealization of depth, fetch and wind, i.e., fully developed waves in shallow water.

From these lakes, we selected data points representing the upper envelope of the dimensionless energy $\tilde{E}$ when plotted against $\tilde{d}$ (see inset of Fig. A.1 in Appendix A) but only in the range where depth-induced breaking dominates (approximately $\tilde{d} < 0.05$; verified with SWAN computations). In the computations, these cases are treated as idealized 1D cases with constant wind and water depth. As the exact wind speed is immaterial for dimensionless quantities, a wind speed of 20 m/s was used.

COASTAL FIELD OBSERVATIONS

Finally, we consider four coastal sites of increasing complexity (see Fig. 3.4), namely a relative simple, straight, and gently sloping beach open to the sea (Petten), a bay with a large shoal half across its entrance (Haringvliet), a complex intertidal region (Amelander Zeegat), and a tropical fringing reef (Guam). In these cases, the wave boundary conditions are 2D spectra inferred from directional wave buoys in deep water. Wave induced set-up is computed with linear wave theory but without calculating wave-induced currents for all but one field case. This is used for Petten, Haringvliet and Guam for which we estimate the current speed < 0.25 m/s (based on observations and tide tables). For Amelander Zeegat, a separate circulation model was used to compute the wind, the wave and tide induced currents, and the wind and wave induced set-up (van der Westhuysen and de Waal, 2008). The wind and tide induced currents and water levels were computed with the same circulation model for Petten (Groeneweg et al., 2003; G.Ph. van Vledder, pers. comm., 2012).

To avoid observations insensitive to depth-induced breaking, only locations demonstrating a 5% variation in the SWAN computed significant wave height between $\gamma_{BJ} = 0.73$ and $\gamma_{BJ} = 1.5$ were considered. Using the latter value essentially disables wave breaking. At the Haringvliet site, this removed all observations in depths > 10 m, while at the Petten site only some of the observations were removed. All other field cases are included in their entirety.

CALIBRATION AND VALIDATION SUBSETS

For the model comparison in Section 3.5, all 225 cases from the 13 data sets were used. This includes 202 laboratory cases, 5 lake cases and 18 coastal cases. For the calibration and verification of our joint scaling in Section 3.6, we split the 225 cases into two mutually exclusive subsets respectively. For the first set (the calibration subset), we used a subset of Wallingford and of Jensen (2002) representing the central and envelope cases i.e., criteria (a) and (b). Similar criteria were also used to add 1 : 100 and 1 : 250 slope cases from Katsardi et al. (2013) to increase the range of slopes in the calibration. These criteria ensured that the calibration subset remained as unbiased as possible to specific experimental parameters. To represent locally generated waves, the lakes data set was also added in its entirety. In total, for the calibration, 84 1D cases were used i.e., 48 from Wallingford, 20 from Jensen (2002), 11 from Katsardi et al. (2013) and 5 from the lakes data set.

For the second set (the verification subset), all remaining laboratory cases were used and all field cases (except the lakes). This included the randomly selected cases from Wallingford and Jensen (2002), the remaining (outside the calibration subset) 12 cases from Katsardi et al. (2013) and Katsardi (2007) and all remaining laboratory data sets,

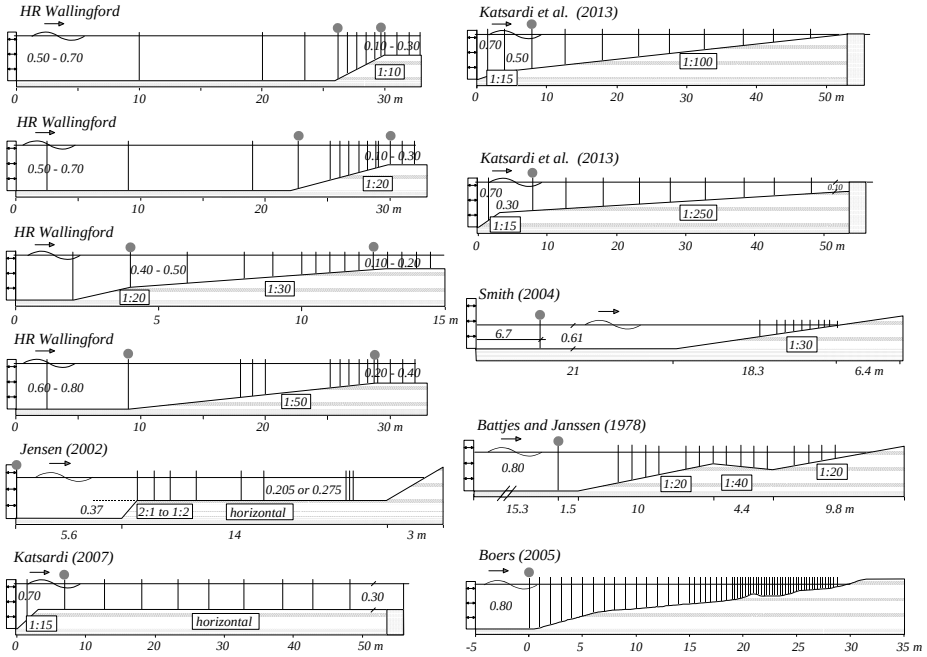

Figure 3.2: The configurations of the laboratory observations. Thin vertical lines indicate wave gauge positions. Solid dots indicate the location of incident spectra for the computations (wave boundary condition).

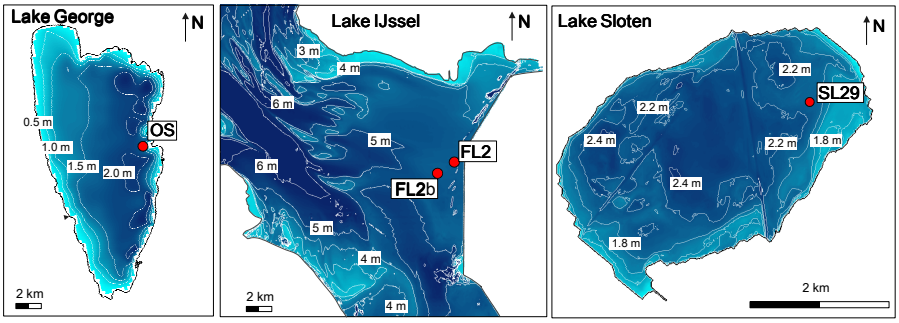

Figure 3.3: The bathymetry of the three lakes with the location of observation sites OS, FL2, FL2b and SL29.

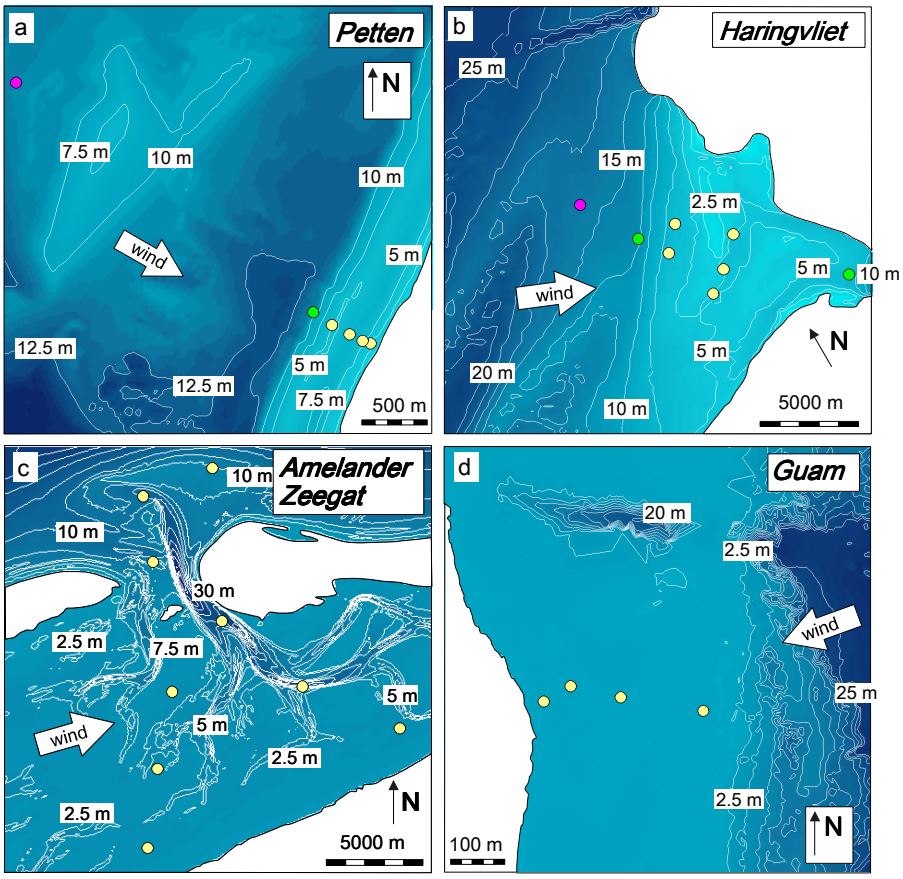

Figure 3.4: The bathymetry of the coastal sites Petten, Haringvliet, Amelander Zeegat and Guam. Water depth for mean sea surface at +1 m above chart datum (Amsterdam Ordnance Datum for Petten, Haringvliet and Amelander Zeegat, and mean lower low water for Guam). The buoy locations are indicated by colored dots: purple (boundary condition), green (occasionally removed when not affected by depth-induced breaking) and yellow (always affected by depth-induced breaking). The indicated wind directions are the average direction over the cases per site (variation over the different cases $< 35^\circ$ for Petten, $< 20^\circ$ for Amelander Zeegat, and $< 25^\circ$ for Guam). The wind direction did not vary significantly for the Haringvliet site.

totaling 123 cases. The addition of the 18 field cases brought the total number of verification cases to 141. Further details of all cases are provided in Appendix A.

3.3.3. METHOD OF ANALYSIS

For our analysis, the errors in the prediction of the significant wave height are expressed in terms of a scatter index (*s.i.*) and a relative bias (*r.b*) as used in previous studies Janssen et al. (1984); Komen et al. (1994); van der Westhuysen (2010). They are defined here as:

$$s.i. = \sqrt{\frac{1}{N}\sum\left(H_{m0,comp} - H_{m0,obs}\right)^2} \Big/ \overline{H_{m0,obs}} \tag{3.3}$$

$$r.b. = \frac{1}{N}\sum\left(H_{m0,comp} - H_{m0,obs}\right) \Big/ \overline{H_{m0,obs}} \tag{3.4}$$

The subscripts *obs* and *comp* refer to the observed and computed values, N is the number of data points and the overbar indicates the mean value. We use these metrics only to indicate the magnitude of the errors.

To determine characteristic averages of these metrics, we divided the data sets into cases with sloping profiles; typically well predicted in the literature and those with horizontal profiles; typically poorly predicted. The distinction is evident in all cases except the Guam reef. The Guam reef is often assumed to be horizontal with a fairly steep approach slope (e.g. Demirbilek et al., 2007), but actually the slope is 1 : 700 and negative with most of the wave breaking occurring over an elevated threshold at the deep water edge. Nevertheless, we consider 1 : 700 gentle enough to be included in the horizontal subset. Furthermore, we also make the distinction between laboratory and field cases.

For each subset (slopes, horizontals, laboratory and field), we compute the metrics for each individual data set and compute the average, unweighted by the number of cases in each sample data set to avoid biasing towards large sample data sets. The overall average is the unweighted average of the sloping and horizontal subsets. We consider the scatter index to be the primary metric to assess performance as it includes the systematic and random error of the prediction. The relative bias represents only the systematic error.

3.4. NEW PARAMETERIZATIONS

3.4.1. A JOINT SCALING FOR DEPTH-INDUCED WAVE BREAKING

THE $\beta - kd$ SCALING

Following the depth-induced wave breaking models outlined in Section 3.3.1, we propose a joint scaling dependent on both local bottom slope, β and local normalized characteristic wave number, $\tilde{k}d$ (see below). In very shallow water ($\tilde{k}d \to 0$), waves behavior converges to that of a solitary wave. Theoretically, the wavelength of such waves is infinitely long and therefore wavelength, and therefore the value of $\tilde{k}d$ becomes less and less relevant as waves propagate into shallower water. For instance, Fenton (1990, his Fig. 6-1) shows that for such waves, the maximum wave height and therefore γ is virtually independent of $\tilde{k}d$. We therefore argue that at some lower limit for $\tilde{k}d$ (to be determined through calibration), wave breaking is only controlled by β. At larger $\tilde{k}d$

values, waves are assumed to be dependent on both β and $\tilde{k}d$. To accommodate this, we represent the two different dependencies on local bottom slope and normalized wave number, respectively, as linear scalings, equivalent to those proposed in previous studies, with $\gamma_1(\beta) = \gamma_0 + a_1 tan\beta \geq 0$ and $\gamma_2(\tilde{k}d) = a_2 + a_3\tilde{k}d \geq 0$ where γ_0, a_1, a_2 and a_3 are tunable coefficients. To provide a smooth transition from the linear dependency on the local normalized wave number in deep water ($\tilde{k}d > 1$) to a linear dependency on the local bottom slope in shallower water ($\tilde{k}d < 1$), we introduce a hyperbolic tangent:

$$\gamma_{\beta-kd} = \gamma_1(\beta) / tanh\left[\gamma_1(\beta)/\gamma_2(\tilde{k}d)\right] \tag{3.5}$$

As waves progress into shallower water, $\tilde{k}d \to 0$ and the proposed scaling for gamma converges to a linear dependency only dependent on β i.e., $\gamma_{\beta-kd} \to \gamma_1(\beta)$. In deeper water, $\tilde{k}d \to \infty$ and $\gamma_{\beta-kd} \to \gamma_2(\tilde{k}d)$. The $\tilde{k}d$ range between these two extremes is determined by the coefficients a_2 and a_3.We refer to this joint scaling as the $\beta - kd$ scaling.

The bottom slope in Eq. (3.5) is (implicitly) assumed to be positive, i.e., decreasing depth in the mean wave direction. In arbitrary and naturally occurring 2D bathymetries, backwards or sideways sloping profiles (relative to the mean wave direction) occur. As we do not have a rationale for estimating γ under such conditions, we estimate the bottom slope as the magnitude of the bottom gradient taken from the computational grid i.e., $tan\beta = |\nabla d|$, thus not discriminating between forward, backward or sideways sloping profiles. Whitford (1988, p. 110) supports this to some extent through his observations of H_{rms}/d as a function of $tan\beta$ in a saturated surf zone where he shows the observations to cluster around a common regression line, with the same degree of scatter, for both positive and negative slopes. Our approach also avoids estimating bottom slopes as horizontal in the mean wave direction when that direction is parallel to the depth contours of a sideways sloping bathymetry. In such a situation, the bottom slope in the mean wave direction would be zero, although approximately half the wave energy would be propagating up-slope and the other half down-slope. It is noteworthy however that in trial computations with negative slopes (Boers, 2005 and Guam cases; see Section 3.6.3), a high local value of $\gamma_{BJ} \sim O(1)$ for negative slopes reduced errors. Furthermore, to prevent physically unrealistic values of $\gamma_1(\beta)$ over very steep slopes, an upper limit of $n = tan^{-1}(\beta)$, i.e. a limiting 1 : 10 slope is imposed.

CHARACTERISTIC WAVE NUMBER

Often in modeling wave breaking, the characteristic wave number is taken at the peak of a typically unimodal spectrum. However, this is not very robust in arbitrary conditions. Its value tends to behave erratically when small variations in a multi-modal spectrum randomly shift the peak from one frequency to another, in particular off an oceanic coast where the spectrum will generally have multiple peaks due to the presence of multiple swell fields. Using a higher-order mean wave number is also not robust. It is sensitive to the exact shape of the high-frequency tail of the spectrum which spectral wave models cannot accurately predict in very shallow water as triad wave–wave interactions – which tend to generate high-frequency peaks – are poorly accounted for, if at all. We therefore propose using a lower-order mean wave number, as used for white capping (WAMDI Group, 1988) $\tilde{k} = k_{-1/2} = \left[\iint k^{-1/2} E(\sigma,\theta)\, d\sigma d\theta / E\right]^{-2}$. This is less sensitive to the presence of multiple peaks or to the exact shape of the spectral tail.

CALIBRATION

The dependency of $\gamma_{\beta-kd}$ on normalized *wave number* is most evident when the *bottom slope* is zero as under such conditions Eq. (3.5) reduces to $\gamma_{\beta-kd} = \gamma_0 / tanh\left[\gamma_0 / \left(a_2 + a_3 \tilde{k}d\right)\right]$. For the calibration of γ_0, a_2 and a_3, we therefore use horizontal profile cases with a wide $\tilde{k}d$ range; namely the Wallingford and Jensen (2002) calibration subsets with $0.4 \leq \tilde{k}d \leq 1.1$ and $0.5 \leq \tilde{k}d \leq 1.0$ respectively and the lakes data set with $1.1 \leq \tilde{k}d \leq 1.4$. However, in the first two (low $\tilde{k}d$, laboratory) data sets a few dozen cases are available whereas in the third (high $\tilde{k}d$, lakes) data set only five cases are available. A calibration using all three data sets simultaneously would therefore be seriously biased towards the lower $\tilde{k}d$ values. To avoid this, we follow van der Westhuysen (2010, his Fig. 7) to estimate the optimal $\gamma_{\beta-kd}$ value for the high $\tilde{k}d$ data set by calibrating $\gamma_{\beta-kd}$ independently from β or $\tilde{k}d$. This calibration consisted of systematically varying the value of $\gamma_{\beta-kd}$ in the range $0 < \gamma_{\beta-kd} \leq 1.5$ and calculating the corresponding scatter index.

We subsequently calibrate γ_0 and a_2 by systematically varying these coefficients over the low $\tilde{k}d$ data sets. For each $\gamma_0 - a_2$ pair, we calculated the average scatter index by equally weighting Wallingford and Jensen (2002). Applying the optimum value for $\gamma_{\beta-kd}$ at the lower $\tilde{k}d$ limit for the lakes data set allowed a_3 to be determined. Following Roelvink (1993), the optimum combination of γ_0 and a_2 was determined by plotting the isolines of the average scatter index in the $\gamma_0 - a_2$ plane and determining the location of the minimum.

The coefficient for slope dependence, a_1 was calibrated last using the sloping calibration cases of Wallingford and Katsardi et al. (2013) from the equally weighted scatter indices.

3.4.2. EXTENSION OF DISSIPATION MODELS FOR WAVE DIRECTIONALITY

For waves breaking in a laboratory flume, the 1D bore analogy used in most dissipation models is a reasonable assumption. However, in reality, all waves in the field are essentially short-crested, even if refraction elongates the crests near a straight coastline. Therefore, in these cases, we expect the inherent short-crestedness of the waves to detract from the 1D bore analogy. As a preliminary investigation on the extent of directional effects, we consider a modification for dissipation models to account for the inapplicability of the 1D bore assumption for waves in 2D conditions.

The directional spreading of waves can be defined as the standard deviation of the frequency integrated 2D spectrum (Kuik et al., 1988):

$$\sigma_\theta = 2 \left[\int_{\theta_0-\pi}^{\theta_0+\pi} sin^2\left(\frac{\theta-\theta_0}{2}\right) D(\theta)\, d\theta \right]^{1/2} \tag{3.6}$$

in which θ_0 is the mean wave direction and $D(\theta)$ is the direction distribution defined as $D(\theta) = \int E(f,\theta)\, df / E$.

We assume that the analogy between the dissipation of a 1D breaking bore and a breaking wave holds for long-crested waves i.e., directionally narrow spectra with a directional spreading, $\sigma_\theta < \sigma_\theta^*$ (to be determined later). For more directionally spread spectra ($\sigma_\theta > \sigma_\theta^*$), we assume the same for each partitioning of the spectrum of width

σ_θ^*. Such a partitioning can be considered as an expansion of the frequency partitioning of Filipot and Ardhuin (2012). As a step towards a fully 2D frequency and directionally partitioned spectrum and to maintain the simplicity, we only consider a simple directional partitioning by defining the number of partitions as $K_\theta = \sigma_\theta / \sigma_\theta^*$. To implement this, we divide the energy in the dissipation formulations by K_θ (equivalent to $\sqrt{K_\theta}$ for rms-wave height) to represent the energy in each partitioning and multiply the bulk dissipation by K_θ to represent the sum of the dissipation from all the partitions. This implicitly assumes a uniform energy distribution. It should be clear that this is not the same as spectral partitioning of e.g. Hanson and Phillips (2001) who considered a partitioning of the 2D spectrum into different wave systems. This technique can be used for all models based on the 1D bore assumption i.e., BJ78, TG83, B98. To illustrate this, BJ78 (Eqs. 3.A1 and 3.A2) is modified to:

$$\varepsilon_{BJ}^{\theta} = -\frac{1}{4} K_\theta \alpha_{BJ} \bar{f} Q_b \rho g H_{max}^2 \tag{3.7}$$

with

$$\frac{1-Q_b}{lnQ_b} = -\left(\frac{H_{rms}/\sqrt{K_\theta}}{H_{max}} \right)^2 \tag{3.8}$$

It is arguable, from a physical perspective, that instead of modifying the dissipation directly, the underlying wave height distribution should be revised or a more rigorous implementation applied. However, here we only explore the limitations of the 1D bore assumption and the possible effects of wave directionality. We discuss the effect of this directional partitioning in Section 3.7.

3.5. COMPARISON OF AVAILABLE DEPTH-INDUCED WAVE BREAKING MODELS

3.5.1. MODEL COMPARISON

The validation metrics are shown for all 12 models and 13 data sets separately in Figs. 3.5 and 3.6. The performance of the different models varies widely with individual scatter indices between 2% and 79% with the *overall* scatter index per model varying between 13% and 43%. The scatter index for the seven best performing models (indicated with green highlights in Fig. 3.5) clusters around 14%. This result agrees with Apotsos et al. (2008) who demonstrates errors between 10% and 20% and concludes that no default (or tuned) model provides the best prediction for their observations. This relatively small error is mostly due to a very good performance over the sloping laboratory cases (typically scatter indices < 10%), combined with a reasonable performance in the field cases except the Guam reef.

The correction to the B98 model (e.g. Janssen, 2006) is shown to have only a marginal effect on the performance. The kd-scaling from Ting (2001) performs slightly worse with an overall scatter index ~ 20% and demonstrates a particularly poor performance for non-locally generated waves over a (near-)horizontal bathymetry (the Haringvliet; Jensen, 2002 and Guam cases). The performance of the remaining five models vary from

			DISSIPATION MODELS + SCALINGS												
	Scatter index	**#**	**BJ78**				**TG83**					**B98**		**D85**
			BJ	Mad'76	Ting'01+	T&M'02	S&Hol'85	S&How'89	Lipp'96+	vdW'09	FA'12	Rue'03		R&S'03/07
SLOPE DATA SETS	**Slopes**												*corrected*	
	Wallingford*	49	0.06	0.10	0.11	0.18	0.08	0.13	0.16	0.07	0.06	0.07	0.08	0.06
	Katsardi*	18	0.13	0.14	0.23	0.34	0.16	0.22	0.24	0.15	0.10	0.16	0.17	0.12
	Smith*	31	0.08	0.08	0.13	0.26	0.14	0.22	0.28	0.08	0.11	0.10	0.10	0.09
	Boers*	3	0.05	0.07	0.15	0.41	0.19	0.31	0.36	0.06	0.13	0.11	0.08	0.10
	B-J*	2	0.05	0.13	0.15	0.34	0.13	0.24	0.32	0.06	0.07	0.07	0.07	0.10
	Petten**	8	0.15	0.17	0.19	0.57	0.45	0.53	0.55	0.15	0.23	0.15	0.13	0.15
HORIZONTAL DATA SETS	**Horizontal**													
	Wallingford*	49	0.07	0.07	0.10	0.29	0.11	0.13	0.13	0.08	0.07	0.07	0.07	0.06
	Katsardi*	5	0.10	0.10	0.11	0.40	0.19	0.26	0.27	0.10	0.03	0.11	0.11	0.10
	Jensen*	45	0.21	0.21	0.37	0.30	0.11	0.14	0.14	0.27	0.21	0.24	0.26	0.26
	AZG**	3	0.16	0.15	0.10	0.58	0.47	0.53	0.55	0.10	0.24	0.15	0.14	0.20
	Lakes**	5	0.16	0.17	0.08	0.64	0.66	0.71	0.71	0.10	0.27	0.02	0.02	0.11
	Guam**	4	0.38	0.29	0.52	0.79	0.41	0.45	0.48	0.56	0.47	0.39	0.29	0.44
	Haringvliet**	3	0.17	0.17	0.37	0.51	0.31	0.56	0.60	0.20	0.12	0.19	0.20	0.14
AVERAGES	**Averages**													
	slopes	111	0.09	0.12	0.16	0.35	0.19	0.27	0.32	0.10	0.12	0.11	0.10	0.10
	horizontal	114	0.18	0.17	0.24	0.50	0.32	0.40	0.41	0.21	0.20	0.17	0.15	0.19
	laboratory*	202	0.09	0.11	0.17	0.32	0.14	0.20	0.24	0.11	0.10	0.12	0.12	0.11
	field**	23	0.20	0.19	0.25	0.62	0.46	0.55	0.58	0.23	0.27	0.18	0.16	0.21
	overall	225	0.13	0.14	0.20	0.43	0.26	0.33	0.37	0.15	0.16	0.14	0.13	0.14
			s.i.< 0.10		0.10<s.i.<0.20		s.i.>0.20						# 1-7	# 8-12

DISSIPATION MODELS

BJ78 = Battjes & Janssen (1978)
TG83 = Thornton & Guza (1983)
B98 = Baldock et al. (1998)
corrected = correction of B98 by Janssen (2008), Janssen and Battjes (2008) and Alsina and Baldock (2008); Rue model
D85 = Dally et al. (1985)

GAMMA SCALINGS

BJ = γBJ = 0.73 (BJ model)
Mad'76 = Madsen (1976)
Ting'01+ = Ting (2001, present authors)
T&M'02 = Tajima & Madsen (2002)
S&Hol'85 = Sallenger & Holman (1985)
S&How'89 = Sallenger & Howd (1989)
Lipp'96+ = Lippmann et al. (1996, present authors)
vdW'09 = van der Westhuysen (2009)
FA'12 = Filipot & Ardhuin (2012)
Rue'03 = Ruessink et al. (2003)
R&S'03/'07 = Rattanapitikon et al. (2003) + Rattanapitikon [2007]

Figure 3.5: Scatter index of the 12 models (columns) based on four different dissipation models for 13 data sets (rows) containing a total of 225 cases consisting of laboratory observations (*) and field observations (**). The highlight colors indicate two classes of performance and three ranges of scatter index. The best performing parameterizations on average (overall scatter index < 20%) are shown in green. The individual performance for each parameterization per data set is indicated in blue for scatter indices < 10%, orange for scatter indices > 20% and blank for values between these two limits. Averaged values as described in Section 3.3.3 are also provided.

			DISSIPATION MODELS + SCALINGS											
	Relative	#	BJ78				TG83					B98		D85
	bias		BJ	Mad'76	Ting'01+	T&M'02	S&Hol'85	S&How'89	Lipp'96+	vdW'09	FA'12	Rue'03		R&S'03/07
	Slopes												corrected	
SLOPE DATA SETS	Wallingford*	49	0.04	0.08	0.09	-0.15	-0.05	-0.11	-0.14	0.05	0.01	0.05	0.06	0.03
	Katsardi*	18	0.11	0.13	0.22	-0.29	-0.08	-0.16	-0.19	0.13	0.07	0.14	0.15	0.06
	Smith*	31	0.00	0.06	0.03	-0.22	-0.11	-0.18	-0.24	0.02	-0.05	0.00	0.04	0.01
	Boers*	3	-0.02	0.05	-0.01	-0.39	-0.17	-0.28	-0.34	0.00	-0.09	-0.07	-0.01	-0.08
	B-J*	2	0.00	0.11	0.12	-0.31	-0.11	-0.22	-0.30	0.03	-0.03	0.01	0.03	0.05
	Petten**	8	0.01	0.03	0.06	-0.17	-0.09	-0.13	-0.15	0.02	-0.02	0.01	0.02	0.00
	Horizontal													
HORIZONTAL DATA SETS	Wallingford*	49	0.04	0.06	0.07	-0.24	-0.08	-0.12	-0.14	0.05	0.02	0.03	0.05	0.01
	Katsardi*	5	0.09	0.09	0.10	-0.40	-0.19	-0.25	-0.27	0.10	0.02	0.10	0.10	0.09
	Jensen*	45	0.17	0.18	0.33	-0.29	0.00	-0.04	-0.05	0.23	0.16	0.21	0.22	0.22
	AZG**	3	-0.12	-0.11	0.00	-0.49	-0.41	-0.47	-0.49	-0.06	-0.21	-0.08	-0.08	-0.15
	Lakes**	5	-0.16	-0.17	0.08	-0.63	-0.64	-0.69	-0.70	-0.10	-0.27	0.01	0.01	-0.11
	Guam**	4	-0.21	-0.02	-0.38	-0.69	-0.31	-0.37	-0.40	-0.46	-0.25	-0.25	-0.12	-0.33
	Haringvliet**	3	0.14	0.14	0.33	-0.44	-0.26	-0.49	-0.53	0.18	-0.05	0.15	0.17	0.11
	Averages													
AVERAGES	slopes	111	0.02	0.07	0.09	-0.25	-0.10	-0.18	-0.23	0.04	-0.02	0.02	0.05	0.01
	horizontal	114	-0.01	0.02	0.08	-0.45	-0.27	-0.35	-0.37	-0.01	-0.08	0.02	0.05	-0.02
	laboratory*	202	0.05	0.09	0.12	-0.28	-0.10	-0.17	-0.21	0.08	0.02	0.06	0.08	0.05
	field**	23	-0.07	-0.02	0.02	-0.49	-0.34	-0.43	-0.45	-0.08	-0.16	-0.03	0.00	-0.09
	overall	225	0.01	0.05	0.08	-0.35	-0.19	-0.26	-0.30	0.02	-0.05	0.02	0.05	0.00
			rel. bias > 0		rel. bias < 0								# 1-7	# 8-12

Figure 3.6: Same as Fig. 3.5 for the relative bias. Highlights indicate positive (light blue) and negative or ~zero (dark blue) bias over horizontal bathymetries for the cluster of seven best performing models.

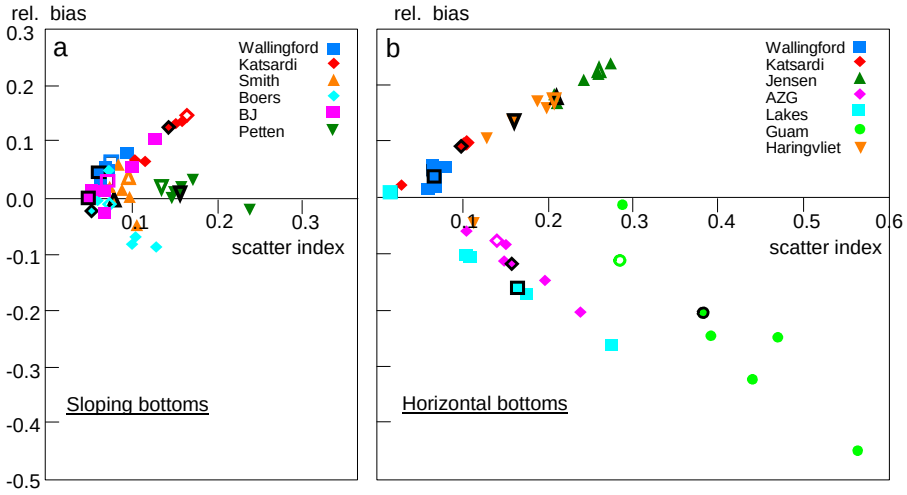

Figure 3.7: The scatter diagram of the relative bias versus the scatter index for all data sets and the cluster of seven best performing models (not identified individually). The reference BJ model is shown with a solid black outline and the reference Rue model is shown with only a symbol outline. The Amelander Zeegat data set is indicated with AZG and the Battjes and Janssen (1978) data set with BJ.

reasonable in some laboratory cases to poor in the field cases where scatter indices are typically ~ 50% or higher.

Concentrating on the seven best performing models with rms-errors ~ 14%, shows that the largest errors occur in the cases with *horizontal* bathymetries where the highest overall scatter index per model varies between 29% and 56% compared with 15% and 23% for sloping bathymetries. Over horizontal bathymetries, the errors are mostly systematic as shown by the relative bias in Fig. 3.6, of which the average absolute value is 0.72 times the average scatter index.

3.5.2. CORRELATION WITH BOTTOM SLOPE AND NORMALIZED WAVE NUMBER

To find a possible cause for the errors, we plot the scatter index and the relative bias of the seven best performing models in Fig. 3.7. These models are not individually indicated, except the BJ model and the best overall performing model; the corrected B98 model with the scaling of Ruessink et al. (2003) (subsequently referred to as the Rue model) as references. For the sloped bottom data sets (Fig. 3.7A), the bias is only weakly correlated with the scatter index. In the horizontal bottom data sets (Fig. 3.7B), the Guam data set is obviously an outlier with high scatter indices, however as discussed previously, its classification is questionable. If therefore, for this analysis, we ignore the Guam data set, we see that in contrast to the slope data sets, for the horizontal cases, the bias is highly correlated with the scatter index. In addition, there is a sharp distinction between data sets with a negative or ~zero bias (under-prediction of locally generated waves in the lakes and the Amelander Zeegat) and with a positive bias (over-prediction of non-locally generated waves in the Wallingford; Katsardi, 2007; Jensen, 2002 and Haringvliet data sets).

Typically for locally generated wave cases, the relative bias is on average ~ 64% (negative) of the total error suggesting a severe systematic under-prediction in agreement with previous studies (e.g. van der Westhuysen, 2010). In cases of finite depth wave growth, models with either a direct dependency on the normalized wave number (kd; Ting, 2001; Ruessink et al., 2003) or indirect (van der Westhuysen, 2009, 2010, through the Ursell number) perform significantly better with averaged scatter indices typically half those from models without such a dependency. However, none of these models provide the smallest errors for both Amelander Zeegat and the lakes.

A similar analysis for non-locally generated wave cases show a severe over-prediction of significant wave heights with larger errors for horizontal bathymetries (~ 73% of the mean bias) than for sloping bathymetries (~ 28% of the mean bias). This is in agreement with Nelson (1997) and Katsardi (2007) who both demonstrate higher dissipation for wave breaking over horizontal bathymetries than over sloping bathymetries.

These contrasts support a joint dependency on both local bottom slope (shown by the contrast in horizontal and sloping bathymetries for non-locally generated waves) and on normalized wave number (shown by the contrast in locally and non-locally generated waves over horizontal bathymetries). Such joint dependencies have been considered before (e.g. Goda, 2004, 2009, 2010; Raubenheimer et al., 1996), however these are not applicable for use in 2D spectral wave models (see Section 3.3.1).

3.6. CALIBRATION AND VERIFICATION OF THE $\beta - kd$ SCALING

3.6.1. DISSIPATION MODEL

Following the model comparison, it is clear from Fig. 3.5 that the simplest dissipation models with constant γ (the BJ and the D85 model with $\gamma_D = 0.266$), in terms of overall scatter index, are among the best performing models and occasionally perform slightly better than the more complex models of van der Westhuysen (2009) and Filipot and Ardhuin (2012). Following these observations, in addition to its proven robustness (Battjes and Janssen, 2008), we choose to address the scaling of the BJ78 dissipation model. Other alternatives may have a better foundation in physics, particularly in regards to the assumed statistical distribution of the wave heights, but we agree with Battjes and Janssen (1978) that the details of the distribution are not important when only integral parameters are required.

3.6.2. CALIBRATION

Using our calibration procedure in Section 3.4.1, the four calibration parameters of the $\beta - kd$ scaling (γ_0, a_1, a_2 and a_3) were calibrated over the calibration subset. For the high $\tilde{k}d$ cases (lakes data set), we present our calibration for $\gamma_{\beta-kd}$ (independent of β and kd) in Fig. 3.8A. These results agree with van der Westhuysen (2010) and demonstrate a sharp decrease in the scatter index from ~ 100% to an asymptote at ~ 5% for $\gamma_{\beta-kd} \geq 0.95$.

Using this limit so that $\gamma_{\beta-kd} = 0.95$ for $\beta = 0$ and $\tilde{k}d = 1.1$ (assumed to be the limit between high and low $\tilde{k}d$), a_3 was determined for each $\gamma_0 - a_2$ pair. From the average scatter indices over the horizontal Wallingford and Jensen (2002) calibration subsets, an error contour plot is shown in Fig. 3.8B. The relatively flat error gradient in the a_2 axis compared to the γ_0 axis demonstrates a sensitivity on γ_0 rather than a_2 for low $\tilde{k}d$ cases over horizontal bathymetries. For these conditions, a minimum error of ~ 6%, was achieved with $\gamma_0 = 0.54$ and $a_2 = -8.06$ (so that $a_3 = 8.09$). This lower limit, γ_0, is identical to the value found by Katsardi (2007) through numerical experiments and similar to the observations of Nelson, 1997; $\gamma_0 = 0.55$). The calibration coefficient a_2 defines the lower limit of $\tilde{k}d$ dependency which, from calibration, is given at $\tilde{k}d \approx 1$. This is consistent with van der Westhuysen (2010, his Fig. 7) who demonstrates $\gamma_{BJ} > \gamma_0$ for horizontal cases over deep water depths ($\tilde{k}d > 1$).

Finally, a_1, the bottom slope dependency coefficient is calibrated from the sloping bottom calibration subsets of Wallingford and Katsardi et al. (2013). This is shown in Fig. 3.8C with a well-defined minimum at $a_1 = 7.59$ and averaged error of ~ 9%. This positive β-variation is consistent with the $\gamma(\beta)$ scalings considered in the model comparison, however for the $\beta - kd$ scaling the variation of γ with β is stronger. This is needed to account for a wider range of γ-values given by the lower limit γ_0. The commonly used value $\gamma_{BJ} = 0.73$ is reproduced for slopes of 1 : 40 in shallow to intermediate water depths. The fully calibrated $\beta - kd$ scaling is shown in Fig. 3.9.

3.6.3. VERIFICATION

To verify the performance of the calibrated $\beta - kd$ scaling ($\gamma_0 = 0.54$, $a_1 = 7.59$, $a_2 = -8.06$ and $a_3 = 8.09$), we show our results over the verification subset as described in Section 3.3.2 in Figs. 3.10 and 3.11. The BJ and Rue models are also shown as references rep-

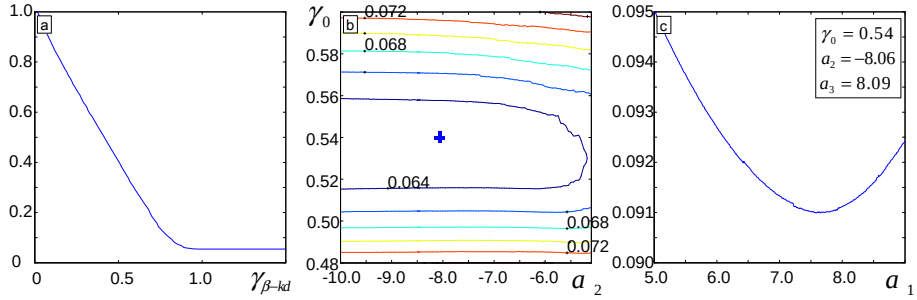

Figure 3.8: Variation of the scatter index for significant wave height during calibration. Shown are A: scatter index using a fixed $\gamma_{\beta-kd}$ per computation in the lakes data set, B: isolines of scatter index for the calibration of γ_0 and a_2 in the horizontal bottom calibration cases of Wallingford and Jensen (2002) (minima denoted by the blue cross) with $\gamma_{\beta-kd} = 0.95$ for $\tilde{k}d = 1.1$ and C: scatter index for the calibration of a_1 in the sloping bottom calibration cases of Wallingford and Katsardi et al. (2013) with $\gamma_0 = 0.54$, $a_2 = -8.06$ and $a_3 = 8.09$.

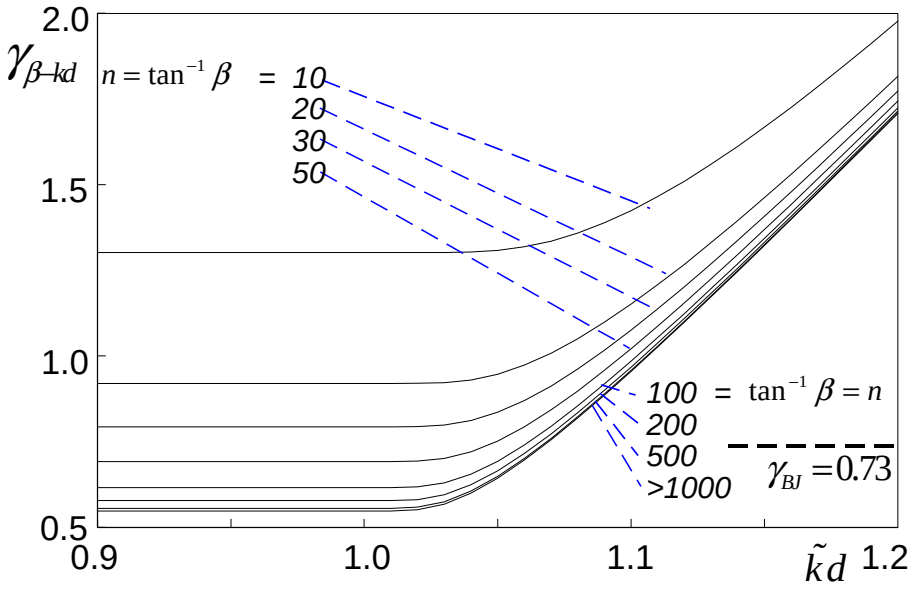

Figure 3.9: Calibrated $\gamma_{\beta-kd}$ as a function of bottom slope $n = tan^{-1}\beta$ and normalized characteristic wave number $\tilde{k}d$ and $\gamma_{BJ} = 0.73$ for reference.

			WAVE BREAKING PARAMETERIZATION					
	Scatter index	**#**	BJ	Rue	$\beta - kd$		BJ	Rue
			no correction			$\sigma_\theta^* = 15^o$	$\sigma_\theta^* = 25^o$	$\sigma_\theta^* = 25^o$
SLOPE DATA SETS	**Slopes**							
	Wallingford*	25	0.08	0.09	0.11	(0.11)	(0.08)	(0.09)
	Katsardi*	7	0.14	0.15	0.12	(0.12)	(0.14)	(0.15)
	Smith*	31	0.08	0.10	0.07	(0.07)	(0.08)	(0.10)
	Boers*	3	0.05	0.07	0.07	(0.07)	(0.05)	(0.07)
	B-J*	2	0.05	0.07	0.10	(0.10)	(0.05)	(0.07)
	Petten**	8	0.15	0.13	0.20	0.15	0.15	0.13
HORIZONTAL DATA SETS	**Horizontal**							
	Wallingford*	25	0.08	0.08	0.08	(0.08)	(0.08)	(0.08)
	Katsardi*	5	0.10	0.11	0.05	(0.05)	(0.10)	(0.11)
	Jensen*	25	0.21	0.26	0.08	(0.08)	(0.21)	(0.26)
	AZG**	3	0.16	0.14	0.23	0.08	0.09	0.09
	Guam**	4	0.38	0.29	0.28	0.27	0.36	0.29
	Haringvliet**	3	0.17	0.20	0.16	0.12	0.18	0.21
	Lakes	*5*	*0.16*	*0.02*	*0.02*	*0.05*	*0.12*	*0.05*
AVERAGES	**Averages**							
	slopes	76	0.09	0.10	0.11	0.10	0.09	0.10
	horizontal	65	0.18	0.18	0.15	0.12	0.17	0.17
	laboratory*	123	0.10	0.12	0.09	(0.09)	(0.10)	(0.12)
	field**	18	0.21	0.19	0.22	0.16	0.19	0.18
	overall	141	0.14	0.14	0.13	0.11	0.13	0.14
			s.i.< 0.10		0.10<s.i.<0.20		s.i.>0.20	

Figure 3.10: Verification of the $\beta - kd$ scaling in terms of the scatter index with or without optimum σ_θ^*. Performance over laboratory observations (*) and field observations (**) are highlighted in three ranges of scatter index (from blue to orange). The Lakes data set, shown in italic type, is not included in computing the average values (as it is used for calibration) but is shown to demonstrate the effect due to directional spreading for this data set. Laboratory cases with their long-crested waves are unaffected by directional partitioning and are shown within parenthesis () where directional partitioning is used.

			WAVE BREAKING PARAMETERIZATION					
	Relative bias	**#**	BJ	Rue	$\beta - kd$		BJ	Rue
			no correction			$\sigma_\theta^* = 15^o$	$\sigma_\theta^* = 25^o$	$\sigma_\theta^* = 25^o$
SLOPE DATA SETS	**Slopes**							
	Wallingford*	25	0.06	0.07	0.08	(0.08)	(0.06)	(0.07)
	Katsardi*	7	0.12	0.13	0.07	(0.07)	(0.12)	(0.13)
	Smith*	31	0.00	0.04	0.04	(0.04)	(0.00)	(0.04)
	Boers*	3	-0.02	-0.01	-0.04	-(0.04)	-(0.02)	-(0.01)
	B-J*	2	0.00	0.03	0.07	(0.07)	(0.00)	(0.03)
	Petten**	8	0.01	-0.01	-0.07	0.03	0.02	-0.01
HORIZONTAL DATA SETS	**Horizontal**							
	Wallingford*	25	0.04	0.05	-0.01	-(0.01)	(0.04)	(0.05)
	Katsardi*	5	0.09	0.10	0.01	(0.01)	(0.09)	(0.10)
	Jensen*	25	0.18	0.22	0.05	(0.05)	(0.18)	(0.22)
	AZG**	3	-0.12	-0.08	-0.15	-0.04	-0.05	-0.03
	Guam**	4	-0.21	-0.12	-0.03	0.02	-0.19	-0.10
	Haringvliet**	3	0.14	0.17	-0.07	0.09	0.15	0.18
	Lakes	*5*	*-0.16*	*0.01*	*-0.01*	*0.04*	-0.12	0.05
AVERAGES	**Averages**							
	slopes	76	0.03	0.04	0.03	0.04	0.03	0.04
	horizontal	65	0.02	0.06	-0.04	0.02	0.04	0.07
	laboratory*	123	0.06	0.08	0.03	(0.03)	(0.06)	(0.08)
	field**	18	-0.04	-0.01	-0.08	0.02	-0.02	0.01
	overall	141	0.02	0.05	-0.02	0.02	0.03	0.06
			rel. bias > 0.10		rel. bias < 0.10			

Figure 3.11: Same as Fig. 3.10 for relative bias. Highlights indicate positive (light blue) and negative (dark blue) bias for relative biases with magnitudes greater than 10%. A consistent underestimation for field cases is demonstrated with the $\beta - kd$ scaling.

resenting, respectively, the most common parameterization used in most wave models and the best performing published parameterization.

The overall performance of the $\beta - kd$ scaling for 1D laboratory cases (scatter index = 9%) is slightly better than for the BJ or Rue models (10% and 12%, respectively). Although this improvement appears insignificant, it is biased by the sloping bottom cases where there is no significant overall improvements with average errors of the models in the range $8\% \leq s.i. \leq 10\%$, implying that the horizontal bottom cases are improved considerably (in fact from ~ 14% to 7%).

For the gentle slopes of Katsardi et al. (2013) and steeper slopes of Smith (2004), we see modest error reductions, from ~ 14% to 12% and ~ 9% to 7%, respectively, with the $\beta - kd$ scaling. However, this is equally diminished by the performance over the remaining sloping bottom cases, particularly over those exhibiting barred beach profiles, i.e., errors increase from ~ 6% for both the Boers (2005) and Battjes and Janssen (1978) data sets to 7% and 10%, respectively. A possible reason may lie in the treatment of negative slopes (see Section 3.4.1).

The improvements for the horizontal laboratory cases are illustrated by significant error reductions of almost 50%. For these cases, by using the $\beta - kd$ scaling the average scatter index fell to 7% from 13% and 15% when using the BJ and Rue models respectively. Most of this improvement comes from error reductions in Jensen (2002) and Katsardi (2007) data sets with decreases of ~ 23% to 8% and ~ 10% to 5%.

It is encouraging to note that over the lakes data set, the calibrated $\beta - kd$ scaling gives significantly smaller errors compared to the BJ model with an error reduction from 16% to 2%. This result is comparable to the performance of the Rue model. The performance of the $\beta - kd$ scaling compared to the lake observations is illustrated in the inset of Fig. A.1 in Appendix A.

In the field cases, the averaged performance of the $\beta - kd$ scaling is shown to be similar to the reference BJ and Rue models with average errors in the range $19\% \leq s.i. \leq 22\%$. The $\beta - kd$ scaling performs better for Guam and Haringvliet with error reductions from 38% (BJ) and 29% (Rue) to 28% and 17% (BJ) and 20% (Rue) to 16% respectively. However, it performs worse for both the sloping Petten and horizontal Amelander Zeegat data sets. In these cases, error increase from ~ 14% to 20% and ~ 15% to 23%, respectively.

3.7. DISCUSSION

The proposed $\beta - kd$ scaling is shown to provide a simple parameterization which improves the modeling skill for the significant wave height over 1D conditions. In particular, it performs well for both locally and non-locally generated waves while being consistent with parameterizations and limits for γ found from previous studies.

The effect of the $\beta - kd$ scaling is twofold. The effect of the bottom slope (i.e., $\beta-$) scaling is to shift from a fixed scaling, i.e., $\gamma_{\beta-kd} = 0.73$ to a value varying between $\gamma_{\beta-kd} = 0.54$ and $\gamma_{\beta-kd} = 1.30$ whereas the effect of the wavenumber (i.e., $\tilde{k}d-$) scaling is to always increase $\gamma_{\beta-kd}$ with increasing $\tilde{k}d$ in intermediate water ($\tilde{k}d >\sim 1$) with no upper limit (until white capping becomes dominant). The physical interpretation of this $\tilde{k}d$-scaling is that it accounts for the inherent differences between non-locally and locally generated waves. For waves arriving from a distant source, for example swell waves at a

reef, $\tilde{k}d <\sim 1$, the waves may be seen as analogous to solitary waves, which are independent of k, and therefore as $\tilde{k}d \rightarrow 0$, $\gamma_{\beta-kd} \rightarrow \gamma_\beta$. For waves locally generated by wind, for example over a lake or tidal flat, $\tilde{k}d >\sim 1$ which corresponds to a relatively high normalized water depth (or wave number). Under these conditions, wind may *indirectly* impact depth-induced wave breaking by changing the spectral shape and therefore the value for $\tilde{k}d$. However, the time scales of these variations are likely to be too short to have a significant impact on depth-induced wave breaking. The physical relevance of the increasing $\gamma_{\beta-kd}$ is to essentially disable depth-induced dissipation in deep water. Of course under such conditions, steepness-induced breaking (white capping) will still continue to limit the wave heights. Therefore under these conditions the impact of wind (the root cause of white capping) cannot be ignored at shallow and intermediate water depths.

The joint scaling encapsulates two different scales for wave breaking. Over relatively shallow water depths where $\tilde{k}d <\sim 1$ e.g. laboratory experiments and near the coast ($d \approx H$), waves will typically be influenced by bathymetric features and therefore the local bottom slope is important. Over locations with greater depth e.g. some distance from the coast ($d \gg H$), waves are less influenced by bottom effects. The expected reduction in depth-induced wave breaking is captured by the kd-scaling. However, under extreme conditions, such as storms, increased wave heights may occur resulting in a reduction of kd. In such conditions, the influence of bottom slope will become important and the scaling of depth-induced breaking will be similar to that found in shallower depths.

However, despite these arguments, for the 2D *field* cases no significant improvements are demonstrated by introducing the $\beta - kd$ scaling. A possible explanation may be in the inherent difference between waves in 1D and 2D conditions. As discussed in Section 3.4.2, the 1D bore analogy is reasonable for laboratory observations. However, for 2D field observations, the inherently short-crested waves are not fully represented by a 1D bore. This discrepancy is most pronounced in the Amelander Zeegat field case where depth-induced refraction causes non-locally generated waves from the North Sea to become focused over and just shoreward of the outer delta. Considering the relative bias for this field case for all the different parameterizations in this study (see Figs. 3.6 and 3.11), a distinct negative bias can be seen for virtually all of them. This suggests that as a wave becomes more short-crested, the observed significant wave height increases and therefore the energy dissipation is reduced.

Further support is provided by a number of studies. Babanin et al. (2011) note, in a hindcast of Typhoon Krosa (2007) in shallow water conditions ($H_{m0}/d \approx 0.63$; $d = 38$ m and $H_{m0} \approx 24$ m), that breaking waves from opposite directions resulted in waves much larger than expected on the basis of the BJ model and suggested that this was due to the large directional spreading of the waves. In this situation, the observed wave field consisted of two modes differing 170° in direction, equivalent to directional spreading of $\sigma_\theta \approx 80°$.

However, Dingemans et al. (1986) and Dingemans (1987) report laboratory experiments in a 2D basin showing a weaker effect with smaller directional spreading. We analyzed two cases (case 25 and 28 in Dingemans, 1987) with wave breaking over a horizontal bar with incident JONSWAP spectrum of 0.1 m significant wave height and with a peak period of 0.8 Hz. The bar reduced the water depth from 0.4 m to 0.1 m over the 2 m wide horizontal bar crest (achieved with a 1 : 20 and 1 : 10 up- and down-slope, respec-

tively) and caused the waves to break and dissipate. However, increasing the observed directional spreading of the incident spectra from $\sigma_\theta \approx 11^\circ$ to $\sigma_\theta \approx 26^\circ$ (the only difference between the two cases), and corresponding to $\sigma_\theta \approx 8^\circ$ to $\sigma_\theta \approx 20^\circ$ over the top of a bar, resulting in an energy dissipation reduction of only ~ 5%. Furthermore, Katsardi (2007) and van Vledder et al. (2013) show with numerical models that wave breaking is somewhat affected by the degree of short-crestedness of the waves in shallow water.

These studies suggest that wave directionality enhances the maximum possible breaking wave height in shallow water, but less so as σ_θ reduces. To investigate this, we apply our extension with wave directionality as described in Section 3.4.2. In Figs. 3.10 and 3.11, we show the results for the reference BJ and Rue models and the $\beta - kd$ scaling. For the reference models, $\sigma^*_\theta = 25^\circ$ was used and for the $\beta - kd$ scaling, $\sigma^*_\theta = 15^\circ$. These optimum values were obtained from computations with $\sigma^*_\theta = 10^\circ, 15^\circ, 20^\circ, 25^\circ$ and 30°.

We thus find that the proposed directional partitioning improves all three models for the Amelander Zeegat data set. Errors decrease from 16% and 14% for the BJ and Rue models to 9% for both, and for the $\beta - kd$ scaling, the errors reduce from 23% to 8%. Almost all of the error reduction is seen in the relative bias which suggests a removal of systematic error. These improvements demonstrate that directional effects, which are not captured by the 1D bore analogy, are significant in complex 2D field cases. In the case of the Amelander Zeegat, over the outer delta, very short-crested waves with $\sigma_\theta >\sim 50^\circ$ occur which are under-predicted by all the models with default settings. By accounting for directional effects, dissipation is reduced for these conditions resulting in a smaller negative bias and improved model performance.

In the remaining field cases (Petten, Haringvliet and Guam), the reference BJ and Rue models are almost insensitive to the directional partitioning whereas some improvements are shown for the $\beta - kd$ scaling. With $\sigma^*_\theta = 15^\circ$, the $\beta - kd$ performs better with an overall average reducing to 11% (from 13%) compared to a mostly unchanged overall average for the reference models of ~ 14%. From Fig. 3.11, the decrease in the magnitude of the relative biases (8% to 2% for field cases) demonstrates that the systematic errors are largely removed.

A possible explanation for the insensitivity of the reference models in the remaining field cases may be seen in how these models were calibrated by the original authors. For calibrating these models, field observations are included which may lead to 2D directional effects being implicitly included, i.e., through higher γ-values. This would then result in larger optimum values for σ^*_θ than if only 1D conditions were considered. In comparison, the $\beta - kd$ scaling is calibrated only over 1D and 1D idealized cases. Therefore, a greater reduction of dissipation is required resulting in a smaller optimum value for σ^*_θ. This provides a consistent explanation for the negative bias seen in the field case verification and the differences over the Petten and Amelander Zeegat cases compared to the reference models.

Wave models are increasingly coupled to circulation models with the resulting radiation stress gradients used to predict wave-induced circulation and set-up. Although much success has been reported in this coupling with wave models where the BJ model is applied (e.g. Dietrich et al., 2012), a number of recent studies have shown this to provide poor modeling skill for currents and set-up. Part of the problem originates from the inflexibility of the BJ model which is constrained to fixed scaling (γ_{BJ}) over the whole

domain. For example Mulligan et al. (2010) show the over-prediction of wave breaking and resulting current velocities over the steep slopes of a rocky shoal (foreslope gradient of the shoal is 1 : 10 over 100 m, and locally 1 : 1) whereas Lowe et al. (2009a) show improved results over a more gently sloping reef-lagoon system when using lower constant scaling coefficient $\gamma_{BJ} = 0.64$. We expect that our joint parameterization will improved the performance of coupled models to predict wave-induced currents and set-up. Over steep bathymetries, the $\beta - kd$ scaling increases the ratio between the characteristic maximum wave height over local depth with increasing slope which would reduce the over-predictions demonstrated by Mulligan et al. (2010). Over the gentler slopes of the reef-lagoon cases of Lowe et al. (2009a,b), the reef slope was $\sim 1:60$. From the $\beta - kd$ scaling, this yields a value of $\gamma_{\beta-kd} \approx 0.67$ for non-locally generated waves (low kd) which is in close agreement with the value used by Lowe et al. (2009a) in their simulations. Further support for the applicability of a lower value for γ_{BJ} in reef cases is shown by the results over the Guam reef cases in Figs. 3.10 and 3.11 by the reduced underestimation over the relatively horizontal bathymetries.

In conclusion, the $\beta - kd$ scaling, while accounting for directional partitioning, provides significant improvements over a wide range of 1D and 2D wave conditions, particularly over horizontal bathymetries. In the laboratory cases, errors are reduced to an average error between 5% and 12% compared to 5% and 21% for the BJ model and 7% and 26% for the Rue model. This improvement demonstrates the applicability of the $\beta - kd$ scaling for non-locally generated 1D cases including significant improvements for observations of wave breaking over horizontal bathymetries. With directional partitioning, improvements are shown for the field cases with the average errors between 8% and 27% compared to 15% and 38% for the BJ model and 13% and 29% for the Rue model. This improvement comes from both the joint scaling and the directional partitioning, particularly over horizontal bathymetries.

The main advantage of the proposed parameterization is that it combines two concepts which have been predominant in the depth-induced wave breaking literature i.e., a dependency on β and a dependency on kd in a simple expression. This scaling is consistent with our current physical interpretation for depth-induced breaking. For conditions where kd is low, the waves can be considered to converge on solitary wave behavior. The lower limit $\gamma_0 = 0.54$ is consistent with theoretical limits for the crest height of solitary waves (see Appendix 3.A). For high kd conditions, the physical interpretation of a reduction of wave nonlinearity (e.g. van der Westhuysen, 2010) is also captured by the positive dependency with kd which acts to reduce depth-induced breaking. Finally, the directional partitioning provides an adjustment for the 2D nature of 'real' wave fields and is shown to provide improvements for both the proposed joint scaling as well as the reference models.

The implication of this work is that attention is required when developing dissipation models based on the 1D analogy and calibrating over 2D field cases. It may be also noted that similar tendencies have been demonstrated in greater detail for deep water waves (e.g. Onorato et al., 2009; Latheef and Swan, 2013) with regards to directionality. Such work may be applicable in our understanding of *shallow* water wave evolution and may potentially result in new source terms which inherently include wave directionality. This work was built upon a large proportion of the parametric wave breaking literature,

and although such work can provide useful insights towards wave modeling, future research needs to focus more on third-generation wave modeling i.e., source terms of a non-parametric or first-principles nature, and the detailed balance between the various source terms. With the increased recognition of the importance of breaking waves at the surf zone interface and the increased use of coupled models, better source terms for shallow water wave physics are still needed. Although both the $\beta - kd$ scaling and directional partitioning provide a better parametric representation of this, they are both still heuristic and require further substantiation with theory and empirical evidence.

ACKNOWLEDGEMENTS

We greatly appreciate receiving the details of the laboratory observations of Jane Smith of the Coastal and Hydraulics Laboratory, US Army Engineer Research and Development Center in Vicksburg (USA). We are equally grateful to the partners of the LOWISH project (Limits on Waves in Shallow Water; a joint initiative project of British Petroleum, Chevron, ConocoPhillips, Shell, Total and Woodside) who provided us with the observations of Imperial College. We thank in particular Kevin Ewans of Shell International Exploration and Production B.V. in The Hague for his assistance and acknowledge with pleasure that these observations were made by Chris Swan and Vanessa Katsardi of Imperial College. The authors also thank Pieter Smit and the anonymous reviewers for their constructive comments and suggestions. The first author (J.S.) is financially supported by the US Office of Naval Research under Grant N00014-10-1-0453 and Grant N00014-12-1- 0534.

APPENDICES

3.A. DEPTH-INDUCED WAVE BREAKING MODELS

Here we provide a summary of the parameterizations of depth-induced breaking that have been assessed in the present study. It is not our purpose here to provide an extensive review; such reviews can be found in e.g. Rattanapitikon (2007) and Apotsos et al. (2008).

3.A.1. THE BATTJES-JANSSEN MODEL

The Battjes–Janssen model assumes $H_{max} \approx d$ which results in a bulk dissipation:

$$\varepsilon_{BJ} = -\frac{1}{4}\alpha_{BJ}\bar{f}Q_b\rho g H_{max}^2 \tag{3.A1}$$

where α is a tunable coefficient of $O(1)$, $\bar{f} = f_{m01}$ and Q_b is the fraction of breakers:

$$\frac{1-Q_b}{lnQ_b} = -\left(\frac{H_{rms}}{H_{max}}\right)^2 \tag{3.A2}$$

The bulk dissipation is scaled with $\gamma_{BJ} = H_{max}/d$; the simplest scalings are given by:

- Battjes and Janssen (1978): $\gamma_{BJ} = 0.80$
- Nelson (1985, 1987, 1994a,b, 1997): $\gamma_{BJ} = 0.55$
- *SWAN et al.: $\gamma_{BJ} = 0.73$

*Formulations used in this study are indicated here and below with an asterisk (*).

Nelson (1985, 1987, 1994a,b, 1997) has long advocated $\gamma_{BJ} = 0.55$ for waves over horizontal bathymetries in (very) shallow water. Such low values ($0.45 < \gamma_{BJ} < 0.65$) for irregular waves are supported by a variety of field and laboratory observations (e.g. Keating et al., 1977; Tucker et al., 1983; Riedel and Byrne, 1986; Hardy et al., 1990; Sulaiman et al., 1994; Hardy and Young, 1996; Moritz, 2001). Katsardi (2007) shows with numerical experiments that for irregular waves in finite depth water over a horizontal profile, $\gamma_{BJ} = 0.54$. Horikawa and Kuo (1966, their Figs. 5 and 3 as analysed by Dally et al., 1985) find $\gamma_{BJ} \approx 0.25$.

Massel (1998) gives theoretical support for $\gamma_{BJ} \leq 0.55$. In very shallow water, a wave in an irregular wave field may behave as a solitary wave. The theoretical limit for the *crest* height of a solitary wave over a horizontal profile has been variously estimated from $\eta_{crest} = 1.78d$ (McCowen, 1894) to $\eta_{crest} = 1.86d$ (Longuet-Higgins, 1974) where d is the far field depth (i.e., undisturbed by the waves). If we take the average depth $\bar{d}$ to lie half way between the trough elevation $\eta_{trough} = d$ and the crest elevation $\eta_{crest} = \beta d$ (Seyama and Kimura, 1988; Kamphuis, 1991), then $H/\bar{d} = \left[\beta - 1\right] / \left[1 + \left(\beta - 1\right)/2\right]$. This

yields $1.78 \leq \beta \leq 1.86$, so $0.56 \leq H/\bar{d} \leq 0.60$. A low value of $\gamma_{BJ} = 0.50$ was also found to be needed on a relatively steep beach (slope $\sim 1:38$) in the SWAN computations of Gorrell et al. (2011).

Several dependencies on bottom slope have been suggested based on a suggestion of Madsen (1976) for regular waves. His expression was modified by Ostendorf and Madsen (1979) to include wave-steepness induced breaking and subsequently modified by Rattanapitikon and Shibayama (2000). Although these scalings have been applied to irregular waves e.g. Black and Rosenberg (1992), Gonzalez-Rodriguez (2006) and Zheng et al. (2008), due to their inclusion of steepness-induced breaking (i.e. white capping), they are not applicable to our study.

- *Madsen (1976): $\gamma_{BJ} = 0.76\left(1 + 6.4 tan\beta\right)$
- Ostendorf and Madsen (1979, reduced): $\gamma_{BJ} = \begin{cases} 0.8 + 5 tan\beta & tan\beta < 0.1 \\ 1.3 & tan\beta \geq 0.1 \end{cases}$
- Rattanapitikon and Shibayama (2000): $\gamma_{BJ} = 0.91 + 5.01 tan\beta - 11.21 tan^2\beta$
- *Tajima and Madsen (2002): $\gamma_{BJ} = 0.3 + 4 tan\beta$

All these formulations suggest a positive dependency with a lower limit over a horizontal profile between $0.3 \leq \gamma_{BJ} \leq 0.91$. It may be noted, without further comment, that Raubenheimer et al. (1996) find for the ratio of *significant* wave height over depth, on the basis of field observations, a similar positive trend with bottom slope $\gamma_s = H_{m0}/d = 0.2 + 5.98 tan\beta$.

Although we did not find scalings of the form $\gamma_{BJ}\left(k_p d\right)$ in the literature, the laboratory observations of irregular waves over a $1:35$ slope of Ting (2001, his Fig. 6) demonstrated an almost linear increase of γ_{BJ} (from 0.43 to 1.21) with $k_p d$ (from 0.253 to 0.735; see Fig. A.1). Our least-squares best-fit gives a range of $0.56 \leq \gamma_{BJ} \leq 1.29$.

- *Ting (2001): $\gamma_{BJ} = 0.17 + 1.53 k_p d$

3.A.2. THE THORNTON–GUZA MODEL

The Thornton–Guza model shifts the Rayleigh distribution for the breaking waves to higher wave heights with a weighting function $W_{TG}(H)$:

$$W_{TH}(H) = M_{TG}\left\{1 - exp\left[-\left(\frac{H}{\gamma_{TG} d}\right)^2\right]\right\} \leq 1 \tag{3.A3}$$

where $M_{TG} = \left(H_{rms}/\gamma_{TG} d\right)^2$. The bulk dissipation is then given as:

$$\varepsilon_{TG} = -\frac{3\sqrt{\pi}}{16} \alpha_{TG} \bar{f} \rho g \frac{H_{rms}^3}{d} M_{TG} \left[1 - \frac{1}{\left(1 + \left(H_{rms}/\left(\gamma_{TG} d\right)\right)^2\right)^{5/2}}\right] \tag{3.A4}$$

Most scalings for γ_{TG} depend on β:

- Thornton and Guza (1983): $\gamma_{TG} = 0.42$

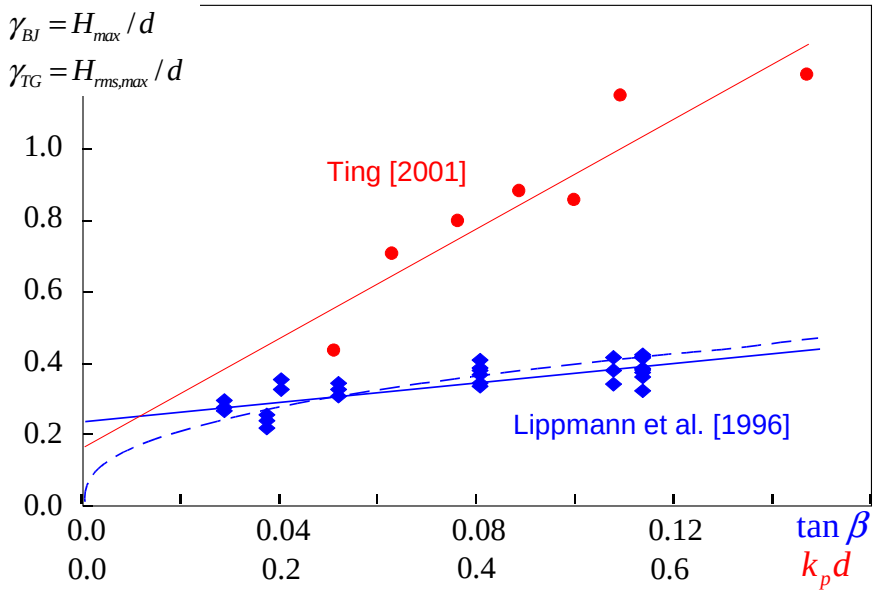

Figure A.1: The approximation by the present authors of the γ_{BJ} estimates of Ting (2001) as a function $k_p d$ (for $tan\beta = 1/35$; solid red line) and the γ_{TG} estimates of Lippmann et al. (1996) as a function of $tan\beta$ (for $0.09 < k_p d < 0.42$; solid blue line). The power relationship with local bottom slope approximation of Lippmann et al. (1996) for γ_{TG} is also presented for reference (dashed blue line).

- *Sallenger Jr. and Holman (1985): $\gamma_{TG} = 0.3 + 3.2tan\beta$
- *Sallenger Jr. and Howd (1989): $\gamma_{TG} = 0.24 + 2.7tan\beta$
- *Lippmann et al. (1996): $\gamma_{TG} = 0.23 + 1.42tan\beta$

Thornton and Guza (1983) find (on average) that $\alpha_{TG} \approx 0.5$ for laboratory conditions and $\alpha \approx 3.4$ for field conditions. Whitford (1988) finds $\alpha_{TG} \approx 0.98$ (average from his Figs. 50–52) from calibrating the expression of Sallenger Jr. and Holman (1985) to his γ_{TG} field observations using his modified conditional probability of breaking. However, Sallenger Jr. and Howd (1989) find ~ 20% lower values in their additional observations. Rattanapitikon (2007, his Table 3) finds in his calibration study very different values $\gamma_{TG} = 0.168$ and $\alpha_{TG} = 0.10$. With calibrated γ_{TG} values, Lippmann et al. (1996) predict the H_{rms} through the surf zone with practically the same error as the original Thornton and Guza (1983) model with $\alpha_{TG} = 1.0$ and calibrated γ_{TG} values. Lippmann et al. (1996) provides an approximation of $\gamma_{TG} = tan^{0.4}\beta$ with $\alpha_{TG} = 1.0$. We approximate this with a least-square linear fit (see Fig. A.1) to avoid $\gamma_{TG} = 0$ over horizontal bathymetries. Using linear wave theory, we infer that these observations (Lippmann et al., 1996, their Fig. 2 and Table 1) were made for the range $0.09 < k_p d < 0.42$.

3.A.3. THE BALDOCK ET AL. MODEL

Baldock et al. (1998) provide an explicit expression for Q_b:

$$Q_b = exp\left[-(H_b/H_{rms})^2\right] \tag{3.A5}$$

and an expression for the bulk energy dissipation, originally formulated as:

$$\varepsilon_B^* = -\frac{\alpha_B}{4}\bar{f}\rho g H_{rms}^2\left(1+R^2\right)exp\left[-R^2\right] \tag{3.A6}$$

but later corrected by Janssen (2006), Janssen and Battjes (2007) and Alsina and Baldock (2007) to:

$$\varepsilon_B = -\frac{3\sqrt{\pi}}{16}\alpha_B\bar{f}\rho g \times \frac{H_{rms}^3}{d}\left[1+\frac{4}{3\sqrt{\pi}}\left(R^3+\frac{3}{2}R\right)exp\left[-R^2\right]-erf\left(R\right)\right] \tag{3.A7}$$

in which $R = H_b/H_{rms}$. In the original work, the expression by Nairn (1990) was used, however due to its dependency on deep water wave steepness, it is not suitable for our purposes. The only scaling we found applicable was:

- *Ruessink et al. (2003): $\gamma_B = 0.29 + 0.76k_p d$

This scaling is based on a large number of field cases and inverse modeling. These γ_B values ($0.48 \leq \gamma_B \leq 0.86$) over the experimental range $0.25 \leq k_p d \leq 0.75$) are considerably lower than the γ_{BJ} values of Ting (2001) which were taken over virtually the same $k_p d$ range. This is remarkable as nominally both γ_{BJ} and γ_B are the upper limit of the non-breaking (irregular) waves, but then, one data set was calibrated with field observations and the other was directly observed in a laboratory flume.

Raubenheimer et al. (1996) found a better fit with their observations by adding a $k_p d$ dependency: $\gamma_s = 0.19 + 1.05 tan\beta / (k_p d)$. Sénéchal et al. (2001) also found a similar inverse trend but with considerably higher γ_s values. This is opposite to the trend found in Ting (2001) and Ruessink et al. (2003), however these observations relate to individual wave heights and not to the significant wave height.

3.A.4. THE DALLY ET AL. / RATTANAPITIKON MODEL

Rattanapitikon et al. (2003a, their Eq. 28) gives an expression for bulk dissipation which does not depend on deep water parameters:

$$\varepsilon_D = -\frac{K_1 c_g \rho g}{8d}\left[H_{rms}^2 - H_{rms,st}^2\right] \tag{3.A8}$$

in which c_g is the group velocity of the peak frequency (W. Rattanapitikon, pers. comm., 2012). We use Rattanapitikon (2007, his M37 model) to scale the dissipation with $\gamma_D = H_{rms.st}/d = 0.266$ as this is shown on that study to be the best performing model suitable for 2D spectral wave models.

3.B. SPECTRAL DISTRIBUTION FOR THE BULK DISSIPATION

In all parameterizations, apart from the implementation of Filipot and Ardhuin (2012), the source term for depth-induced breaking is taken as proportional to the spectral density[1]:

$$S_b(\sigma,\theta) = \frac{\varepsilon_b E(\sigma,\theta)}{\rho g E} \tag{3.B1}$$

Support for this spectral distribution is given by the observations of Beji and Battjes (1993) who observed that the *shape* of the wave spectrum seems to be unaffected by wave breaking. This seems to be inconsistent with the change of the spectrum during breaking. Initially, at the outer edge of the surf zone, higher harmonics of the spectral peak are generated, evident as secondary peaks, but deeper in the surf zone, these peaks typically disappear and the tail of the spectrum becomes featureless (Smith, 2004; Kaihatu et al., 2007, 2008). Such evolution seems to be almost entirely due to triad wave–wave interactions (Herbers et al., 2000) and not the breaking process. Even if the spectral distribution of Eq. (3.B1) is only approximately correct, triad wave–wave interactions will force the universal shape of the tail (Chen et al., 1997; Eldeberky, 2011). There are strong indications that the dissipation is actually proportional to σ^2 (Mase and Kirby, 1992; Kaihatu and Kirby, 1995; Kirby and Kaihatu, 1996; Chen et al., 1997). However, we consider these issues to be outside the scope of this paper as we are mostly concerned with the bulk dissipation (the prediction of the significant wave height) which is virtually independent of the spectral shape.

To verify the insensitivity between the proposed parameterization in this paper and the triad source term used, we also calibrated and verified our parameterization with the triad source term switched off (not shown). Over the verification data sets, the differences in model performance for the prediction of H_{m0} was negligible.

[1] Modified to be consistent with Chapter 2.

4

MODELLING DEPTH-INDUCED WAVE BREAKING OVER COMPLEX COASTAL BATHYMETRIES

James SALMON, Leo HOLTHUIJSEN

The correct representation of depth-induced wave breaking is important for understanding coastal morphology and for design and management in the coastal zone. Although numerous studies have demonstrated the applicability of a constant scaling of the Battjes and Janssen (1978) dissipation model for depth-induced breaking, recent studies have shown its inability to sufficiently reproduce wave dissipation over complex field cases. In the present study, we contrast the application of such a constant scaling to two alternative wave breaking parameterizations with a variable scaling based on either the wave nonlinearity (the φ parameterization) or on both bottom slope and normalized wavelength supplemented with wave directionality (the $\beta - kd$ parameterization). We consider three field data sets characteristic of a simple beach-bar profile, a bay partially protected by a shoal and a complex intertidal region. We demonstrate that in these cases the $\beta - kd$ parameterization provides a better alternative to the use of a constant scaling or the φ parameterization. To illustrate the operational consequences, we up-scale the conditions over the case of the intertidal region to correspond to design conditions for the Dutch coast (storm conditions with a 4000 year return period). Under these extreme conditions, for *locally* generated waves both the $\beta - kd$ and φ parameterizations predict qualitatively similar increased significant wave heights but the $\beta - kd$ parameterization increased the waves twice as much as the φ parameterization. Under other conditions, when *non-locally* generated waves (swell) dissipates over a gently sloping bottom, the $\beta - kd$ parameterization predicts lower significant wave heights compared to either the constant scaling or φ parameterization.

This chapter has been published as SALMON, J.E. and HOLTHUIJSEN, L.H. (2015). Modeling depth-induced wave breaking over complex coastal bathymetries. *Coastal Engineering*, **105**, pp. 21–35.

4.1. INTRODUCTION

Depth-induced wave breaking is one of the most dominant hydro-dynamic processes occurring in the coastal region. It not only controls the amount of wave energy impacting our coastlines and coastal defenses, but also plays a crucial role in driving many nearshore processes such as sediment transport, bottom morphology (Hoefel and Elgar, 2003) and turbulence (which has been shown to be important for the local ecology; Feddersen, 2012). Wave breaking also induces radiation stresses which drive wave-induced set-up and currents (Longuet-Higgins and Stewart, 1964), both of which are of importance for coastal engineering design and management. However, despite the importance and relevance towards our knowledge of wave hydrodynamics, depth-induced wave breaking is still poorly understood partially due to its highly nonlinear nature and is therefore heavily parameterized in most wave models.

For the prediction of various wave parameters in finite water depth, phase-averaging stochastic spectral wave models based on an action (or energy) balance (e.g. Komen et al., 1984; WAMDI Group, 1988; Holthuijsen, 2007; WISE Group, 2007) are used on an operational basis. Under the assumption that the wave field can be modeled as a stationary Gaussian process, a number of statistical parameters such as significant wave height, defined as the average wave height of the highest one-third waves (Longuet-Higgins, 1952) can be estimated from the wave spectrum (see Section 2.4). Although it can be argued that phase-resolving models of the Boussinesq-type (e.g. Peregrine, 1967; Lynett, 2006) or non-hydrostatic type (e.g. Zhou and Stansby, 1998; Zijlema et al., 2011) may be more applicable for resolving nonlinear processes such as wave breaking, in practice, such models are constrained for larger areas ($> 1 \times 1$ km^2, say) by computational expense and inability to account for wave generation by wind.

Extensive research has therefore been carried out into the parameterization of dissipation due to depth-induced breaking for spectral wave models (e.g. Battjes and Janssen, 1978; Thornton and Guza, 1983; Baldock et al., 1998) and the scaling of these dissipation models (e.g. Battjes and Stive, 1985; Rattanapitikon and Shibayama, 2000; Ruessink et al., 2003; Apotsos et al., 2008, and many others). Despite fundamental shortcomings of using these source terms, which are at best quasi-linear, these dissipation models have been used with considerable success. In particular, the use of the Battjes and Janssen (1978) dissipation model in combination with a fixed calibration parameter $\gamma_{BJ} = 0.73$ (the ratio of maximum possible individual wave height to local depth) has been shown to be effective, particularly over sloping beach profiles (e.g. Salmon et al., 2015). It is therefore often the default parameterization for depth-induced wave breaking in spectral wave models, even in third-generation wave models in which many of the other processes affecting the waves are considerably better founded in theory and observations (e.g. WAMDI Group, 1988).

However, although effective, this parameterization does not provide much physical insight towards our understanding of irregular wave breaking over varying bathymetry. Furthermore, it has been reported that even a calibrated constant γ_{BJ} is unable to always give optimum results (Apotsos et al., 2008; van der Westhuysen, 2010). In particular, the commonly used value $\gamma_{BJ} = 0.73$ has been shown to consistently overestimate the dissipation of *locally* generated waves over horizontal bathymetries (e.g. de Waal, 2001; Bottema and Beyer, 2002; van Vledder et al., 2008) while underestimating the dissipation

for *non-locally* generated waves (e.g. Nelson, 1997; Katsardi, 2007).

The focus of this study is to analyze the effect of bottom topography and local wave characteristics for the prediction of depth-induced wave breaking by considering two recent alternative parameterizations with variable scalings, proposed by van der Westhuysen (2009, 2010) and Salmon et al. (2015). These parameterizations are considered as they represent the most recent formulations which have been shown to provide improved model performance for the depth-induced breaking under *locally* generated wave conditions (e.g. Salmon et al., 2015). These improvements are expected to be important for representing complex coastal regions as well as for design conditions. Here, we analyze the differences between these alternatives compared to $\gamma_{BJ} = 0.73$ to predict the significant wave height and address the implications of their use for coastal applications. We consider three data sets representing coastal systems of increasing complexity, namely a fairly simple beach-bar profile (Petten); a bay partially protected by a shoal (Haringvliet) and a complex intertidal region with a number of characteristic coastal features such as tidal channels and extended shoals (Amelander Zeegat). Finally, we scale the boundary conditions for three cases over the Amelander Zeegat to represent a hypothetical 1:4000 year storm corresponding to Dutch design conditions for coastal defenses.

Here, we demonstrate that both alternatives perform better than $\gamma_{BJ} = 0.73$ for the prediction of significant wave height of locally-generated waves. Furthermore, in our up-scaled storm over the Amelander Zeegat, we show significant differences in using the two alternatives with higher waves predicted by both parameterizations over intertidal areas dominated by *locally* generated waves and lower waves by the parameterization of Salmon et al. (2015) for *non-locally* generated waves (swell) over gently sloping slopes.

This paper is organized as follows. In Section 4.2, we outline the field cases and methodology and in Section 4.3, we present the host wave model and introduce the three breaking parameterizations. The results of our comparison study is presented in Section 4.4 where we first show the performance of using $\gamma_{BJ} = 0.73$ and then compare and contrast this to the alternative parameterizations. We discuss the implications, particularly for design conditions, in Section 4.5 and finally present our conclusions in Section 4.6.

4.2. FIELD OBSERVATIONS

To provide an objective comparison between the default and alternative parameterizations, they are applied to three separate field data sets. Each data set consists of a number of cases considered to be stationary. Together they cover a wide range of wave conditions including locally (wind-sea) and non-locally (swell) generated waves, over a variety of bathymetric profiles including a gently sloping beach, a near-horizontal shoal and an intertidal region.

4.2.1. PETTEN (1995 AND 2002) OBSERVATIONS

The Petten site is located off the west coast of the Netherlands near the town of Petten (Figure 4.1). The location represents a gently sloping beach profile with a large offshore shoal with a minimum depth of ~ 5.7 m and a smaller nearshore bar with a minimum depth of ~ 4.0 m. Wave conditions were measured along a transect normal to the beach

with three to five instruments depending on when the observations were taken (shown in magenta (×) in Fig. 4.1A). Following a hindcast study to investigate the performance of the wave model SWAN (Booij et al., 1999; see Section 4.3.1) under instationary conditions (Groeneweg et al., 2003), a number of instances, typically four per storm, were chosen representing variations in the tide and development of the storm. Over the selected 21 cases, the offshore significant wave height varied between $3.0 < H_{m0} < 6.7$ m and the offshore mean wave period varied between $4.2 < T_{m01} < 9.9$ s as provided in Table 4.1. Computations were carried out in the frequency range between 0.03 Hz to 0.5 Hz with 31 discrete frequencies. Groeneweg et al. (2003) used similar settings in their hindcast but with an upper frequency limit of 0.8 Hz. We modified our frequency range to be consistent with the constraint for the DIA ($\Delta f = 0.1 f$; see Section 4.3.2). However, in a sensitivity analysis, this difference was found to be negligible.

For the 1995 storms, a fine inner computational grid over the region shown in Figure 4.1A is nested within a coarser outer grid to calculate the spectral boundary conditions for the inner grid. The outer grid uses 2D spectra inferred from a directional Waverider buoy located approximately 5 km north-west (shown as an empty dot in Fig. 4.1D) of the directional Waverider buoy which provides the boundary conditions for the 2002 campaign (shown in red in Fig. 4.1A). The same inner grid is applied for the 2002 campaign with no need for nesting.

For the 1995 storms, wind speeds are estimated from three wind measurement locations in the vicinity of Petten (Texalhors, TXH; Noordwijk, MPN and K13; see Fig. 4.1D) to estimate the wind variation both along the coast and perpendicular to it. For the 2002 storms, digital wind fields were available and only two locations (TXH and IJmuiden Semafoor; YMS) were used to scale the computed wind speeds. Although this latter technique provides a wind field with more structure, the effect on the wave hindcasts cannot be verified. However, small differences in the computed H_{m0} error between the 1995 and 2002 storm hindcasts (Groeneweg et al., 2003, their Table 4.4a) indicate that both storms are predicted with similar error and can be combined into a single data set. A two-dimensional circulation model (WAQUA) was used in an independent study to compute both the water level and depth-averaged current fields for all storms (Groeneweg et al., 2003). Bathymetric data was obtained from measurements made between 1996 and 1997 and supplemented with transect measurements taken in September to November 1994 and in February and November 2002.

4.2.2. HARINGVLIET (1982) OBSERVATIONS

The Haringvliet represents a 10 km × 10 km bay in the south-west of the Netherlands which is partially protected from the southern North Sea by a fairly flat shoal (the 'Hinderplaat') extending across half of its entrance. In the considered area, the water depth varies between 4 and 6 m with a depth over the Hinderplaat varying between 1.0 and 2.2 m (Fig. 4.1B). The up-slope of the shoal in the mean wave direction varies from 1 : 500 to horizontal (at the shoal crest).

Waves were measured at various locations around the shoal with six buoys and one wave gauge, excluding the deep water buoy used to provide the boundary conditions (shown with a red dot in Fig. 4.1B). Four cases during a storm on the 14th October 1982 representing conditions with a stationary wind field and relatively high waves were cho-

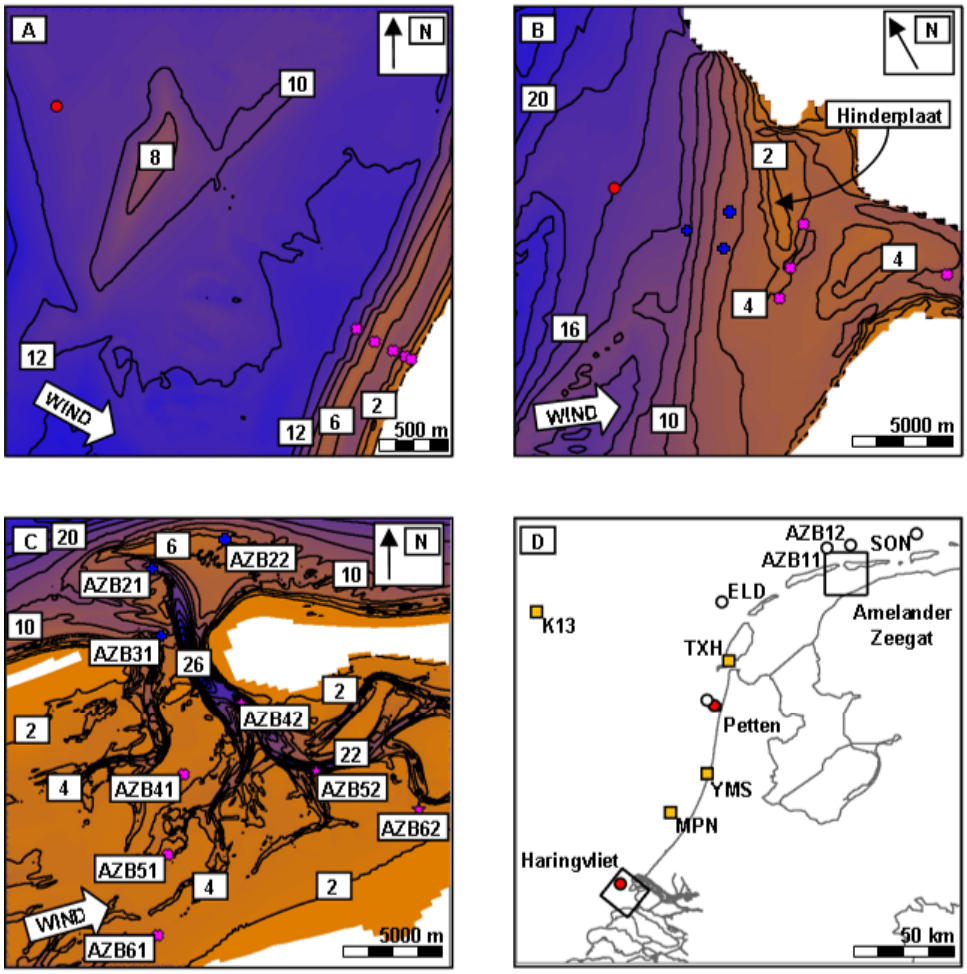

Figure 4.1: Bathymetry for Petten (A), Haringvliet (B) and Amelander Zeegat (C) given at +1 m above Amsterdam Ordnance Datum (NAP) with the regions indicated along the Dutch coastline shown in Panel D. Contour lines are shown at 2 m intervals. All buoys used to provide the boundary conditions are indicated with a red dot or an empty dot in Panel D. For the Petten 1995 campaign, the buoy used for the boundary conditions is located 4.8 km NW from that shown in Panel A for the Petten 2002 campaign. For the Amelander Zeegat 2007 campaign, boundary conditions for waves from the west and east are provided by the ELD and SON buoys located, respectively, 65 km WSW and 40 km ENE from the tidal inlet. Boundary conditions for the northern boundary are provided by buoys AZB11 and AZB12 located, respectively, 5 km NW from AZB21 and NNE from AZB22. The seaward measurement location subsets are indicated in blue (+) whereas the shoreward locations are indicated in magenta (×). In Panel C, the shoreward intertidal measurement locations are further differentiated into × for the western transect and * for the eastern transect. Wind measurement locations used for the Petten data set are indicated in Panel D as orange squares.

Table 4.1: Cases for Petten, Haringvliet and Amelander Zeegat. Times are given in Coordinated Universal Time (UTC)+01:00. Wind velocity, $U_{w,10}$ and direction, θ_w are averaged over the entire computational domain. The subscript $_0$ relates to the averaged offshore significant wave height, H_{m0} and mean wave period, T_{m01}. This is taken at the ELD and YMW buoys for Petten, at the deep water buoys for Haringvliet and at the ELD and SON buoys for Amelander Zeegat. Current velocity, U_c and direction, θ_c is taken at the most shoreward buoy location from the Petten 1995 campaign for Petten and at buoy location AZB42 for Amelander Zeegat.

Case	***Date***	***Time***	$\mathbf{U_{w,10}}$	θ_w	$\mathbf{H_{m0,0}}$	$\mathbf{T_{m01,0}}$	$\mathbf{U_c}$	θ_c
Reference		***UTC +01:00***	**[m/s]**	**[°N]**	**[m]**	**[s]**	**[m/s]**	**[°N]**
Petten								
P95_01	01 Jan. 1995	01:00	12.5	335.4	2.99	6.57	0.0	280.0
P95_02		02:00	11.8	335.4	3.42	6.88	0.2	283.2
P95_03		06:40	14.7	324.3	4.96	8.02	0.3	98.1
P95_04		10:00	13.9	325.3	5.47	8.96	0.2	102.7
P95_05	02 Jan. 1995	04:20	15.7	335.7	6.48	9.90	0.2	276.4
P95_06		14:40	14.2	353.9	5.03	8.80	0.0	100.0
P95_07		16:40	12.7	370.4	4.58	8.74	0.2	280.0
P95_08		21:20	9.7	366.7	3.62	7.87	0.3	102.1
P95_09	10 Jan. 1995	09:20	14.1	308.1	5.56	9.45	0.1	280.0
P95_10		11:20	12.6	305.1	4.96	8.72	0.1	273.5
P95_11		16:20	10.6	293.6	3.69	8.16	0.2	103.2
P95_12		20:20	4.0	279.4	3.04	8.02	0.0	100.0
P02_01	23 Feb. 2002	07:20	17.3	266.0	4.78	7.55	0.1	109.2
P02_02		10:20	14.8	273.7	4.83	7.26	0.2	280.0
P02_03		13:20	15.9	276.1	5.03	7.28	0.2	276.9
P02_04		19:20	15.6	299.3	4.63	7.51	0.1	100.0
P02_05	26 Oct. 2002	07:00	18.5	262.9	4.96	5.61	0.3	276.2
P02_06	27 Oct. 2002*	06:00	14.7	193.8	3.91	4.23	0.3	281.9
P02_07		11:00	20.9	227.9	3.87	5.66	0.2	276.5
P02_08		14:20	24.8	246.7	5.50	6.75	0.2	280.0
P02_09		17:00	22.7	272.7	6.70	6.88	0.4	277.3
Haringvliet								
H82_01	14 Oct. 1982	21:00	12.0	261.2	3.19	6.70	-	-
H82_02		22:00	17.0	261.2	3.19	6.72	-	-
H82_03		23:00	14.0	261.2	3.56	6.65	-	-
H82_04	15 Oct. 1982	00:00	15.0	261.2	3.53	6.95	-	-
Amelander Zeegat								
A07_01	11 Jan. 2007	22:00	17.9	275.0	4.76	7.41	0.1	9.2
A07_02		22:40	18.8	279.0	4.98	7.55	0.4	305.4
A07_03	18 Jan. 2007	12:20	21.1	233.0	3.64	6.23	1.2	129.6
A07_04		14:00	20.2	263.0	4.09	6.83	0.9	129.0
A07_05		17:20	20.3	267.0	4.49	6.92	0.7	304.2
A07_06		20:40	18.9	274.0	4.57	6.98	0.5	131.5
A07_07	19 Mar. 2007	10:00	13.8	279.0	3.56	6.51	0.0	192.2
A07_08		14:40	18.1	266.0	5.23	8.09	1.2	129.8
A07_09		15:40	17.9	271.0	5.60	8.48	0.8	129.0
A07_10		17:00	17.1	268.0	5.51	8.30	1.0	306.2

*Offshore parameters were only available at YMW, T_{m01} values are estimated from T_{m-10} (see Section 2.4).

sen as provided in Table 4.1 (Ris et al., 1999). During this period, the incident significant wave heights generated by an offshore north-westerly wind varied between $3.2 < H_{m0} < 3.6$ m with a mean wave period varying between $6.7 < T_{m01} < 7.0$ s. Computations were carried out in the frequency range between 0.05 Hz to 1.0 Hz with 32 discrete frequencies (Ris et al., 1999). With the estimated tidal currents < 0.25 m/s (from tide tables) mostly orthogonal to the waves, current effects are considered to be negligible.

Comparisons of observations made both in front of and behind the Hinderplaat suggest that depth-induced breaking occurs over the shoal. Therefore, in our analysis we distinguish between observations made seaward ($d \geq 6$ m) and shoreward ($d < 6$ m) from the Hinderplaat. These observation locations are shown in Figure 4.1B in blue (+) for the seaward locations and magenta (×) for the shoreward location. This distinction permits a less biased statistical analysis of the depth-induced dissipation which would otherwise be affected by observations of typically larger non-breaking waves in deeper water.

4.2.3. AMELANDER ZEEGAT (2007) OBSERVATIONS

The Amelander Zeegat represents a relatively protected tidal inlet of the Wadden Sea in the southern North Sea with a depth of ~ 30 m between the barrier islands of Terschelling to the west and Ameland to the east. The inlet is characterized with a seaward ebb tidal delta with a main inlet which branches off into a complex network of smaller tidal channels. Shoreward of the barrier islands (extending 15 km towards the mainland of the Netherlands) is a relatively flat and shallow intertidal area (tidal range between 0 and 3 m) featuring numerous shoals and channels. Seaward of the barrier islands, the bathymetry can be considered to be a beach-bar profile with a typical slope between 1 : 30 to 1 : 60.

In this study, 10 cases considered representative of depth-limited conditions with high stationary wind speeds are taken from previous studies (Lansen et al., 2007; van der Westhuysen, 2010) and represent conditions with offshore significant wave heights of $3.6 < H_{m0} < 5.6$ m and mean wave period of $6.2 < T_{m01} < 8.5$ s as provided in Table 4.1. Computations were carried out in the frequency range 0.03 Hz to 1.0 Hz with 38 discrete frequencies Lansen et al. (2007). Waves were measured with 14 buoys, 12 of which are located along two more-or-less parallel arrays east and west of the main channel and continuing on to the flats. A coarse outer grid is used to provide the boundary conditions for the east and west boundary of a finer inner grid from the deep water buoys ELD and SON. Boundary conditions for the northern boundary of the finer grid are provided by AZB11 and AZB12 (not shown in Fig. 4.1C). Of the remaining 10 buoys, AZB32 was mostly unavailable and therefore we only analyze observations taken at the remaining nine buoy locations shown in Figure 4.1C.

The water level and current fields used were computed with the Delft3D circulation model and calibrated with measured water levels (van der Westhuysen and de Waal, 2008). A uniform wind field is assumed from the average measured values taken at three wind measuring sites near the measurement location (Hoorn, Huibertgat and Lauwersoog). Bathymetries were obtained from a number of depth soundings taken over the period between 1996 to 2006.

To focus on the different dependencies of the wave breaking parameterizations con-

sidered, we subdivide the Amelander Zeegat observations by geographical region. The ebb tidal delta shelters much of the intertidal area from the wave energy coming from the North Sea (van der Westhuysen, 2012) and divides the region seaward of the tidal inlet, which is swell dominated, from the wind-sea conditions found over the intertidal region shoreward of the tidal inlet. It is evident from Figure 4.1C that over the intertidal region the bathymetry over the western transect is different to that over the eastern transect. The western region is more characteristically represented as a tidal flat with shallow horizontal depths of $d \approx 2$m whereas the eastern region is more complex with deeper regions due the presence of tidal channels. It is therefore likely that waves in this region are affected by other processes such as wave-current interactions in addition to wave breaking. We therefore define three distinct regions for consideration. Firstly, the region over the tidal delta (AZB21, AZB31 and AZB22) which is dominated by non-locally generated waves (swell); secondly, the western intertidal (AZB41 to AZB61) region which represents the limit of locally generated wave growth over horizontal bathymetries (van der Westhuysen, 2009) and finally, the eastern transect (AZB42 to AZB62) which represents a more complex case with the included effects of the tidal currents and channels. These observation subsets are indicated in Panel 4.1C in blue (+) over the tidal delta and magenta (× or *) over the intertidal region. Magenta crosses (×) are used to indicated the western transect whereas stars (*) are used to indicated the eastern transect.

UP-SCALING TO A 1 IN 4000 YEAR DESIGN STORM

To demonstrate the effect of choosing either of the alternative wave breaking parameterizations for engineering purposes, we consider extreme design conditions. For this, we first choose three cases from the 18th January 2007 storm cases (14:00, 20:00 and 03:00 UTC+01:00) to represent a major storm prior, during and after the peak of the storm. To subsequently represent a storm with a return period of 4000 years, wind and pressure fields were equally scaled by a factor 1.4 to produce a water level field which matched the desired exceedance level (van Vledder and Adema, 2007). The computed water levels and current fields as well as the scaled wind and pressure fields were then used in the SWAN computations using identical settings as for the field observations (see Section 4.3.2) with the use of two nested curvilinear grids.

4.3. WAVE MODEL FOR DEPTH-INDUCED BREAKING

In this section, we first present SWAN, the host wave model used and the underlying wave action balance. We then outline the default parameterization of depth-induced wave breaking with a constant scaling parameter $\gamma_{BJ} = 0.73$, followed by the alternative parameterizations of van der Westhuysen (2009, 2010) and Salmon et al. (2015).

4.3.1. MODEL DESCRIPTION

SWAN (Simulating WAves Nearshore; Booij et al., 1999) solves the wave action density in five dimensions i.e., $N(\sigma,\theta;x,y,t) = E(\sigma,\theta;x,y,t)/\sigma$ (Bretherton and Garett, 1968) where $E(\sigma,\theta;x,y,t)$ represents the energy density of the random surface elevation as a function of the relative radian frequency σ and spectral direction θ at each geographic location as a function of time. The evolution of the wave spectrum is given by the Eulerian action balance:

$$\frac{\partial N}{\partial t} + \frac{\partial c_{g,x} N}{\partial x} + \frac{\partial c_{g,y} N}{\partial y} + \frac{\partial c_{g,\sigma}}{\partial \sigma} + \frac{\partial c_{g,\theta}}{\partial \theta} = \frac{S_{tot}}{\sigma} \tag{4.1}$$

The left-hand side of Eq. (4.1) represents the conservative wave kinematics with the terms representing, respectively, the temporal change in the wave action and the propagation of wave action in four dimensions with propagation velocities $c_{g,x}$, $c_{g,y}$, $c_{g,\sigma}$ and $c_{g,\theta}$. The propagation in x and y accounts for shoaling and energy bunching, whereas the last two terms represent the shifting of σ due to variations in depth and current (the Doppler effect) and the propagation of wave action in θ-space due to depth- and current-induced refraction. The right-hand side of Eq. (4.1) represents the wave dynamics through a number of source and sink terms which represent the process of wave generation by wind, the redistribution of wave energy by nonlinear wave-wave interactions (quadruplet and triad interactions) and the dissipation due to white capping, bottom friction and depth-induced breaking.

4.3.2. MODEL SETTINGS

All computations with SWAN are carried out in stationary mode as the residence times of the waves in the computational regions of this study are small compared to the time scales of the varying conditions. Apart from the depth-induced breaking source term, all of the source terms applied in our computations are the present default of the public domain version of SWAN (version 40.91A; `swan.tudelft.nl`).

To represent generation by wind, the source term of Snyder et al. (1981) as re-scaled by Komen et al. (1984) with the wind drag coefficient of Zijlema et al. (2012) is used. For the nonlinear wave-wave interactions, the Discrete Interaction Approximation (DIA) of Hasselmann et al. (1985) scaled for shallow water by the WAMDI Group (1988) is used for the quadruplets and the Lumped Triad Approximation (LTA) of Eldeberky (1996) for the triads. For the dissipation source terms, white capping is represented by the pulse model of Hasselmann (1974) as modified by the WAMDI Group (1988) and weighted to the higher frequencies as suggested by Rogers et al. (2003) and bottom friction is represented by Hasselmann et al. (1973) with a bottom friction coefficient of 0.038 $m^2 s^{-3}$ (Zijlema et al., 2012). The source terms used for depth-induced breaking (the subject matter of the present study) are described in Section 4.3.3.

A frequency resolution, $\Delta f = 0.1 f$ (constrained by the DIA) and directional resolution of $\Delta\theta = 10^\circ$ over a complete circle is applied. In order to terminate the SWAN computations per case, the numerical settings for the curvature-based criterion of Zijlema and van der Westhuysen (2005) are used. Computations are terminated if, over 99.5% of the spatial computational grid points, the curvature of the normalized significant wave height iteration curve is less than 0.005 and either the absolute or relative change in significant wave height change by less than 0.005 m or 0.01 respectively with a cap of 50 iterations.

These defaults do not necessarily represent the most accurate settings or physically justified source terms available, but are chosen to be representative of most model simulations and most commonly applied source terms for coastal applications. These choices often reflect a compromise between accuracy and computational cost, as well as prior knowledge and experience. It is not our intention to show the best possible modelling

skill for wave dissipation, but to focus on the relevance and contrasts between different depth-induced wave breaking parameterizations.

Holthuijsen et al. (2008, their Fig. 7) demonstrates that in the surf zone for Amelander Zeegat, i.e., seaward of the barrier islands presented in Figure 4.1C, depth-induced breaking has *relatively* the most importance with the smallest time scales. We expect this to be characteristic for all our field cases and that any slight inaccuracies in the remaining source terms will not significantly detract from the conclusions made in this study. After depth-induced breaking, Holthuijsen et al. (2008) shows that the remaining shallow water source terms, i.e., the triad interactions and bottom friction, as well as the quadruplet interactions are the next *relatively* most important source terms. The remaining deep water source terms, i.e., wind input and white capping are shown to play an almost negligible role in the surf zone. The only exception to this was found in regions of locally generated wave growth such as that found over the intertidal regions at the leeside of the barrier islands of the Amelander Zeegat (Figure 4.1C). There, the deep water source terms may become *relatively* more important. However, much debate still exists as to the correct form for the wind input and white capping source terms with still no universally agreed consensus (see WISE Group, 2007; Tolman et al., 2013). A comparison of results for the Amelander Zeegat as presented by van der Westhuysen (2010) and Salmon et al. (2015) suggests an insensitivity of the deep water source terms on the prediction of the significant wave height. We therefore choose to use formulations and settings for wind input and white capping which most wave modelers working in the coastal zone are familiar with.

Our choice of source term for the triad and quadruplet interactions is primarily due to considerations of computational cost. Although exact methods for the quadruplet source term exist and have been shown to provide improved modeling skill (e.g. van der Westhuysen et al., 2007), these methods are typically three to four orders of magnitude more expensive than the DIA (van Vledder, 2006). In the present study, trial runs with such an exact computation of these quadruplet wave-wave interactions (the XNL code of van Vledder, 2006) were found to give only marginally different results and therefore did not change the conclusions of this study. Potentially more accurate approximations also exist for the triad wave-wave interactions, however even the cheapest alternatives are of an order of magnitude more expensive than the LTA used in the present study (Salmon et al., 2014). Both of these source terms are responsible for the transfer of energy between interacting frequencies and therefore they result in the evolution of the spectral shape. By itself, this does not directly affect the total wave energy, but through the evolution of the mean wave frequency (see Eq. 4.2 below), this may have an indirect effect on the depth-induced breaking dissipation. However, this effect is considered outside the scope of this study and is not considered further.

We choose our bottom friction model and friction coefficient based on the work of Zijlema et al. (2012) who show improved agreement with observations for fully developed waves over shallow water as well as the penetration of low-frequency energy into the intertidal region of the Amelander Zeegat. These improvements are independent of the proposed wind drag formulation of Zijlema et al. (2012) and were further verified by van der Westhuysen et al. (2012). Guillou (2014) showed that the proposed wind drag of Zijlema et al. (2012) improves the modeling skill over observations in the English channel

with a slight sensitivity to the choice of bottom friction model and friction coefficient to the prediction of the significant wave height. However, only small improvements (~ 5%) were demonstrated if regional effects e.g. sand ripples were ignored (error reductions increased to ~ 10% if they are included). As detailed bottom morphology is unavailable, the settings proposed by Zijlema et al. (2012) are considered reasonable.

4.3.3. DEPTH-INDUCED WAVE BREAKING

DEFAULT PARAMETERIZATION

Most parameterizations for the depth-induced breaking in spectral wave models are based on the work of Battjes and Janssen (1978) who coupled a Rayleigh distribution to represent the wave heights in a random wave field with the dissipation of a single breaking wave, assumed analogous to the dissipation of a 1D bore (per unit time and per unit bottom area; Lamb, 1932 and Le Méhauté, 1962). The bulk dissipation can then be given as:

$$\varepsilon_{BJ} = -\frac{1}{4}\alpha_{BJ}\bar{f}\rho g Q_b H_m^2 \tag{4.2}$$

where $\alpha_{BJ} = O(1)$ is a tunable coefficient, $\bar{f}$ is the mean wave frequency (based on the first and zero-th order moment of the wave variance density spectrum i.e., $\bar{f} = f_{m01}$; see Section 2.4), ρ is the density of water, g is the gravitational acceleration, Q_b is the fraction of breakers and H_m is the maximum possible wave height in the local water depth.

Since the details of the distribution function for the wave heights is not required to estimate overall properties, Battjes and Janssen (1978) use an approximate distribution. They assume a Rayleigh distribution for the non-breaking waves and truncate this at H_m with a delta function at this limit to represent the breaking waves. This yields an implicit expression for the fraction of breakers dependent on the root-mean square wave height H_{rms}:

$$\frac{1-Q_b}{lnQ_b} = -\left(\frac{H_{rms}}{H_m}\right)^2 \tag{4.3}$$

To estimate H_m, Battjes and Janssen (1978) used an estimate based on Miche (1944):

$$H_m = 0.88k^{-1}tanh\left(\gamma kd/0.88\right) \tag{4.4}$$

where $k = 2\pi/L$ is the wave number and L is the wavelength, γ is introduced as an adjustable coefficient and d is the local water depth. This expression has two limits: in deep water as $kd \to \infty$, the expression reduces to $H_m = 0.88k^{-1}$ and in shallow water as $kd \to 0$, the expression reduces to $H_m = \gamma d$. The first limit represents a limiting steepness where waves begin to break in deep water which is often referred to as white capping whereas the second limit represents depth-induced breaking. As most spectral wave models use a separate source terms for white capping, Eq. (4.4) is reduced in SWAN to $H_m = \gamma_{BJ} d$. Battjes and Janssen (1978) showed that $\gamma_{BJ} = 0.80$ provided reasonable results over their observations, however most operational third-generation wave models use $\gamma_{BJ} = 0.73$ which is taken as the averaged value over a larger data set (Battjes and Stive, 1985, their Table 1). This has been shown to provide reasonable results over a large

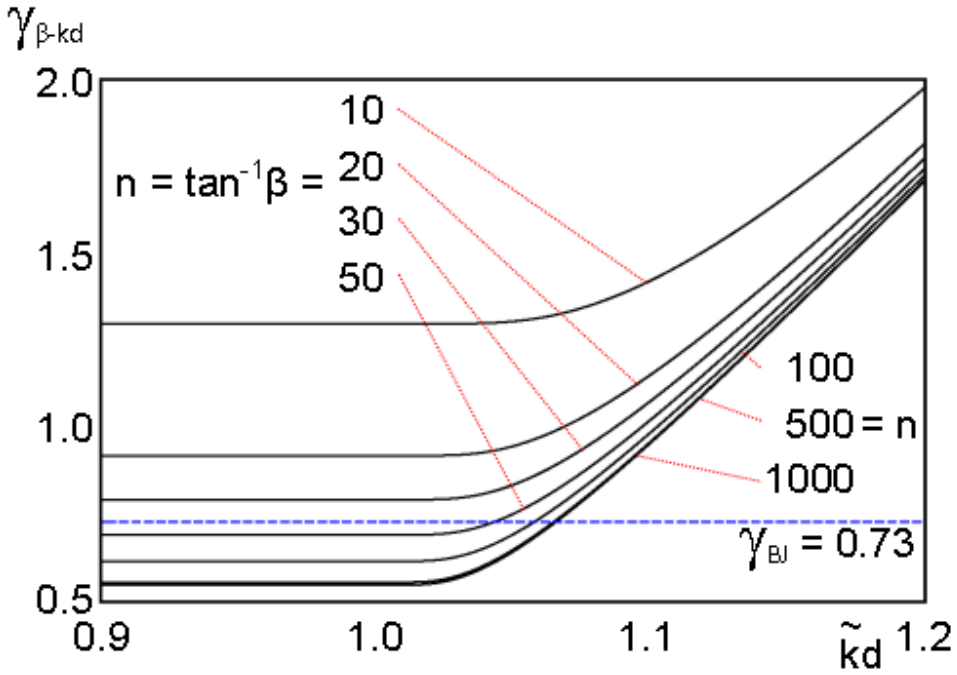

Figure 4.2: Calibrated $\gamma_{\beta-kd}$ as a function of the local bottom slope $n = tan^{-1}\beta$ and local normalized wave number $\tilde{kd}$ with $\gamma_{BJ} = 0.73$ for reference (from Salmon et al., 2015).

range of bathymetries and wave conditions, particularly for slopes and non-locally generated waves (e.g. Salmon et al., 2015). We subsequently refer to the Battjes and Janssen (1978) dissipation model as the BJ78 model and its use with $\gamma_{BJ} = 0.73$ as the 'default'.

ALTERNATIVE PARAMETERIZATIONS

Beta-kd ($\beta - kd$) parameterization Many studies that have addressed improving the modeling of depth-induced wave breaking have focused on re-scaling the dissipation in terms of either local topography i.e., bottom slope (e.g. Madsen, 1976) or wave parameters either offshore or local i.e., wave number or wave steepness (e.g. Ruessink et al., 2003; Apotsos et al., 2008). However previous studies (e.g. Rattanapitikon, 2007) have shown that these scalings do not provide substantially better results than using the default parameterization. Salmon et al. (2015) suggest an alternative approach of combining both local bottom slope (β) and normalized wave number (kd) in a joint scaling and show this to provide similar results to using $\gamma_{BJ} = 0.73$ in laboratory cases with sloping bathymetries and significantly improved results over horizontal laboratory cases. This $\beta - kd$ scaling is shown in Figure 4.2.

In their scaling, they assume that in shallow water ($kd < 1$) waves behave more like solitary waves so that wave number becomes irrelevant for the kinematics and dynamics of such waves. Therefore, under such conditions, the waves are only dependent on the

local bottom slope, β. However, in deeper water ($kd > 1$), van der Westhuysen (2010) suggests an equilibrium state where the wave growth limit of locally generated waves is due to a balance between the local wind-wave growth and dissipative sources i.e., depth-induced breaking, white capping and bottom friction. Over (near-) horizontal bottoms, the influence of depth-induced breaking was shown to be small in this balance and not well represented with $\gamma_{BJ} = 0.73$. To account for this, under these conditions, a positive kd-dependency on $\gamma_{\beta-kd}$ to represent a reduction in Q_b (as for example Ting, 2001; Ruessink et al., 2003) is introduced so that waves become dependent on both β and kd. To represent these dependencies Salmon et al. (2015) suggest:

$$\gamma_{\beta-kd} = \gamma_\beta / tanh\left[\gamma_\beta / \gamma_{\tilde{k}d}\right] \tag{4.5}$$

and their extensive calibration finds $\gamma_\beta = 0.5 + 7.59|\nabla d| \geq 0$ for the bottom slope, β-dependency where the bottom slope is estimated as the magnitude of the bottom gradient i.e., $tan\beta = |\nabla d|$ (as taken from the computational grid; Salmon et al., 2015) and $\gamma_{\tilde{k}d} = -8.06 + 8.09\tilde{k}d \geq 0$ for the $\tilde{k}d$-dependency where $\tilde{k} = k_{-1/2}$ is a characteristic wave number (to be determined from the local spectrum; WAMDI Group, 1988; see Section 2.4).

To account for inherent differences between 1D long-crested (directionally narrow) and 2D short-crested (directionally spread) wave conditions, Eqs. (4.2) and (4.3) are modified by Salmon et al. (2015) to:

$$\varepsilon^\theta_{BJ} = -\frac{1}{4} K_\theta \alpha_{BJ} \bar{f} \rho g Q_b H_m^2 \tag{4.6}$$

with

$$\frac{1 - Q_b}{lnQ_b} = -\left(\frac{H_{rms}/\sqrt{K_\theta}}{H_{max}}\right)^2 \tag{4.7}$$

where $K_\theta = \sigma_\theta / \sigma^*_\theta \geq 1$ is the number of directional partitions which are each assumed to be sufficiently long-crested so that the 1D bore assumption of Battjes and Janssen (1978) is applicable to that partition, σ_θ is the directional spreading of the spectrum (Kuik et al., 1988) and σ^*_θ is the upper limit for directional spreading where the 1D bore assumption holds. This was shown to provide the best results with $\sigma^*_\theta = 15°$ (Salmon et al., 2015). We subsequently refer to this parameterization, i.e., the BJ78 dissipation model with both bottom slope and wave number dependency (Eq. 4.5) and modified with the directional partitioning (Eqs. 4.6 and 4.7) as the beta-kd or $\beta - kd$ parameterization.

Bi-phase (φ) parameterization A development of the Battjes and Janssen (1978) model was proposed by Thornton and Guza (1983) who suggested, based on their field observations, using a Rayleigh distribution for the breaking waves shifted toward the higher waves. This is achieved by the use of a weighting function (their Eq. 21) to give the bulk dissipation as:

$$\varepsilon_{TG} = -\frac{3\sqrt{\pi}}{16} \alpha_{TG} \bar{f} \rho g \frac{H^5_{rms}}{\gamma^2_{TG} d^3} \left[1 - \frac{1}{\left[1 + \left(H_{rms}/\left(\gamma_{TG} d\right)\right)^2\right]^{5/2}}\right] \tag{4.8}$$

where α_{TG} is a calibration coefficient ($\alpha_{TG} \approx 0.5$ for laboratory cases and $\alpha_{TG} \approx 3.4$ for field cases in their study) and $\gamma_{TG} = H_{rms,max}/d$, the ratio of the maximum *rms* wave height to local depth. This dissipation model is subsequently referred to as the TG83 model.

An alternative weighting function was suggested by van der Westhuysen (2009, 2010) who argued that the weighting function should be based on wave nonlinearity which is introduced through the bi-phase parameterization of Eldeberky (1996). The bulk dissipation is then given as:

$$\varepsilon_{TG,vdW} = -\frac{3\sqrt{\pi}}{16}\alpha_{TG}\bar{f}\rho g\frac{H_{rms}^3}{d}\left(\frac{\varphi}{\varphi_{ref}}\right)^n \tag{4.9}$$

For which van der Westhuysen (2009) calibrated $\alpha_{TG} \approx 0.95$; $\varphi = 0.5\,\pi\,[tanh(0.2/Ur) - 1]$ represents the parameterization of the bi-phase of the self-self triad interaction at the peak of the spectrum as a function of Ur, the Ursell number (see Section 2.4); $\varphi_{ref} = -4\pi/9$ and $n = 4\left\{1 - \pi^{-1}arctan\,[s - 0.038]\right\}$ with the local wave steepness s as defined by WAMDI Group (1988, see Section 2.4). In contrast to the $\beta - kd$ parameterization, the relaxation of the depth-induced breaking criterion for locally generated waves is provided by a reduction of nonlinearity (φ) and therefore dissipation. We subsequently refer to the TG83 model with the weighting function of van der Westhuysen (2009, 2010) as the bi-phase or φ parameterization.

4.4. RESULTS

To assess the performance of the three parameterizations introduced in Section 4.3.3, we calculate two commonly applied performance metrics which have been used in previous studies: the scatter index (*s.i.*) and the relative bias (*r.b.*) for the field data sets as described in Section 4.2 (e.g. Janssen et al., 1984; Komen et al., 1994). These performance metrics are defined in Section 3.3.3. Following previous studies of depth-induced wave breaking over field data sets (e.g. Rattanapitikon, 2007; Salmon et al., 2015), scatter indices of < 10% are considered very good; between 10% and 20% as reasonable and > 20% as poor.

4.4.1. DEFAULT PARAMETERIZATION

PETTEN (1995 AND 2002)

The modeling performance of significant wave height for the default parameterization for Petten is presented in Figure 4.3A as a scatter plot. The performance of the default parameterization is shown to perform reasonably well with a scatter index of 17% and a relative bias of ~ 0%. This is further illustrated the proximity of the line of best-fit, shown as a dashed magenta line, to the line of unity which suggest a good correspondence between the simulated and observed significant wave heights. This negligible bias demonstrates the limited potential for further error reductions through model calibration. This result is consistent with previous studies (e.g. Salmon et al., 2015) which demonstrate the applicability of most parameterizations for depth-induced wave breaking for non-locally generated waves over simple gently sloping beach profiles.

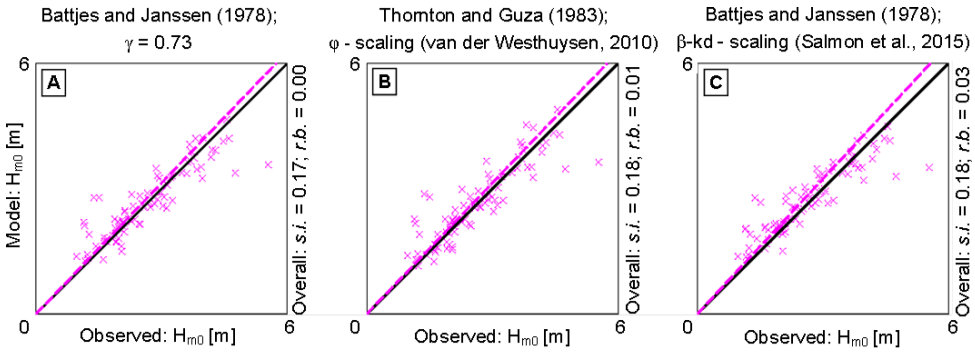

Figure 4.3: Performance of the default, φ and $\beta - kd$ parameterizations for predicting significant wave heights for the Petten data set. The dashed magenta line shows the line of best-fit forced through the origin with the solid black unity line as reference. Averaged performance metrics of the scatter index (*s.i.*) and relative bias (*r.b.*) are also shown for all data points (overall).

4

HARINGVLIET (1982)

Figure 4.4A shows the computed significant wave height for the default parameterization for the Haringvliet field case. A distinct reduction in wave energy is shown across the Hinderplaat by the reduction in the observed (and computed) significant wave height between the seaward (+) and shoreward (×) side of the shoal. At the three seaward locations, the observed average significant wave height was 2.6 m whereas at the four shoreward locations this value was 1.1 m and therefore represents the dissipation of non-locally generated waves over a near-horizontal shoal.

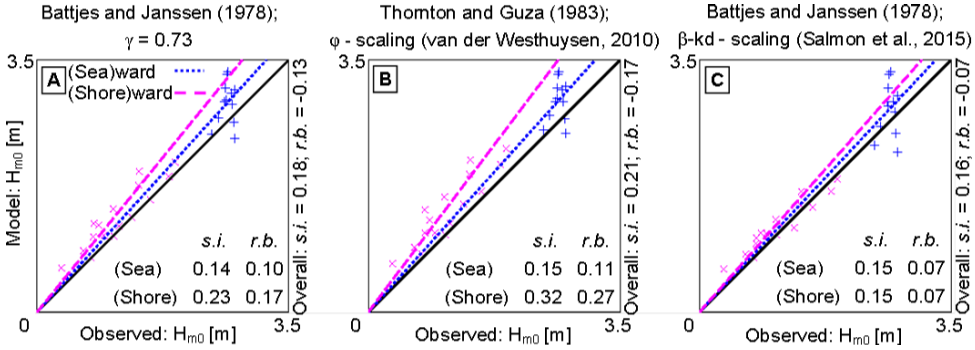

Figure 4.4: Performance of the default, φ and $\beta - kd$ parameterizations for predicting significant wave heights for the seaward and shoreward Haringvliet data set. The dashed magenta and dotted blue lines show the line of best-fit forced through the origin for buoys observations taken seaward (blue +) and shoreward (magenta ×) of the Hinderplaat respectively with the solid unity line as reference. Averaged performance metrics of the scatter index (*s.i.*) and relative bias (*r.b.*) are also shown for the observation subsets (Sea) and (Shore) in addition to all data points (overall).

From the overall computed average performance metrics, the default parameterization is shown to perform reasonably with a scatter index of 18%, but unlike for the Petten

data set, a significant proportion of this error is shown by the relative bias (+13%) to be systematic. As explained in Section 4.2.2, this result is biased towards the observations made seawards of the Hinderplaat which are not significantly affected by depth-induced breaking (2.6 m significant wave height in ~ 7 m water depth).

If we analyze the observations shoreward of the Hinderplaat, i.e., that *are* significantly affected by depth-induced breaking, a larger error is seen compared to the overall average, suggesting a decrease in model performance. At the shoreward observations, the scatter index is rather poor with a value of 23% and a positive relative bias of 17%. This overestimation is consistent with previous studies which suggest that the use of $\gamma_{BJ} = 0.73$ leads to an underestimation of the dissipation for non-locally generated waves over horizontal bathymetries, e.g. Nelson (1997) and Katsardi (2007), resulting in a corresponding overestimation of the predicted wave height.

AMELANDER ZEEGAT (2007)

We present our results for the Amelander Zeegat in Figure 4.5. Data points in blue (+) represent the non-locally generated wave measurements taken seawards of the tidal inlet whereas the magenta points represent measurements of locally generated wave measurements taken over the western (×) and eastern (*) shoreward intertidal regions. From the overall performance metrics, the default parameterization, shown in Figure 4.5A, performs reasonably with a scatter index of 17% and relative bias of −9%. To evaluate its performance further, we consider the three subsets of the observations as described in Section 4.2.3.

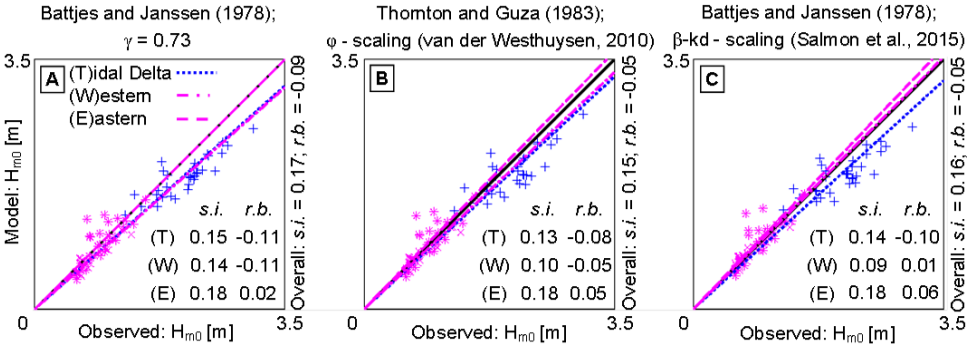

Figure 4.5: Performance of the default, φ and $\beta - kd$ parameterizations for predicting significant wave heights for the Amelander Zeegat data set. The dotted blue line shows the line of best-fit forced through the origin for buoy observations taken seaward (+) for the tidal inlet. The dot-dashed and dashed magenta line show equivalent best-fit lines for observations taken shoreward of the tidal inlet taken from the western (×) and eastern (*) transects respectively. Averaged statistical measures of the scatter index (*s.i.*) and relative bias (*r.b.*) are also shown for the observation subsets (T), (W) and (E) in addition to all data points (overall).

The results for the non-locally generated waves over the ebb tidal delta are shown in Figure 4.5A (blue +). The corresponding scatter index for the default is 15% (−11% relative bias). This underestimation is also illustrated by the line of best-fit shown (dotted blue). In contrast to the similar conditions in the Haringvliet, i.e., non-locally generated waves breaking over a shoal, a significant underestimation is demonstrated rather than

an overestimation as shown previously.

Over the *western* intertidal region (magenta ×), a similar underestimation can be seen with a scatter index of 14% and a negative relative bias of −11%. This is consistent with numerous studies which suggests the overestimation of the dissipation of *locally* generated waves over horizontal bathymetries e.g. de Waal, 2001; Bottema and Beyer, 2002; van Vledder et al., 2008. Over the *eastern* transect, the agreement with the observations is worse with a scatter index of 18%, however the bias is significantly less (+2%). This reflects the increased complexity of the region represented by the eastern transect and limited scope for improvement over this region through calibration.

4.4.2. BI-PHASE (φ) AND BETA-KD ($\beta - kd$) PARAMETERIZATION

PETTEN (1995 AND 2002)

The model performance for the alternative parameterizations is shown in Figures 4.3B and 4.3C with a similar trend to that of the default parameterization given in Figure 4.3A. From the computed performance metrics, all parameterizations are shown to perform comparably with a reasonable averaged scatter index of 18% and a negligible bias. As with the default parameterization, the good agreement between the line of best-fit (dashed magenta) with the line of unity further demonstrates minimal systematic error.

HARINGVLIET (1982)

From the overall computed averaged performance metrics given in Figure 4.4, both the default and $\beta - kd$ parameterizations are shown to perform comparably with an averaged scatter index of ~ 17%. In contrast, the φ parameterization performs worse with a scatter index of 21%. Focusing on the shoreward and seaward locations, it is clear that these differences, as expected, originate from the model performance at the shoreward locations as at the seaward locations, all three models perform comparably with a scatter index of ~ 15%.

In Figure 4.4B, it is apparent that the decrease in the overall model performance for the φ parameterization is due to the increased overestimation of significant wave height at the shoreward location as demonstrated with a scatter index of 32% and a positive relative bias of 27%. This poor performance is likely due to the presence of horizontal and negative slopes i.e., increasing depth at the Hinderplaat. Over positively sloping beaches and bar profiles where most of the dissipation is expected to occur over the seaward side of the bar, e.g. Petten, the φ parameterization performs well because the inverse square relationship between Ur and d dominates and rapidly increases Q_b (Salmon et al., 2015). This is not the case for the Haringvliet data set. Van der Westhuysen (2010, his Figure 11b) shows that just shoreward of a bar i.e., for negative bottom slopes, the power relationship in Eq. (4.9) underestimates Q_b in comparison to the observations resulting in an overestimation of the significant wave height. This problem is further compounded by the strong dependency of the φ parameterization on Ur which is sensitive to the estimate of the mean wave period which is typically under-predicted in spectral wave models. This leads to an underestimation of Ur and a further reduction of Q_b.

In contrast, Figure 4.4C shows an improvement with the $\beta - kd$ parameterization at the shoreward location with both the seaward and shoreward locations equally well represented with a scatter index of ~ 15% and a positive relative bias of ~ 7%. This repre-

sents an error reduction of at least 30% compared to the other parameterizations. Much of this improvement is due to the contribution of the bottom slope ($\beta-$) dependency of the $\beta - kd$ scaling and the directional partitioning of the dissipation model. As the waves are non-locally generated, the values of $\tilde{k}d$ are small enough that the dissipation is $\tilde{k}d$ insensitive. Therefore, the scaling of the dissipation is only dependent on the local slope (β), which approaches a value of $\gamma_{BJ} = 0.54$ for horizontal bathymetries in shallow water (Fig. 4.2); a value smaller than that of the default and in closer agreement to studies which suggest $\gamma_{BJ} \approx 0.55$ over horizontal bottoms, e.g. Nelson, 1997; Katsardi, 2007. By itself, this bottom slope dependency would result in increased dissipation and a reduction in the predicted significant wave height. However, for these cases, the wave directional spreading behind the shoal exceeds $\sigma^*_\theta = 15°$ (typically $\sigma_\theta > 45°$ just behind the shoal) due to the waves propagating both over and around the shoal. Therefore the overall effect of the $\beta - kd$ scaling on the dissipation is then a balance between an increase due to the β-scaling and a decrease due to the wave directional spreading. As shown by the reduced positive relative bias and predicted wave heights, the effect of the β-dependency dominates this balance.

4

AMELANDER ZEEGAT (2007)

From the scatter plots given in Figures 4.5B and 4.5C for the alternative parameterizations, only marginal improvements are seen over the tidal delta (blue +) with a decrease in the scatter index from 15% to ~ 14% and virtually no difference is seen over the *eastern* intertidal region (magenta *) with a scatter index of ~ 18% for all three parameterizations.

The most significant differences between the default and alternative parameterizations is shown only over the *western* transect (magenta ×) where it is clear from the dot-dashed magenta best-fit lines that both alternative parameterizations (Figure 4.5B and C) produce significantly less error and bias than the default parameterization (Figure 4.5A). Compared to the default parameterization with a scatter index of 14% (relative bias −11%), the performance metrics for the φ and $\beta - kd$ parameterizations are 10% (−5% relative bias) and 9% (+1% relative bias) respectively. These differences suggest a reduction of error of up to ~ 40% with significant reduction in the negative bias.

To illustrate the differences in modelling performance, the computed spectra and the observed spectra for case A07_03 are presented in Figure 4.6. This case is chosen as it represents observations during the highest wind speeds and represents conditions with strong finite-depth wave growth. Six buoy locations, three from the western transect (top row) and three from the eastern transect (bottom row) are chosen. The first column, corresponding to buoys AZB21 and AZB22 and represents the observations taken at the tidal delta, the middle column corresponds to buoys AZB41 and AZB42 and represents observations taken near the center of the intertidal region and the final column corresponds to buoys AZB61 and AZB62 and represents observations close to the Dutch mainland. These locations are indicated by the magenta dots in Figures 4.7 and 4.8.

The prediction of the spectra in the delta region (at buoys AZB21 and AZB22; first column of Fig. 4.6) shows that all three parameterizations underestimate the spectral densities, with slightly smaller errors with the alternative parameterizations. A possible reason for the slight improvement of the $\beta - kd$ parameterization is suggested by Salmon et al. (2015) who discuss the influence of wave directionality on depth-induced breaking.

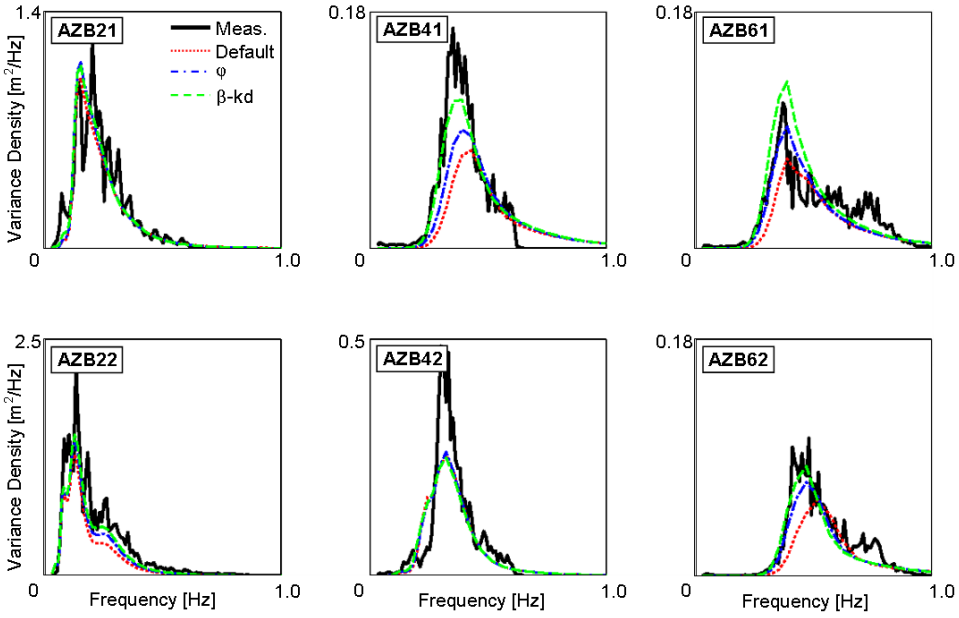

Figure 4.6: Variance density spectra for case A07_03 (Amelander Zeegat 18th Jan. 2007 12:20) at six buoy locations (note differences in vertical scaling; for locations see Fig. 4.2C). The top panels represent buoys located along the western transect moving towards the shore from left to right while the bottom panels represent corresponding buoys from the eastern transect. The first column shows spectra observed or computed over the ebb tidal delta whereas the remaining columns represent spectra over the intertidal region. Measured spectra is given in black (thick solid) with computed spectra in red (dotted; default), blue (dashed-dot; φ parameterization) and green (dashed; $\beta - kd$ parameterization).

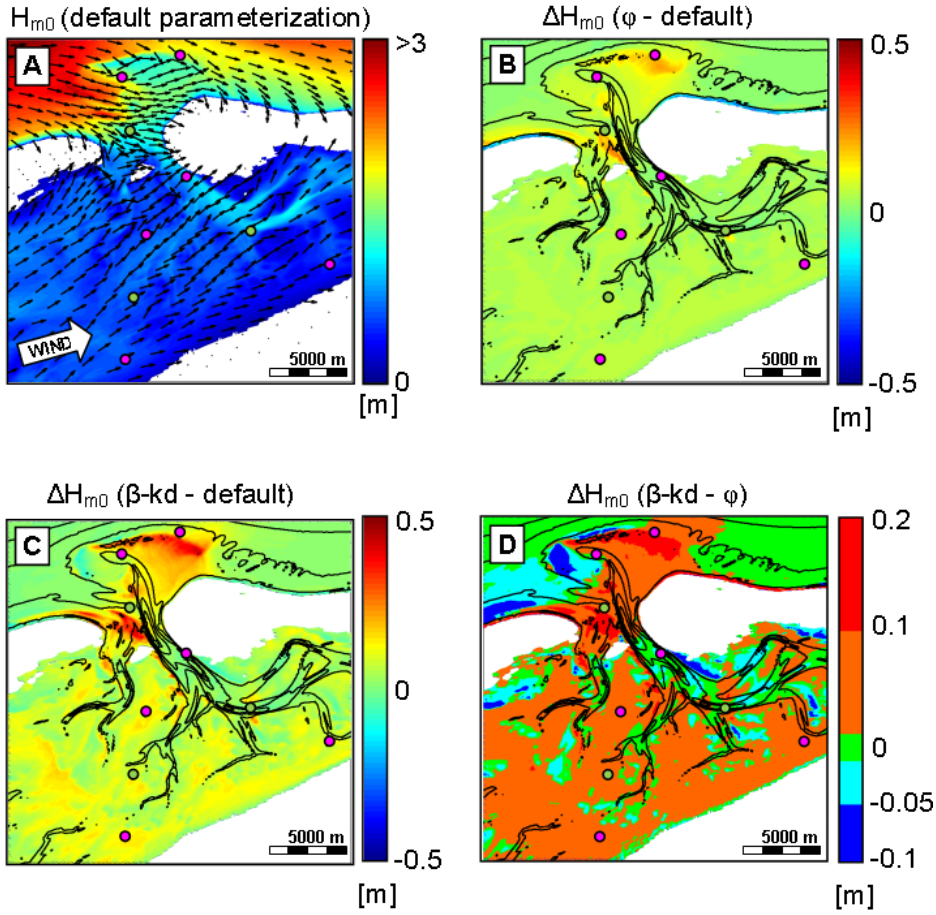

Figure 4.7: Comparison of predicted significant wave heights for the three parameterizations over the Amelander Zeegat region for case A07_03 (Amelander Zeegat 18th Jan. 2007 12:20). Panel A shows the predicted significant wave height and mean wave direction using the default parameterization. Panels B and C show the respective differences in predicted significant wave height for the φ and $\beta - kd$ parameterizations to those shown in Panel A. Panel D shows banded differences in computed significant wave height between the $\beta - kd$ and φ parameterizations. Depth contours are shown at 5 m intervals and buoys locations used in this study are indicated with colored dots with the selected buoys from Figure 4.6 shown in magenta.

They argued that when wave directional spreading increases i.e. due to refraction around a shoal, the assumption of a 1D bore analogy for wave breaking should not be applicable and results in a reduction of dissipation. Therefore the modification of the dissipation model (Eq. 4.6 and 4.7) to include this effect seems justified. This is supported by observations in *deep* water (e.g. Onorato et al., 2009; Latheef and Swan, 2013) and numerical simulations in *shallow* water (Katsardi, 2007; van Vledder et al., 2013) which suggest that directionally narrow wave fields exhibit greater nonlinearity and are steeper and more dissipative than their short-crested counterparts (directionally broader but otherwise identical spectra). This is to some extent at least captured by the φ parameterization which is based on wave nonlinearity.

From the top right two panels of Figure 4.6, representing the western intertidal region (AZB41 and AZB61), higher variance densities in agreement with the observations are predicted with the φ and $\beta - kd$ parameterizations reinforcing their applicability for locally generated wind-wave growth compared to the default parameterization. In particular, the $\beta - kd$ parameterization is shown to produce the best agreement with the energy observed at the peak frequency, but the tail is still poorly predicted. This is possibly related to the rather simplistic representation in SWAN of the triad wave-wave interactions which dominates the evolution of the tail.

For the eastern intertidal region, represented by the bottom right two panels (AZB42 and AZB62) of Figure 4.6, improvements are only seen at the most shoreward buoy (AZB62). For buoy AZB42 (and AZB52; not shown), the differences are found between the three parameterization are small. This is probably due to the fact that these observations are taken in deep water where depth-induced breaking will not be dominant and therefore only small differences between the three parameterizations are seen. Other processes such as the effect of currents on waves or wind-wave growth are likely to be more important. Van der Westhuysen (2012) and van der Westhuysen et al. (2012) shows that at these locations wave-current interactions are important, especially for the negative current gradients found during the ebb tide which are shown to be responsible for enhanced dissipation of waves.

In order to show the model prediction comparison over the entire Amelander Zeegat region, in addition to highlighting the different characteristic regions of interest, a geographical plot for the predicted significant wave height and mean wave direction using the default parameterization is shown in Figure 4.7A. Westerly waves with significant wave heights of over 3 m are shown to dissipate over the tidal delta resulting in reduced significant wave heights at the lee side of the delta. The tidal delta is shown to be an effective dissipater of the wave energy coming off the North Sea with a clear distinction between the significant wave heights predicted in front of and behind the tidal inlet. In agreement with Figures 4.5 and 4.6, smaller waves are seen over the tidal flats with significant wave heights of < 2 m, although higher waves are predicted over the tidal channels.

The geographical differences in predicted significant wave height between the default and the φ and $\beta - kd$ parameterizations are presented in Figure 4.7B and C respectively. As shown previously in Figures 4.5 and 4.6, similar increases in the predicted significant wave height are shown over the tidal flats with an average respective increase of ~ 0.05 m and ~ 0.07 m by the φ and $\beta - kd$ parameterizations. Corresponding increases over the tidal delta are ~ 0.1 m and ~ 0.2 m with maximum increases of ~ 0.25 m and

~ 0.51 m.

The difference between the φ and $\beta - kd$ parameterizations is shown in Figure 4.7D. Over the tidal delta, waves up to 0.2 m higher are predicted by the $\beta - kd$ parameterization and over the intertidal region, particularly towards the west, waves up to 0.1 m higher are predicted. Over the tidal channels, towards the offshore region and seaward of the Ameland (eastern barrier island) coast, negligible differences of < 0.05 m are predicted. However, seaward of the Terschelling (western barrier island) coast, waves up to 0.1 m smaller are predicted by the $\beta - kd$ parameterization. This effect is considered in greater detail below.

4.5. DISCUSSION

In this study we have shown that the alternative φ and $\beta - kd$ parameterizations for depth-induced wave breaking in third-generation spectral wave models perform similarly or better than the default parameterization (with a constant scaling $\gamma_{BJ} = 0.73$). For simple beach cases (Petten), the default parameterization performs reasonably, but for locally (Amelander Zeegat) or non-locally (Haringvliet) generated waves breaking over (near-)horizontal bottoms, improvements are demonstrated by the φ parameterization for *locally* generated waves or the $\beta - kd$ parameterization for both locally and non-locally generated wave conditions (and therefore the preferred parameterization).

It is not clear from the above how the three different contributions in the $\beta - kd$ parameterization i.e., the β-scaling, $\tilde{k}d$-scaling, and directional partitioning contribute to the final result. To illustrate this, we consider case A03_07, the case with the highest wind speed, from the Amelander Zeegat data set as shown previously in Section 4.4.2. We choose to consider this data set over the Haringvliet and Petten, as the Amelander Zeegat represents the most complex field case with a number of characteristic regions.

We present the effect of these contributions in Figure 4.8 in which we show the sequential effect of the β-scaling (Fig. 4.8D), the $\tilde{k}d$-scaling (Fig. 4.8E) and the directional partitioning σ_θ^* (Fig. 4.8F) compared to the φ-parameterization. The corresponding dependencies are given in Figure 4.8A to C. From Figure 4.8D, the effect of the β-scaling compared to the φ-parameterization is to force a reduction of significant wave height over the outer delta and seaward of the Terschelling coast (west barrier island) coast by up to ~ 0.5 m and by ~ 0.2 m over the intertidal flats. As explained in Section 4.4.2, a lower limit for γ_{BJ} over (near-)horizontal bottoms (shown in Fig. 4.8A) increases the wave dissipation and reduces the significant wave height. Such reductions are not seen seaward of the Ameland (eastern barrier island) coast despite similar horizontal bathymetries due to the sheltering effect of the tidal delta resulting in smaller waves which do not break until the shallower water depths found closer to the shore are reached.

The effect of the $\tilde{k}d$-scaling, as shown in Figure 4.8E, is to counteract the reduction of significant wave height over the intertidal flats as predicted by the β-scaling resulting in waves up 0.1 m higher when the joint $\beta-$ and $\tilde{k}d-$scaling is applied, i.e., an increase of up to ~ 0.3 m compared to the β-scaling. From Figure 4.8B it is clear to see that the $\tilde{k}d$-scaling only contributes in the relatively shallow water ($k_p d > 0.5$) found over the intertidal area and does not account for the increased significant wave heights as shown in Figure 4.7C and D found over the deeper regions found seawards of the tidal inlet over

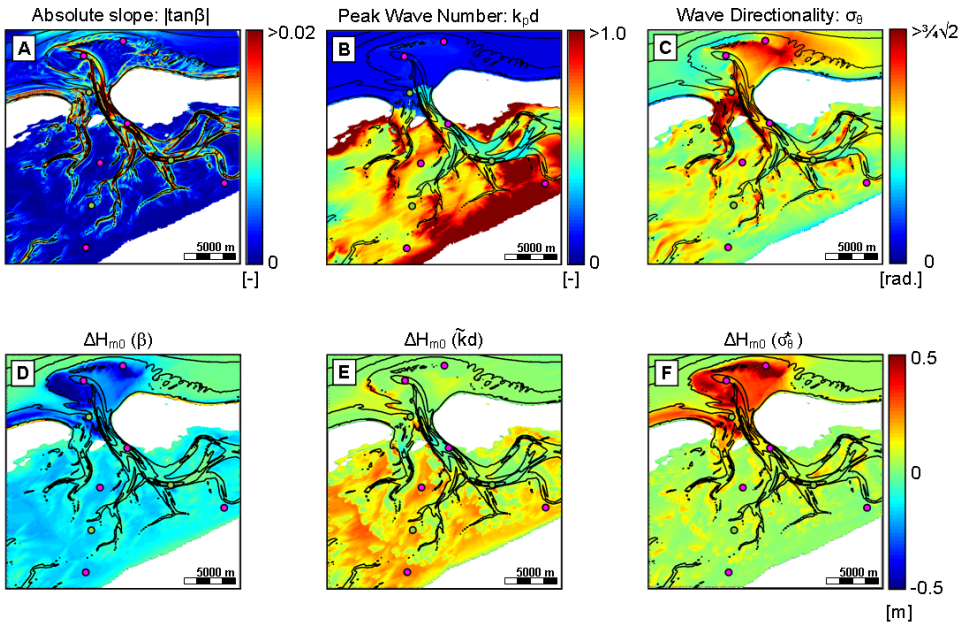

Figure 4.8: Contributions to the significant wave height for the $\beta - kd$ parameterization by bottom slope, normalized wave number and directional partitioning for case A07_03 (Amelander Zeegat 18th Jan. 2007 12:20). Upper panels A-C show, respectively, the magnitude of the absolute bottom slope ($|tan\beta|$), peak wave number ($k_p d$), and wave directionality (σ_θ; as defined by the directional width of the spectrum of Kuik et al., 1988). Lower panels D-F show the sequential effect of the $\beta - kd$ parameterization. Panel D shows the effect on the predicted significant wave height of the β-scaling of the $\beta - kd$ parameterization compared to the φ parameterization with Panels E and F demonstrating the subsequent change of including the $\tilde{k}d$-scaling and directional partitioning (σ^*_θ). The summation of Panels D-F is equivalent to the differences shown in Figure 4.7D. Depth contours are shown at 5 m intervals and buoys locations used in this study are indicated with colored dots with the selected buoys from Figure 4.6 shown in magenta.

the tidal delta. This difference relates to a distinction made in the $\beta - kd$ parameterization between locally and non-locally generated waves (by virtue of the $\tilde{k}d$ dependency) with a smaller contribution of depth-induced breaking in the equilibrium balance for locally generated waves.

For the non-locally generated waves observed over the ebb tidal delta, the directional partitioning acts to reduce dissipation resulting in higher significant wave heights as shown in Figure 4.8F. In this region, as non-locally generated waves propagate and break over the tidal delta, they are also refracted by the shoal leading to a wave field characterized by a directionally confused sea state with different directional modes, i.e., short-crested waves. This trend can be clearly seen in the mean wave direction plots superimposed in Figure 4.7A and is further quantified by large values of directional spreading ($\sigma_\theta > 50°$) in Figure 4.8C. The effect of the directional partitioning is to increase the significant wave height almost everywhere. Over the tidal delta, this increase is up to 0.5 m, whereas over the intertidal area, this is effect is smaller with a maximum increases of ~ 0.15 m. This difference is partially due to the reduced directional spreading over the intertidal region ($\sigma_\theta \approx 35°$) as well as the effect of the $\tilde{k}d$ dependency to essentially disable the depth-induced wave breaking. Correspondingly, the effect of the directional partitioning then becomes reduced.

4.5.1. 1 IN 4000 YEAR STORM

Figure 4.9 shows the effect of up-scaling the above 18th January 2007 storm as described in Section 4.2.3. Panel A shows the predicted significant wave height at the peak of the storm using the default parameterization. Waves with significant wave heights of up to 6 m are shown to propagate southward from the North Sea towards the barrier islands where they dissipate to a wave height of ~ 3 m near the 5 m depth contour prior to fully dissipating. Even under these severe conditions, the tidal delta is still shown to be an effective dissipater of wave energy with significant wave heights of ~ 2 m predicted over most of the intertidal area with slightly larger waves predicted over the tidal channels and smaller waves, up to ~ 1 m predicted on the shoreward side of the barrier islands. However, in comparison to the unscaled simulation shown in Figure 4.7A, the effect of larger waves over the tidal channels is less pronounced.

Figure 4.9D and E show the comparison between using the φ and $\beta - kd$ parameterizations compared to the default parameterization as shown in Figure 4.9A. The φ parameterization is shown to increase the significant wave heights by up to ~ 0.25 m over the tidal delta and at the tidal inlet around AZB31 and by between ~ 0.1 and ~ 0.2 m seawards of the barrier islands to about 10 m water depth and over the western intertidal region and seawards off the mainland coast. The $\beta - kd$ parameterization shows many similar qualitative features, but with stronger upward deviations over the landward shoals, as shown in the scatter plot in Figure 4.9C and by the red regions in Figure 4.9E and 4.9F. However, downwards deviations seawards of the barrier islands are also shown by the blue regions in Figure 4.9E and 4.9F. This downwards effect of the $\beta - kd$ parameterization relates to higher waves in this up-scaled storm propagating over a relatively horizontal bathymetry (Fig. 4.8A), which is (properly in the context of this parameterization) uncompensated by either the $\tilde{k}d$-scaling or the directional partitioning. This dominance of the β-scaling over the remaining dependencies is almost negligible

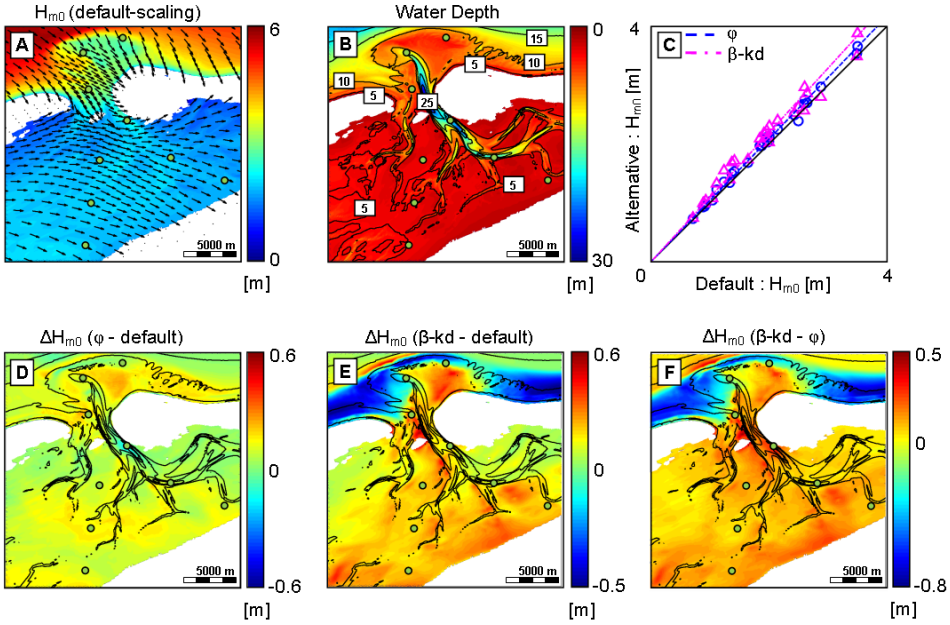

Figure 4.9: Comparison of predicted significant wave height for the three parameterizations over the 18th January 2007 storm re-scaled to reproduce 1 in 4000 year storm conditions. Panel A shows the predicted significant wave heights and mean wave direction using the default parameterization at the peak of the storm (20:00 UTC+01:00) with the water depth shown in Panel B. Panel C summarizes the performance of the φ (○) and $\beta - kd$ (△) parameterizations compared to the default for all cases considered (14:00, 20:00 03:00 UTC+01:00) at the buoy locations with the dashed blue and dotted-dashed magenta lines showing the respective lines of best-fit through the origin. Panels D and E show the respective differences in predicted significant wave height compared to those shown in Panel A. Panel F presents the difference in predicted significant wave height between the $\beta - kd$ and φ parameterizations. Depth contours are provided at 5 m intervals and buoys locations used in this study are indicated by the colored dots.

for the unscaled cases (Fig. 4.7C) as for these cases the waves typically remain small enough that they propagate mostly undisturbed up to the sloping beaches of the barrier islands. However, in severe storm conditions, waves may become depth-limited in more offshore regions and, due to the β-scaling, become more dissipative than predicted by previous parameterizations.

The distribution and dissipation of wave energy as represented by the significant wave height shown in Figure 4.9 not only has a direct significant importance for the design and management at the coastline but also through other processes, in particular wave-induced currents and water level set-up. To illustrate the effects of the different breaking parameterizations, Figure 4.10A shows the variation in the magnitude of the radiation stress gradient computed with the default wave breaking parameterization, defined as $\|\mathbf{F}\|\, sgn\left(F_y\right)$ (i.e., the sign is taken from the north-south component of the gradient). With the beaches orientated in an almost east-west direction, this approximates the cross-shore variation in the wave-induced forces.

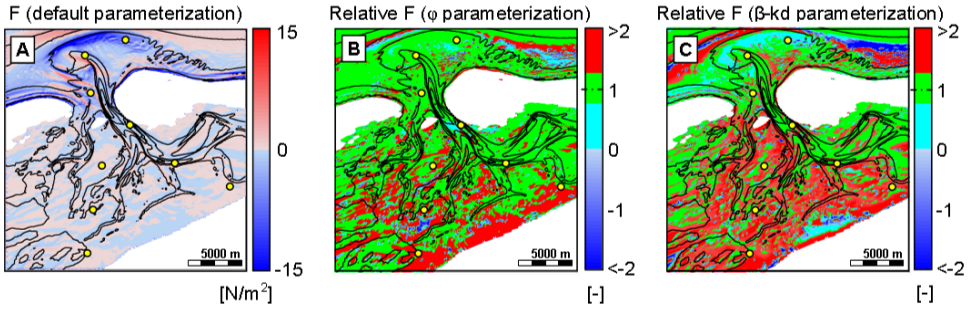

Figure 4.10: Comparison of predicted radiation stress gradients at the peak of the 1 in 4000 year storm. Panel A shows the computed magnitude of the wave-induced forces with the sign taken from F_y, the wave-induced force taken in the north-south direction, i.e., $\|\mathbf{F}\|\, sgn\left(F_y\right)$ using the default parameterization. Panels B and C show the relative magnitudes compared to the default parameterization within banded ranges for the wave-induced forces computed from the φ and $\beta - kd$ parameterizations. Depth contours are provided at 5 m intervals and buoys locations used in this study are indicated by the colored dots.

At the seaward side of the islands, positive values i.e., northward decreasing radiation stresses (in red in Fig. 4.10A; computed with the default breaking parameterization) are shown typically in a band along the tidal delta edge, extending east and westwards along the coast. This corresponds to increasing wave heights, mostly due to shoaling, and the generation of a slight, local set-down of the mean sea surface. The negative values (in blue in Fig. 4.10A) occur shoreward of this band and corresponds to decreasing wave heights, mostly due to breaking, generally resulting in a set-up over the tidal delta and north-facing beaches. Behind the islands, a complex pattern of negative and positive wave-induced forces reflecting the complex bathymetry is shown. Because these gradients are relatively small and scattered, they will not contribute significantly to the set-up along the mainland coast (which is therefore mostly due to the set-up generated over the tidal delta).

The effects of using the φ and $\beta - kd$ parameterizations are shown with the relative magnitudes of the radiation stress gradients in Figures 4.10B and C respectively. The

most obvious differences are the fairly large change in magnitude (more than a factor 2; deep red and blue) and the occasional change in sign (in blue in Fig. 4.10B and C; indicating a shift in the geographical pattern). The regions indicated in green correspond to regions with values of similar magnitude and sign i.e., small differences in comparison to the default parameterization. Both effects of increased magnitude and change of sign are more pronounced for the $\beta - kd$ parameterization than for the φ parameterization. The increased values in the intertidal region (in both parameterizations) suggest an increase in wave heights as demonstrated in Figure 4.9. Since these increased radiation stress gradients dominate almost everywhere, without a change of sign, both parameterizations will increase the set-up along all the coasts in the computational area; the $\beta - kd$ more so than the φ parameterization. The location of the blue regions in Figures 4.10B and C indicates that the $\beta - kd$ parameterizations shifts the region where depth-induced breaking occurs further offshore than the φ parameterization, most notably just north of the island of Ameland.

It should be noted however that for the up-scaled storm, the wind, current and water level fields are all hypothetical and cannot be verified. In particular, van Vledder and Adema (2007), discuss their concerns of the application of the one-way coupling applied between the circulation and wave model, i.e., the influence of wave-induced forces on the water level and current fields.

4.6. CONCLUSIONS

In this study, we show that over the three field sites considered, representing a gently sloping beach, a near-horizontal shoal and an intertidal region, the $\beta - kd$ scaling of Salmon et al. (2015) with directional partitioning included provides the best results for depth-induced breaking compared to the default and φ parameterizations.

For the Haringvliet field cases, representative of non-locally generated waves breaking over a fairly flat shoal, only the $\beta - kd$ parameterization performs equally well at both the seaward and shoreward locations. Similar improvements are expected when the $\beta - kd$ parameterization is applied to similar coastal environments e.g. swell breaking over reef platforms.

Over the complex intertidal field cases of the Amelander Zeegat, the $\beta - kd$ parameterization performs better over regions of local finite-depth wave growth than the default parameterization. On average, these improvements over the Amelander Zeegat are shown to be comparable to the φ parameterization of van der Westhuysen (2009, 2010). In particular, for the Amelander Zeegat A07_03 case (with the highest wind speed; 21.1 m/s), the $\beta - kd$ parameterization is shown to provide the best agreement with the observed spectra. However, all three parameterization are shown to perform equally poorly over the tidal channels, underestimating the energy near the peak frequency. Wave-current interactions and the effect of currents on wave growth may well be responsible.

For the Petten cases, i.e., simple coastal environments with an open beach and straight coastline, all three parameterizations perform comparably with no preferred parameterization identified.

Overall, the $\beta - kd$ parameterization performs best and it is therefore recommended for use instead of the currently used default parameterization for operational purposes,

particularly for complex coastal environments which are characterized by extended horizontal bathymetries and local wave generation.

These improvements in the prediction capability for spectral wave models with the $\beta - kd$ parameterization is shown to be a balance between the effects of local bathymetry and local normalized wave number (or water depth). This balance distinguishes between locally and non-locally generated waves (swell) and allows for *reduced* depth-induced breaking for locally generated waves as suggested by van der Westhuysen (2010) but, in contrast, also for *increased* depth-induced breaking for non-locally generated waves (swell) over horizontal bottoms (reefs and shoals) as proposed in previous studies e.g. Nelson (1997). Our computations show that these contrasting effects are occasionally modified by any excessive directional spreading of the waves, e.g., due to refraction.

Despite these improvements, further research is still required to derive a more universal 2D wave breaking source term. Errors are still found for directional wave conditions, say $\sigma_\theta > 50°$, and for the most complex bathymetries, e.g. the tidal channels found over the eastern transect of the Amelander Zeegat. Some of these errors may also be due to the uncertainties in the remaining wave physics such as wave-current interaction and wind-wave growth. Therefore, greater focus on the spectral balance is required. In particular, depth-induced dissipation has been shown to be quadratic (e.g. Chen et al., 1997; Smit et al., 2014), however this is still not applied on a routine basis. This is partially due to the uncertainties in the parameterization of the triad wave-wave interactions which are poorly represented, if at all, which in turn restricts the reliability of the computed spectral shape.

The contributions of the $\beta - kd$ parameterization are illustrated under the design conditions for the Dutch coast near the complex coastal bathymetry of the Amelander Zeegat. In comparison to the results with the default parameterization, larger significant wave heights were predicted over both the tidal delta and intertidal regions. Significant wave heights up to ~ 0.4 m higher, i.e., from ~ 2 m to ~ 2.4 m were predicted just off the Dutch mainland (behind the barrier islands). Qualitatively, the φ parameterization is shown to provide a similar trend of increasing the significant wave height, however this increase is approximately half that predicted with the $\beta - kd$ parameterization. This is reflected in wave-induced forces computed with the $\beta - kd$ parameterization that are larger than those computed with the φ parameterization, which in turn are larger than those computed with the default parameterization. This implies increased wave-induced set-up and currents along all coasts in the computational domain. The most significant difference however, under these design conditions, is the reduction of the predicted significant wave height of the $\beta - kd$ parameterization *seawards* of the barrier islands. There, significant wave heights up to ~ 0.8 m smaller than those predicted with the default and φ parameterizations are shown corresponding to a reduction from ~ 5 m significant wave height to ~ 4 m. This results in a surf zone region located further offshore with a significantly increased wave-induced set-up.

In the context of engineering applications, these differences in wave heights and radiation stresses (with corresponding differences in set-up and wave-induced currents) are large and are expected to be important for the design and management of sea defenses under extreme conditions. However, continued model exercises with fully coupled wave and hydrodynamic models are called for to refine the estimated effects of the

alternative breaking parameterizations under extreme conditions.

ACKNOWLEDGEMENTS

The first author (J.S.) is financially supported by the US Office of Naval Research under Grant N00014-10-1-0453 and Grant N00014- 12-1-0534. We are indebted to our colleagues Gerbrant van Vledder and Marcel Zijlema for their support and suggestions during this study. The authors also thank the reviewers for their feedback and suggestions and Deltares for providing the outline of the Dutch coastline (openearth.deltares.nl).

5

A CONSISTENT COLLINEAR TRIAD APPROXIMATION FOR OPERATIONAL WAVE MODELS

James SALMON, Pieter SMIT, Tim JANSSEN, Leo HOLTHUIJSEN

In shallow water, the spectral evolution associated with energy transfers due to three-wave (or triad) interactions is important for the prediction of nearshore wave propagation and wave-driven dynamics. The numerical evaluation of these nonlinear interactions involves the evaluation of a weighted convolution integral in both frequency and directional space for each frequency-direction component in the wave field. For reasons of efficiency, operational wave models often rely on a so-called collinear approximation that assumes that energy is only exchanged between wave components travelling in the same direction (collinear propagation) to eliminate the directional convolution. In this work, we show that the collinear approximation as presently implemented in operational models is inconsistent. This causes energy transfers to become unbounded in the limit of unidirectional waves (narrow aperture), and results in the underestimation of energy transfers in short-crested wave conditions. We propose a modification to the collinear approximation to remove this inconsistency and to make it physically more realistic. Through comparison with laboratory observations and results from Monte Carlo simulations, we demonstrate that the proposed modified collinear model is consistent, remains bounded, smoothly converges to the unidirectional limit, and is numerically more robust. Our results show that the modifications proposed here result in a consistent collinear approximation, which remains bounded and can provide an efficient approximation to model nonlinear triad effects in operational wave models.

This chapter has been published as SALMON, J.E., SMIT, P.B., JANSSEN, T.T. and HOLTHUIJSEN, L.H. (2016). A consistent collinear triad approximation for operational wave models. *Ocean Modelling*, **104**, pp. 203–212.

5.1. INTRODUCTION

The evolution of ocean waves due to three-wave (or triad) interactions near the coast and in shallow water is important for the prediction of nearshore wave characteristics (see e.g. Herbers et al., 2000) and wave-driven dynamics (see e.g. Hoefel and Elgar, 2003). In deep water, these interactions are generally off-resonant and the nonlinear evolution is governed by higher-order resonances (Hasselmann, 1962). In contrast, near the coast, due to reduced water depth, these three-wave interactions approach resonance and can drive $O(1)$ energy transfers on length scales of $O(10)$ wavelengths (see e.g. Janssen et al., 2006). In particular, in the surf zone, the evolution of the wave spectrum is almost entirely dictated by the balance between nonlinear triad interactions and depth-induced breaking (e.g. Kaihatu and Kirby, 1995; Herbers et al., 2000; Smit et al., 2014). Accounting for these effects in operational wave models for coastal wave propagation (e.g. Tolman, 1990b; Komen et al., 1994; Booij et al., 1999) is therefore important.

Operational wave models describe the spatial 2D evolution of the directional wave spectrum $E(\sigma,\theta;\mathbf{x},t)$ through geographical space $\mathbf{x}=(x,y)$, and through frequency σ and directional space θ, by solving a wave action balance equation of the form (e.g. WAMDI Group, 1988):

$$\frac{\partial N}{\partial t}+\frac{\partial c_{g,x}N}{\partial x}+\frac{\partial c_{g,y}N}{\partial y}+\frac{\partial c_{\sigma}N}{\partial \sigma}+\frac{\partial c_{\theta}N}{\partial \theta}=\frac{S}{\sigma} \tag{5.1}$$

Here, $N(\sigma,\theta;\mathbf{x},t)=E/\sigma$ is the wave action density, $\sigma=2\pi f$ is the radian frequency, $c_{g,x}$, $c_{g,y}$, c_{σ}, c_{θ} denote transport velocities in geographical, frequency and directional space, respectively, and S represents the source terms that account for non-conservative and nonlinear processes, including triad interactions. The difficulty with incorporating three-wave nonlinearity is that these interactions will result in the development of high-order correlations for which a separate transport equation should be evaluated, and some closure approximation invoked (e.g. Eldeberky, 1996; Becq-Girard et al., 1999; Herbers et al., 2003; Janssen, 2006). Because of the inherent complexity of the problem and for reasons of efficiency, much effort has gone into developing efficient approximations for the evolution of the unidirectional energy density spectrum $E(\sigma;\mathbf{x},t)$ (e.g. Eldeberky, 1996; Becq-Girard et al., 1999; Toledo and Agnon, 2012). In this context, one of the first – and perhaps most widely used – of these approximations is the Lumped Triad Approximation (LTA; Eldeberky, 1996). This efficient approximation, which amongst numerous other simplifications (see e.g. Becq-Girard et al., 1999), accounts only for self-self interactions and takes the form

$$S_{nl3}^{1D}(\sigma_1)\propto (W_1)^2\left[(E_2)^2-2E_1E_2\right]-2(W_3)^2\left[(E_1)^2-2E_1E_3\right] \tag{5.2}$$

where $W_i=W(\sigma_i,x)$ is an interaction coefficient (given by Madsen and Sørensen, 1993, their Eq. 5.4) and $E_i=E(\sigma_i)$ with $\sigma_1=\sigma$, $\sigma_2=\sigma/2$ and $\sigma_3=2\sigma$. For brevity, the dependence on x (or $\mathbf{x}$) and t is implied in the spectral quantities. To apply this unidirectional self-self formulation in a fully directional model, Booij et al. (1999) proposed to use Eq. (5.2) along each spectral direction. This is achieved by simply replacing each occurrence of E_i in Eq. (5.2) with its directional counterpart $E_i^1=E(\sigma_i,\theta_1)$ to obtain the directional source term

$$S_{nl3}(\sigma_1,\theta_1) \propto (W_1)^2\left[\left(E_2^1\right)^2 - 2E_1^1E_2^1\right] - 2(W_3)^2\left[\left(E_1^1\right)^2 - 2E_1^1E_3^1\right] \tag{5.3}$$

The source term defined in Eq. (5.3) is what is known as the collinear approximation which we will refer to as the Original Collinear Approximation (OCA). In this approximation, directional components are completely isolated so that each discrete direction is treated as an independent unidirectional wave field. The assumption that energy transfers predominantly occur between (almost) collinear waves is probably reasonable for harmonic generation and transfer of energy to shorter waves in wave fields propagating over a relatively uniform beach. However, over complicated topography, where energy transfers between waves at significant angles may be important (Toledo, 2013; Groeneweg et al., 2015), this approximation should generally be used with care. Moreover, the collinear approximation is not at all suited for modelling infragravity wave generation for which full directionality would have to be retained (Herbers et al., 1995).

Even though directionally-coupled models are available (e.g. the full directional SPB model; Becq et al., 1998), the collinear approximation is still the most widely applied triad model (for instance in e.g. WAVEWATCH III, SWAN, TOMAWAC), principally because the numerical evaluation of these less restrictive models is prohibitively expensive for routine operational use. Despite its continued use, the performance of the directional version of the LTA is highly unsatisfactory, which is often ascribed to the shortcomings of the underlying LTA model. As a consequence, efforts towards the improvement of the OCA have focused on improving the underlying LTA approximation (see e.g. Booij et al., 2009).

Although the LTA model is undoubtedly a crude approximation, the principal source of the errors in the OCA is not due to the LTA. Instead, it results from the directional decoupling as applied in the OCA. For instance, from Eq. (5.3) it can be shown that the OCA predicts unbounded energy transfers in the limit of unidirectional waves, and generally underestimates nonlinear transfers in short-crested seas. To illustrate this numerically, we consider energy transfers predicted by $S_{nl3}(\sigma,\theta)$ (as implemented in SWAN) for a directional wave spectrum of the form $E(\sigma,\theta) = D(\theta)E(\sigma)$. In the simulations, we increasingly reduce the aperture of the directional distribution $D(\theta)$, while maintaining the same frequency spectrum $E(\sigma) = \int E(\sigma,\theta)\,d\theta$. From these simulations (see Figure 5.1), we see that the energy transfers as predicted by the OCA become excessively large as the directional width is reduced. In fact these transfers greatly exceed the energy transfers predicted by the unidirectional triad model of Eldeberky (1996) on which the SWAN collinear model is based, and to which it should reduce to if the collinear model is consistent.

Clearly, the excessive energy transfers for narrow directional apertures indicates that the collinear approximation fails to reduce to the unidirectional limit. This inconsistency is the principal motivation for the present study. To identify the source of the error, we revisit the formulation of the collinear approximation as used in various models and provide a more consistent formulation that removes the unrealistic sensitivity to directional aperture, while retaining similar efficiency gains (Section 5.2). By no means do we argue that the collinear approximation, even in a more consistent form, represents a complete description of the three-wave interactions. However, we acknowledge that approximations for increasing efficiency are a reality for many operational applications and our

objective here is to improve the collinear approximation to ensure it is at the very least internally consistent to improve its potential for operational use.

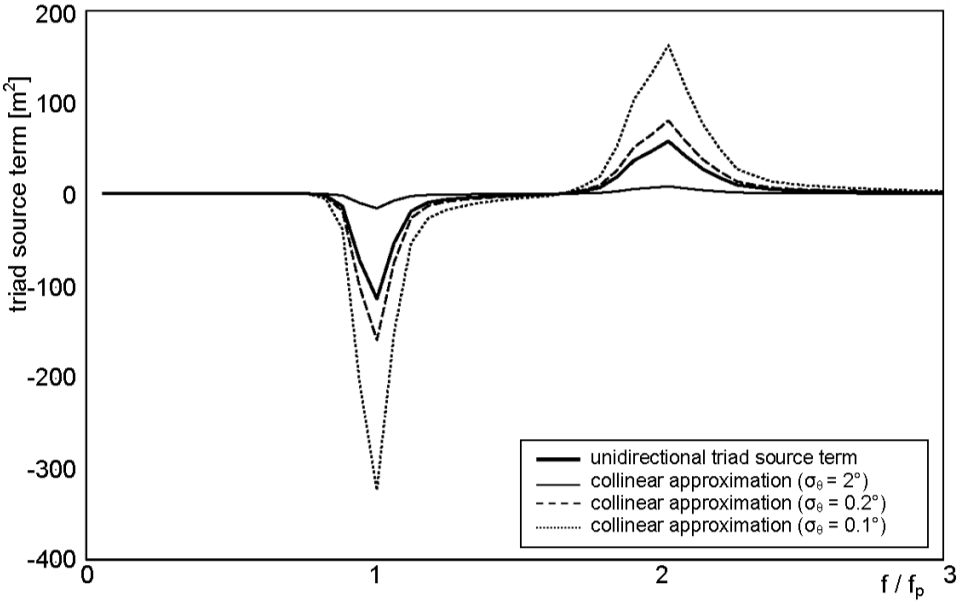

Figure 5.1: Energy transfers due to nonlinear triad interactions for a wave field with a JONSWAP spectrum (H_{m0} = 5 m and T_p = 12 s) in 5 m water depth for varying directional widths as computed by the OCA implementation in SWAN (see Booij et al., 1999). As the directional width is reduced, energy transfers greatly exceed the transfers predicted by the unidirectional triad model of Eldeberky (1996, thick solid line) on which the OCA model is based, and to which it should – in theory – reduce to. The fact that it does not suggests that there is an inconsistency in the collinear approximation.

To show the differences between the original and proposed approximation, we calibrate and validate both collinear models using laboratory data, and with Monte Carlo simulations with a deterministic model (Section 5.3 and 5.4). We discuss and summarize our principal results and their implications in Section 5.5 and 5.6.

5.2. COLLINEAR TRIAD APPROXIMATIONS

In order to identify the source of the inconsistency in the OCA, and derive an improved version of the collinear approximation, the Consistent Collinear Approximation (CCA), we consider the source term for energy transfers due to triad interactions for weakly nonlinear waves over slowly varying bathymetry. This can be written as (e.g. Eldeberky, 1996; Becq et al., 1998; Smit and Janssen, 2016)

$$S_{nl3}(\sigma_1,\theta_1) = c_{g,1}\int_0^{2\pi}\int_{-\infty}^{\infty} W_{2,1-2}^{2,1-2}\, Im\left\{B_{2,1-2}^{2,1-2}\right\} d\sigma_2 d\theta_2 \tag{5.4}$$

where W is a real coupling coefficient, B denotes the bispectrum and $Im\{\ldots\}$ denotes the imaginary part of the argument. The shorthand notation $W_{2,1-2}^{2,1-2}$ (and for B, E etc.)

relates to $W(\sigma_2, \sigma_1-\sigma_2, \theta_2, \theta_1-\theta_2)$ where the subscript and superscript denote the frequency and directional components involved, respectively. Equation (5.4) gives the complete source term for a WKB approximation of weakly nonlinear waves. In order to arrive at a collinear approximation we need to introduce a series of assumptions, and we will step through them systematically. As a first step, all the interaction coefficients are replaced by their unidirectional equivalents (i.e. $W^{2,1-2}_{2,1-2} \rightarrow W^{1,1}_{2,1-2} \equiv W_{2,1-2}$) and the bispectrum is expressed in terms of local products of the spectral components while making use of its symmetries, so that S_{nl3} can be written as

$$S_{nl3}(\sigma_1,\theta_1) = 2c_{g,1}\left[\int_0^{\sigma_1} W_{2,1-2}\overline{B^1_{2,1-2}}d\sigma_2 - 2\int_0^{\infty} W_{2,1}\overline{B^1_{2,1}}d\sigma_2\right] \tag{5.5}$$

where the first and second integrals represent contributions due to the sum and difference interactions, respectively, and

$$\overline{B^1_{2,1-2}} = \Phi^1_{2,1-2}\int_0^{2\pi} Q^{2,1-2}_{2,1-2}d\theta_2 \tag{5.6}$$

Here $\Phi^1_{2,1-2} = \Phi(\sigma_2, \sigma_1-\sigma_2, \theta_1)$ is an (empirical) factor that approximately accounts for the closure approximation implied and the development of the bispectrum towards resonance for collinear shallow waves (see e.g. Becq-Girard et al., 1999), and

$$Q^{2,1-2}_{2,1-2} = \left[W_{2,1-2}E^2_2E^{1-2}_{1-2} - E^1_1\left(W_{1,-2}E^2_2 + W_{1,2-1}E^{1-2}_{1-2}\right)\right] \tag{5.7}$$

Equivalent expressions for the difference term is achieved by replacing the subscript and superscript pairs. The expression of the bispectrum in terms of an algebraic relation to products of local energies is possible by introducing a quasi-normal closure approximation for the nonlinear hierarchy and assuming that three-wave correlations can be expressed in terms of the products of local spectral components (see Herbers et al., 2003; Janssen, 2006). Although all the assumptions to approximate the nonlinear term can be questioned independently, we will assume here that they are reasonable for the intended range of application of the collinear approximation.

From here, the final step towards the collinear approximation is to replace all the spectral components by the directional components, simply drop the directional integration, and add a calibration constant for tuning. The Original Collinear Approximation (OCA) can then be written as

$$\overline{B^1_{2,1-2}} \approx \overline{B^{1,(OCA)}_{2,1-2}} = \alpha\Phi^1_{2,1-2}Q^1_{2,1-2} \tag{5.8}$$

with

$$Q^1_{2,1-2} = \left[W_{2,1-2}E^1_2E^1_{1-2} - E^1_1\left(W_{1,-2}E^1_2 + W_{1,2-1}E^1_{1-2}\right)\right] \tag{5.9}$$

and where α is a (dimensional) calibration constant. Effectively, with these approximations each direction is considered in isolation as if it was a unidirectional wave field and energy is only exchanged between collinear components. From the series of approximations, it is this last step which introduces the inconsistency that causes the erratic behavior for narrow-aperture waves (see Figure 5.1).

By simply dropping the directional integration, the effects of directional width are effectively (but implicitly) moved to the calibration coefficient, which thus becomes strongly dependent on the directional aperture of the wave field. The consequence of this is that, once calibrated, energy transfers become exaggerated when applied to wave fields with narrower apertures than for which it was calibrated. This can be readily seen if we consider the special case of a wave field with directional aperture $\Delta\theta$, and a uniform distribution of wave energy in directional space, such that $E(\sigma,\theta) = E(\sigma)/\Delta\theta$ for $\theta \in \Delta\theta$ (and 0 elsewhere). For this case, due to the omission of the directional integral, without making any provisions to ensure dimensional consistency, we have

$$\overline{B^{1,(OCA)}_{2,1-2}} = \frac{\alpha}{\Delta\theta}\overline{B^{1}_{2,1-2}} \tag{5.10}$$

This shows that for a given, and fixed, value of the calibration coefficient α, the dropping of the directional integration introduces a strong dependency on the directional aperture $\Delta\theta$ and in the limit of $\Delta\theta \to 0$ the result becomes unbounded. This is what causes the erratic behavior for the energy transfers in general and unrealistic amplification of energy transfers for small aperture wave fields specifically, as seen in Figure 5.1.

5

5.2.1. A CONSISTENT COLLINEAR APPROXIMATION (CCA)

Although the collinear approximation relies on a number of assumptions to simplify the numerical evaluation, it is principally the dropping of the directional integration that introduces an inconsistency and limits the potential of the collinear approximation in operational wave models. To maintain a similar level of efficiency, while bypassing this inconsistency, we propose a slight modification of the collinear terms, which can be written as

$$\overline{B^{1,(CCA)}_{2,1-2}} = \alpha\Phi^{1}_{2,1-2}\overline{Q^{1}_{2,1-2}} \tag{5.11}$$

where

$$\begin{aligned}\overline{Q^{1}_{2,1-2}} \;=\; & \frac{1}{2}\left(W_{2,1-2}\overline{E^{1}_{2}}E^{1}_{1-2} - \overline{E^{1}_{1}}\left\{W_{1,-2}E^{1}_{2} + W_{1,2-1}E^{1}_{1-2}\right\}\right)\\ & + \frac{1}{2}\left(W_{2,1-2}E^{1}_{2}\overline{E^{1}_{1-2}} - E^{1}_{1}\left\{W_{1,-2}\overline{E^{1}_{2}} + W_{1,2-1}\overline{E^{1}_{1-2}}\right\}\right)\end{aligned} \tag{5.12}$$

in which

$$\overline{E^{j}_{i}} = \int_{\theta_j - p_\theta/2}^{\theta_j + p_\theta/2} E(\sigma_i,\theta)\,d\theta \tag{5.13}$$

and where p_θ is a tuning parameter which determines how close the approximation mimics a unidirectional model. Effectively thus, in this approximation, which we refer to as the Consistent Collinear Approximation (CCA), instead of simply dropping the directional convolution integral (see Eq. 5.4) we assume that

$$\int_0^{2\pi} E^{2}_{2}E^{1-2}_{1-2}\,d\theta_2 \propto \frac{1}{2}\left[\overline{E^{1}_{2}}E^{1}_{1-2} + E^{1}_{2}\overline{E^{1}_{1-2}}\right] \tag{5.14}$$

and absorb the dimensionless constant of proportionality into the calibration factor α. By re-writing the collinear approximation in this way, we prevent the inconsistency and potential singularity as present in the original formulation. Moreover, since $\overline{E_2^1} \leq \int_0^{2\pi} E_2^1 d\theta = E_2$ it follows that $\frac{1}{2}\int_0^{2\pi}\left[\overline{E_2^1}E_{1-2}^1 + E_2^1\overline{E_{1-2}^1}\right]d\theta \leq E_2 E_{1-2}$ so that the directionally-integrated energy transfers are always less than or equal to the transfers in an equivalent unidirectional wave field. The latter is internally consistent with the underlying premise that the collinear interactions are closest to resonance and are the most efficient contributors to the nonlinear transfers. In fact, with $p_\theta = 2\pi$, the integrated energy transfer becomes

$$S_{nl3}(\sigma) = \int_0^{2\pi} S_{nl3}(\sigma,\theta)\, d\theta = S_{nl3}^{1D}(\sigma) \qquad \text{with} \qquad p_\theta = 2\pi.$$

In this sense, the parameter p_θ is an independent calibration parameter, such that if the magnitude of p_θ is reduced (and thus the integration aperture in the interaction term), the strength of the interactions in wide-aperture wave fields is suppressed, consistent with what is typically observed. Although the CCA (Eq. 5.11) does require an additional directional integral (compared to the OCA), its efficiency is similar to the OCA since it reduces the full convolution to a simple one-dimensional integral and a multiplication, while still reproducing the qualitative features of Eq. (5.8).

For a complete model, we would still need to introduce suitable approximations for the closure factor $\Phi_{2,1-2}^1$, which in itself has not been resolved in the literature (see, for example Orszag, 1974; Janssen, 2006, for an overview) and is outside the scope of this work. Since our primary goal is to resolve the directional sensitivity issue in the OCA, and to allow a direct comparison between the models, we will continue to use the closure assumption and other simplifications as implied by the LTA. However, to emphasize that the collinear approximation, and the improvement proposed in this work is in essence an approximation layer on top of an underlying 1D triad model, we also implement an OCA and CCA version of the Stochastic Parametric Boussinesq (SPB) model by Becq-Girard et al. (1999). This model differs from the LTA-based collinear model in that it accounts for triad interactions between all frequency components and not just the self-self interactions. In essence, the collinear SPB implementation has the same decoupling between directional components, but includes all wave-wave interactions for each directional component individually and does not suffer from the limitations of the restriction to only self-self interactions as does the LTA. For further details regarding the two different models, we refer to Appendix 5.A.

5.3. MODEL SETUP AND OBSERVATIONS

In what follows, we compare simulations with the SWAN wave model (version 40.91A) using both the Original Collinear Approximation (OCA, Eq. 5.8) and the Consistent Collinear Approximation (CCA, Eq. 5.11) for a range of different wave conditions. We couple the collinear approximations to both the LTA model (Eldeberky, 1996) and the SPB model (Becq-Girard et al., 1999). Furthermore, in the CCA, we set $p_\theta = 2\pi$ for all the numerical results, and discuss the implications of other choices for p_θ in Section 5.5. Model simulations are run with the dissipative source terms suggested by Zijlema et al.

(2012) with the Battjes and Janssen (1978) depth-induced wave breaking model scaled with $\gamma = 0.73$ and the curvature-based stopping criteria of Zijlema and van der Westhuysen (2005) with a cap of 50 iterations.

To calibrate the models, we consider two unidirectional laboratory data sets described by Beji and Battjes (1993) and Boers (1996) with random waves (characterized by a JONSWAP spectrum at the wavemaker) propagating over a barred-beach profile (see Figure 5.2). The Beji and Battjes (1993) data set consists of a single wave condition with a significant wave height of $H_{m0} = 0.023$ m and a peak period of $T_p = 2.0$ s. The Boers (1996) data set consists of three wave conditions with $H_{m0} = 0.160$, 0.220 and 0.107 m and $T_p = 2.1$, 2.1 and 3.4 s, respectively. We chose these data sets as they have been used extensively for calibration in previous triad studies (see e.g. Booij et al., 1999; van der Westhuysen, 2007). Following those studies, we approximate the unidirectional conditions with a small (but otherwise arbitrary) directional width of $\sigma_\theta = 2^\circ$ (as defined by Kuik et al., 1988) uniformly over all frequencies. Furthermore, computations are performed with frequency resolution $\Delta f = 0.05 f$ and frequency range [0.0837, 2.5] Hz and [0.15, 2.0] Hz for the Beji and Battjes, and Boers data set, respectively. Computations include a 20° directional sector, centered about the mean wave direction with $\Delta\theta = 0.05^\circ$. Subsequently, to demonstrate the sensitivity of the collinear approximations to the directional aperture of the incident wave field, we perform simulations with varying directional widths ranging from $0.1^\circ \leq \sigma_\theta \leq 5^\circ$.

To verify the effect of the collinear approximation for directional wave fields, for which detailed observations are less readily available, we compare the collinear approximation models to Monte Carlo simulations with a second-order accurate deterministic Boussinesq model based on an angular-spectrum decomposition (Herbers and Burton, 1997). Although the interaction coefficients in the Herbers and Burton (1997) model are slightly different from those in the LTA and SPB models (which also differ), these differences are negligible compared to the effects of the collinear and closure approximations in these models. The only physical processes included in the deterministic model and the SWAN models are the triad interactions and depth-induced wave breaking dissipation (all other source terms are turned off in SWAN). Since dissipation in the deterministic model is implemented consistently with SWAN, we can ascribe any differences between the Monte Carlo simulations and the collinear approximations to the collinear approximation, and the closures implied by the LTA and SPB models.

The directional wave simulations are run over a plane beach using the same beach profile as in the laboratory setup of Smith (2004, see Figure 5.3). However, instead of unidirectional incident waves, we generate directional wave conditions at the incident wave boundary. We use the laboratory setup by Smith (2004) so that we can verify the deterministic model for unidirectional wave propagation against observations for the same beach profile (not shown).

The simulations are initialized at Station 1 (see Figure 5.3) with spectra identical to that measured by Smith (2004). The incident wave field consists of a TMA spectrum with $H_{m0} = 0.09$ m, $T_p = 2.5$ s and $\gamma_{TMA} = 3.3$ for Case A (broad-banded in frequency space) and $\gamma_{TMA} = 100$ for Case B (narrow-banded). For the directional distribution, we apply a $cos^m\theta$ model uniformly to all frequencies and consider the directional widths $\sigma_\theta = 2^\circ$, 4°, 10°, 20° and 30°.

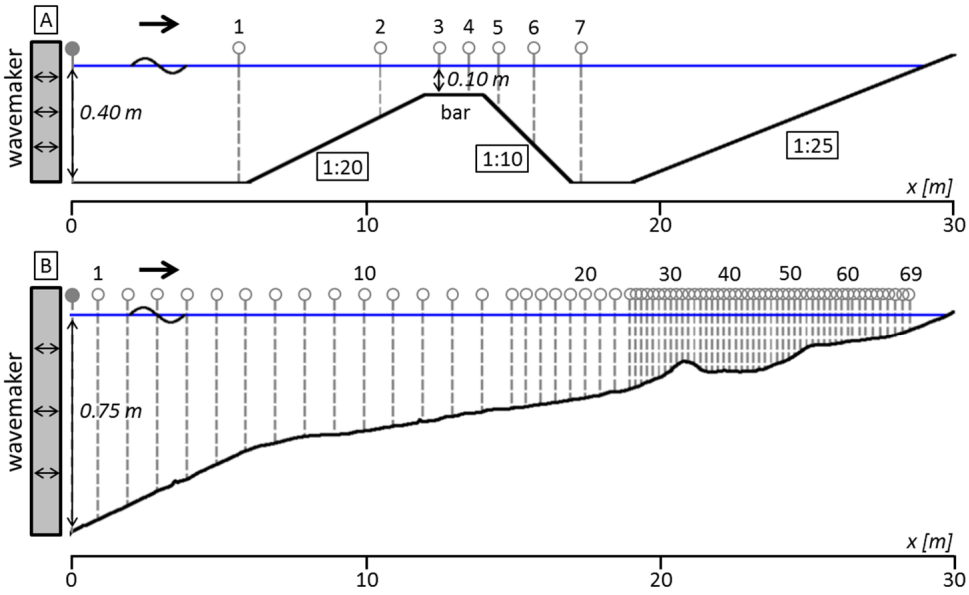

Figure 5.2: Configuration of the Beji and Battjes (1993, Panel A) and Boers (1996, Panel B) laboratory flume experiments. The measurement locations are indicated by the vertical dashed lines and the location of the offshore boundary is indicated by the solid dot near the wavemaker.

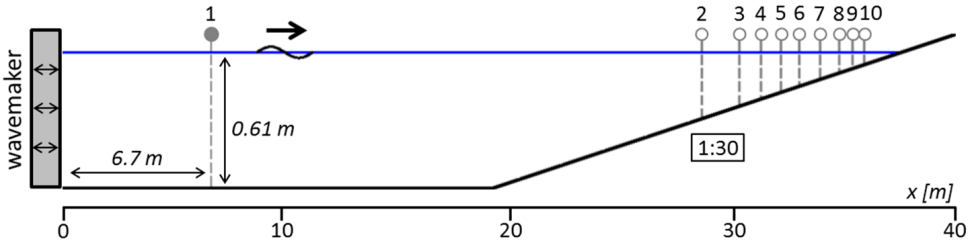

Figure 5.3: Configuration of the Smith (2004) laboratory flume experiment. Annotations are as in Figure 5.2.

Monte Carlo simulations with the deterministic model consist of 128 realizations with a spatial resolution $\Delta x = 0.025$ m, a lateral wavenumber array defined as $\Delta k_y\,[-M/2+1,\ldots,M/2]$ with $M = 32$ and $\Delta k_y = 0.1$, and a frequency array consisting of 120 frequencies with $\Delta f = 0.025$ Hz. In what follows, we consider the deterministic model results as a proxy for observations, and compare these with SWAN computations with similar settings as before but with $\Delta f = 0.1 f$ (over the range [0.2, 3.0] Hz) and $\Delta\theta = 1°$ over a full circle.

5.4. RESULTS

5.4.1. UNIDIRECTIONAL RANDOM WAVES

To calibrate α for both collinear models (OCA and CCA) and both triad closure models (LTA and SPB), α was varied over the range $0.01 \leq \alpha \leq 1.50$ with $\Delta\alpha = 0.01$. For each data set, the scatter index, $s.i. = \sqrt{N\sum\left(\chi_{comp.} - \chi_{obs.}\right)^2} / \sum \chi_{obs.}$ was computed where N denotes the sample size and χ represents either the significant wave height, H_{m0} or the mean wave period, T_{m02} computed from the spectral moment $m_n = \iint \sigma^n E(\sigma,\theta)\, d\sigma d\theta$ (i.e., $H_{m0} = 4\sqrt{m_0}$ and $T_{m02} = 2\pi\sqrt{m_0 m_2^{-1}}$). The subscripts *comp.* and *obs.* refer to the computed and observed values, respectively.

From the scatter indices for H_{m0} and T_{m02}, the optimal calibration coefficients for the OCA model were found to be $\alpha_{LTA}^{OCA} = 0.04$ and $\alpha_{SPB}^{OCA} = 0.07$ with an averaged scatter index of $\overline{s.i.} = 5\%$ and $\overline{s.i.} = 8\%$, respectively. These low α values are consistent with previous studies (e.g. Booij et al., 1999; van der Westhuysen, 2007). However, they are small compared to the original calibration values of Eldeberky (1996) and Becq-Girard et al. (1999), i.e., $\alpha = 1$. Using the CCA implementation, optimal values closer to $\alpha = 1$ are found with $\alpha_{LTA}^{CCA} = 0.52$ ($\overline{s.i.} = 5\%$) and $\alpha_{SPB}^{CCA} = 0.87$ ($\overline{s.i.} = 8\%$).

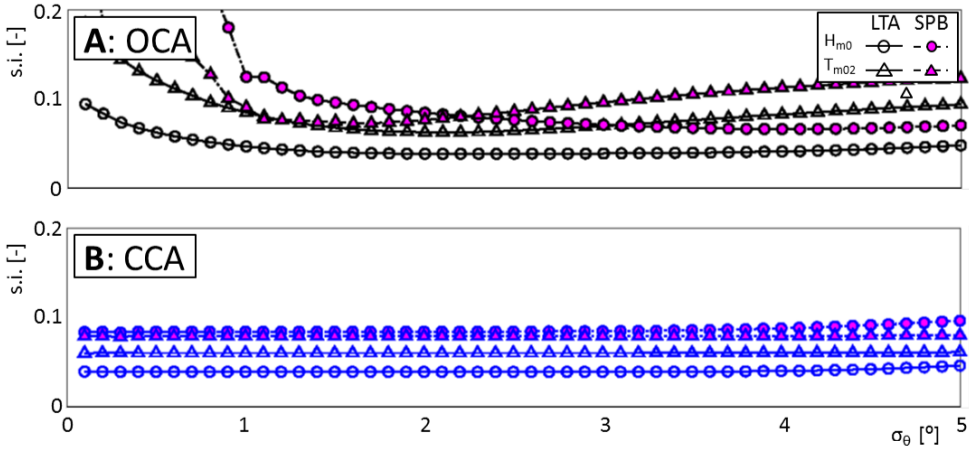

Figure 5.4: Scatter indices for the computed H_{m0} (○) and T_{m02} (△), averaged over the Beji and Battjes (1993) data set and all cases from the Boers (1996) data sets for OCA and CCA models (Panels A and B, respectively).

Using the calibrated model values, we consider the influence of changing the direc-

tional aperture of the incident spectra between $0.1^\circ \leq \sigma_\theta \leq 5^\circ$ (Figure 5.4). From the scatter index, it is seen that the CCA implementation (Figure 5.4B) is insensitive to the directional width of the incident wave spectrum for $\sigma_\theta \leq 4^\circ$, and appears to converge to the unidirectional limit, which is consistent with what we would expect on physical grounds. In contrast, the scatter index for the OCA implementation (Figure 5.4A) shows a strong sensitivity to the directional width of the incident spectrum. In particular, as the unidirectional limit is reached, the OCA errors increase significantly, consistent with what was seen in Figure 5.1.

5.4.2. SENSITIVITY TO DIRECTIONAL SPREADING

For the idealized directional cases considered, error characteristics for T_{m02} are shown in Figure 5.5. While these results demonstrate a decrease in modeling performance with increased σ_θ, which is likely caused by the models' inability to account for the non-collinear interactions, there is a clear reduction of error between the OCA (blue lines) and the CCA (black lines) for directional wave conditions. For the conditions shown, with $\sigma_\theta \geq 4^\circ$, the typical error in the CCA simulations, for both LTA and SPB models, is less than 50% of the errors in the OCA simulations. The errors for H_{m0} (not shown) are significantly smaller with $\overline{s.i.} \approx 6\%$ and less variability in errors between the directional cases ($\overline{\Delta s.i.} \approx 3\%$). This is consistent with the fact that triad interactions redistribute energy, thus primarily affect the spectral shape, to which T_{m02} is very sensitive.

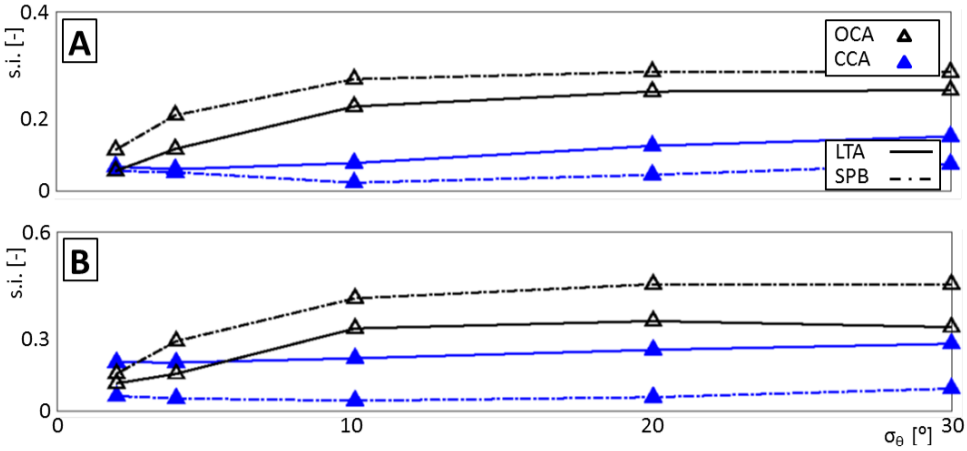

Figure 5.5: Scatter index of T_{m02} as a function of directional width for Cases A and B. Comparison is between the OCA (combined with LTA or SPB model) and CCA (with the LTA or SPB model).

To further investigate these differences, the computed spectra for Case A with $\sigma_\theta = 30^\circ$ are presented for three locations in the first row of Figure 5.6 (Panels A-C). At Station 2, negligible differences between the two model variants occur (OCA; black lines and CCA; blue lines) and overall both are in good agreement with the deterministic model (dashed red lines) irrespective of the choice of triad model (LTA or SPB). However, as the waves propagate into shallower water and the influence of the triad interactions be-

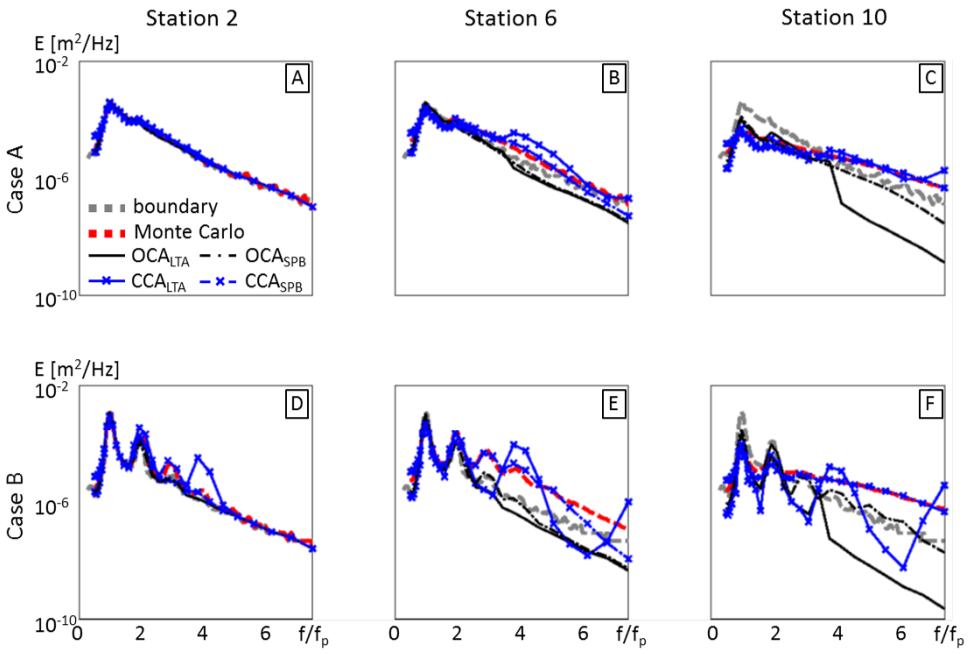

Figure 5.6: Variance density spectra for the Case A and B directional wave conditions with $\sigma_\theta = 30^\circ$ at Stations 2, 6 and 10. The gray and red dashed lines represent incident spectra and the Monte Carlo model results, respectively. The spectra computed with the OCA are represented by the black lines and with the CCA in blue with additional (×) markers. The solid and dashed-dotted lines represent spectra computed with the LTA and SPB triad models, respectively.

comes stronger, the differences become more apparent. At Station 6, just outside the surf zone, the OCA (coupled to either the LTA or SPB) generally underestimates energy transfers. This underestimation of energy transfers in the OCA particularly affects the higher frequencies, i.e., $f/f_p \geq 4$ and results in an underestimation of the high-frequency tail by an order of magnitude. At Station 10, which is deep inside the surf zone, this effect is further enhanced. In contrast, with the CCA both triad models perform much better. In particular when combined with the SPB, the overall agreement with the Monte Carlo simulations is excellent.

The more narrow-banded incident spectrum of Case B shows well-defined harmonic peaks in the Monte Carlo simulations at Station 2 and Station 6 (Figure 5.6D-F; second row). By Station 10, the high-frequency tail is again largely featureless due to the continued action of the triad interactions (Smith and Vincent, 1992). As in Case A, the OCA models transfer insufficient energy to the higher frequencies, whereas the CCA models predict significant amplification of energy, in better agreement with the Monte Carlo simulations. In particular when coupled with the SPB, the CCA reproduces both the harmonic generation and the eventual development into a featureless tail very well, and is in good quantitative agreement with the Monte Carlo simulations. In contrast, the CCA combined with the LTA cannot reproduce the enhanced energy levels at the non-self-self interaction frequencies (e.g. at $3f_p$) nor does it predict the featureless high-frequency tail (e.g. Booij et al., 2009). Furthermore, with the LTA, energy levels at self-self interaction frequencies (e.g. at $4f_p$) are typically overestimated. These discrepancies appear due to fundamental limitations of the LTA to capture these dynamics and are not associated with the collinear approximation.

In any case, the application of the CCA is shown to significantly reduce the total rms-error for T_{m02} for both the LTA and SPB models. When combined with the LTA, the average rms-error for T_{m02} for Case A and B with $\sigma_\theta = 30^\circ$ goes from 26% for the OCA to 18% for the CCA. With the SPB model, this error goes from 36% for the OCA to 7% for the CCA. These error reductions are shown to be at least comparable, if not larger than the error differences between the LTA and SPB triad models themselves (either with OCA or CCA implementation).

5.5. DISCUSSION

In this study, we revisited the collinear approximations used in operational wave models. We showed that in its conventional form, the OCA can become unbounded resulting in unrealistic transfers of energy away from the spectral peak which results in large errors and potential numerical instabilities. Historically, this inconsistency has mostly gone unnoticed likely because collinear triad models are typically calibrated with flume-type experiments using a fixed, and small, directional distribution with directional spreading, σ_θ^0 (as done here in Section 5.4.1). As a consequence, the calibration parameter formally becomes a representative angle that is only valid for that particular directional distribution. If the calibrated model is subsequently applied to waves with a different directional spreading, σ_θ (but otherwise identical spectral characteristics), the integrated energy transfers change approximately by a factor $\sigma_\theta^0/\sigma_\theta$. Therefore, for wider directional distributions, the predicted energy transfers rapidly decrease, whereas for narrow distributions, these transfers grow without limit. The net result in operational conditions (where

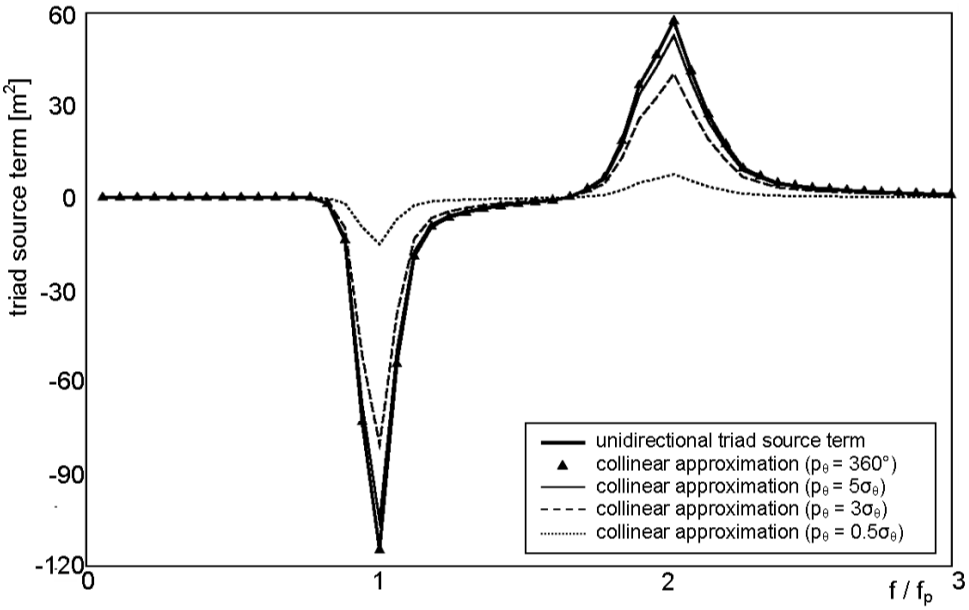

Figure 5.7: Energy transfers due to nonlinear triad interactions for a wave field as in Figure 5.1 for varying directional bandwidths as computed with the CCA.

typically $\sigma_\theta > \sigma_\theta^0$) is that these energy transfers are almost always underestimated. While heuristically, one could argue that this is qualitatively reasonable since we would expect lower transfers in short-crested seas, this result relies on a completely arbitrary directional spreading σ_θ^0 used to represent unidirectional conditions with which the model was calibrated. Furthermore, in the few cases where the wave field is indeed more narrowly supported (where nonlinear transfers are stronger and important), predicted energy transfers become effectively unbounded, which may produce unphysical results, and possibly introduces numerical stability issues. For these reasons, a formulation that is internally consistent, reduces to the correct limits for narrow-band wave fields, always produces bound results, and for which we have, through p_θ, some degree of control over how strongly the interactions attenuate with increased directional spreading, is much to be preferred.

In this work, to focus our discussion, we used $p_\theta = 360°$ for all numerical simulations. In this case the integrated energies (Eq. 5.13) are determined by computing the full directional integral over the energy spectrum. The fact that this gives reasonable results is encouraging as the assumption $p_\theta = 360°$ is actually the least compatible with the collinear assumption on which the approximation is based. The principal effect of p_θ is to reduce the strength of the energy transfers. For instance, using a similar setup as Figure 5.1, we see that by reducing p_θ we have some control on the strength of the interaction (Figure 5.7).

To assess the sensitivity and robustness of the proposed collinear approximation to p_θ, we present the scatter indices normalized by the full directional integral equivalent

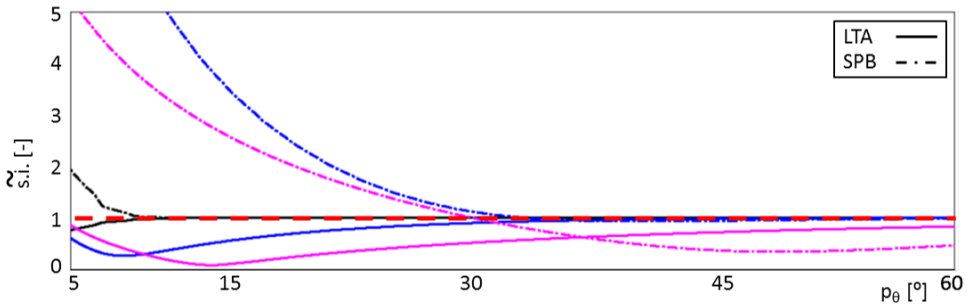

Figure 5.8: Sensitivity of the CCA to the directional integration bandwidth p_θ for Case B for varying σ_θ (2°, black; 10°, blue and 30°, magenta). The vertical axis represents the scatter index normalized with the scatter index with the full directional integral. The horizontal dashed red line indicates unity.

for Case B with $\sigma_\theta = 2°$, 10° and 30° in Figure 5.8. For all three wave conditions the normalized scatter index asymptotes to unity for $p_\theta \gg \sigma_\theta$ and convergence to the full integral is mostly found for $p_\theta \approx 3\sigma_\theta$ in agreement with Figure 5.7. A notable exception is found for $\sigma_\theta = 30°$ where smaller scatter indices are found for lower values of p_θ. This suggests that the use of the full directional integral, in very short-crested seas may lead to some overestimation of the energy transfers (which are small to begin with). The increased scatter index for T_{m02} for smaller values of p_θ is counterintuitive since we would anticipate that results should improve (albeit possible slightly) for more realistic values for p_θ. This effect is due to an overestimation of T_{m02} due to the insufficient transfer of energy to the higher frequencies.

In this work, we set out to identify the source of the unrealistic behavior of the triad source terms when using the OCA to increase the computational efficiency when coupled to the LTA or a different triad model. We propose an alternative collinear formulation (CCA) and compare results for the CCA coupled to two different triad models (LTA and SPB). However, the optimum choice of triad model is clearly outside the scope of this paper. Our objective is to identify the source of the unrealistic behavior of triad source terms when used together with the OCA to increase the computational efficiency. Clearly, the overall quality of the model will greatly depend on the underlying triad model to which the CCA is coupled. The use of any collinear approximation (such as the CCA), and the implied decoupling of non-collinear components remains an admittedly crude approximation driven primarily by the need for efficiency in operational wave models. Possibly, with the improvements proposed here, we can make these collinear models more useful for operational models, and allow larger-scale models to capture some of the principal nonlinear shallow-water effects at reasonable computational cost.

5.6. CONCLUSIONS

In this study, we consider collinear approximations used in operational wave models to compute the nonlinear source term for three-wave interactions for directional wave fields by eliminating the interactions between non-collinear wave components. We demonstrate that the Original Collinear Approximation (OCA), which is presently used in

operational wave models (e.g. SWAN), severely overestimates energy transfers in the unidirectional limit (where energy transfers in that approximation become unbounded). At the same time, the OCA underestimates energy transfers in short-crested seas. We propose a Consistent Collinear Approximation (CCA) which has the proper asymptotic behavior in the unidirectional limit and remains well behaved for wave fields with a wider directional aperture. Comparisons with flume experiments demonstrate that the CCA is a significant improvement over the OCA, is more robust and performs much better overall. Comparisons of the CCA model to Monte Carlo simulations show a significant improvement in overall performance over the OCA. Further improvements are expected through improvements to the underlying triad model.

ACKNOWLEDGEMENTS

This research is supported by the U.S. Office of Naval Research (Littoral Geosciences and Optics Program and Physical Oceanography Program), the National Oceanographic Partnership Program, and the National Science Foundation (Physical Oceanography Program). The first author (James Salmon) is financially supported by the US Office of Naval Research under Grant N00014-10-1-0453 and Grant N00014-12-1-0534. The first author also thanks the Environmental Fluid Mechanics section of Delft University of Technology for additional financial support.

APPENDICES

5.A. COLLINEAR VERSIONS OF THE LTA AND SPB MODELS

The collinear approximations discussed in the main text take the form (repeated for convenience)

$$S_{nl3}(\sigma_1,\theta_1) = 2c_{g,1}\left[\int_0^{\sigma_1} W_{2,1-2}\overline{B^1_{2,1-2}}d\sigma_2 - 2\int_0^{\infty} W_{2,1}\overline{B^1_{2,1}}d\sigma_2\right] \tag{5.A1}$$

where the first integral term represents the sum interactions $(\sigma_2, \sigma_1-\sigma_2)$ and the second the difference interactions $(\sigma_2, \sigma_1+\sigma_2)$. The OCA and CCA are then obtained using the corresponding estimates for the bispectrum

$$\overline{B^{1,(OCA)}_{2,1-2}} = \alpha\Phi^1_{2,1-2}Q^1_{2,1-2} \qquad \overline{B^{1,(CCA)}_{2,1-2}} = \alpha\Phi^1_{2,1-2}\overline{Q^1_{2,1-2}} \tag{5.A2}$$

with $Q^1_{2,1-2}$ and $\overline{Q^1_{2,1-2}}$ defined as in Eqs. (5.9) and (5.12), respectively.

The LTA model expresses the imaginary part of the bispectrum in terms of its magnitude and phase (Kim and Powers, 1979) and uses a parameterization for the bi-phase φ using the spectrally-based Ursell number (Doering and Bowen, 1995; Eldeberky, 1996, his Eq. 3.19) to control the magnitude of the energy transfers. The quasi-normal closure then takes the form

$$\Phi^{LTA}_{2,1-2} = \frac{sin\left|\varphi_{Ur}\right|}{\Delta k_{2,1-2}} \tag{5.A3}$$

where $\Delta k_{2,1-2} = k_1 - k_2 - k_{1-2}$ represents the wave number mismatch. To further reduce the computational costs of the integrals in Eq. (5.A1), the LTA model makes the following additional simplifications. First, it is assumed that the coupling coefficients are equivalent, i.e., $W_{2,1-2} = W_{1,-2} = W_{1,2-1}$ in the expressions for $Q^1_{2,1-2}$ and $\overline{Q^1_{2,1-2}}$. Secondly, the integrals are approximated by the product of a representative value of the integrand, taken to be the self-self interactions and an effective frequency interaction bandwidth $\delta\sigma$. Applying this approximation and arguing that $\delta\sigma$ and δk scale with σ_1 and k_1, using the notation $\sigma_2 = \sigma_1/2$ for convenience, the CCA version of the LTA is given as

$$S_{LTA}(\sigma_1,\theta) = 2\pi\alpha_{LTA}c_{g,1}c_1 sin\left|\varphi_{Ur}\right|\left[W_{2,2}\overline{Q^1_{2,2}} - 2W_{1,1}\overline{Q^1_{1,1}}\right] \tag{5.A4}$$

The OCA version is obtained by replacing $\overline{Q}$ with Q in Eq. (5.A4).

The SPB model of Becq-Girard et al. (1999) assumes a closure approximation based on Holloway and Hendershott (1977). In this case the closure factor takes the form

$$\Phi^{SPB}_{2,1-2} = \frac{\mu}{\left(\Delta k_{2,1-2}\right)^2 + \mu^2} \tag{5.A5}$$

where μ represents a proportionality constant between the bispectrum and the fourth-order cumulant. In the SPB model, $\mu = 0.95k_{p,0} - 0.75$, a dimensional parameter where $k_{p,0}$ is the deep water peak wave number. For application in a 2D wave model, where the offshore region is not well defined, we replace the deep water peak wave number with the local peak wave number, k_p. The CCA version of the SPB may then be expressed as

$$S_{SPB}(\sigma_1,\theta) = 8\pi\alpha_{SPB}c_{g,1}\mu\left[\int_0^{\sigma_1} W_{2,1-2}\frac{\overline{Q^1_{2,1-2}}}{\left(\Delta k_{2,1-2}\right)^2+\mu^2}d\sigma_2 - 2\int_0^{\infty} W_{2,1}\frac{\overline{Q^1_{2,1}}}{\left(\Delta k_{2,1}\right)^2+\mu^2}d\sigma_2\right] \tag{5.A6}$$

As with Eq. (5.A4), the OCA version of the SPB is obtained by replacing $\overline{Q}$ with Q in Eq. (5.A6).

6

CONCLUSIONS AND OUTLOOK

IN this thesis, new source terms suitable for 2D stochastic wave models were developed and validated for application in the coastal environment. Two of the dominant wave processes in the coastal zone, depth-induced wave breaking and nonlinear triad wave-wave interactions, were considered independently. In Chapter 3, the process of depth-induced wave breaking was studied and a new joint scaling suitable for a wide range of bathymetries and wave conditions was developed. Noting the 1D limitation of the underlying dissipation model, directional partitioning for bulk dissipation models was introduced and tested to include the effect of wave directionality. Subsequently, in Chapter 4, the implications of the new depth-induced wave breaking source term were examined from an operational context: both for the hindcasting of wave conditions and for the prediction of wave statistics under design conditions. Finally, in Chapter 5, the parameterization of nonlinear triad interactions was explored and a new collinear approximation suitable for both unidirectional and directional wave conditions was introduced. Furthermore, a less approximate triad source term was implemented for application in operational wave models. The main conclusions with respect to the two research subjects of this thesis are presented below, as is their implications for the future of stochastic wave model development and application in the coastal environment.

6.1. CONCLUSIONS

DEPTH-INDUCED WAVE BREAKING

On the basis of an analysis over an extensive set of observations of wave breaking, both in laboratory and field conditions, the $\beta - kd$ scaling, dependent on both wave field characteristics (normalized wave number) and bottom topography (bottom slope) was developed. This dependency was found to be consistent with much of the depth-induced wave breaking literature and to have comparable limits to those reported in previous studies.

At the limit of shallow water, where depth effects are strong, i.e., $kd \ll 1$, the scaling of depth-induced wave breaking was found to be independent of the wave conditions (kd)

and to depend solely upon the local bottom slope (β). For bathymetries of a constant depth, an optimal scaling of $H_{max} = 0.54d$ was determined; a value in good agreement with observations (Nelson, 1997), theory (Massel, 1998) and numerical simulations (Katsardi, 2007) which all support a limiting value of $H_{max} \approx 0.55d$. These values were shown to be comparable to the theoretical limits for the *crest* height of solitary waves propagating over constant water depth (McCowen, 1894; Longuet-Higgins, 1974) which is shown to be $0.56\bar{d} \leq H \leq 0.60\bar{d}$. An analogy with solitary waves provides a possible explanation for the insensitivity of the joint scaling to kd under the aforementioned conditions. Furthermore, for bathymetries with steeper slopes, a positive dependency of $\gamma = H_{max}/d$ on β was found in agreement with previous β-dependent scalings (e.g. Madsen, 1976).

In intermediate to deep water, i.e., $kd > 1$, both bottom slope and normalized wave number (kd) were found to be relevant to wave breaking. The effect of increasing kd was shown to increase the limit of H_{max} and essentially disable the influence of depth-induced breaking. This is consistent with the physical interpretation of van der Westhuysen (2010) who suggests that under these conditions, which are typical for locally generated waves, depth-induced wave breaking has a reduced influence on the equilibrium balance between wind input and wave breaking (both white capping and depth-induced) due to a reduction in nonlinearity. This positive dependency of γ on kd is also consistent with previous studies (e.g. Ting, 2001; Ruessink et al., 2003).

An extensive comparison of the $\beta - kd$ scaling to 12 alternative parameterizations for 1D wave conditions demonstrated that the $\beta - kd$ model accurately predicts the bulk dissipation and evolution of significant wave height. In particular, significant error reductions were demonstrated for bathymetries of constant water depth and for wave conditions with local wave growth. A potential limitation of the underlying 1D bore-based dissipation model was indicated by the mediocre performance of the new scaling for 2D wave conditions. To address this, a heuristic directional partitioning was introduced to relax this restriction. With this, improved model performance was realized with the $\beta - kd$ scaling for 2D wave conditions. In addition, error reductions were also found for the two best performing alternative parameterizations (the Battjes and Janssen (1978) dissipation model with a constant scaling, and the corrected Baldock et al. (1998) dissipation model with the scaling of Ruessink et al. (2003)). With this directional partitioning, the $\beta - kd$ scaling was shown to be the most applicable parameterization for depth-induced wave breaking for the widest range of bathymetries and wave conditions.

To ascertain the effect of the new parameterization for hindcasting and design purposes, the $\beta - kd$ parameterization was further verified against a larger set of field observations and applied to a hypothetical 1 in 4000 year super storm (equivalent to Dutch design conditions). Compared to two reference models: the bulk dissipation model of Battjes and Janssen (1978) model with a constant scaling of $H_{max} = 0.73d$ and the recent nonlinear model of van der Westhuysen (2010), the $\beta - kd$ parameterization was shown to perform the best on average for the prediction of H_{m0}. For the prediction of locally-generated waves over intertidal regions, the $\beta - kd$ parameterization performance was similar to that of van der Westhuysen (2010) but unlike this model it did not overestimate H_{m0} over horizontal shoals. For typical beach bathymetries characterized by non-locally generated wave conditions, all three wave breaking models are comparable.

For the super storm, the $\beta - kd$ parameterization was shown to provide qualitatively

similar results to the nonlinear model of van der Westhuysen (2010). Both models predicted higher significant wave heights in regions of local wave growth and in regions of high wave directionality than that predicted with the constant scaling. In the case of the $\beta - kd$ parameterisation, this increase was up to twice that predicted by the nonlinear model. It is not clear however which of these two models is better for this hypothetical design condition. Despite this, both the $\beta - kd$ and nonlinear wave models predict increased wave-induced set-up and currents along the coasts shoreward of intertidal regions which is of great importance for engineering design and research.

However, the most surprising result was found in regions characterized by predominantly non-locally generated waves propagating over gently sloping bottom in extreme conditions. Under these circumstances, the $\beta - kd$ parameterization predicts that these waves may become depth-limited and dissipate in more offshore regions than that predicted by previous parameterizations. This may result in a different patterns of wave-induced set-up and currents to those predicted by previous models. Understanding these differences is essential for understanding the different processes occurring along our coasts.

In conclusion, the comparison suggests that the $\beta - kd$ parameterization can be applied over a larger range of field conditions, both of wave conditions and bottom topography, than currently available parameterizations. In particular, the use of the $\beta - kd$ parameterization is recommended both in regions of constant water depth e.g. intertidal regions, reefs and rocky shoals, and in regions of locally-generated wave conditions.

NONLINEAR TRIAD WAVE-WAVE INTERACTIONS

The prediction of the spectral shape or distribution of wave energy in frequency space is typically worse than the prediction of the total wave energy. Although this is invariably due to the crudeness of the underlying triad models, necessitated by computational considerations, the present work also highlighted the significant impact the collinear approximation can have on model performance.

Near the unidirectional limit, the conventional collinear approximation (OCA) was found to be inconsistent with the underlying directional triad model. At this limit, energy transfers as computed with the OCA were found to become unbounded and diverge from the underlying source term. This was shown to be a peculiarity of the OCA which rendered the resulting source term dependent on the inverse of the directional width of the spectrum, σ_θ^{-1}.

The most immediate problem of this inconsistency was demonstrated at the unidirectional limit where the predicted energy transfers were shown to be unbounded with physically unrealistic energy transfers. On re-calibration of two of the simplest unidirectional triad models with the conventional collinear approximation (LTA, Eldeberky (1996); SPB, Becq-Girard et al. (1999)), the calibration results suggested that this inconsistency has likely gone unnoticed due to this systematic error having been removed through calibration over unidirectional conditions. In agreement with previous calibration exercises (e.g. Booij et al., 1999; van der Westhuysen, 2007), a low value for the optimal calibration coefficient was found for both models ($\alpha^{OCA} \approx 0.05$); a value significantly smaller than those used by the original authors ($\alpha = 1$).

The effect of using such small calibration values is to attenuate the predicted en-

ergy transfers to physically realistic values. However, two serious implications of this approach are emphasized. First, any calibration exercise carried out over unidirectional wave conditions becomes specific to the small, but finite, directional width required to define unidirectional waves in 2D spectral wave models. Second, and more importantly, any calibration over unidirectional wave conditions becomes irrelevant for *directional* wave conditions. Under these conditions, such calibrated triad models will severely underestimate the energy transfers due to both the effects of the reduced value of α and the inverse scaling of σ_θ which both act to attenuate the magnitude of the underlying source term. This results in the poor estimation of wave parameters that are dependent on the spectral shape such as mean wave period (or frequency).

To resolve this problem, a consistent framework for implementing 1D unidirectional triad source terms in 2D wave models is introduced through a new collinear approximation (Consistent Collinear Approximation; CCA). Unlike the OCA, the CCA is shown to converge correctly at the unidirectional limit to the underlying source term. The proposed CCA resolved this inconsistency by accounting for the amount of energy contained within a finite directional bandwidth, p_θ. While α still remains relevant to unidirectional wave conditions, the new parameter p_θ permits the effect of directionality to be incorporated.

A comparison with model predictions from a second-order accurate deterministic wave model (Herbers and Burton, 1997; Janssen, 2006) for idealized wave conditions demonstrated that the CCA significantly reduced the modelling error for T_{m02}. Unlike the OCA, the CCA was shown to transfer sufficient energy to the higher frequencies. As a result, the rms-errors for T_{m02} reduced from 26% to 18% for the LTA model and from 36% to 7% for the SPB model (with $\sigma_\theta = 30°$). Furthermore, near the unidirectional limit, the calibration coefficients of the re-calibrated triad models were found to be in better agreement with the original authors with $\alpha_{LTA}^{CCA} = 0.52$ and $\alpha_{SPB}^{CCA} = 0.87$.

In conclusion, the error reductions shown between the collinear approximations is occasionally more significant than the error reductions provided by the use of different triad approximations. Therefore, it is important to first ensure that new triad approximations are correctly implemented in 2D spectral wave models with a suitable collinear approximation. For both unidirectional and directional wave conditions, the CCA provides consistent and physically realistic energy transfers compared to the the OCA and therefore is preferred. It is not unexpected that the less approximate SPB model is in better qualitative agreement with the spectral shape predicted by the deterministic wave model than the LTA model. This is because it computes all the interactions between each of the frequency bins. However, further verification of more complete triad models is required, as is their computational trade-off, as greater emphasis is placed both on the spectral balance in the surf zone, and on the coupled dynamics between depth-induced wave breaking and nonlinear triad interactions.

6.2. OUTLOOK

The modelling of surf wave dynamics in the coastal zone has always been a challenging endeavour due to both a lack of a complete physical description of the dominant processes in addition to their representation in a phase-averaged sense. Despite this, much success has been achieved from the use of simple 1D idealizations in 2D stochastic mod-

els; even if occasionally they require re-calibration (see e.g. Appendix B). An underlying theme of this thesis has been the exploration of the limitations of these 1D idealizations imposed on the stochastic modeling of 2D wave conditions. Even if refraction acts to reduce the directionality of incident waves such as swell, in the coastal environments they are still essentially directional, notwithstanding the additional effects of local current and wind. Therefore, although the parameterizations presented in this study aim to extend the limits of applicability and accuracy of 1D idealizations, care must still be taken when these models are calibrated over 1D (laboratory) conditions and are subsequently applied to 2D (field) conditions.

Although modifications to include directional effects in shallow water have been proposed here, it seems inevitable that future progress must focus on modelling frameworks that incorporate 2D effects over alternative source terms based on 1D idealizations; even if initially they may come at the cost of decreased computational efficiency. Both the $\beta - kd$ parameterization and SPB triad model with the Consistent Collinear Approximation (CCA) may provide a starting point towards these developments as both source terms have been shown to be more applicable to directional wave conditions than the alternative parameterizations considered.

It is anticipated that research along these lines will lead to the development of 'third-generation' source terms where the spectral energy balance at each frequency (and directional) component can be taken into account. In particular, the balance between depth-induced wave breaking and nonlinear triad wave-wave interactions needs to be addressed as demonstrated in Figure 2.3. Progress towards this has likely been hampered by the widespread application of the LTA model which does not sufficiently reproduce the evolution of the spectral shape.

If progress is to be made, the application of more complex and less restrictive triad models is warranted. Such examples include 2D source terms (e.g. Becq et al., 1998), combined models (e.g. van der Westhuysen, 2007) and better representations for the evolution of the bispectrum (e.g. Janssen, 2006; Smit and Janssen, 2016) which include both collinear and non-collinear interactions. Whilst computationally prohibitive, these alternatives should be used to verify the limits and conditions to which the collinear approximations are justified in operational wave models. In particular, recent studies demonstrate the importance of the non-collinear interactions for the transfer of wave energy to the infragravity frequencies (e.g. Herbers et al., 1995; Toledo, 2013; Groeneweg et al., 2015). These effects may potentially be parameterized in the CCA by modifying the form of the directional function, D.

A potential solution to balance computational expense with accuracy may be to develop hybrid models which enable a compromise between computing all frequency interactions and only the self-self interactions. This may be implemented by only considering the interactions between frequency components over a characteristic frequency bandwidth determined by the frequency width of the primary peak.

Furthermore, effort should be made to translate more generalized deterministic evolution equations into the stochastic domain. For example, Janssen (2006) suggests that nonlinear shoaling coefficients based on Boussinesq-type equations will likely be underestimated in intermediate to deep water ($kd > 1$) compared to the use of alternative evolution equations. This may provide an explanation for the underestimated energy

transfers demonstrated by both the LTA and SPB triad models.

An additional issue with the triad source term is the problem of finding an appropriate closure hypothesis to account for the bispectrum. Progress towards this has been demonstrated by including the effects of wave breaking through the introduction of a relaxation length scale (Herbers et al., 2003; Janssen, 2006). This essentially accounts for the balance between the nonlinearities and the weakening of phase-coupling through wave dissipation permitting a return to Gaussian statistics. However, this balance has been shown to be strongly dependent on the spectral distribution of the bulk dissipation (Chen et al., 1997; Elgar et al., 1997) and is expected to be weighted with the frequency-squared (Mase and Kirby, 1992; Chen et al., 1997; Kaihatu and Kirby, 1995; Smit et al., 2014) rather than uniformly to the spectrum. As such both processes cannot be considered strictly independent of each other, which is consistent with our physical understanding of the shoaling and breaking of shallow water waves.

In addition to including a quadratic weighting of the depth-induced wave breaking dissipation, it is expected that the $\beta - kd$ parameterization may be improved by unifying its dependency on the normalized wave number (kd) and wave directionality (σ_θ). It is anticipated that both of these dependencies are not independent and that their effects can be combined. Waves in deeper water ($kd > 1$) are expected to be more directional than waves in shallow water due to refraction and therefore the predicted reduction of wave breaking for increasing kd and σ_θ can likely be expressed in terms of each other. Preferably the effects of kd should be incorporated in the bulk dissipation model. Physically, this may be interpreted as the effect of reducing water depth (kd) to increase the crest length of breaking waves and therefore increase the bulk dissipation.

Parallel to these developments, more complex analysis techniques will be required which not only consider the basic parameters such as the significant wave height and mean wave period, but other intrinsic properties of the spectral shape such as the spectral (frequency) width (e.g. Rogers and van Vledder, 2013; Dabbi et al., 2015) and the energy contained within defined frequency bandwidths (e.g. Becq-Girard et al., 1999).

Many of these proposed developments may be expedited by the ever increasing availability of computational resources, both in processing power and in data storage. Physically more complete wave models such as phase-resolving models will become more accessible and applicable to ever larger geographical domains. They should however not be seen as a replacement for stochastic models but as an opportunity to further understand shallow water wave processes. For example, much of the framework for the triad source terms comes from the development of Boussinesq-type models (e.g. Madsen and Sørensen, 1993). Contemporary examples include the application of non-hydrostatic models to estimate the probability density function of the wave height for breaking waves in directional wave conditions (e.g. van Vledder et al., 2013) and to demonstrate the quadratic weighting of wave breaking dissipation (e.g. Smit et al., 2014). In the foreseeable future, it is unlikely that these models will supersede stochastic models due to their operationally prohibitive costs in addition to fundamental issues such as the inclusion of wave generation due to wind. As such, the role of stochastic models will likely remain relevant for engineering purposes such as for the generation of boundary conditions and in their coupling to other models.

Technological advancement will also allow the availability of more extensive data

sets encompassing a greater range of wave conditions over a greater diversity of coastal environments. These are not only useful for the validation of our models but also for our understanding of the underlying wave physics. For example, Catalán et al. (2011) demonstrate the capabilities of remote sensing techniques to measure parameters such as the fraction of breakers Q_b which is crucial for understanding wave breaking. Such observations will be invaluable to the future advancement of wave modelling as we develop and refine better source terms and balances to represent the wave dynamics in the coastal environment.

REFERENCES

AGNON, Y. and SHEREMET, A. (1997). Stochastic nonlinear shoaling of directional spectra. *Journal of Fluid Mechanics*, **345**, pp. 79–99.

AGNON, Y. and SHEREMET, A. (2000). Stochastic evolution models for nonlinear gravity waves over uneven topography. In: *Advances in Coastal and Ocean Engineering* (edited by P.L.F. LIU), World Scientific, vol. 6, pp. 103–132.

ALSINA, J.M. and BALDOCK, T.E. (2007). Improved representation of breaking wave energy dissipation in parametric wave transformation models. *Coastal Engineering*, **54** (10), pp. 765–769.

APOTSOS, A., RAUBENHEIMER, B., ELGAR, S. and GUZA, R.T. (2008). Testing and calibrating parametric wave transformation models on natural beaches. *Coastal Engineering*, **55** (3), pp. 224–235.

ARDHUIN, F., HERBERS, T.H.C. and O'REILLY, W.C. (2001). A hybrid Eulerian-Lagrangian model for spectral wave evolution with application to bottom friction on the continental shelf. *Journal of Physical Oceanography*, **31** (6), pp. 1498–1516.

BABANIN, A.V., HSU, T.W., ROLAND, A., OU, S.H., DOONG, D.J. and KAO, C.C. (2011). Spectral wave modelling of Typhoon Krosa. *Natural Hazards and Earth System Science*, **11** (2), pp. 501–511.

BALDOCK, T.E., HOLMES, P., BUNKER, S. and VAN WEERT, P. (1998). Cross-shore hydrodynamics within an unsaturated surf zone. *Coastal Engineering*, **34** (3-4), pp. 173–196.

BATTJES, J.A. (1994). Shallow water wave modelling. In: *Proceedings of the International Symposium: Waves - Physical and Numerical Modelling*, University of British Columbia, Vancouver, Canada, pp. 1–23.

BATTJES, J.A. and GROENENDIJK, H.W. (2000). Wave height distributions on shallow foreshores. *Coastal Engineering*, **40** (3), pp. 161–182.

BATTJES, J.A. and JANSSEN, J.P.F.M. (1978). Energy loss and set-up due to breaking of random waves. In: *Proceedings of the 16th International Conference on Coastal Engineering*, ASCE, Hamburg, Germany, pp. 569–587.

BATTJES, J.A. and JANSSEN, T.T. (2008). Random wave breaking models - history and discussion. In: *Proceedings of the 31st International Conference on Coastal Engineering*, World Scientific, Hamburg, Germany, pp. 25–37.

BATTJES, J.A. and STIVE, M.J.F. (1985). Calibration and verification of a dissipation model for random breaking waves. *Journal of Geophysical Research: Oceans*, **90** (C5), pp. 9159–9167.

BECQ, F., BENOIT, M. and FORGET, P. (1998). Numerical simulations of directionally spread shoaling surface gravity waves. In: *Proceedings of the 26th International Conference on Coastal Engineering*, ASCE, Copenhagen, Denmark, pp. 523–536.

BECQ-GIRARD, F., FORGET, P. and BENOIT, M. (1999). Non-linear propagation of unidirectional wave fields over varying topography. *Coastal Engineering*, **38** (2), pp. 91–113.

BEJI, S. and BATTJES, J.A. (1993). Experimental investigation of wave propagation over a bar. *Coastal Engineering*, **19** (1-2), pp. 151–162.

BENOIT, M., MARCOS, F. and BECQ, F. (1996). Development of a third generation shallow-water wave model with unstructured spatial meshing. In: *Proceedings of the 25th International Conference on Coastal Engineering*, ASCE, Orlando, FL, pp. 465–478.

BERKOFF, J.C.W. (1972). Computation of combined refraction-diffraction. In: *Proceedings of the 13th International Conference on Coastal Engineering*, ASCE, Vancouver, Canada, pp. 471–490.

BLACK, K.P. and ROSENBERG, M.A. (1992). Semi-empirical treatment of wave transformation outside and inside the breaker line. *Coastal Engineering*, **16** (3), pp. 313–345.

BOERS, M. (1996). *Simulations of a surf zone with a barred beach. Report 1: Wave heights and wave breaking*. Tech. Rep. 69 (5), Delft University of Technology.

BOERS, M. (2005). *Surf zone turbulence*. Ph.D. thesis, Delft University of Technology.

BOOIJ, N., HOLTHUIJSEN, L.H. and BÉNIT, M.P. (2009). A distributed collinear triad approximation in SWAN. In: *Coastal Dynamics 2009*, pp. 1–10.

BOOIJ, N., RIS, R.C. and HOLTHUIJSEN, L.H. (1999). A third-generation wave model for coastal regions: 1. Model description and validation. *Journal of Geophysical Research: Oceans*, **104** (C4), pp. 7649–7666.

BORSBOOM, M., DOORN, N., GROENEWEG, J. and VAN GENT, M.R.A. (2000). A Boussinesq-Type wave model that conserves both mass and momentum. In: *Proceedings of the 27th International Conference on Coastal Engineering*, ASCE, Sydney, Australia, pp. 148–161.

BOTTEMA, M. and BEYER, D. (2002). Evaluation of the SWAN wave model for the Dutch IJsselmeer area. In: *Ocean Wave Measurement and Analysis* (edited by B. EDGE and J. HEMSLEY), ASCE, Reston, VA, pp. 580–609.

BOTTEMA, M. and VAN VLEDDER, G.P. (2009). A ten-year data set for fetch- and depth-limited wave growth. *Coastal Engineering*, **56** (7), pp. 703–725.

BOTTEMA, M., DE WAAL, J.P. and REGELING, E.J. (2002). Some applications of the Lake IJssel/Lake Sloten data set. In: *Proceedings of the 28th International Conference on Coastal Engineering*, World Scientific, Cardiff, UK, pp. 413–425.

BOUWS, E., GÜNTHER, H., ROSENTHAL, W. and VINCENT, C.L. (1985). Similarity of the wind wave spectrum in finite depth water: 1. Spectral form. *Journal of Geophysical Research: Oceans*, **90** (C1), pp. 975–986.

BRETHERTON, F.P. and GARETT, C.J.R. (1968). Wavetrains in inhomogeous moving media. *Proceedings of the Royal Society A: Mathematical, Physical and Engineering Sciences*, **302** (1471), pp. 529–554.

BROCCHINI, M. (2013). A reasoned overview on Boussinesq-type models: the interplay between physics, mathematics and numerics. *Proceedings of the Royal Society A: Mathematical, Physical and Engineering Sciences*, **469** (2160), pp. 1–27.

CAMENEN, B. and LARSON, M. (2007). Predictive formulas for breaker depth index and breaker type. *Journal of Coastal Research*, **23** (4), pp. 1028–1041.

CATALÁN, P.A., HALLER, M.C., HOLMAN, R.A. and PLANT, W.J. (2011). Optical and microwave detection of wave breaking in the surf zone. *IEEE Transactions on Geoscience and Remote Sensing*, **49** (6), pp. 1879–1893.

CAVALERI, L. and RIZZOLI, P.M. (1981). Wind wave prediction in shallow water: Theory and applications. *Journal of Geophysical Research: Oceans*, **86** (C11), pp. 10,961–10,973.

CHEN, Y., GUZA, R.T. and ELGAR, S. (1997). Modeling spectra of breaking surface waves in shallow water. *Journal of Geophysical Research: Oceans*, **102** (C11), pp. 25,035–25,046.

COATES, T.T., JONES, R.J. and BONA, P. (1998). *Wave flume studies on responses to wind/swell seas and steep approach slopes*. Tech. Rep. TR 24, HR Wallingford.

COLLINS, J.I. (1972). Prediction of shallow-water spectra. *Journal of Geophysical Research*, **77** (15), pp. 2693–2707.

COST ACTION 714 WORKING GROUP (2005). *Measuring and Analysing the Directional Spectra of Ocean Waves*. Office for Official Publications of the European Communities, Luxembourg, 184 pp.

DABBI, E.P., HAIGH, I.D., LAMBKIN, D., HERNON, J., WILLIAMS, J.J. and NICHOLLS, R.J. (2015). Beyond significant wave height: A new approach for validating spectral wave models. *Coastal Engineering*, **100**, pp. 11–25.

DALLY, W.R. (1992). Random breaking waves : field verification of a wave-by-wave algorithm for engineering application. *Coastal Engineering*, **16** (4), pp. 369–397.

DALLY, W.R., DEAN, R.G. and DALRYMPLE, R.A. (1985). Wave height variation across beaches of arbitrary profile. *Journal of Geophysical Research: Oceans*, **90** (C6), pp. 11,917–11,927.

DALRYMPLE, R.A. and DEAN, R.G. (1991). *Water Wave Mechanics for Engineers and Scientists*, vol. 2 of *Advanced Series on Ocean Engineering*. World Scientific, 368 pp.

DALRYMPLE, R.A. and ROGERS, B.D. (2006). Numerical modeling of water waves with the SPH method. *Coastal Engineering*, **53** (2-3), pp. 141–147.

DEMIRBILEK, Z., NWOGU, O.G. and WARD, D.L. (2007). *Laboratory study of wind effect on runup over fringing reefs. Report 1: data report*. Tech. Rep. ERDC/CHL TR-07-4, US Army Corps of Engineers.

DEMIRBILEK, Z., NWOGU, O.G., WARD, D.L. and SÁNCHEZ, A. (2009). *Wave transformation over reefs: evaluation of one-dimensional numerical models*. Tech. Rep. ERDC\CHL TR-09-1, US Army Corps of Engineers.

DEMIRBILEK, Z. and PANCHANG, V. (1998). *CGWAVE: A coastal surface water wave model of the mild slope equation*. Tech. Rep. CHL-98-26, US Army Corps of Engineers.

DIETRICH, J.C., TANAKA, S., WESTERINK, J.J., DAWSON, C.N., LUETTICH JR., R.A., ZIJLEMA, M., HOLTHUIJSEN, L.H., SMITH, J.M., WESTERINK, L.G. and WESTERINK, H.J. (2012). Performance of the unstructured-mesh, SWAN+ADCIRC model in computing hurricane waves and surge. *Journal of Scientific Computing*, **52** (2), pp. 468–497.

DINGEMANS, M.W. (1987). *Verification of numerical wave propagation models with laboratory measurements: HISWA verification in the directional wave basin*. Tech. Rep. No. H228, Delft Hydraulics.

DINGEMANS, M.W. (1997). *Water Wave Propagation over Uneven Bottoms*, vol. 13 of *Advanced Series on Ocean Engineering*. World Scientific, 1016 pp.

DINGEMANS, M.W., STIVE, M.J.F., BOSMA, J., DE VRIEND, H.J. and VOGEL, J.A. (1986). Directional nearshore wave propagation and induced currents. In: *Proceedings of the 20th International Conference on Coastal Engineering*, ASCE, Taipei, Taiwan, pp. 1092–1106.

DOERING, J.C. and BOWEN, A.J. (1995). Parametrization of orbital velocity asymmetries of shoaling and breaking waves using bispectral analysis. *Coastal Engineering*, **26** (1-2), pp. 15–33.

ELDEBERKY, Y. (1996). *Nonlinear transformation of wave spectra in the nearshore zone*. Ph.D. thesis, Delft University of Technology.

ELDEBERKY, Y. (2011). Modeling spectra of breaking waves propagating over a beach. *Ain Shams Engineering Journal*, **2** (2), pp. 71–77.

ELDEBERKY, Y. and BATTJES, J.A. (1996). Spectral modeling of wave breaking: Application to Boussinesq equations. *Journal of Geophysical Research: Oceans*, **101** (C1), pp. 1253–1264.

ELDEBERKY, Y. and MADSEN, P.A. (1999). Deterministic and stochastic evolution equations for fully dispersive and weakly nonlinear waves. *Coastal Engineering*, **38** (1), pp. 1–24.

ELGAR, S. and GUZA, R.T. (1985). Observations of bispectra of shoaling surface gravity waves. *Journal of Fluid Mechanics*, **161**, pp. 425–448.

ELGAR, S., GUZA, R.T., RAUBENHEIMER, B., HERBERS, T.H.C. and GALLAGHER, E.L. (1997). Spectral evolution of shoaling and breaking waves on a barred beach. *Journal of Geophysical Research: Oceans*, **102** (C7), pp. 15,797–15,805.

EMERY, W.J. and THOMSON, R.E. (2001). *Data Analysis Methods in Physical Oceanography*. Elsevier, 2nd ed., 654 pp.

FEDDERSEN, F. (2012). Scaling surf zone turbulence. *Geophysical Research Letters*, **39** (18), pp. 1–5.

FENTON, J.D. (1990). Nonlinear wave theories. In: *The Sea* (edited by B. LEMÉHAUTÉ and D.M. HANES), Wiley, vol. 9 of *Ocean Engineering Science*, pp. 3–25.

FILIPOT, J.F. and ARDHUIN, F. (2012). A unified spectral parameterization for wave breaking: From the deep ocean to the surf zone. *Journal of Geophysical Research: Oceans*, **117** (C11), pp. 1–19.

GODA, Y. (2004). A 2-D random wave transformation model with gradational breaking index. *Coastal Engineering Journal*, **46** (1), pp. 1–38.

GODA, Y. (2009). A performance test of nearshore wave height prediction with CLASH datasets. *Coastal Engineering*, **56** (3), pp. 220–229.

GODA, Y. (2010). Reanalysis of regular and random breaking wave statistics. *Coastal Engineering Journal*, **52** (1), pp. 71–106.

GONZALEZ-RODRIGUEZ, D. (2006). *Modeling of nearshore hydrodynamics for sediment transport calculations*. Ph.D. thesis, Massachusetts Institute of Technology.

GORRELL, L., RAUBENHEIMER, B., ELGAR, S. and GUZA, R.T. (2011). SWAN predictions of waves observed in shallow water onshore of complex bathymetry. *Coastal Engineering*, **58** (6), pp. 510–516.

GRABER, H.C. and MADSEN, O.S. (1988). A finite-depth wind-wave model. Part I: Model description. *Journal of Physical Oceanography*, **18** (11), pp. 1465–1483.

GREEN, M.O. and COCO, G. (2014). Review of wave-driven sediment resuspension and transport in estuaries. *Reviews of Geophysics*, **52** (1), pp. 77–117.

GROENEWEG, J., VAN GENT, M.R.A., VAN NIEUWKOOP, J.C.C. and TOLEDO, Y. (2015). Wave propagation into complex coastal systems and the role of nonlinear interactions. *Journal of Waterway, Port, Coastal, and Ocean Engineering*, **141** (5), pp. 1–17.

GROENEWEG, J., VAN VLEDDER, G.P., HURDLE, D.P., DOORN, N. and KUIPER, C. (2003). *Reliability of SWAN at the Petten Sea Defence*. Tech. Rep. No. H4197/A1044, WL|Delft Hydraulics & Alkyon.

GROENEWEG, J., VAN DER WESTHUYSEN, A.J., VAN VLEDDER, G.P., JACOBSE, S., LANSEN, J. and VAN DONGEREN, A.R. (2008). Wave modelling in a tidal inlet: Performance of SWAN in the Wadden Sea. In: *Proceedings of the 31st International Conference on Coastal Engineering*, World Scientific, Hamburg, Germany, pp. 411–423.

GUILLOU, N. (2014). Wave-energy dissipation by bottom friction in the English Channel. *Ocean Engineering*, **82**, pp. 42–51.

HANSON, J.L. and PHILLIPS, O.M. (2001). Automated analysis of ocean surface directional wave spectra. *Journal of Atmospheric and Oceanic Technology*, **18** (2), pp. 277–293.

HARDY, T.A. and YOUNG, I.R. (1996). Field study of wave attenuation on an offshore coral reef. *Journal of Geophysical Research: Oceans*, **101** (C6), pp. 14,311–14,326.

HARDY, T.A., YOUNG, I.R., NELSON, R.C. and GOURLAY, M.R. (1990). Wave attenuation on an offshore coral reef. In: *Proceedings of the 22nd International Conference on Coastal Engineering*, ASCE, Delft, The Netherlands, pp. 330–344.

HASSELMANN, K. (1962). On the non-linear energy transfer in a gravity-wave spectrum. Part 1. General Theory. *Journal of Fluid Mechanics*, **12** (4), pp. 481–500.

HASSELMANN, K. (1974). On the spectral dissipation of ocean waves due to white capping. *Boundary-Layer Meteorology*, **6** (1-2), pp. 107–127.

HASSELMANN, K., BARNETT, T.P., BOUWS, E., CARLSON, H., CARTWRIGHT, D.E., ENKE, K., EWING, J.A., GIENAPP, H., HASSELMANN, D.E., KRUSEMAN, P., MEERBURG, A., MÜLLER, P., OLBERS, D.J., RICHTER, K., SELL, W. and WALDEN, H. (1973). *Measurements of wind-wave growth and swell decay during the Joint North Sea Wave Project (JONSWAP)*. Tech. Rep. Reihe A (80), Nr. 12, Deutschen Hydrographischen Zeitschrift, Hamburg.

HASSELMANN, S., HASSELMANN, K., ALLENDER, J.H. and BARNETT, T.P. (1985). Computations and parameterizations of the nonlinear energy transfer in a gravity-wave spectrum. Part II: Parameterizations of the nonlinear energy transfer for application in wave models. *Journal of Physical Oceanography*, **15** (11), pp. 1378–1391.

HAWKES, P.J., COATES, T.T. and JONES, R.J. (1998). *Impact of bi-modal seas on beaches and control structures*. Tech. Rep. SR 07, HR Wallingford.

HAWKES, P.J., JONES, R.J. and DURAND, N. (1999). *Supply and further analysis of TR24 wave time series data*. Tech. Rep. 4114, HR Wallingford.

HERBERS, T.H.C. and BURTON, M.C. (1997). Nonlinear shoaling of directionally spread waves on a beach. *Journal of Geophysical Research: Oceans*, **102** (C9), pp. 21,101–21,114.

HERBERS, T.H.C., ELGAR, S. and GUZA, R.T. (1995). Generation and propagation of infragravity waves. *Journal of Geophysical Research: Oceans*, **100** (C12), pp. 24,863–24,872.

HERBERS, T.H.C., ORZECH, M., ELGAR, S. and GUZA, R.T. (2003). Shoaling transformation of wave frequency-directional spectra. *Journal of Geophysical Research: Oceans*, **108** (C1), pp. 1–17.

HERBERS, T.H.C., RUSSNOGLE, N.R. and ELGAR, S. (2000). Spectral energy balance of breaking waves within the surf zone. *Journal of Physical Oceanography*, **30** (11), pp. 2723–2737.

HOEFEL, F. and ELGAR, S. (2003). Wave-induced sediment transport and sandbar migration. *Science*, **299** (5614), pp. 1885–1887.

HOLLOWAY, G. (1980). Oceanic internal waves are not weak waves. *Journal of Physical Oceanography*, **10** (6), pp. 906–914.

HOLLOWAY, G. and HENDERSHOTT, M.C. (1977). Stochastic closure for nonlinear Rossby waves. *Journal of Fluid Mechanics*, **82** (4), pp. 747–765.

HOLTHUIJSEN, L.H. (2007). *Waves in Oceanic and Coastal Waters*. Cambridge University Press, 404 pp.

HOLTHUIJSEN, L.H. and BOOIJ, N. (2006). Experimental wave breaking in SWAN. In: *Proceedings of the 30th International Conference on Coastal Engineering*, World Scientific, San Diego, CA, pp. 392–402.

HOLTHUIJSEN, L.H., HERMAN, A. and BOOIJ, N. (2003). Phase-decoupled refraction–diffraction for spectral wave models. *Coastal Engineering*, **49** (4), pp. 291–305.

HOLTHUIJSEN, L.H., ZIJLEMA, M. and VAN DER HAM, P.J. (2008). Wave physics in a tidal inlet. In: *Proceedings of the 31st International Conference on Coastal Engineering*, World Scientific, Hamburg, Germany, pp. 437–447.

HORIKAWA, K. and KUO, C.T. (1966). A study on wave transformation inside surf zone. In: *Proceedings of the 10th International Conference on Coastal Engineering*, ASCE, Tokyo, Japan, pp. 217–233.

JANSSEN, P.A.E.M., KOMEN, G.J. and DE VOOGT, W.J.P. (1984). An operational coupled hybrid wave prediction model. *Journal of Geophysical Research: Oceans*, **89** (C3), pp. 3635–3654.

JANSSEN, T.T. (2006). *Nonlinear surface waves over topography*. Ph.D. thesis, Delft University of Technology.

JANSSEN, T.T. and BATTJES, J.A. (2007). A note on wave energy dissipation over steep beaches. *Coastal Engineering*, **54** (9), pp. 711–716.

JANSSEN, T.T., HERBERS, T.H.C. and BATTJES, J.A. (2006). Generalized evolution equations for nonlinear surface gravity waves over two-dimensional topography. *Journal of Fluid Mechanics*, **552**, pp. 393–418.

JENSEN, M.S. (2002). *Breaking of waves over a steep bottom slope*. Ph.D. thesis, Aalborg University.

KAIHATU, J.M. and KIRBY, J.T. (1995). Nonlinear transformation of waves in finite water depth. *Physics of Fluids*, **7** (8), pp. 1903–1914.

KAIHATU, J.M., VEERAMONY, J. and EDWARDS, K.L. (2008). Spatial evolution of the frequency distribution of dissipation and implications on frequency domain modeling. In: *Proceedings of the 31st International Conference on Coastal Engineering*, World Scientific, Hamburg, Germany, pp. 293–301.

KAIHATU, J.M., VEERAMONY, J., EDWARDS, K.L. and KIRBY, J.T. (2007). Asymptotic behavior of frequency and wave number spectra of nearshore shoaling and breaking waves. *Journal of Geophysical Research: Oceans*, **112** (C6), pp. 1–15.

KAMPHUIS, J.W. (1991). Incipient wave breaking. *Coastal Engineering*, **15** (3), pp. 185–203.

KATSARDI, V. (2007). *Surface water waves in intermediate and shallow water depths*. Ph.D. thesis, Imperial College London.

KATSARDI, V., DE LUTIO, L. and SWAN, C. (2013). An experimental study of large waves in intermediate and shallow water depths. Part I: Wave height and crest height statistics. *Coastal Engineering*, **73**, pp. 43–57.

KATSARDI, V. and SWAN, C. (2011). An experimental study of shallow water wave statistics on mild bed slopes. In: *ASME 30th International Conference on Ocean, Offshore and Arctic Engineering*, pp. 711–719.

KEATING, T., WEBBER, N.B. and HAVELOCK, T.H. (1977). The generation of periodic waves in a laboratory channel: a comparison between theory and experiment. *Proceedings of the Institution of Civil Engineers*, **63** (4), pp. 819–832.

KIM, Y.C. and POWERS, E.J. (1979). Digital bispectral analysis and its applications to nonlinear wave interactions. *IEEE Transactions on Plasma Science*, **7** (2), pp. 120–131.

KINSMAN, B. (1965). *Wind Waves: Their generation and propagation on the ocean surface*. Dover Publications Inc., 676 pp.

KIRBY, J.T. (2003). Boussinesq models and applications to nearshore wave propagation, surfzone processes and wave-induced currents. In: *Advances in Coastal Modeling* (edited by V.C. LAKHAN), Elsevier, vol. 67 of *Elsevier Oceanography Series*, chap. 1, pp. 1–41.

KIRBY, J.T. and DALRYMPLE, R.A. (1994). *Combined refraction/diffraction model REF/DIF 1 Version 2.5. Documentation and User's Manual*. Tech. Rep. No. CACR-94-22, Center for Applied Coastal Research, University of Delaware.

KIRBY, J.T. and KAIHATU, J.M. (1996). Structure of frequency domain models for random wave breaking. In: *Proceedings of the 25th International Conference on Coastal Engineering*, ASCE, Orlando, FL, pp. 1144–1155.

KIRBY, J.T., WEI, G., CHEN, Q., KENNEDY, A.B. and DALRYMPLE, R.A. (1998). *FUNWAVE 1.0 Fully Nonlinear Boussinesq Wave Model Documentation and User's Manual*. Tech. Rep. No. CACR-98-06, Center for Applied Coastal Research, University of Delaware.

KLOPMAN, G., VAN GROESEN, B. and DINGEMANS, M.W. (2010). A variational approach to Boussinesq modelling of fully nonlinear water waves. *Journal of Fluid Mechanics*, **657**, pp. 36–63.

KOMEN, G.J., CAVALERI, L., DONELAN, M., HASSELMANN, K., HASSELMANN, S. and JANSSEN, P.A.E.M. (1994). *Dynamics and Modelling of Ocean Waves*. Cambridge University Press, 556 pp.

KOMEN, G.J., HASSELMANN, S. and HASSELMANN, K. (1984). On the existence of a fully developed wind-sea spectrum. *Journal of Physical Oceanography*, **14** (8), pp. 1271–1285.

KUIK, A.J., VAN VLEDDER, G.P. and HOLTHUIJSEN, L.H. (1988). A method for the routine analysis of pitch-and-roll buoy wave data. *Journal of Physical Oceanography*, **18** (7), pp. 1020–1034.

LAMB, H. (1932). *Hydrodynamics*. Dover Publications, 6th ed., 738 pp.

LANSEN, J., JACOBSE, S., KLUYVER, M. and ARNOLD, E. (2007). *Hindcast tidal inlet of Ameland storms January and March 2007*. Tech. Rep. No. 9S8833.A0, Royal Haskoning.

LATHEEF, M. and SWAN, C. (2013). A laboratory study of wave crest statistics and the role of directional spreading. *Proceedings of the R*, **469** (2152), pp. 1–24.

LE MÉHAUTÉ, B. (1962). On non-saturated breakers and the wave run-up. In: *Proceedings of the 8th International Conference on Coastal Engineering*, Council on Wave Research, Mexico City, Mexico, pp. 77–92.

LEBLOND, P.H. and MYSAK, L.A. (1981). *Waves in the Ocean*. Elsevier, 602 pp.

LENTZ, S.J., FEWINGS, M., HOWD, P., FREDERICKS, J. and HATHAWAY, K. (2008). Observations and a model of undertow over the inner continental shelf. *Journal of Physical Oceanography*, **38** (11), pp. 2341–2357.

LIN, P. and LIU, P.L.F. (1998). A numerical study of breaking waves in the surf zone. *Journal of Fluid Mechanics*, **359**, pp. 239–264.

LIPPMANN, T.C., BROOKINS, A.H. and THORNTON, E.B. (1996). Wave energy transformation on natural profiles. *Coastal Engineering*, **27** (1-2), pp. 1–20.

LONGUET-HIGGINS, M.S. (1952). On the statistical distributions of the heights of sea waves. *J. Mar. Res.*, **11** (3), pp. 245–265.

LONGUET-HIGGINS, M.S. (1974). On the mass, momentum, energy and circulation of a solitary wave. *Proceedings of the Royal Society A: Mathematical, Physical and Engineering Sciences*, **337** (1608), pp. 1–13.

LONGUET-HIGGINS, M.S., CARTWRIGHT, D.E. and SMITH, N.D. (1963). Observations of the directional spectrum of sea waves using the motions of a floating buoy. In: *Ocean Wave Spectrum*, Prentice-Hall, pp. 111–136.

LONGUET-HIGGINS, M.S. and STEWART, R.W. (1964). Radiation stresses in water waves; a physical discussion, with applications. *Deep Sea Research and Oceanographic Abstracts*, **11** (4), pp. 529–562.

LOWE, R.J., FALTER, J.L., MONISMITH, S.G. and ATKINSON, M.J. (2009a). A numerical study of circulation in a coastal reef-lagoon system. *Journal of Geophysical Research: Oceans*, **114** (C6), pp. 1–18.

LOWE, R.J., FALTER, J.L., MONISMITH, S.G. and ATKINSON, M.J. (2009b). Wave-driven circulation of a coastal reef-lagoon system. *Journal of Physical Oceanography*, **39** (4), pp. 873–893.

LUBIN, P. and GLOCKNER, S. (2015). Numerical simulations of three-dimensional plunging breaking waves: generation and evolution of aerated vortex filaments. *Journal of Fluid Mechanics*, **767**, pp. 364–393.

LYNETT, P.J. (2006). Nearshore wave modeling with high-order Boussinesq-type equations. *Journal of Waterway, Port, Coastal, and Ocean Engineering*, **132** (5), pp. 348–357.

MA, G., SHI, F. and KIRBY, J.T. (2012). Shock-capturing non-hydrostatic model for fully dispersive surface wave processes. *Ocean Modelling*, **43**, pp. 22–35.

MADSEN, O.S. (1976). Wave climate of the continental margin: elements of its mathematical description. In: *Marine Sediment Transport in Environmental Engineering* (edited by D.J. STANLEY and D.J.P. SWIFT), Wiley, pp. 65–87.

MADSEN, O.S., POON, Y.K. and GRABER, H.C. (1988). Spectral wave attenuation by bottom friction: Theory. In: *Proceedings of the 21st International Conference on Coastal Engineering*, ASCE, Torremolinos, Spain, pp. 492–504.

MADSEN, P.A. and SCHAFFER, H.A. (1999). A review of boussinesq-type equations for surface gravity waves. In: *Advances in Coastal and Ocean Engineering* (edited by P.L.F. LIU), World Scientific, vol. 5, pp. 1–94.

MADSEN, P.A. and SØRENSEN, O.R. (1992). A new form of the Boussinesq equations with improved linear dispersion characteristics. Part 2. A slowly-varying bathymetry. *Coastal Engineering*, **18** (3-4), pp. 183–204.

MADSEN, P.A. and SØRENSEN, O.R. (1993). Bound waves and triad interactions in shallow water. *Ocean Engineering*, **20** (4), pp. 359–388.

MARTÍNEZ, M.L., INTRALAWAN, A., VÁZQUEZ, G., PÉREZ-MAQUEO, O., SUTTON, P. and LANDGRAVE, R. (2007). The coasts of our world: Ecological, economic and social importance. *Ecological Economics*, **63** (2-3), pp. 254–272.

MASE, H. and KIRBY, J.T. (1992). Hybrid frequency-domain KdV equation for random wave transformation. In: *Proceedings of the 23rd International Conference on Coastal Engineering*, ASCE, Venice, Italy, pp. 474–487.

MASSEL, S.R. (1996). *Ocean Surface Waves: Their physics and prediction*, vol. 11 of *Advanced Series on Ocean Engineering*. World Scientific, 508 pp.

MASSEL, S.R. (1998). The limiting wave height in wind-induced wave trains. *Ocean Engineering*, **25** (9), pp. 735–752.

MCCOWEN, J. (1894). On the highest wave of permanent type. *Philosophical Magazine Series 5*, **38** (233), pp. 351–358.

VAN DER MEER, J.W., HURDLE, D.P., VAN VLEDDER, G.P., VAN GENT, M.R.A. and RIS, R.C. (2000). *Uni- and bi-modal spectra on steep foreshores - validation of the SWAN model, wave height statistics and wave overtopping, based on HR Wallingford data*. Tech. Rep. i230/A509/H3510, Delft Hydraulic/Alkyon/INFRAM.

MICHE, R. (1944). Mouvements ondulatoires de la mer en profondeur constante ou décroissante. Forme limite de la houle lors de son déferlement. Application aux digues maritimes. Troisième partie. Forme et propriétés des houles limites lors du déferlement. Croissance ... *Annals des Ponts et Chaussées*, **114**, pp. 369–406.

MILES, J.W. (1957). On the generation of surface waves by shear flows. *Journal of Fluid Mechanics*, **3** (2), pp. 185–204.

MITSUYASU, H., TASAI, F., SUHARA, T., MIZUNO, S., OHKUSU, M., HONDA, T. and RIKIISHI, K. (1975). Observations of the directional spectrum of ocean waves using a cloverleaf buoy. *Journal of Physical Oceanography*, **5** (4), pp. 750–760.

MONBALIU, J., PADILLA-HERNÁNDEZ, R., HARGREAVES, J.C., ALBIACH, J.C.C., LUO, W., SCLAVO, M. and GÜNTHER, H. (2000). The spectral wave model, WAM, adapted for applications with high spatial resolution. *Coastal Engineering*, **41** (1-3), pp. 41–62.

MORITZ, H.R. (2001). Observing large waves using bottom-mounted pressure and current meters. In: *Ocean Wave Measurement and Analysis* (edited by B. EDGE and J. HEMSLEY), ASCE, Reston, VA, pp. 44–53.

MULLIGAN, R.P., HAY, A.E. and BOWEN, A.J. (2010). A wave-driven jet over a rocky shoal. *Journal of Geophysical Research*, **115** (C10), pp. 1–13.

NAIRN, R.B. (1990). *Prediction of cross-shore sediment transport and beach profile evolution*. Ph.D. thesis, Imperial College London.

NELSON, R.C. (1985). Wave heights in depth limited conditions. *Transactions of the Institution of Engineers, Australia. Civil engineering*, **27**, pp. 210–215.

NELSON, R.C. (1987). Design wave heights on very mild slopes - an experimental study. *Transactions of the Institution of Engineers, Australia. Civil engineering*, **29**, pp. 157–161.

NELSON, R.C. (1994a). Depth limited design wave heights in very flat regions. *Coastal Engineering*, **23** (1-2), pp. 43–59.

NELSON, R.C. (1994b). Height limit anomalies in laboratory waves. In: *Proceedings of the International Symposium: Waves - Physical and Numerical Modelling*, University of British Columbia, Vancouver, Canada, pp. 580–589.

NELSON, R.C. (1997). Height limits in top down and bottom up wave environments. *Coastal Engineering*, **32** (2-3), pp. 247–254.

NWOGU, O.G. (1993). Alternative form of Boussinesq equations for nearshore wave propagation. *Journal of Waterway, Port, Coastal, and Ocean Engineering*, **119** (6), pp. 618–638.

NWOGU, O.G. and DEMIRBILEK, Z. (2001). *BOUSS-2D : A Boussinesq Wave Model for Coastal Regions and Harbors Coastal and Hydraulics Laboratory*. Tech. Rep. ERDC/CHL TR-01-25, US Army Corps of Engineers.

OCHI, M.K. (2005). *Ocean Waves: The stochastic approach*, vol. 6 of *Cambridge Ocean Technology Series*. Cambridge University Press, 332 pp.

ONORATO, M., CAVALERI, L., FOUQUES, S., GRAMSTAD, O., JANSSEN, P.A.E.M., MONBALIU, J., OSBORNE, A.R., PAKOZDI, C., SERIO, M., STANSBERG, C.T., TOFFOLI, A. and TRULSEN, K. (2009). Statistical properties of mechanically generated surface gravity waves: a laboratory experiment in a three-dimensional wave basin. *Journal of Fluid Mechanics*, **627**, pp. 235–257.

ORSZAG, S.A. (1974). *Lectures on the statistical theory of turbulence*. Massachusetts Institute of Technology, 216 pp.

OSTENDORF, D.W. and MADSEN, O.S. (1979). *An analysis of long-shore current and associated sediment transport in the surf zone*. Tech. rep., Massachusetts Institute of Technology.

PÉQUIGNET, A.C., BECKER, J.M., MERRIFIELD, M.A. and BOC, S.J. (2011). The dissipation of wind wave energy across a fringing reef at Ipan, Guam. *Coral Reefs*, **30** (S1), pp. 71–82.

PEREGRINE, D.H. (1967). Long waves on a beach. *Journal of Fluid Mechanics*, **27** (4), pp. 815–827.

PHILLIPS, O.M. (1957). On the generation of waves by turbulent wind. *Journal of Fluid Mechanics*, **2** (5), pp. 417–445.

PHILLIPS, O.M. (1960). On the dynamics of unsteady gravity waves of finite amplitude. Part 1. The elementary interactions. *Journal of Fluid Mechanics*, **9** (2), pp. 193–217.

PHILLIPS, O.M. (1977). *The Dynamics of the Upper Ocean*. Cambridge University Press, 2nd ed., 336 pp.

PIERSON JR., W.J., NEUMANN, G. and JAMES, R.W. (1955). *Practical methods for observing and forecasting ocean waves by means of wave spectra and statistics*. Tech. Rep. H.O. Pub. No. 603, US Navy Hydrographic Office.

RATTANAPITIKON, W. (2007). Calibration and modification of energy dissipation models for irregular wave breaking. *Ocean Engineering*, **34** (11-12), pp. 1592–1601.

RATTANAPITIKON, W., KARUNCHINTADIT, R. and SHIBAYAMA, T. (2003a). Irregular wave height transformation using representative wave approach. *Coastal Engineering Journal*, **45** (3), pp. 489–510.

RATTANAPITIKON, W. and SHIBAYAMA, T. (1998a). Energy dissipation model for irregular breaking waves. In: *Proceedings of the 26th International Conference on Coastal Engineering*, ASCE, Copenhagen, Denmark, pp. 112–125.

RATTANAPITIKON, W. and SHIBAYAMA, T. (1998b). Energy dissipation model for regular and irregular breaking waves. *Coastal Engineering Journal*, **40** (4), pp. 327–346.

RATTANAPITIKON, W. and SHIBAYAMA, T. (2000). Verification and modification of breaker height formulas. *Coastal Engineering Journal*, **42** (4), pp. 389–406.

RATTANAPITIKON, W., VIVATTANASIRISAK, T. and SHIBAYAMA, T. (2003b). A proposal of new breaker height formula. *Coastal Engineering Journal*, **45** (1), pp. 29–48.

RAUBENHEIMER, B., GUZA, R.T. and ELGAR, S. (1996). Wave transformation across the inner surf zone. *Journal of Geophysical Research: Oceans*, **101** (C11), pp. 25,589–25,597.

RIEDEL, H.P. and BYRNE, A.P. (1986). Random breaking waves - horizontal seabed. In: *Proceedings of the 20th International Conference on Coastal Engineering*, ASCE, Taipei, Taiwan, pp. 903–908.

RIJNSDORP, D.P., RUESSINK, G. and ZIJLEMA, M. (2015). Infragravity-wave dynamics in a barred coastal region, a numerical study. *Journal of Geophysical Research: Oceans*, **120** (6), pp. 4068–4089.

RIS, R.C., HOLTHUIJSEN, L.H. and BOOIJ, N. (1999). A third-generation wave model for coastal regions. 2. Verification. *Journal of Geophysical Research: Oceans*, **104** (C4), pp. 7667–7681.

ROELVINK, J.A. (1993). Dissipation in random wave groups incident on a beach. *Coastal Engineering*, **19** (1-2), pp. 127–150.

ROGERS, W.E., HWANG, P.A. and WANG, D.W. (2003). Investigation of wave growth and decay in the SWAN model: Three regional-scale applications. *Journal of Physical Oceanography*, **33** (2), pp. 366–389.

ROGERS, W.E. and VAN VLEDDER, G.P. (2013). Frequency width in predictions of windsea spectra and the role of the nonlinear solver. *Ocean Modelling*, **70**, pp. 52–61.

ROLAND, A. (2009). *Development of the WWM II (Wind Wave Model II) - Spectral wave modelling on unstructured meshes*. Ph.D. thesis, Technische Universität Darmstadt.

ROLAND, A., ZANKE, U., HSU, T.W., OU, S.H. and LIAU, J.M. (2006). Spectral wave modelling on unstructured grids with WWM (Wind Wave Model) I: The deep water cases. In: *Third Chinese-German Joint Symposium on Coastal and Ocean Engineering*, National Cheng Kung University, Tainan, Taiwan.

RUESSINK, B.G., WALSTRA, D.J.R. and SOUTHGATE, H.N. (2003). Calibration and verification of a parametric wave model on barred beaches. *Coastal Engineering*, **48** (3), pp. 139–149.

SALLENGER JR., A.H. and HOLMAN, R.A. (1985). Wave energy saturation on a natural beach of variable slope. *Journal of Geophysical Research: Oceans*, **90** (C6), pp. 11,939–11,944.

SALLENGER JR., A.H. and HOWD, P.A. (1989). Nearshore bars and the break-point hypothesis. *Coastal Engineering*, **12** (4), pp. 301–313.

SALMON, J.E. and HOLTHUIJSEN, L.H. (2011). Re-scaling the Battjes-Janssen model for depth-induced wave-breaking. In: *12th International Workshop on Wave Hindcasting and Forecasting and Coastal Hazards Symposium*, WMO/IOC Joint Technical Commission for Oceanography and Marine Meteorology (JCOMM), Kohala Coast, HI, pp. 1–6.

SALMON, J.E. and HOLTHUIJSEN, L.H. (2015). Modeling depth-induced wave breaking over complex coastal bathymetries. *Coastal Engineering*, **105**, pp. 21–35.

SALMON, J.E., HOLTHUIJSEN, L.H., SMIT, P.B., VAN VLEDDER, G.P. and ZIJLEMA, M. (2014). Alternative source terms for SWAN in the coastal region. In: *Proceedings of the 34th International Conference on Coastal Engineering*, Coastal Engineering Research Council, Seoul, South Korea, pp. 1–13.

SALMON, J.E., HOLTHUIJSEN, L.H., ZIJLEMA, M., VAN VLEDDER, G.P. and PIETRZAK, J.D. (2015). Scaling depth-induced wave-breaking in two-dimensional spectral wave models. *Ocean Modelling*, **87**, pp. 30–47.

SALMON, J.E., SMIT, P.B., JANSSEN, T.T. and HOLTHUIJSEN, L.H. (2016). A consistent collinear triad approximation for operational wave models. *Ocean Modelling*, **104**, pp. 203–212.

SÉNÉCHAL, N., DUPUIS, H., BONNETON, P., HOWA, H. and PEDREROS, R. (2001). Observation of irregular wave transformation in the surf zone over a gently sloping sandy beach on the French Atlantic coastline. *Oceanologica Acta*, **24** (6), pp. 545–556.

SEYAMA, A. and KIMURA, A. (1988). The measured properties of irregular wave breaking and wave height change after breaking on the slope. In: *Proceedings of the 21st International Conference on Coastal Engineering*, ASCE, Torremolinos, Spain, pp. 419–432.

SHEREMET, A., KAIHATU, J.M., SU, S.F., SMITH, E.R. and SMITH, J.M. (2011). Modeling of nonlinear wave propagation over fringing reefs. *Coastal Engineering*, **58** (12), pp. 1125–1137.

SMIT, P.B. and JANSSEN, T.T. (2013). The evolution of inhomogeneous wave statistics through a variable medium. *Journal of Physical Oceanography*, **43** (8), pp. 1741–1758.

SMIT, P.B. and JANSSEN, T.T. (2016). The evolution of nonlinear wave statistics through a variable medium. *Journal of Physical Oceanography*, **46** (2), pp. 621–634.

SMIT, P.B., JANSSEN, T.T., HOLTHUIJSEN, L.H. and SMITH, J.M. (2014). Non-hydrostatic modeling of surf zone wave dynamics. *Coastal Engineering*, **83**, pp. 36–48.

SMITH, J.M. (2004). Shallow-water spectral shapes. In: *Proceedings of the 29th International Conference on Coastal Engineering*, World Scientific, Lisbon, Portugal, pp. 206–217.

SMITH, J.M. and VINCENT, C.L. (1992). Shoaling and decay of two wave trains on beach. *Journal of Waterway, Port, Coastal, and Ocean Engineering*, **118** (5), pp. 517–533.

SNYDER, R.L., DOBSON, F.W., ELLIOTT, J.A. and LONG, R.B. (1981). Array measurements of atmospheric pressure fluctuations above surface gravity waves. *Journal of Fluid Mechanics*, **102**, pp. 1–59.

SØRENSEN, O.R., KOFOED-HANSEN, H., RUGBJERG, M. and SØRENSEN, L.S. (2004). A third generation spectral wave model using an unstructured finite volume technique. In: *Proceedings of the 29th International Conference on Coastal Engineering*, World Scientific, Lisbon, Portugal, pp. 894–906.

STELLING, G.S. and ZIJLEMA, M. (2003). An accurate and efficient finite-difference algorithm for non-hydrostatic free-surface flow with application to wave propagation. *International Journal for Numerical Methods in Fluids*, **43** (1), pp. 1–23.

STIASSNIE, M. and DRIMER, N. (2006). Prediction of long forcing waves for harbor agitation studies. *Journal of Waterway, Port, Coastal, and Ocean Engineering*, **132** (3), pp. 166–171.

STOKER, J.J. (1957). *Water Waves: The mathematical theory with applications*. Interscience Publishers Inc., 567 pp.

SU, S.F., SHEREMET, A. and SMITH, J.M. (2010). Parametric wave-breaking on steep reefs. In: *Proceedings of the 32nd International Conference on Coastal Engineering*, Coastal Engineering Research Council, Shanghai, China, pp. 1–12.

SULAIMAN, D.M., TSUTSUI, S., YOSHIOKA, H., YAMASHITA, T., OSHIRO, S. and TSUCHIYA, Y. (1994). Prediction of the maximum wave on the coral flat. In: *Proceedings of the 24th International Conference on Coastal Engineering*, ASCE, Kobe, Japan, pp. 609–623.

SUZUKI, T., ZIJLEMA, M., BURGER, B., MEIJER, M.C. and NARAYAN, S. (2012). Wave dissipation by vegetation with layer schematization in SWAN. *Coastal Engineering*, **59** (1), pp. 64–71.

SVENDSEN, I.A. (1987). Analysis of surf zone turbulence. *Journal of Geophysical Research: Oceans*, **92** (C5), pp. 5115–5124.

TAJIMA, Y. and MADSEN, O.S. (2002). Shoaling, breaking and broken wave characteristics. In: *Proceedings of the 28th International Conference on Coastal Engineering*, World Scientific, Cardiff, UK, pp. 222–234.

THORNTON, E.B. and GUZA, R.T. (1983). Transformation of wave height distribution. *Journal of Geophysical Research: Oceans*, **88** (C10), pp. 5925–5938.

TING, F.C.K. (2001). Laboratory study of wave and turbulence velocities in a broad-banded irregular wave surf zone. *Coastal Engineering*, **43** (3-4), pp. 183–208.

TOLEDO, Y. (2013). The oblique parabolic equation model for linear and nonlinear wave shoaling. *Journal of Fluid Mechanics*, **715**, pp. 103–133.

TOLEDO, Y. and AGNON, Y. (2012). Stochastic evolution equations with localized nonlinear shoaling coefficients. *European Journal of Mechanics B/Fluids*, **34**, pp. 13–18.

TOLMAN, H.L. (1990a). The influence of unsteady depths and currents of tides on wind-wave propagation in shelf seas. *Journal of Physical Oceanography*, **20** (8), pp. 1166–1174.

TOLMAN, H.L. (1990b). *Wind wave propagation in tidal seas*. Ph.D. thesis, Delft University of Technology.

TOLMAN, H.L. (2009). *User manual and system documentation of WAVEWATCH III version 3.14*. Tech. Rep. 276, NOAA/NWS/NCEP/MMAB.

TOLMAN, H.L., BANNER, M.L. and KAIHATU, J.M. (2013). The NOPP operational wave model improvement project. *Ocean Modelling*, **70**, pp. 2–10.

TOLMAN, H.L. and CHALIKOV, D. (1996). Source terms in a third-generation wind wave model. *Journal of Physical Oceanography*, **26** (11), pp. 2497–2518.

TROCH, P. (1998). *MILDwave - A numerical model for propagation and transformation of linear water waves*. Tech. rep., Ghent University.

TUCKER, M.J., CARR, A.P. and PITT, E.G. (1983). The effect of an offshore bank in attenuating waves. *Coastal Engineering*, **7** (2), pp. 133–144.

VINCENT, C.L. (1985). Depth-controlled wave height. *Journal of Waterway, Port, Coastal, and Ocean Engineering*, **111** (3), pp. 459–475.

VINK, A.S. (2001). *Transformation of wave spectra across the surf zone*. Master thesis, Delft Univesity of Technology.

VAN VLEDDER, G.P. (2006). The WRT method for the computation of non-linear four-wave interactions in discrete spectral wave models. *Coastal Engineering*, **53** (2-3), pp. 223–242.

VAN VLEDDER, G.P. and ADEMA, J. (2007). *Hydro-dynamics in the Wadden Sea during storm conditions*. Tech. Rep. No. A1848R2, Alkyon.

VAN VLEDDER, G.P., GROENEWEG, J. and VAN DER WESTHUYSEN, A.J. (2008). Numerical and physical aspects of wave modeling in a tidal flat. In: *Proceedings of the 31st International Conference on Coastal Engineering*, World Scientific, Hamburg, Germany, pp. 424–436.

VAN VLEDDER, G.P., RUESSINK, G. and RIJNSDORP, D.P. (2013). Individual wave height distributions in the coastal zone: Measurements and simulations and the effect of directional spreading. In: *Coastal Dynamics 2013*, pp. 1799–1810.

DE WAAL, J.P. (2001). Wave growth limit in shallow water. In: *Ocean Wave Measurement and Analysis* (edited by B. EDGE and J. HEMSLEY), ASCE, Reston, VA, pp. 560–569.

WAMDI GROUP (1988). The WAM Model - A third generation ocean wave prediction model. *Journal of Physical Oceanography*, **18** (12), pp. 1775–1810.

WARNER, J.C., SHERWOOD, C.R., SIGNELL, R.P., HARRIS, C.K. and ARANGO, H.G. (2008). Development of a three-dimensional, regional, coupled wave, current, and sediment-transport model. *Computers & Geosciences*, **34** (10), pp. 1284–1306.

VAN DER WESTHUYSEN, A.J. (2007). *Advances in the spectral modelling of wind waves in the nearshore*. Ph.D. thesis, Delft University of Technology.

VAN DER WESTHUYSEN, A.J. (2009). Modelling of depth-induced wave breaking over sloping and horizontal beds. In: *11th International Workshop on Wave Hindcasting and Forecasting and Coastal Hazards Symposium*, WMO/IOC Joint Technical Commission for Oceanography and Marine Meteorology (JCOMM), Halifax, Canada, pp. 1–10.

VAN DER WESTHUYSEN, A.J. (2010). Modeling of depth-induced wave breaking under finite depth wave growth conditions. *Journal of Geophysical Research: Oceans*, **115** (C1), pp. 1–19.

VAN DER WESTHUYSEN, A.J. (2012). Spectral modeling of wave dissipation on negative current gradients. *Coastal Engineering*, **68**, pp. 17–30.

VAN DER WESTHUYSEN, A.J., VAN DONGEREN, A.R., GROENEWEG, J., VAN VLEDDER, G.P., PETERS, H., GAUTIER, C. and VAN NIEUWKOOP, J.C.C. (2012). Improvements in spectral wave modeling in tidal inlet seas. *Journal of Geophysical Research: Oceans*, **117** (C11), pp. 1–23.

VAN DER WESTHUYSEN, A.J. and DE WAAL, J.P. (2008). *Observed finite depth wave growth limit in the Wadden Sea*. Tech. Rep. H5107.35, Deltares.

VAN DER WESTHUYSEN, A.J., ZIJLEMA, M. and BATTJES, J.A. (2007). Nonlinear saturation-based whitecapping dissipation in SWAN for deep and shallow water. *Coastal Engineering*, **54** (2), pp. 151–170.

WHITFORD, D.J. (1988). *Wind and wave forcing of longshore currents across a barred beach*. Ph.D. thesis, Naval Postgraduate School, Monterey, CA.

WISE GROUP (2007). Wave modelling - The state of the art. *Progress in Oceanography*, **75** (4), pp. 603–674.

YOUNG, I.R. and BABANIN, A.V. (2006). The form of the asymptotic depth-limited wind wave frequency spectrum. *Journal of Geophysical Research: Oceans*, **111** (C6), pp. 1–15.

ZAKHAROV, V. (1999). Statistical theory of gravity and capillary waves on the surface of a finite-depth fluid. *European Journal of Mechanics B/Fluids*, **18** (3), pp. 327–344.

ZHENG, J., MASE, H., DEMIRBILEK, Z. and LIN, L. (2008). Implementation and evaluation of alternative wave breaking formulas in a coastal spectral wave model. *Ocean Engineering*, **35** (11-12), pp. 1090–1101.

ZHOU, J.G. and STANSBY, P.K. (1998). An arbitrary Lagrangian-Eulerian σ (ALES) model with non-hydrostatic pressure for shallow water flows. *Computer Methods in Applied Mechanics and Engineering*, **178** (1-2), pp. 199–214.

ZIJLEMA, M. (2010). Computation of wind-wave spectra in coastal waters with SWAN on unstructured grids. *Coastal Engineering*, **57** (3), pp. 267–277.

ZIJLEMA, M. (2012). Modelling wave transformation across a fringing reef using SWASH. In: *Proceedings of the 33rd International Conference on Coastal Engineering*, Coastal Engineering Research Council, Santander, Spain, pp. 1–12.

ZIJLEMA, M., STELLING, G.S. and SMIT, P.B. (2011). SWASH: An operational public domain code for simulating wave fields and rapidly varied flows in coastal waters. *Coastal Engineering*, **58** (10), pp. 992–1012.

ZIJLEMA, M., VAN VLEDDER, G.P. and HOLTHUIJSEN, L.H. (2012). Bottom friction and wind drag for wave models. *Coastal Engineering*, **65**, pp. 19–26.

ZIJLEMA, M. and VAN DER WESTHUYSEN, A.J. (2005). On convergence behaviour and numerical accuracy in stationary SWAN simulations of nearshore wind wave spectra. *Coastal Engineering*, **52** (3), pp. 237–256.

A

FURTHER DETAILS FOR WAVE BREAKING OBSERVATIONS

A.1. LABORATORY OBSERVATIONS

The laboratory observations were all made in 15 m – 50 m long 1D wave flumes obtained by HR Wallingford Ltd., United Kingdom (with 210 cases; Coates et al., 1998; Hawkes et al., 1998, 1999; van der Meer et al., 2000), Aalborg University, Department of Civil Engineering, Hydraulics & Coastal Engineering Laboratory, Denmark (with 110 cases; Jensen, 2002), Imperial College London, Department of Civil and Environmental Engineering, England (with 23 cases; Katsardi, 2007; Katsardi and Swan, 2011; Katsardi et al., 2013) and the US Army Engineer Research and Development Center, Coastal and Hydraulics Laboratory, Vicksburg, USA (with 31 cases; Smith, 2004). Two data sets with variable bathymetry were obtained by Battjes and Janssen (1978, 2 cases) for a schematic beach profile with one bar and by Boers (1996, 2005, 3 cases) for a fixed but otherwise natural beach profile with two nearshore bars.

In all these laboratory data sets, the waves were mechanically generated with incident spectra resembling the JONSWAP spectrum (Hasselmann et al., 1973) or the TMA spectrum (Bouws et al., 1985) or a log-normal distribution. The shape of these spectra was varied in the experiments by modifying the peakedness of the spectrum or by adding a second peak. In the Wallingford data set, double-peaked spectra were generated by super-imposing a JONSWAP spectrum onto the high-frequency tail of the primary JONSWAP spectrum containing either 20%, 50% or 80% of the total energy. A similar technique was used in the Smith (2004) data set with TMA spectra with the super-imposed spectra containing two-thirds of the total wave energy.

A.2. LAKE OBSERVATIONS

The lakes (Lake George, Lake IJssel and Lake Sloten) were typically 0.5 m – 4.5 m deep during the observations and have a nearly horizontal bathymetry (up-wind bottom slope between 1 : 7000 and 1 : 10000). The wind speed varied $10 < U_{10} < 25$ m/s approximately.

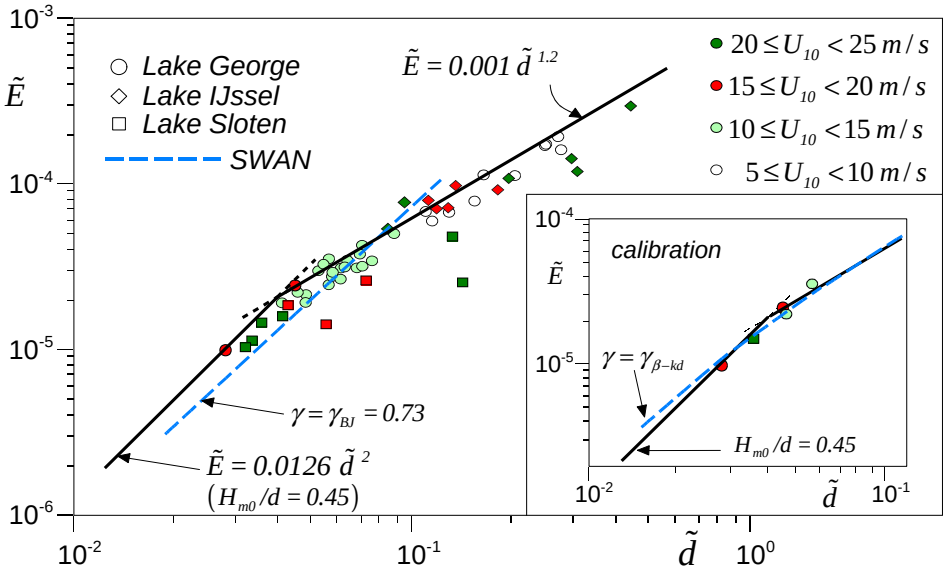

Figure A.1: The observed values of the dimensionless wave energy as a function of the dimensionless water depth for fully developed waves in shallow water of Young and Babanin (2006) and Bottema and van Vledder (2009). The shape of the symbol indicates the site. The color of the symbol indicates wind speed range. Solid lines represent the upper envelope suggested by Young and Babanin (2006) and the alternative suggested by the present authors for approximately $\tilde{d} < 0.05$. The dashed blue line represents the SWAN results for $\gamma = \gamma_{BJ} = 0.73$ and $U_{10} = 20$ m/s. Inset: solid lines identical to those in main figure; the symbols represent the data used in this study; the dashed blue line represents the calibrated SWAN results for $\gamma = \gamma_{\beta-kd}$.

Young and Babanin (2006) and Bottema and van Vledder (2009) consider these conditions to be idealized with the maximum significant wave height determined only by a constant wind speed and depth, i.e., they consider these values to represent fully developed waves in shallow water. They accordingly present their observations in dimensionless form, with the dimensionless wave variance (often referred to as dimensionless energy as it differs only by a constant ρg) $\tilde{E} = g^2 m_0 / U_{10}^4$ as a function of the dimensionless depth $\tilde{d} = gd/U_{10}^2$. Based on an upper envelope of their observations, Young and Babanin (2006) propose a universal relationship for the fully developed waves $\tilde{E} = 0.001\tilde{d}^{1.2}$. We re-examined the upper envelope of both data sets and found that when depth-induced breaking dominates (approximately $\tilde{d} < 0.05$, which we verified with SWAN computations), the envelope corresponds closer to a constant ratio of H_{m0}/d (which is identical to $\tilde{E} = 0.0126\tilde{d}^2$) than to the proposed relationship (see Fig. A.1). Because of this dominance of depth-induced breaking, the computations of the present study concentrate on the range $0.01 \le \tilde{d} \le 0.06$. This range was divided into 5 bins of equal width $\Delta\tilde{d} = 0.01$ and the maximum observed dimensionless energy $\tilde{E}$ was determined (see inset of Fig. A.1) for each bin. This provided us with five observations representing five different cases.

A.3. COASTAL OBSEVATIONS

We considered four coastal sites, three of which are found along the Dutch coast in the southern North Sea and the fourth, Guam, in the Pacific Ocean. In all cases, the wave boundary conditions for the computations were taken from the 2D spectra observed with buoys (reconstructed from the observed 1D frequency spectrum and the observed mean direction and directional spreading per frequency with an assumed directional distribution at each frequency). Locations insensitive to wave breaking were removed and are shown in Figure 3.4.

A.3.1. PETTEN

The Petten site is located near the town of Petten on the west coast of the Netherlands. The beach is fairly straight with a gently sloping profile and a large offshore shoal (minimum depth ~ 5.7 m) and a smaller nearshore sand bar (minimum depth ~ 4.0 m). The waves were measured along a transect normal to the beach extending from the approach to the nearshore bar to the beach with 3 to 5 instruments (depending on the date of observation). We selected 8 cases from three westerly storms in 1995 and 2002. The tidal currents (< 0.6 m/s) were computed with a circulation model (Groeneweg et al., 2003). The incident significant wave heights varied $3.9 < H_{m0} < 5.4$ m and the (onshore) wind speed $14.1 < U_{10} < 22.1$ m/s from directions $264° < \theta_{wind} < 336°$N. The location of the buoy providing the boundary conditions for the Petten 2002 campaign is shown in Figure 3.4B. For the Petten 1995 campaign, the buoy providing the boundary conditions was located 4.8 km NW from the location shown for the 2002 campaign.

A.3.2. HARINGVLIET

The Haringvliet is a 10×10 km^2 bay in the Netherlands, partly protected from the southern North Sea by a shoal extending across half its entrance. During the observations, the minimum water depth over the shoal varied between 1.0 and 2.2 m. The up-slope of the shoal in the mean wave direction varies from 1 : 500 to horizontal. The waves were measured at various locations around the shoal with 6 buoys and 1 wave gauge (not counting the deep water buoy). We selected 3 cases from a north-westerly local storm over the southern North Sea on October 14, 1982 (22:00, 23:00, 00:00 UTC; Ris et al., 1999) with incident significant wave heights $3.2 < H_{m0} < 3.6$ m generated by an offshore north-westerly storm with wind speeds $14.0 < U_{10} < 17.0$ m/s from ~ 300° N. With the estimated tidal currents < 0.25 m/s (from tide tables) mostly orthogonal to the waves, current effects were considered to be negligible.

A.3.3. AMELANDER ZEEGAT

The Amelander Zeegat is a 30 m deep tidal inlet of the Wadden Sea between the barrier islands of Terschelling and Ameland in the southern North Sea. It is an intertidal area with shoals and channels over a distance of 15 km to the mainland. In fair weather, the water over the shoals is typically ~ 1 m deep. The waves were measured with 13 buoys, 11 of which were located along two more-or-less parallel arrays west and east of the main channel and continuing farther onto the flats. Only observations at the nine buoys closest to the coast were sensitive to depth-induced breaking. The remaining two buoys

from the arrays provided the northern boundary conditions and are located approximately 5 km NW and NNE, respectively, from the most seaward buoy of the western and eastern transects shown in Figure 3.4A. The two other (offshore) buoys (ELD and SON) provided the eastern and western boundary conditions for the computations. These are located 65 km WSW and 40 km ENE from the tidal inlet. We selected three cases from one westerly storm which occurred on January 18, 2007 (12:20, 14:00, 17:20 UTC+1) with winds of $U_{10} \approx 20$ m/s from $233° < \theta_{wind} < 267°$N. The water levels and currents were computed with a circulation model (van der Westhuysen and de Waal, 2008) that was calibrated with nearby water level observations. The error in water depth in the three cases was estimated from nearby observations to be < 0.07 m for local water depths 1.5−2.5 m. The deep water incident significant wave height varied $2.7 < H_{m0} < 5.4$ m and the mean period $5.4 < T_{m01} < 7.6$ s. The significant wave height of the locally generated waves on the flats was typically ~ 1 m.

A.3.4. GUAM

The Guam site is a reef fringing the south-east coast of Guam in the Pacific Ocean. Over the transect of the buoy locations, the sea bottom rises at the reef edge from ~ 25 m depth to ~ 1.5 m depth at the reef crest over a distance of 200 m (the fore reef). Behind the crest, the depth slightly increases again to ~ 2 m over the reef flat with a characteristic negative slope of ~ 1 : 700. Schematized 1D versions of this profile, typically with a horizontal reef flat and no crest, have been used in other studies (Demirbilek et al., 2009; Su et al., 2010; Sheremet et al., 2011; Zijlema, 2012). Here, we consider the actual 2D situation. At the location of the observations, the reef is 400 m wide. Péquignet et al. (2011) estimated the bulk frictional dissipation using the *bottom friction* model of Thornton and Guza (1983) with a bottom roughness coefficient of $C_{f,TG} = 0.06$ on the reef flat and $C_{f,TG} = 0.2$ on the fore reef (outside the breaking region). The waves were measured with current meters and pressure transducers at 4 locations. We selected 4 cases under very mild wind conditions ($2.2 < U_{10} < 4.2$ m/s) from $46° < \theta_{wind} < 85°$N and with the incident significant wave height varying between $4.04 < H_{m0} < 4.52$ m. Two cases were taken from a storm event (defined as $H_{m0,max} > 3.0$ m and duration > 8 hours) between July 7-8, 2006 and the other two between December 5-8, 2006. These cases were chosen in conditions where the observed tidal current was < 0.5 m/s and are considered negligible. Boundary conditions were taken from a location 1.5 km SE from the most seaward buoy on the reef.

Table A.1: Summary of laboratory and field conditions used in this study. The averaged significant wave height, $\overline{H_{m0,0}}$; mean wave period, $\overline{T_{m01,0}}$ and peak wave period, $\overline{T_{p,0}}$ enforced at the boundary are provided. The averaged normalized characteristic wave number, $\overline{\tilde{k}d}$ is also provided for all locations used in this study which were sensitive to depth-induced wave breaking (Section 3.3.2).

Cases	**#**	$\overline{H_{m0,0}}$	$\overline{T_{m01,0}}$	$\overline{T_{p,0}}$	$\overline{\tilde{k}d}$	**Notes**
Slopes	111					
Wallingford	49	0.12	1.60	4.16	0.89	JONSWAP uni-/bimodal; slopes 1:10, 20, 30 and 50
Katsardi	18	0.09	1.15	1.44	0.89	JONSWAP log-normal; slopes 1:100 and 250
Smith	31	0.09	1.24	1.71	0.65	TMA uni-/bimodal; slope 1:30
Boers	3	0.16	1.75	2.50	0.46	JONSWAP unimodal; fixed barred profile
Battjes-Janssen	2	0.17	1.63[a]	1.95[b]	0.73[b]	JONSWAP unimodal; fixed barred profile
Petten	8	4.63	7.73	10.38	0.59	Predominantly unimodal (swell) with wind-sea
Horizontal	114					
Wallingford	49	0.12	1.48	1.48	0.48	JONSWAP uni-/bimodal; horizontal slope
Katsardi	5	0.12	1.14	1.14	0.85	JONSWAP log-normal; horizontal slope
Jensen	45	0.15	1.56[a]	1.84[b]	0.80[b]	JONSWAP unimodal; horizontal slope
Amelander Zeegat	3	3.52	6.24	8.41	3.71	Unimodal swell at boundary; wind-sea in interior
Lakes	5	-	-	-	1.40	No spectra enforced; wind generated waves
Guam	4	4.35	6.95	9.41	0.33[b]	Unimodal swell
Haringvliet	3	3.43	6.77	8.33	1.12[b]	Predominantly unimodal (swell) with wind-sea

[a] Estimated from a parametric JONSWAP spectrum
[b] Nominal value

B

COMBINED SOURCE TERMS FOR SWAN IN THE COASTAL REGION

The following Appendix presents the combined effect the new $\beta - kd$ parameterization for depth-induced wave breaking as presented in Chapters 3 and 4 with the SPB model for nonlinear triad interactions with the Consistent Collinear Approximation as presented in Chapter 5. The computed results are compared to present modelling defaults for the representation of the dominant water wave physics for the coastal zone, namely the Battjes and Janssen (1978) dissipation model with a constant scaling of $\gamma_{BJ} = 0.73$ and the Lumped Triad Approximation of Eldeberky (1996) with the Original Collinear Approximation. The comparison highlights increased modelling skill for the prediction of the significant wave height and the qualitative representation of the evolution of the spectral shape and suggests a greater range of applicability of the new source terms for operational applications. However, a number of shortcomings are also highlighted which need to be addresses in future work, namely the occasional increase in error for the prediction of lower order mean wave periods, i.e., T_{m01} and the increased computational time required.

A significant part of following has been taken from SALMON, J.E., HOLTHUIJSEN, L.H., SMIT, P.B., VAN VLEDDER, G.P. and ZIJLEMA, M. (2014). Alternative source terms for SWAN in the coastal region. In: *Proceedings of the 34th International Conference on Coastal Engineering*, Coastal Engineering Research Council, Seoul, South Korea, pp. 1–13.

B.1. INTRODUCTION

SWAN is a third-generation wave model (Booij et al., 1999) specifically developed for operational use in the coastal zone. Although it has been used over the past 15 years with numerous developments including the support for parallelization and unstructured grids, the representation for the dominant shallow water-wave physics: depth-induced wave breaking and triad wave-wave interactions have remained virtually unchanged despite known shortcomings, particularly in the estimation of wave period measures, and alternatives available. Here, we consider the combined effects of using the new $\beta - kd$ source term for depth-induced wave breaking (Chapters 3 and 4) in conjunction with the SPB triad source term for the nonlinear triad wave-wave interactions with the proposed Consistent Collinear Approximation (CCA; Chapter 5) to present defaults.

First, we compare the the depth-induced wave breaking parameterizations over observations taken over a 1 : 30 laboratory slope (Smith, 2004) and laboratory observations of an idealized horizontal reef (Jensen, 2002). We then compare the Stochastic Parametric model based on Boussinesq equations (SPB; Becq-Girard et al., 1999) model with the Consistent Collinear Approximation for the triad source term over these cases. Finally, we present a comparison between the default shallow water physics and these alternatives over observations taken at Haringvliet (Ris et al., 1999). The intention of this work is to demonstrate preliminary results of using these alternative source terms and the limitations of the currently used default source terms.

B.2. MODEL SETTINGS

We use the default settings of the latest public domain version of SWAN (41.01; `swan.tudelft.nl`) apart from the applied depth-induced breaking and triad interaction source terms; the focus of this Appendix. The source terms used for depth-induced wave breaking and nonlinear triad wave-wave interactions are described in Chapters 3 and 4, and Chapter 5, respectively, with one exception. For the SPB model, a calibration coefficient of $\alpha_{SPB}^{CCA} = 0.75$ was used (instead of $\alpha_{SPB}^{CCA} = 0.87$), a value obtained from a number of trial computations over laboratory cases (not shown). The modified SPB model is subsequently referred to as the mSPB model.

Wave generation due to wind is computed with the source term of Komen et al. (1984) with the wind drag coefficient of Zijlema et al. (2012). For the nonlinear quadruplet wave-wave interactions, the Discrete Interactions Approximation (DIA; Hasselmann et al., 1985) as scaled by the WAMDI Group (1988) for shallow water is used. For computational efficiency, this source term is switched off for 1D cases as quadruplets do not play a role in unidirectional waves. For the sink terms, white capping is represented by the pulse model of Hasselmann et al. (1973) as modified by the WAMDI Group (1988) and weighted to higher frequencies as suggested by Rogers et al. (2003), and for bottom friction, the model of Hasselmann et al. (1973) with a bottom friction coefficient of 0.038 $m^2 s^{-3}$ (Zijlema et al., 2012) is used.

For the laboratory cases, a frequency resolution of $\Delta f = 0.05 f$ and a directional resolution of $\Delta\theta = 0.5°$ is used. For the field cases, $\Delta f = 0.1 f$ (constrained by the DIA) and $\Delta\theta = 10°$ is used. For terminating the iterative SWAN computations, the curvature-based criterion of Zijlema and van der Westhuysen (2005) are applied.

B.3. OBSERVATIONS

To verify the performance of the proposed alternative source terms, we compared the model performance of the default source terms and the alternative source terms to two laboratory cases and one field case as described in the following.

B.3.1. LABORATORY CASES

SMITH (2004)

The Smith (2004) laboratory data set consists of 31 cases performed at the US Army Engineer Research and Development Center, Coastal and Hydraulics Laboratory encompassing a variety of spectra including unimodal and bimodal incident spectra with varying degrees of wave steepness and spectral width. The wave flume consisted of a 1 : 30 slope and waves were measured at 10 locations, nine of which are located on the slope (Fig. B.1A).

Irregular waves are generated at a piston wave generator as either unimodal or bimodal spectra described with the parametric TMA spectral shape (Bouws et al., 1985). For the case of the double-peaked spectra, the spectra is formed by the linear combination of the two underlying TMA spectra. For these cases, two-thirds of the total energy is contained at the higher peak, set at 1 Hz. For all cases, the peak wave period varied between $1.0 \leq T_p \leq 2.5$ s with a significant wave height of either $H_{m0} = 0.06$ or 0.09 m. The spectral peakedness parameter, γ_{TMA} varied between three values from 3.3 for a broad spectrum, 20 and 100 for a narrow spectrum.

JENSEN (2002)

The Jensen (2002) laboratory data set consists of a total of 301 cases with regular waves and 110 tests with irregular waves over 4 different reef approach slopes (varying between 1 : 0.5, 1 : 1, 1 : 1 's'-shape and 1 : 2) and a horizontal section. Waves were measured at 14 different locations, however wave measurements at only four locations over the horizontal are considered here (Fig. B.2A).

We chose a random selection of 25 cases from the 110 irregular wave cases. The corresponding range of incident peak frequencies for the unimodal JONSWAP spectra were $1.4 \leq T_p \leq 2.6$ s with a significant wave height between $0.11 \leq H_{m0} \leq 0.21$ m.

B.3.2. FIELD CASES

HARINGVLIET (OCTOBER 14, 1982)

The Haringvliet is characterized as a relatively shallow $10 \times 10\,\text{km}^2$ bay in the southwest of the Netherlands. It is partially protected by a shoal (the 'Hinderplaat') which extends across half of its entrance (Fig. B.3A). Four cases at 21:00, 22:00, 23:00 and 00:00 UTC are selected from observations taken from a north-westerly local storm over the southern North Sea on October 14, 1982. These cases were chosen as negligible currents (< 0.25 m/s) occurred during the observations, the wind conditions were fairly constant, the waves were relatively high and the water level was sufficiently low to observe the generation of a secondary peak.

Over the observation period, the minimum water depth over the shoal varied between 1.0 and 2.2 m and the incident significant wave height varied between $3.2 \leq H_{m0} \leq$

3.6 m. The wind speed varied between $14.0 < U_{10} < 17$ m/s from $\sim 300^{\circ}N$. Further details are given in Ris et al. (1999).

B.4. RESULTS

B.4.1. DEPTH-INDUCED WAVE BREAKING

The default source terms for depth-induced breaking and triad nonlinear interactions were applied to the above cases. The results over the sloping Smith (2004) data set is shown in Figure B.1 (in red). The comparison between the observed and the predicted significant wave height shown in the scatter plot in Fig. B.1B shows good modelling skill over relatively steep slopes as demonstrated in previous studies (e.g. Rattanapitikon, 2007). For illustration purposes, Case 31 ($H_{m0} = 0.09$ m, $T_p = 2.5$ s, $\gamma_{TMA} = 100$), shown in Fig. B.1A, illustrates the typically good agreement between the observations and model results for H_{m0}. The modelling skill for each test case can be expressed by calculating performance metrics: scatter index ($s.i.$) and the relative bias ($r.b.$) as used in previous studies (e.g. Janssen et al., 1984, see Section 3.3.3).

For each data set, the performance metrics were computed for each case, and then averaged over the number of cases to give an averaged $s.i.$ and averaged $r.b.$. The corresponding values over the Smith (2004) data set with default source terms are $s.i. = 0.08$ and $r.b. = -0.00$.

Conversely, over the horizontal bathymetries of the Jensen (2002) data set, as shown in Fig. B.2B, a large overestimation of the significant wave height is shown. The corresponding performance metric were $s.i. = 0.21$ and $r.b. = +0.17$. This overestimation H_{m0} of can be seen in the example shown in Fig. B.2A. In comparison with the sloping laboratory cases, the magnitude of the total error is more than double and the relative bias forms a significant contribution to the total error.

Also shown in Figs. B.1B and B.2B is the performance of the $\beta - kd$ model with the LTA source term (in blue). Over the Smith (2004) data set, the performance is comparable to the BJ model with $s.i. = 0.07$ and $r.b. = +0.04$ whereas over the Jensen (2002) data set, the $\beta - kd$ model is also shown to provide comparable modelling performance as shown in the Smith (2004) data set with $s.i. = 0.08$ and $r.b. = +0.05$.

B.4.2. NONLINEAR TRIAD WAVE-WAVE INTERACTION

Although the previous comparison illustrates reasonable results for the prediction of H_{m0} over relatively steep slopes (1 : 30) with the default source terms, for the prediction of integral parameters which are more sensitive to the spectral shape e.g. mean wave period measures, the performance is relatively poorer. This is due to the poor representation, if at all, of the nonlinear triad interactions. This is illustrated in Fig. B.1C for the LTA model with $s.i. = 0.13$, of which a significant amount is negative bias ($r.b. = -0.10$) for the mean wave period T_{m01}. Conversely, the mSPB model appears to give better results with slightly smaller errors ($s.i. = 0.10$) and a significantly reduced bias ($r.b. = +0.04$).

These differences are illustrated in Figure B.4 where the observed and computed spectra for Case 31 are presented. Following Booij et al. (2009), we scale the energy density so that the universal $k^{-4/3}$ tail appears as a horizontal line. It is clear that the LTA is only able to transfer energy to $f_{2^n \times p}$ where n is a positive integer. Furthermore, it is

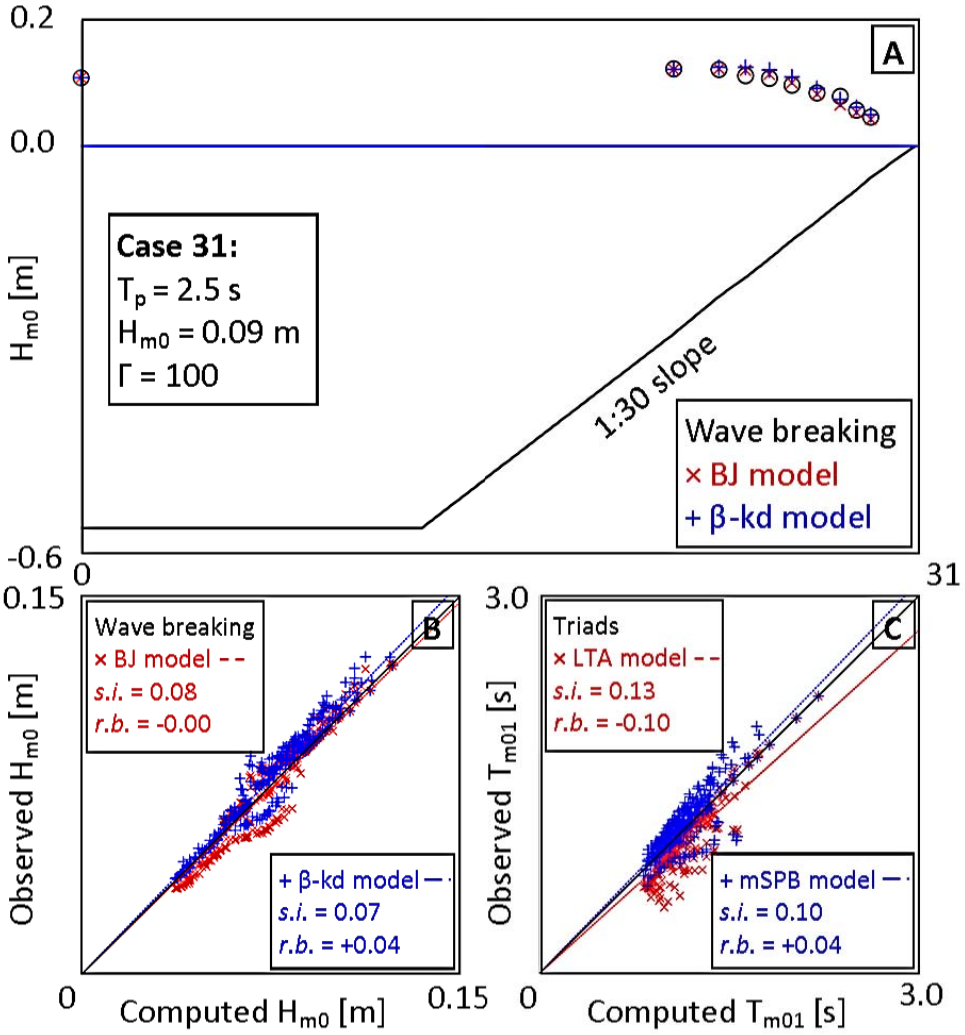

Figure B.1: Experimental setup and computational results for the Smith (2004) data set. Top panel (A) shows the flume profile and measuring locations with computed H_{m0} using the BJ (red ×) and $\beta - kd$ (blue +) breaker models for Case 31 with the LTA triad model. Panel B shows the performance of these breaker models in predicting H_{m0} for all 31 cases. Panel C shows the performance in predicting T_{m01} of the LTA triad model (red ×) and the mSPB triad model (blue +) with the BJ breaker model. The performance metrics: *s.i.* and *r.b.* are presented in Panels B and C as defined in Eqs. (3.3) and (3.4).

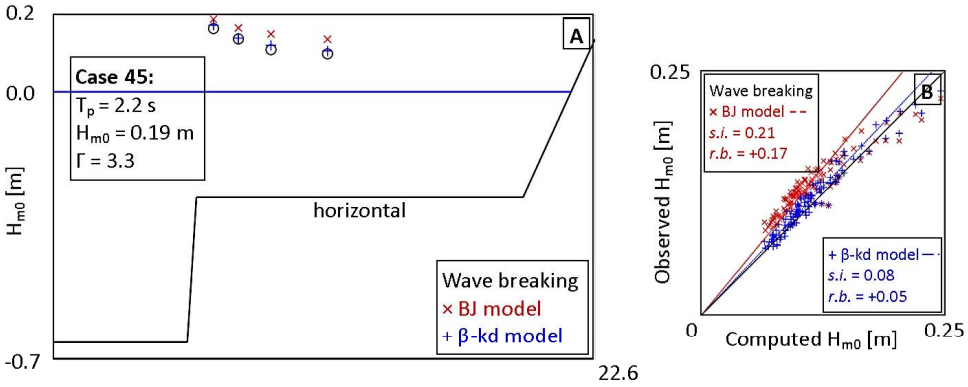

Figure B.2: Experimental setup and computational results for the Jensen (2002) data set. Panel A shows the flume profile and measuring locations with computed H_{m0} using the BJ (red ×) and $\beta - kd$ (blue +) breaker models for Case 45 with the LTA triad model. Panel B shows the performance of these breaker models in predicting H_{m0} for all 25 cases (random selection). Wave period measures were not available for this data set. The performance metrics: *s.i.* and *r.b.* are presented in Panel B as defined in Eqs. (3.3) and (3.4).

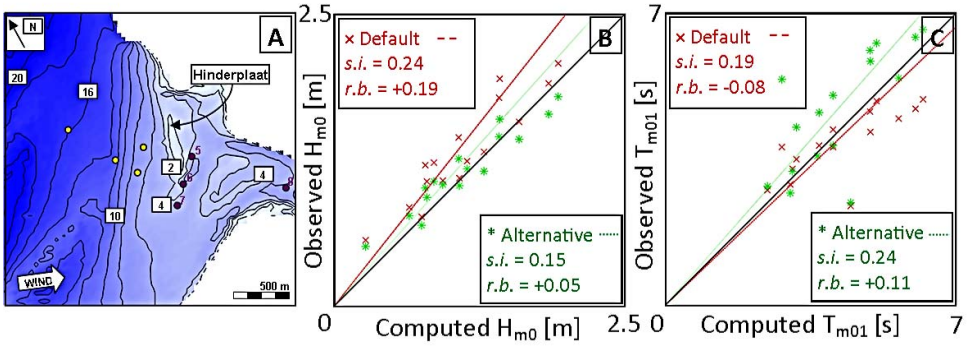

Figure B.3: Bathymetry and computational results for the Haringvliet (October 14, 1982) data set. Panel A provides the bathymetry for the region at +1 m above Amsterdam Ordnance Datum (NAP) with contour lines given at 2 m intervals. Wave observation stations are shown as dots. Only locations shown in purple (5, 6, 7, 8) are considered. Panel B shows the performance of default SWAN (BJ + LTA; red ×) and the alternative source terms ($\beta - kd$ + mSPB; green *) in predicting H_{m0}. Panel C shows the equivalent for T_{m01}. The performance metrics: *s.i.* and *r.b.* are presented in Panels B and C as defined in Eqs. (3.3) and (3.4).

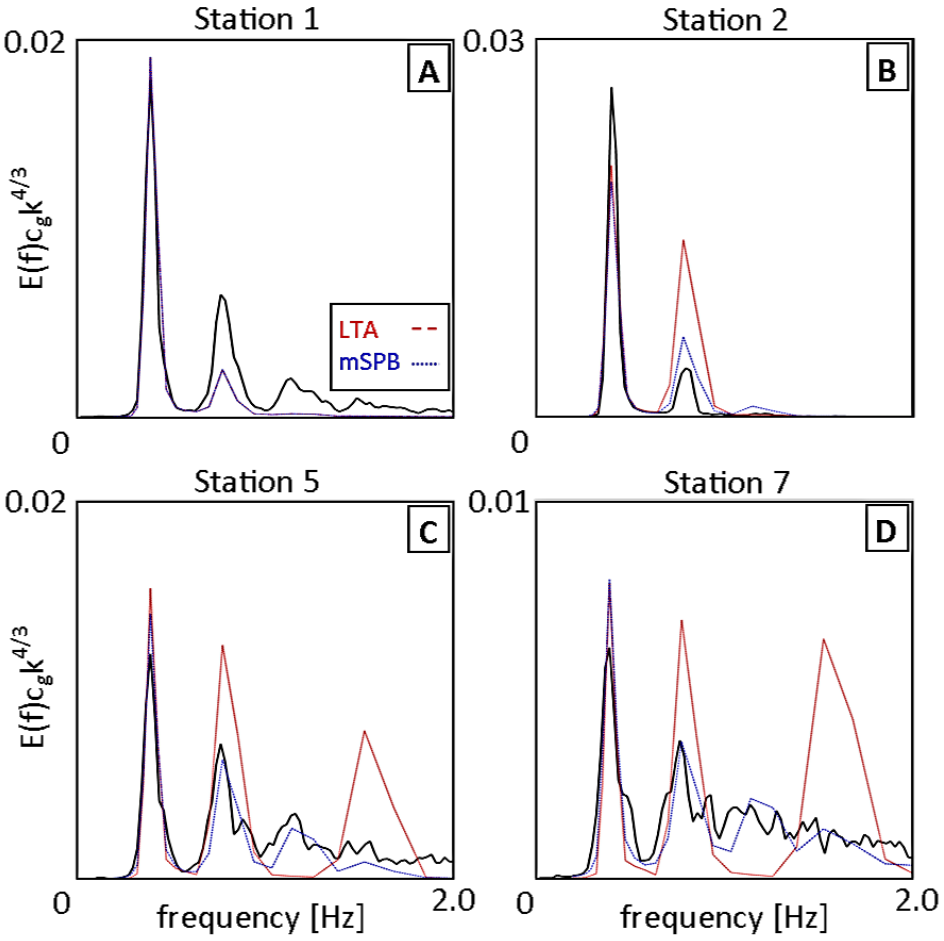

Figure B.4: Observed and computed scaled variance density spectra for Case 31 of the Smith (2004) data set. Panels A to D show the evolution of the spectra in the surf zone from at the wavemaker (Location 1) to deep in the surf zone (Location 7). Spectra computed with the LTA are shown in red (–) and the spectra computed with the mSPB are shown in blue (..). Note that the spectra are scaled so that a $k^{-4/3}$ tail appears horizontal.

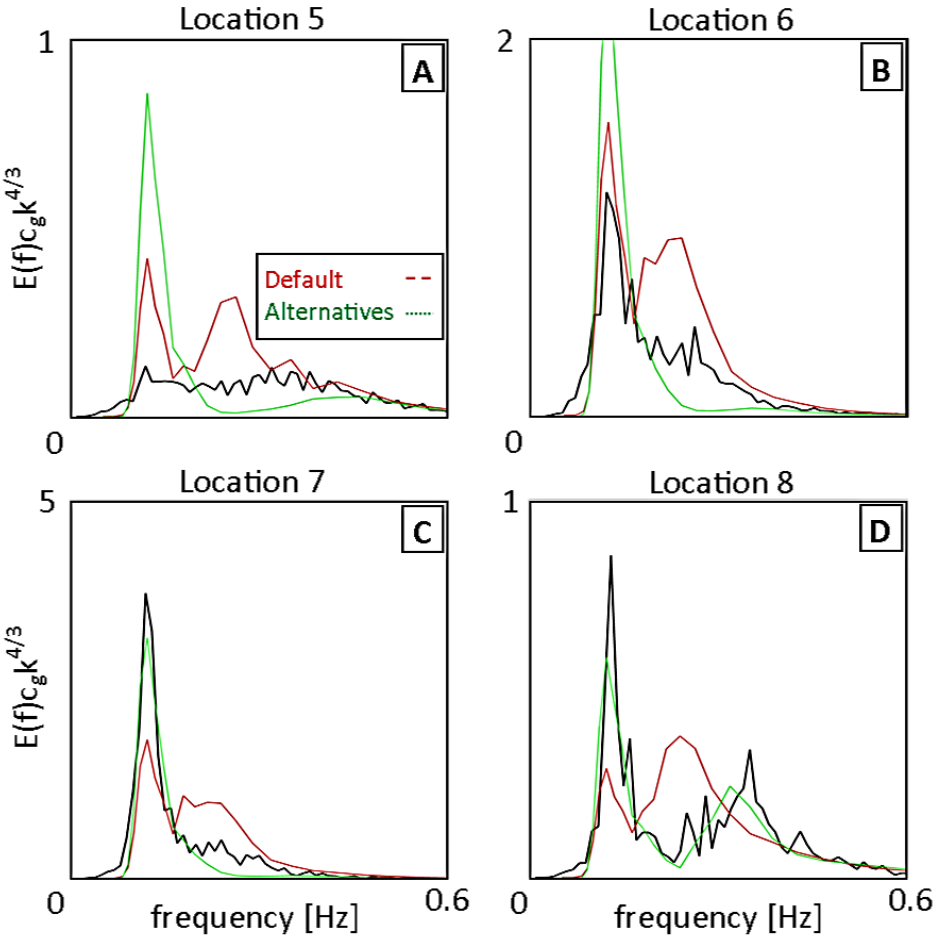

Figure B.5: Observed and computed scaled variance density spectra for case 23:00 UTC of the Haringvliet data set at the four most shoreward locations. Spectra computed with the default source terms (LTA + BJ model) are shown in red (–) and the spectra computed with the alternative source terms ($\beta - kd$ + mSPB) are shown in green (..). Note that the spectra are scaled so that a $k^{-4/3}$ tail appears horizontal.

clear that for this case these peaks are severely overestimated with energy not removed deeper in the surf zone e.g. Stations 5 and 7. In contrast, the mSPB model provides better agreement with the observations. All higher harmonics are predicted relatively well, including locations deep in the surf zone. In addition, the universal tail is also in better agreement with the observations compared to the LTA model results.

B.4.3. COMBINED SOURCE TERMS OVER A FIELD CASE

To verify the combined use of both the $\beta - kd$ and mSPB model, we compared the combined use of these source terms to default SWAN i.e., the BJ and LTA model over the Haringvliet data set. This case represents depth-induced wave breaking over a relatively horizontal shoal (the 'Hinderplaat') as well as the generation of a significant secondary peak behind the shoal (Ris et al., 1999). To reduce the bias from observations taken in deeper water, which would be largely be unaffected by wave breaking and triad interactions, we only considered wave observations taken in depths of $d < 6$ m (Locations 5, 6, 7 and 8; shown as purple dots in Fig. B.3A).

Figure B.3B demonstrates the model comparison for the prediction of H_{m0} over the Haringvliet data set. Similar to the Jensen (2002) cases shown in Fig. B.2B, a significant overestimation of H_{m0} is shown with the default source terms (red; $s.i. = 0.24$ and $r.b. = +0.19$). These errors are significantly reduced, particularly the relative bias, with the use of the alternative source terms (green; $s.i. = 0.15$ and $r.b. = +0.05$).

However, compared to the improvements shown in Figure B.1C and Figure B.4, the model comparison shown for T_{m01} in Figure B.3C demonstrate a decrease in modelling skill with the application of the alternative source terms compared to the defaults. Whereas the performance metrics for the default source terms are $s.i. = 0.19$ and $r.b. = -0.08$, the equivalent values for the alternative source terms are $s.i. = 0.24$ and $r.b. = +0.11$. To further investigate this lack of improvement, the observed and predicted spectra for measurements at 23:00 UTC are shown in Figure B.5.

At the wave observation locations just behind the shoal i.e., Location 5 and 6, both the LTA and SPB model perform poorly. Whereas the LTA model transfer too much energy to the second harmonic as shown previously in the Smith (2004) data set, the mSPB transfers too little energy to the higher harmonics. This results in an underestimation of T_{m01} with the LTA and an overestimation with the mSPB.

At Location 7, the mSPB model captures the energy at the primary peak well however as seen at Location 5 and 6 the energy at the higher frequencies is also underestimated. However, compared to the LTA which transfers too much energy from the primary peak to the secondary peak, the mSPB provides better agreement with the observed spectral shape.

At a greater distance from the shoal, at Location 8, good agreement between the observed spectra and the mSPB model results is shown. Although slightly underestimated, the primary peak is reproduced relatively well and the amount of energy at the second harmonic is also in good agreement with the observations. Furthermore, the energy at the higher frequencies is also in good agreement with the observations. Conversely, as shown at Location 7, the LTA still transfers too much energy from the primary peak to the second harmonic.

B.4.4. COMPUTATIONAL EFFICIENCY

The averaged relative contributions of the depth-induced breaking source term and triad source term over all four cases of the Haringvliet data set is shown in Table B.1. It is clear that the default BJ and LTA source terms contribute very little to the total computational cost (< 2% and < 5% of the total respectively). The proposed $\beta - kd$ is also shown to be comparable to the BJ model in terms of computational cost in the $\beta - kd$ + mSPB column.

However, much of the increased computational cost of using alternative source terms, as shown in the last three columns is due to the use of alternative triad source terms to the LTA model. In the case of the mSPB model, the source term is up to three orders of magnitude more expensive. Such a steep increase in computational cost is not surprising due to the introduction of the integral over all other frequencies represented by Eq. (2.49) and a more complex representation of the bispectrum as given in Eq. (2.46). This increase in computational cost results in computations up to 45 times more expensive for a complete model run. In the final row, the average number of iterations for convergence over the four Haringvliet cases is given. A slight change to the convergence behavior between the LTA and mSPB model is demonstrated. However it represents, at most, an additional iteration step with the mSPB model for the Haringvliet cases considered. Therefore, the increased computational cost of the mSPB model can be attributed to the computation of the triad source term rather than a poor convergence behavior.

Table B.1: Averaged relative contributions of the depth-induced wave breaking and nonlinear triad wave-wave interaction source terms for the Haringvliet data set compared to default SWAN 41.01.

	Default	BJ + mSPB	$\beta - kd$ + mSPB	BJ + DCTA*
Total	100.00	4310.92	4415.90	462.23
Wave breaking	1.45	1.56	1.53	1.46
Triad interaction	4.58	4197.82	4304.00	362.01
Other	93.97	111.54	110.37	98.76
Av. # Iterations	8.50	9.35	9.35	9.00

*DCTA: Distributed Collinear Triad Approximation (Booij et al., 2009).

B.5. DISCUSSION

The alternative source terms presented here show good agreement with observations made in laboratory conditions. Over the sloping cases of the Smith (2004) data set, the $\beta - kd$ model perform comparably with the BJ model, whereas over the horizontal cases of the Jensen (2002) data set, the overestimation of the BJ model is largely reduced with the use of the $\beta - kd$ model resulting in better model performance. Much of this improvement comes from the lower value of $\gamma_{\beta-kd} = \gamma_0 = 0.54$ under the wave conditions represented by the Jensen (2002) data set i.e., a horizontal bathymetry ($\beta = 0$) with non-locally generated waves ($\widetilde{kd} < 1$). These improvements are expected to be applicable to other similar wave environments e.g. the dissipation of swell over horizontal bathymetries such as reefs and intertidal flats. Similar conditions are found in the Haringvliet data set where waves from a local storm propagate and break over a fairly flat shoal. For

these cases, the $\beta - kd$ model also shows better modelling skill and a reduced bias compared to the BJ model.

Better agreement with the observed spectral shape of the Smith (2004) data set is demonstrated with the mSPB model in comparison to the LTA model. In these cases, the LTA model demonstrates an excessive transfer of wave energy to the higher frequencies which results in an underestimation of the mean wave period. Conversely, the mSPB model does not transfer too much energy to the higher frequencies and reproduces the primary peak well. For the Haringvliet data set, these improvements are only demonstrated at some distance from the Haringvliet shoal (Locations 7 and 8). At locations closer to the shoal, the mSPB model underestimates the wave energy transfer to the higher frequencies whereas the LTA over-predicts this. However, the almost consistent excessive transfer of wave energy to the second harmonic by the LTA model is not reproduced by the mSPB model in agreement with the observations.

The poorer prediction of T_{m01} by the mSPB model compared to the LTA model over the Haringvliet data set may be due to a number of reasons. In particular, the ad hoc modification of the SPB model to use $K_{mSPB}\left(k_p\right)$ is not physically justified and is dimensional. Therefore it may not be appropriate for scaling the (m)SPB model. Furthermore, the use of α_{mSPB} is determined from simulations over laboratory cases which may not be representative for field cases. Nonetheless, promising results are shown by the mSPB model, particularly in respect to the almost 'out of the box' configuration of the SPB model presented here. In particular, smaller errors in the prediction of higher-order measures for mean wave period are expected with the mSPB model as typically the energy levels at the higher frequencies are better reproduced.

However, a limitation of the application of models such as the mSPB is the increased computational cost. This arises from computing over all interacting frequencies. Although this may result in more physically realistic spectra (e.g. Fig. B.4 and Fig. B.5), it comes at a computational cost prohibitive for operational use. As an alternative, the computational cost of the DCTA (Booij et al., 2009) is presented in the final column of Table (B.1). This source term computes a similar integrals as represented by Eq. (2.49) but is formulated and implemented so that the sum and difference contributions per frequency are computed simultaneously. The difference in computation time between the mSPB and DCTA source terms shows a computational cost of up to an order of magnitude smaller. Therefore, formulation the mSPB model in a similar manner may lead to a similar increase in computational efficiency.

Further gains may be possible by restricting the range of interacting frequency components considered i.e., to a range between the extremes of only considering the self-self interactions, as done in the LTA model, and all interactions, as considered by the mSPB model. This modifications may allow for an efficient and physically more realistic nonlinear triad interaction source term to become available for operational purposes.

B.6. CONCLUSIONS

Alternative source terms for depth-induced wave breaking and nonlinear triad wave-wave interactions have been presented and some preliminary results shown. In general, the $\beta - kd$ model is shown to provide comparable or improved modelling performance for H_{m0} when compared to the BJ model over the data sets presented. These improve-

ments come at no decrease in modelling performance (over the cases considered) or increased computational cost.

The mSPB model is shown to provide better agreement with the observed spectral shapes from the Smith (2004) data set as well in the Haringvliet data set at locations relatively far from the Hinderplaat shoal when compared to the LTA model, particularly in the prediction of the higher harmonics. In the remaining locations, where the mSPB model performed worse, the mSPB model typically under-predicted the transfer of wave energy to higher frequencies in contrast to the LTA model which over-predicted these transfers. This decrease in modelling performance of the mSPB model is likely due to the ad hoc use of $\mu_{mSPB}\left(k_p\right)$ and α_{mSPB} which should be re-assessed in future work. Furthermore, the mSPB comes at a computational cost prohibitive for most operational purposes. In future work, this increased computational cost can likely be reduced by implementing the model to compute the sum and difference terms simultaneously and reviewing the interaction frequencies considered.

List of Common Symbols

Greek Symbols

α	calibration coefficient [−; (typically)]
α_p	wave phase [$rad.$]
β	local bottom slope [°]
γ	breaker index [−]
γ_{TMA}	spectral peakedness parameter for TMA spectrum [−]
δ	Dirac delta function
$\Delta\theta$	directional resolution [°]
$\Delta\sigma$	radial frequency resolution [Hz]
$\Delta\psi$	linear phase mismatch [$rad.$]
Δf	frequency resolution [Hz]
$\Delta k_{m,p-m}$	wave number mismatch [m^{-1}]
Δk_y	spatial resolution in lateral wavenumber [m^{-1}]
Δt	temporal resolution [s]
Δx	spatial resolution in x-axis [m]
Δy	spatial resolution in y-axis [m]
ε	dissipation per unit area [W/m^2]
η	surface elevation [m]
θ	wave direction [°]
θ_0	mean wave direction [°]
θ_c	current direction [°]
θ_w	wind direction [°]
κ	shape coefficient [−]
μ	proportionality constant between B and fourth-order cumulant [m^{-1}]
ρ	density [kgm^{-3}]
σ	radial frequency [Hz]
σ_θ	directional width [°]
σ_θ^*	directional width limit assumed as unidirectional [°]
σ_{peak}	peak radial frequency [Hz]
τ	time lag [s]
φ	biphase [$rad.$]
$\Phi_{m,p-m}$	factor accounting for closure for the bispectrum [m]
ψ_p	phase (linear contribution) [$rad.$]

Roman Symbols

a	wave amplitude [m]
A_p	complex Fourier amplitude [m]
$\widetilde{A}_p$	complex amplitude [m]

$B_{m,p-m}$	bispectrum $[m^3 Hz^{-2}]$
$\overline{B_{m,p-m}}$	parameterization of the bispectrum $[m^3 Hz^{-2}]$
c	phase velocity $[ms^{-1}]$
c_g	group velocity $[ms^{-1}]$
$c_{g,\theta}$ (or c_θ)	propagation velocity in θ-space $[^\circ s^{-1}]$
$c_{g,\sigma}$ (or c_σ)	propagation velocity in σ-space $[Hzs^{-1}]$
$c_{g,x}$	propagation velocity in x $[ms^{-1}]$
$c_{g,y}$	propagation velocity in y $[ms^{-1}]$
d	local water depth $[m]$
$\tilde{d}$	dimensionless depth $[-]$
$D(\theta;\sigma)$	directional distribution $[1/^\circ]$
E	total variance $[m^2]$
$E_p^{'}$	double-sided discrete variance spectrum $[m^2 Hz^{-1}]$
$E(\sigma)$	1D continuous single-sided variance spectrum $[m^2 Hz^{-1}]$
$E(\sigma,\theta)$	2D continuous single-sided variance spectrum $[m^2 Hz^{-1}/^\circ]$
$\tilde{E}$	dimensionless energy $[-]$
f	wave frequency $[Hz]$
$\bar{f}$	mean or characteristic wave frequency (unspecified) $[Hz]$
f_{m01}	first-order moment mean wave frequency $[Hz]$
f_{m02}	second-order moment mean wave frequency $[Hz]$
f_{peak}	peak frequency $[Hz]$
$\mathbf{F}$	radiation stress gradient vector $[Nm^{-2}]$
g	gravitational acceleration $[ms^{-2}]$
H	wave height $[m]$
H_{brk} (or H_b)	characteristic breaking wave height $[m]$
H_{m0}	significant wave height $[m]$
H_{max} (or H_m)	maximum wave height $[m]$
H_r	ratio of H_{rms} to H_b $[-]$
H_{rms}	root-mean squared wave height $[m]$
k	wave number $[m^{-1}]$
$\mathbf{k}$	wave number vector $[m^{-1}]$
$\bar{k}$	mean wave number $[m^{-1}]$
k_{peak} (or k_p)	peak wave number $[m^{-1}]$
$\tilde{k}$	characteristic wave number $[m^{-1}]$
K_θ	number of directional partitions $[-]$
L	wavelength $[m]$
m	directional width parameter $[-]$
m_n	nth-order moment $[m^2 Hz^n]$
M	weighting function $[-]$
N	action density $[m^2 Hz^{-2}]$
p_θ	directional integration bandwidth $[^\circ]$
Q_b	fraction of breaking waves $[-]$
$Q_{m,p-m}$	bispectrum as product of local variance densities $[m^2 Hz^{-2}]$
$\overline{Q^p_{m,p-m}}$	bispectrum as product of local variance densities using CCA $[m^2 Hz^{-2}]$

$R_{\eta\eta}$	autocorrelation of η $[m^2]$
s	local wave steepness $[-]$
S_{total}	sum of all source terms
S_{brk} (or S_b)	source term for depth-induced wave breaking
$S_{dissipation}$	source term for wave dissipation (unspecified)
S_{fric} (or S_{bf})	source term for bottom friction
S_{nl}	source term for nonlinear interactions (unspecified)
S_{nl4}	source term for quadruplet interactions
S_{nl3}	source term for triad interactions
S_{wcap}	source term for white capping
S_{wind}	source term for wind input
t	time $[s]$
T	duration $[s]$
T_{m01}	first-order moment mean wave period $[s]$
T_{m02}	second-order moment mean wave period $[s]$
T_{m-10}	minus first-order moment wave period $[s]$
T_{peak} (or T_p)	peak wave period $[s]$
$T_{m,p-m,-p}$	trispectrum $[m^4 Hz^{-3}]$
U_{10} (or $U_{w,10}$)	average windspeed at 10 m elevation $[ms^{-1}]$
U_c	current velocity $[ms^{-1}]$
Ur	spectral Ursell number$[-]$
W	coupling coefficient $[m^{-2}]$
$\mathbf{x}$	horizontal coordinate vector (x, y) $[m]$
x	principal horizontal axis $[m]$
y	lateral horizontal axis $[m]$

Abbreviations and Acronyms

B	Baldock et al. (1998)
BJ	Battjes and Janssen (1987)
CCA	Consistent Collinear Approximation
CREST	Coupled Rays with Eulerian Source Terms
D	Dally et al. (1985)
DCTA	Distributed Collinear Triad Approximation (Booij et al., 2009)
DIA	Discrete Interation Approximation (Hasselmann et al., 1985)
ELD	Eierland
LTA	Lumped Triad Approximation (Eldeberky, 1996)
MPN	Meetpost Noordwijk
NAP	Amsterdam Ordnance Datum
OCA	Original Collinear Approximation
R	Rattanapitikon (2007)
SON	Schiermonnikoog Noord
SPB	Stochastic Parametric model based on Boussinesq eq. (Becq-Girard, 1999)
SWAN	Simulating WAves in the Nearshore
TG	Thornton and Guza (1983)
TOMAWAC	TELEMAC-based Operational Model Addressing Wave Action Computation

TXH	Texelhors
UTC	Coordinate Universal Time
vdW	van der Westhuysen (2009)
WAM	WAve Model
WAQUA	WAter QUAlity simulation
WWM	Wind Wave Model
YMS	IJmuiden Semafoor

Miscellaneous

*	complex conjugate
$\|\ldots\|$	absolute value
$\|\|\ldots\|\|$	magnitude of vector
$\langle\ldots\rangle$	ensemble average
$[\ldots]$	expected value
$\nabla_{\mathbf{x}}$	horizontal gradient operator
rms	root-mean squared
$r.b.$	relative bias [−]
$s.i.$	scatter index [−]

List of Publications

Journal Articles

Salmon, J.E., Holthuijsen, L.H., Zijlema, M., van Vledder, G.P. and Pietrzak, J.D. (2015). Scaling depth-induced wave-breaking in two-dimensional spectral wave models. *Ocean Modelling*, **87**, pp. 30–47.

Salmon, J.E. and Holthuijsen, L.H. (2015). Modeling depth-induced wave breaking over complex coastal bathymetries. *Coastal Engineering*, **105**, pp. 21–35.

Salmon, J.E., Smit, P.B., Janssen, T.T. and Holthuijsen, L.H. (2016). A consistent collinear triad approximation for operational wave models. *Ocean Modelling*, **104**, pp. 203–212.

Conference Proceedings

Salmon, J.E., Holthuijsen, L.H., Smit, P.B., van Vledder, G.P. and Zijlema, M. (2014). Alternative source terms for SWAN in the coastal region. In: *Proceedings of the 34th International Conference on Coastal Engineering*, Coastal Engineering Research Council, Seoul, South Korea, pp. 1–13.

Salmon, J.E. and Holthuijsen, L.H. (2011). Re-scaling the Battjes-Janssen model for depth-induced wave-breaking. In: *12th International Workshop on Wave Hindcasting and Forecasting and Coastal Hazards Symposium*, WMO/IOC Joint Technical Commission for Oceanography and Marine Meteorology (JCOMM), Kohala Coast, HI, pp. 1–6.

CURRICULUM VITÆ

James Eric SALMON

06-05-1987	Born in London, United Kingdom

EDUCATION

1998–2005	Grammar School Southend High School for Boys, Southend-on-Sea
2005–2009	Civil Engineering with a Year Abroad (MEng; 1:1) Imperial College London, United Kingdom (2005–2008) Delft University of Technology, the Netherlands (2008–2009)
2009	Guest Researcher at Delft University of Technology
2010–2015	Ph.D. Civil Engineering Delft University of Technology